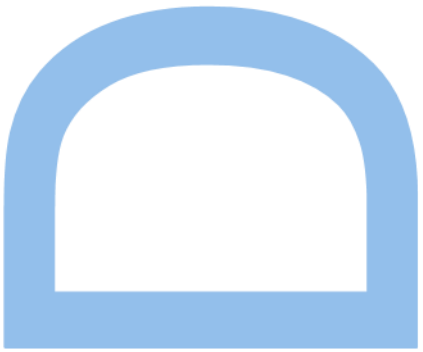
PyranoFlavylium-based Materials as Colorimetric pH-Indicators for Food Spoilage Monitoring

Vânia Patrícia Martins Gomes
PhD in Chemistry
Department of Chemistry and Biochemistry
2023

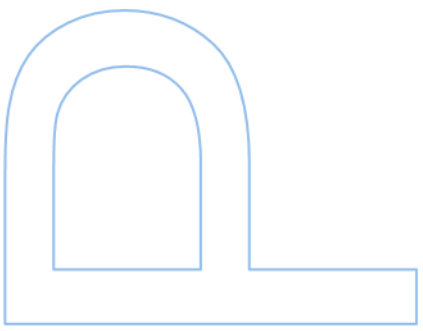
Supervisor
Victor Armando Pereira de Freitas, Full Professor,
Faculty of Sciences of the University of Porto

Co-supervisor
Luís Miguel Neves Ferreira Serra Cruz, Independent Researcher,
REQUIMTE-LAQV


U.PORTO
FACULDADE DE CIÊNCIAS
UNIVERSIDADE DO PORTO







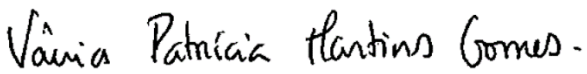
Sworn Statement

I, Vânia Patrícia Martins Homes, enrolled in the Doctor's Degree in Chemistry at the Faculty of Sciences of the University of Porto hereby declare, in accordance with the provisions of paragraph a) of Article 14 of the Code of Ethical Conduct of the University of Porto, that the content of this thesis reflects perspectives, research work and my own interpretations at the time of its submission.

By submitting this thesis, I also declare that it contains the results of my own research work and contributions that have not been previously submitted to this or any other institution.

I further declare that all references to other authors fully comply with the rules of attribution and are referenced in the text by citation and identified in the bibliographic references section. This thesis does not include any content whose reproduction is protected by copyright laws.

I am aware that the practice of plagiarism and self-plagiarism constitute a form of academic offense.



Vânia Patrícia Martins Gomes

January 18, 2023

Acknowledgements | Agradecimentos

À FCT pelo financiamento da minha bolsa de doutoramento.

Ao Luís, por toda a orientação, confiança, compreensão e pela liberdade que me concedeu para desenvolver este projeto.

Ao Professor Victor Freitas, por todas sua palavras sábias, mas também pelas suas piadas à Pai.

À Sofia, porque parte deste trabalho também é dela, mas acima de tudo pela amizade e cumplicidade.

À companheira Joana Azevedo, que foi um pilar em toda esta jornada, por me ter orientado nas questões burocráticas e nos prazos deste doutoramento.

A todo o pessoal do laboratório pela boa disposição, e por todos os docinhos que foram deixando no gabinete, que me alegravam o dia.

Ao Roberto, Noemi e ao Rubén e restante pessoal do CTC, por me te terem acolhido na minha estadia em Ourense.

À Rosa pela amizade, pelo apoio dos tempos que esteve no porto, mas especialmente, pelo apoio na minha estadia em Ourense.

À Cláudia, Mafalda, Luísa, Ana e Cátia pelo nosso almocinho, pela disponibilidade de ouvir todos os desabafos do dia-a-dia, pela amizade e apoio.

A todos os meus amigos que acompanharam esta minha jornada de perto e que me ajudaram sempre com sorrisos e copos.

Aos meus pais e à minha irmã, sem o apoio deles eu nunca teria chegado até aqui.

Ao Nuno, por estar sempre ao meu lado.

E ao meu querido Fausto!

Resumo

O uso de pigmentos naturais e de base natural têm atraído atenção crescente por parte da comunidade científica em diversas áreas de aplicação devido à sua biocompatibilidade, biodegradabilidade e não toxicidade, entre outras propriedades interessantes. Os pigmentos derivados do catião flavílio, particularmente as antocianinas, são uma das mais importantes classes de pigmentos naturais e têm sido amplamente explorados devido às suas excecionais propriedades cromáticas, nomeadamente, a capacidade de mudar de cor dependendo do pH do meio. No entanto, os pigmentos naturais têm geralmente associados problemas de estabilidade, que limitam as suas aplicações. O desenho e síntese de novos pigmentos inspirados em antocianinas pode resolver alguns dos problemas associados aos pigmentos naturais, mantendo ou até mesmo melhorando algumas das suas características físico-químicas e cromáticas.

Os pigmentos do tipo piranoflavílio também se caracterizam por serem sensíveis ao pH do meio devido às reações de transferência de protões, que levam à formação de diferentes espécies em equilíbrio ácido-base com diferentes cores. Além disso, estes pigmentos mostraram propriedades melhoradas em relação aos precursores derivados de flavílio quanto à estabilidade química e fotoquímica. Por estas razões, os piranoflavílios têm grande potencial para serem utilizados em diversas aplicações, nomeadamente, como indicadores ácido-base para o controlo do estado de frescura de alimentos sensíveis ao pH.

Nos últimos anos, têm sido desenvolvidas embalagens alimentares inteligentes para detetar e fornecer informações em tempo real sobre a qualidade dos alimentos. De entre as tecnologias aplicadas em embalagens inteligentes, os indicadores colorimétricos de pH são os mais estudados para deteção da deterioração de alimentos perecíveis através da mudança de cor. Geralmente, a deterioração de alimentos à base de músculos (ou seja, carne e peixe) é caracterizada por um aumento do pH devido à libertação de compostos voláteis baseados em azoto, como resultado da decomposição de proteínas e de outras moléculas de azoto não proteico.

O primeiro objetivo do presente trabalho consistiu no desenho racional e na síntese de pigmentos à base de piranoflavílio com propriedades cromáticas adequadas para aplicação como indicadores de pH na monitorização da frescura de alimentos. A cor dos

pigmentos foi modulada por modificações estruturais da estrutura base dos piranoflavílio e, ainda, pela interação com sistemas micelares (dodecil sulfato de sódio (SDS), brometo de cetiltrimetilamónio (CTAB) e *Triton X-100*). Algumas mudanças estruturais foram realizadas no núcleo do cromóforo de modo a promover a extensão da conjugação π como, por exemplo, a substituição do flavílio por xantílio. Outras alterações envolveram os substituintes ao núcleo do piranoflavílio, nomeadamente, o número e posição dos grupos hidroxilo. As características de cor dos pigmentos e sua dependência ao pH foram investigadas através da determinação de parâmetros físico-químicos e foto-físicos. Foi ainda feito um estudo de citotoxicidade dos pigmentos mais promissores.

Os principais resultados da síntese e caracterização mostraram que a extensão da conjugação π, pela introdução de uma ligação dupla no núcleo do flavílio, resultou numa maior capacidade corante quando comparado com as piranoantocianinas tradicionais. O sistema micelar aniónico SDS promoveu uma melhor estabilização de cor em toda a gama de pH. O piranoxantílio demostrou uma interessante propriedade de fluorescência dependente do pH, tornando-o útil como uma potencial sonda fluorescente do tipo "*off-on-off*" responsiva ao pH para aplicações alimentares e biológicas. No entanto, entre todos os corantes sintetizados, o piranoflavílio simétrico com dois grupos fenóis (cloreto de 2,10-*bis*-(4',4''-hidroxifenil)piranobenzopirílio) mostrou ter uma variação de cor mais destacável dentro da gama de pH correspondente à deterioração de alimentos. Além disso, demonstrou citotoxicidade reduzida, o que o tornou um candidato promissor como indicador colorimétrico responsivo ao pH, em embalagens alimentares inteligentes.

O segundo objetivo consistiu na imobilização do pigmento num suporte sólido para desenvolver o indicador de pH colorimétrico (etiqueta inteligente). Inicialmente, a imobilização foi considerada através de duas abordagens: aprisionado fisicamente ou ligado covalentemente a uma matriz polimérica. Esta última consistiu na conjugação química de pigmentos de piranoflavílio a biopolímeros de origem marinha, nomeadamente o quitosano e o alginato.

No entanto, o desenvolvimento do indicador de pH apenas seguiu a imobilização do pigmento por aprisionamento numa matriz polimérica. O filme indicador foi produzido pela técnica de molde (*casting*) usando uma matriz polimérica de acetato de celulose e glicerol como plastificante. Foram estudadas diferentes formulações através das propriedades físicas dos filmes (espessura, cor, morfologia, barreira e térmicas) e da sua resposta cromática a soluções de diferentes valores de pH (pH 4 a 8). A melhor

formulação foi inicialmente testada no *headspace* de aminas biogénicas e em soluções contendo amónia e, em seguida, com amostras reais (peixe e carne) em condições controladas (4 ± 1 ºC e embalagem em atmosfera modificada). Além disso, foram quantificadas a fotoestabilidade do filme indicador e a migração do pigmento ao longo do tempo.

Entre as formulações testadas, o filme indicador contendo glicerol a 30% (m/m) apresentou a melhor reposta à variação do pH. Essa percentagem originou o aparecimento de poros no filme, resultando no aumento da permeabilidade ao vapor de água e da área superficial de contacto, e consequentemente, a uma resposta cromática mais eficiente e sensível.

Além disso, o pigmento a 0,2% (m/m) favoreceu a eficácia colorimétrica do filme em comparação com 0,1% (m/m). Relativamente à migração do pigmento e à fotoestabilidade, a etiqueta mostrou-se adequada para aplicação em embalagens de carnes e peixes frescos. O melhor desempenho foi observado para a monitorização da frescura das amostras de peixe. A etiqueta demonstrou elevada eficácia na deteção da deterioração do carapau (*Trachurus trachurus*). Após 5 dias de armazenamento, os parâmetros de frescura excederam o limite definido pelos regulamentos da UE, indicando que o peixe estaria impróprio para consumo. Simultaneamente, a etiqueta inicialmente de cor amarela alterou-se para a cor roxa, indicando efetivamente o início do processo de deterioração.

Palavras-chave: corantes de piranoflavílio, mudanças de cor, ajuste da cor, sensibilidade ao pH, filmes indicadores, caracterização físico-química, deterioração de alimentos, frescura de alimentos em tempo real.

Abstract

The use of natural and natural-based pigments has attracted growing attention from the scientific community for several applications due to their biocompatibility, biodegradability, and non-toxicity, among other noteworthy properties. Flavylium-derived pigments, particularly anthocyanins, are one of the most important natural classes of pigments and have been extensively explored due to their remarkable color properties, such as the dependency on the pH of the medium. However, natural pigments generally have associated stability problems, which limit their applications. The design and synthesis of new anthocyanin-inspired pigments can solve some of the problems associated with natural pigments, maintaining, or even improving some of their physical-chemical and chromatic characteristics.

Pigments of the pyranoflavylium type are also characterized by being pH sensitive due to proton transfer reactions, leading to different colored species in acid-base equilibrium. Moreover, they have been shown to improve properties compared to flavylium-derived precursors, such as chemical and photochemical stability. Thus, these dyes have great potential to be used for several applications, namely, as pH indicators to control the freshness state of pH-sensitive foodstuffs.

In recent years, intelligent food packaging is being developed to detect and provide real-time information regarding food quality. Behind the technologies applied in intelligent packaging, colorimetric pH-indicators are the most studied in research for detecting spoilage in perishable food packaging through a color change. Generally, the spoilage of perishable food based on muscles (i.e., meat and fish) is characterized by an increase in pH due to the release of volatile nitrogen-based compounds as a result of the decomposition of proteins and other non-proteic nitrogen molecules.

The present work's first goal was the rationale design and synthesis of pyranoflavylium-based pigments with suitable color features for application as pH-indicators for food freshness monitoring. The color was modulated by structural modifications and interaction with micellar systems (sodium dodecyl sulphate (SDS), cetyltrimethylammonium bromide (CTAB), and Triton X-100). Some structural changes were performed to the chromophore core, promoting the extension of the π-conjugation, by replacing the flavylium cation with a xanthylium. Other alterations involved the substituents on the pyranoflavylium core, namely, the number and position of the

hydroxyl groups. Color features of the pigments and their pH dependency were investigated by determining physicochemical and photophysical parameters, where the most promising ones were also studied in terms of cytotoxicity properties.

The main results of synthesis and characterization showed that the extent of π-conjugation by introducing a double bond in the flavylium core leads to a higher colorant capacity of the pigment when compared with traditional pyranoanthocyanins. The anionic SDS micellar system promoted the best color stabilization at the entire pH range. Pyranoxanthylium showed an interesting pH-dependent fluorescence property, making it useful as a potential "*off-on-off*" pH-responsive fluorescent probe for food and biological applications. Nevertheless, among all the synthesized dyes, a symmetrical phenol-based pyranoflavylium dye (2,10-*bis*-(4',4''-hydroxyphenyl)pyranobenzopyrylium chloride) showed a more noticeable color variation within the pH range of the food spoilage process. Furthermore, this dye demonstrated reduced cytotoxicity, which made it a promising candidate as a pH-dependent colorimetric and fluorescence sensor for food intelligent packaging.

The second goal was the pigment immobilization on a solid support to develop a colorimetric pH-indicator (smart label). Initially, the immobilization was conceived through two approaches: physically entrapped or covalently bonded to a polymeric matrix. This last one consisted of the chemical conjugation of pyranoflavylium pigments onto marine-origin biopolymers, namely chitosan, and alginate. Nevertheless, the development of the pH-indicator only followed the immobilization of the pigment by entrapment into a polymeric matrix. The film indicator was produced by solvent casting technique using a cellulose acetate polymeric matrix and glycerol as a plasticizer. Different formulations were investigated in terms of the physical properties of the films (thickness, color, morphology, barrier, and thermal properties) and their chromatic response to solutions at different pH values (pH 4 to 8). The best formulation was first tested in the headspace of biogenic amines and ammonia-containing solutions and then used in real samples (fish and meat) at controlled conditions (4 ± 1 ºC and modified atmosphere packaging). Moreover, the film indicator photostability and the pigment migration over time were quantified.

Among the tested formulations, acetate cellulose film with glycerol at 30% (w/w) showed the best pH-responsiveness of the film indicator. This percentage originated pores in the film, which increased water permeability and the surface contact area, resulting in a more efficient and sensitive chromatic response to the environment. In addition, pigment at

0.2% (w/w) favored the colorimetric efficacy of the film in comparison with 0.1% (w/w). Regarding pigment migration and photostability, the label was suitable for application in fresh meat and fish packaging. The best performance was observed for the freshness monitoring of fish samples. The indicator demonstrated high efficacy in detecting spoilage in Atlantic horse mackerel (*Trachurus trachurus*). After 5 days of storage, freshness parameters exceeded the limit defined by EU regulations, indicating that the fish was not suitable for consumption. Simultaneously, the yellow label started to turn purple, effectively indicating the beginning of the spoilage process.

Keywords: pyranoflavylium dyes, color changes, color tuning, pH-sensitivity, indicator films, physicochemical characterization, food spoilage, real-time food freshness

Table of Contents

Sworn Statement i
Acknowledgments iii
Resumo iii
Abstract vii
Table of contents xi
List of Publications xii
List of Abbreviations and Symbols xv
Thesis Outline xvii
General Introduction 1
1. Pyranoflavylium-based pigments 3
1.1. The Origin 5
1.2. Synthesis and hemi-synthesis 7
1.3. Properties of Pyranoflavylium pigments 9
1.3.1. Chromatic features and chemical equilibria 9
1.3.2. Color stabilization or modulation 11
1.3.3. Fluorescence Properties 14
1.3.4. Biological Properties 16
2. pH-indicators for food freshness monitoring 19
2.1. Food Packaging 19
2.1.1. Intelligent food packaging 19
2.2. Food spoilage and pH variations 20
2.3. pH-indicators for food freshness monitoring 21
2.3.1. Cellulose acetate films as a solid support for pH-indicators 23

2.3.2. Film production, characterization, and test as pH-indicator 24

2.4. Anthocyanin-based indicators 26

2.4.1. Problems related to ANCs pH-indicators 27

3. Project purpose 31

References 32

Chapter I – Novel pyranoflavylium and related dyes: synthesis and physicochemical characterization 43

Article I – Synthesis and chemical equilibria of a new 10-methylpyrano-2-styrylbenzopyrylium pigment in aqueous solution and its modulation by different micellar systems 45

Article II – A pH-responsive fluorescent sensor based on a new pyranoxanthylium salt 57

Article III – Bioinspired Synthesis and Physical-Chemical Properties of a New 10-Methylpyrano-4′-hydroxyflavylium Chloride Salt 73

Article IV – Synthesis of novel pyrano-3,7-deoxyanthocyanin derivatives and study of their thermodynamic, photophysical and cytotoxicity properties 83

Article V – Colorimetric pH-Responsive Biomaterials Based on Pyranoflavylium-Biopolymer Hybrid Conjugates 95

Chapter II – Development of a pH-indicator label based on a pyranoflavylium for food packaging 117

Article VI – Pyranoflavylium-cellulose acetate films and the glycerol effect towards the development of pH-freshness smart label for food packaging 119

Article VII – FoodSmarTag: An innovative dynamic labeling system based on pyranoflavylium-based colorimetric films for real-time control of food freshness 133

General conclusions and final remarks 161

List of Publications

Articles published in peer-reviewed scientific journals:

Pires, A. P., Gomes, V., Neves, D., Mateus, N., de Freitas, V, Cruz, L., Colorimetric pH-Responsive Biomaterials Based on Pyranoflavylium-Biopolymer Hybrid Conjugates, *ACS Applied Polymer Materials*, **2022**, 4, 7, 4961–4971. DOI: 10.1021/acsapm.2c00514

Gomes, V., Pires, A. P., Mateus, N., de Freitas, V, Cruz, L., Pyranoflavylium-cellulose acetate films and the glycerol effect towards the development of pH-freshness smart label for food packaging, *Food Hydrocolloids*, **2022**, 127, 10750. DOI: 10.1016/j.foodhyd.2022.107501

Gomes, V., Pires, A. P., Fernandes, I., Mateus, N., de Freitas, V, Cruz, L., Synthesis of novel pyrano-3,7-deoxyanthocyanin derivatives and study of their thermodynamic, photophysical and cytotoxicity properties, *Journal of Photochemistry and Photobiology A: Chemistry*, **2021**, 415, 113313. DOI: 10.1016/j.jphotochem.2021.113313

Gomes V., Mateus N., de Freitas V., Cruz L., A pH-responsive fluorescent sensor based on a new pyranoxanthylium salt. *Photochemical and Photobiological Sciences*, **2021**, 20(4), 513-521. DOI:10.1007/s43630-021-00033

Pinto, A. L., Cruz, H, Oliveira, J., Araújo, P., Cruz, L., Gomes, V., Silva, C. P., Silva, G.T.M., Mateus, T., Calogero, G., de Freitas, V., Quina, R.H., Pina, F., Parola, A. J., Lima, J.C., Dye-sensitized solar cells based on dimethylamino-π-bridge-pyranoanthocyanin dyes, *Solar Energy*, **2020**, 206, 188-199. DOI: 10.1016/j.solener.2020.05.101.

Gomes, V., Guimarães, M., Gonçalves, G., de Freitas, V., Cruz, L., Bioinspired Synthesis and Physical-Chemical Properties of a New 10-Methylpyrano-4′-hydroxyflavylium Chloride Salt, *Synlett*, **2020**, 31(04), 334-338. DOI: 10.1055/s-0039-1690744.

Pinto, A. L., Cruz, L., Gomes, V., Cruz, H., Calogero, G., de Freitas, V., Pina, F., Parola, A. J., Lima, J.C.Catechol versus carboxyl linkage impact on DSSC performance of synthetic pyranoflavylium salts, *Dyes and Pigments*, **2019**, 170, 107577 DOI: 10.1016/j.dyepig.2019.107577

Gomes, V., Cruz, L., Mateus, N., de Freitas, V., Synthesis and chemical equilibria of a new 10-methylpyrano-2-styrylbenzopyrylium pigment in aqueous solution and its

modulation by different micellar systems, *Dyes and Pigments*, **2019**, 167, 60–67 DOI: 10.1016/j.dyepig.2019.04.004

Articles in preparation:

Gomes, V., Bermudez, R., Lorenzo, J. M., Mateus, N., de Freitas, V, Cruz, L., FoodSmarTag: An innovative dynamic labeling system based on pyranoflavylium-based colorimetric films for real-time control of food freshness, **2023**.

Gomes, V., Mateus, N., Oliveira, J., de Freitas, V, Cruz, L., Pyranoflavylium-based dyes: from properties to applications. (Review), **2023**.

List of Abbreviations and Symbols

A	quinoidal base
A^-	anionic quinoidal base
AFM	Atomic Force Microscopy
AH^+	flavylium cation
ANC	anthocyanin
a_w	water activity
B2	hemiketal
CA	cellulose acetate
C_C	*cis*-chalcone
C_t	*trans*-chalcone
CTAB	cetyltrimethylammonium bromide
Cy	Cyanidin
Cy-3-glc	Cyanidin-3-*O*-glucoside
DMA	dimethylamine
Dp-3-glc	Delphinidin-3-*O*-glucoside
DPPH	2,2-diphenyl-1-picrylhydrazyl
DSSC	Dye-sensitized solar cell
EB	Elongation at Break
ESPT	Excited State Proton Transfer
FAO	Food and Agriculture Organization of the United Nations
FRAP	Ferric Reducing Antioxidant Power
FT-IR	Fourier Transform Infrared
Gly	glycerol
LbL	layer-by-layer assembly
λ_{max}	maximum wavelength
MAP	Modified atmosphere packaging
Mv	Malvidin

Mv-3-glc	Malvidin3-*O*-glucoside
NMR	Nuclear magnetic resonance
NPN	Nonproteic nitrogen
OP	Oxygen permeability
PDT	Photodynamic therapy
pK_a	acidity constant
ROS	Reactive oxygen species
SDS	sodium dodecyl sulphate
SEM	Scanning electron microscopy
SRB	Sulforhodamine B
Tg	Glass transition temperature
TGA	Thermogravimetric analysis
TMA	Trimethylamine
TS	Tensile strength
TVB-N	Total volatile basic-nitrogen
WHO	World Health Organization
WVP	Water vapor permeability
YM	Young's modulus
ε	molar extinction coefficient

Thesis Outline

This thesis is divided into three parts: introduction, research work, and general conclusion with final remarks. The research work is divided into two chapters (I and II), which in turn are divided into five and two subchapters, respectively. The formal organization of the experimental work does not precisely reflect the order in which it was performed; however, it was chosen for a better organization of the results. Each subchapter consists of an integral article published, except for the last subchapter, whose manuscript is not yet published. A brief description of each part is given below.

The general introduction describes the necessary topics for the broad comprehension of this thesis and is divided into three parts. The first part consists of a bibliographic review of pyranoflavylium dyes, which includes their origin, synthesis, and physical-chemical properties, such as chromatic, fluorescence, and biological properties. In addition, pyranoflavylium applications related to their properties will be introduced. The second part is an introduction to intelligent food packaging, which explains how colorimetric pH-indicators may monitor food's freshness. The last part of the introduction presents the project's purpose, which includes general and specific objectives.

As mentioned above, the experimental section is divided into two chapters (I and II). The first chapter refers to the synthesis and study of new pyranoflavylium and related compounds. The first subchapter (Article I) describes the synthesis of a styryl derivative of pyranoflavylium and the modeling of its color in micellar systems (SDS, CTAB, Triton X-100). The second subchapter (Articles II) consists of the chromatic and fluorescence properties of a pyranoflavylium-related compound, namely, the pyranoxanthylium. Articles III, IV, and V report the synthesis of a new pyranoflavylium lacking a hydroxyl group at position 7 of the basic structure of the pyranoflavylium. Article IV describes the chromatic and fluorescence properties of the studied compounds. Finally, the last subchapter (Article V), in addition to the chromatic properties, also describes the combination of pigments with marine biopolymers (alginate and chitosan).

Chapter II describes the development of the colorimetric pH-indicator label based on the most promising pyranoflavylium pigment. The first article in this chapter (Article VI) describes the development of films containing the optimized formulation with the required properties. The second article (Article VII) reports the tests on food samples and

concerns other questions related to the applicability of the indicator, namely, its photostability and the possible migration of the pigment to the food matrix.

Finally, a brief discussion of the general results obtained is presented in the last part of the thesis. In addition, final considerations and potential direction of future work are presented.

General Introduction

1. Pyranoflavylium-based pigments

The use of natural and natural-based pigments has attracted growing attention from the scientific community for several applications due to their biocompatibility, biodegradability, and non-toxicity, among other interesting properties. In the field of natural-based pigments, flavylium cation (2-phenylbenzopyrylium) derivatives, namely 3-deoxyanthocyanidins and anthocyanins, have played a crucial role in different applications (Figure 1.1). Anthocyanins are one of the most important classes of pigments present in nature, responsible for colors from yellow to the blue of many fruits, flowers, and vegetables. 3-deoxyanthocyanidins, which lack the hydroxyl substituent at position C-3, are considered the chemical ancestor of anthocyanins and may be found in mosses, ferns, and other plants [1].

Besides the amazing colors, these kinds of pigments are also known for their excellent antioxidant activity and other biological properties. Furthermore, the ability of flavylium compounds to change their color according to the pH media is an additional noteworthy characteristic.

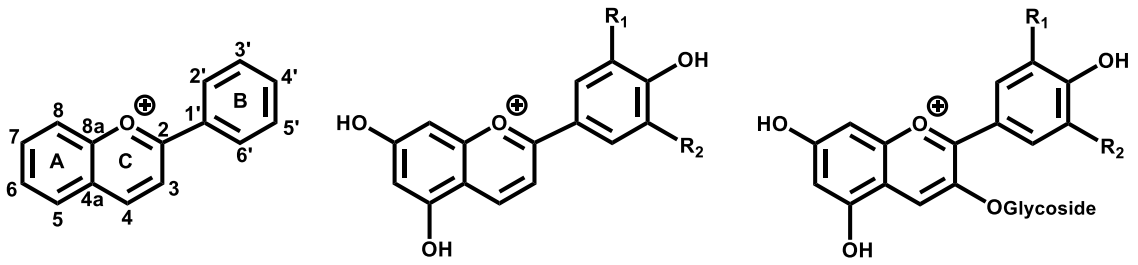


Figure 1.1. Chemical structures of flavylium cation and the most common natural pigments: 3-Deoxyanthocyanidins and Anthocyanins.

A complex multistate equilibrium in an aqueous solution generally characterizes the physicochemical properties of flavylium-based pigments (Figure 1.2). The red cationic form (AH^+) is the predominant specie at very low pH. As the pH increases, the flavylium cation immediately undergoes proton transfer reactions leading to the formation of the violet quinoidal base (A) and the blue anionic quinoidal base (A^-). However, on a small-time scale, the flavylium cation hydrates giving a colorless hemiketal (B_2). This specie quickly reaches the equilibrium with pale a yellow *cis*-chalcone (C_c), which slowly isomerizes to a *trans*-chalcone (C_t) (Figure 1.2) [2,3].

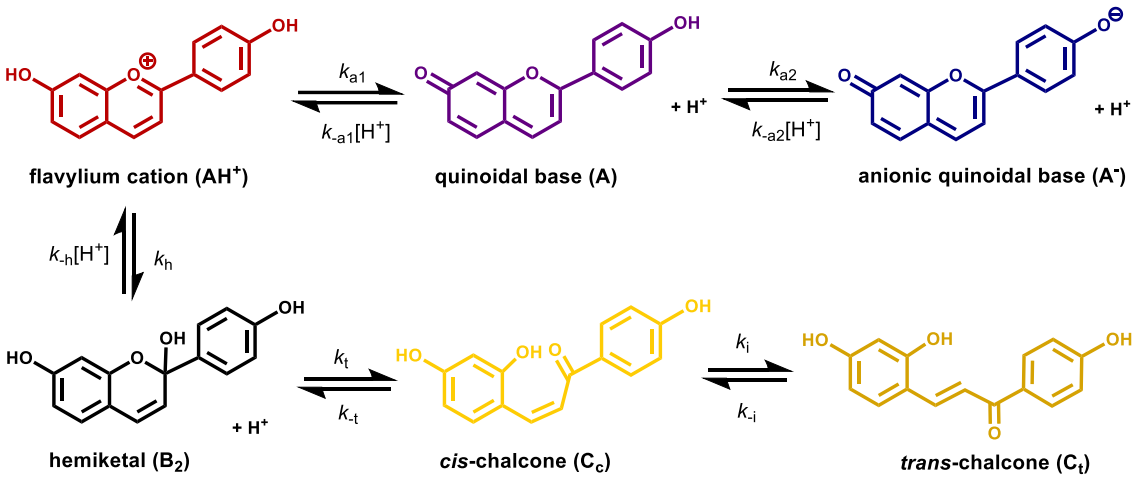


Figure 1.2. General equilibrium forms of flavylium-based pigments in aqueous solutions at different pH values. Adapted from [2,3].

Despite their interesting chemical equilibria, the hemiketal and, subsequently, chalcones formation leads to color fading over time in neutral and basic pH. In addition, these pigments are notoriously unstable outside their native environment, particularly when exposed to light and temperature [4]. These characteristics considerably restrict the use of anthocyanins in several applications.

Pyranoflavylium compounds are flavylium-derived pigments with an additional pyranic ring in the chromophore center, as shown in Figure 1.3. These derivatives are described as having advantages compared to flavylium, namely, their stability and color intensity, which make them promisors' molecules to apply in different applications. Pyranoflavylium properties, their origin, and obtention will be discussed in detail in the following sections.

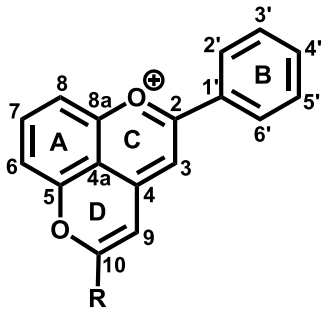


Figure 1.3. Chromophore structure of pyranoflavylium cation.

1.1. The Origin

The first record of a pyranoflavylium-based dye in the literature dated from 1936 when Brockmann and Haase were researching the red color of the "dragon's blood" resin and isolated a pigment called dracorubin [5,6]. However, the chemical structure of dracorubin was only fully elucidated in 1950 (as a quinoidal base form), followed by its synthesis in 1976 by Robertson, Whalley, and co-workers [7,8].

To the best of our knowledge, after that and up to the 1990s, no developments in the discovery of new pyranoflavylium-based pigments were documented. In 1996, the study of the composition of red wine led to the discovery of new anthocyanin-derived pigments by Cameira dos Santos *et al.*, which suggested that the new structure resulted from the condensation reaction between grape anthocyanins and another wine component [9].

In the same year, the new compounds' structural elucidation was achieved using analytical (mass spectrometry and NMR spectroscopy) and synthetic methods by Fulcrand *et al.* [10]. This study showed that the new pigments result from a chemical reaction between the main wine anthocyanins and 4-vinylphenol. They reported a cyclization reaction between the C-4 and the hydroxyl group at C-5 of the flavylium moiety and the vinylphenol double bond, followed by an oxidation step, giving rise to a new pyranic ring with a hydroxyphenyl group in C-10 position (Figure 1.4).

A year later, Bakker and Timberlake isolated and characterized two more new types of pyranoanthocyanins from red wines: the A- and B-type vitisins [11]. They reported that the A-type vitisin had an aldehyde and hydroxyl substituents in C-9 and C-10 positions (Figure 1.4), respectively, in the new pyranic ring; while the B-type vitisin had only hydrogen in the C-10 position. However, the correct structure of A-type vitisin (Figure 1.4) was only elucidated by Fulcrand *et al.* in 1998, as well as its formation mechanism from malvidin-3-monoglucoside and pyruvic acid [12].

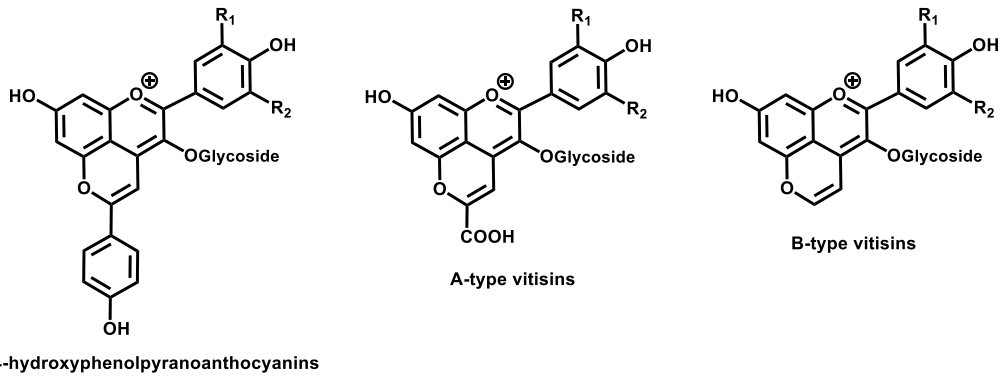


Figure 1.4. Structure of pyranoanthocyanins discovered by Fulcrand *et al.* [10] [12] and Bakker and Timberlake [11].

After that, other pyranoanthocyanins have been identified and isolated from beverages such as fruit and vegetable juices and red wines. Then, they were chemically synthesized according to the formation pathways that also have been described. The formation of pyranoanthocyanins is related to reactions in processed foods containing anthocyanins and where these can react with other compounds also present in the food matrix. In aged red wines, anthocyanins react with yeast metabolites produced during the fermentation process, such as pyruvic acid [12], acetaldehyde [11], acetoacetic acid [13], diacetyl [14], oxaloacetic acid [15], vinyl phenols [10,16–18] and hydroxycinnamic acids [17,19,20], or with flavan-3-ols [21], giving rise to primary or first-generation pyranoanthocyanins. Primary pyranoanthocyanins, namely 10-carboxypyranoanthocyanins and 10-methylpyranoanthocyanins, can react between them or again with yeast metabolites or flavan-3-ols, arising more complex pyranoanthocyanins (second-generation), such as pyranoanthocyanin dimers [22] and Portisins (vinylpyranoanthocyanins) [23–27]. Although the majority of pyranoanthocyanins were discovered in red wine samples, particularly in aged red wine, owing to the time required for their formation, other pigments were identified for the first time in experiments conducted on wine-like solutions [19,28]. All these compounds and the chemistry behind the wine color are well-documented elsewhere [3]. They have also been reported in strawberry and raspberry juices, formed by reactions with sinapic and ferulic acids [29]. Although most pyranoanthocyanins were found in fermented food products, this kind of pigment was also described in plants, such as in scales of red onion *Allium cepa* (carboxypyranocyanidin) [30] and strawberry *Fragaria ananassa* (carboxypyranopelargonidin) [31]. Pyranoflavylium-type pigments that are not anthocyanins (without glycoside moiety) were also discovered in petals of *Rosa hybrida* (rosacyanin B) [32] and sorghum species [33,34]. The pathway formation of pyranoflavylium pigments in plants remains unclear until now. However, some authors do not entirely exclude the possibility of its formation during the extraction process [30,33]. Lu *et al.* [35] reported a clear example of this, describing new 10-methylpyranoanthocyanins from black currant seeds (*Ribes nigrum*), which were shown later to be the result of the oxidative cycloaddition reaction between anthocyanins and acetone as one of the extraction solvents [36].

1.2. Synthesis and hemi-synthesis

Although pyranoflavylium pigments have been discovered in aged red wines or some plants, as mentioned above, their amounts are usually small, which makes their isolation and purification not sustainable for a practical application. Therefore, the obtention of the required amounts for further deep studies is normally achieved through total synthesis or hemi-synthesis procedures starting from the respective flavylium salt. In addition, other pyranoflavylium-based pigments with improved and desired properties could be rationally designed and synthesized.

Generally, pyranoanthocyanins are obtained from anthocyanins previously extracted from a natural product (fruits or vegetables), purified/isolated, and following the same formation pathway that occurs during the aging of the red wine. Other pyranoflavylium salts, such as pyrano-3-deoxyanthocyanidins can be obtained from flavylium salts following the same methodology used to obtain pyranoanthocyanins.

Different flavylium salts can be obtained mainly through two synthetic approaches: 1) C-ring cyclization by an aldol condensation reaction of 2-hydroxybenzaldehydes with acetophenones; 2) reductive or oxidative transformations of flavonoid compounds, which are well-documented elsewhere [1].

The general pathway formation of pyranoflavylium compounds, specifically the new pyranic D-ring, results first from the nucleophilic attack of an enol form of a carbonyl compound (R_2 = OH) or a vinyl group (R_2 = H) to the electrophilic C-4 of the flavylium C-ring. Then the hydroxy group at C-5 adds to the carbonyl group, giving a hemiketal. Finally, a new pyranic ring is obtained following H_2O elimination and some oxidation steps (Figure 1.5) [1].

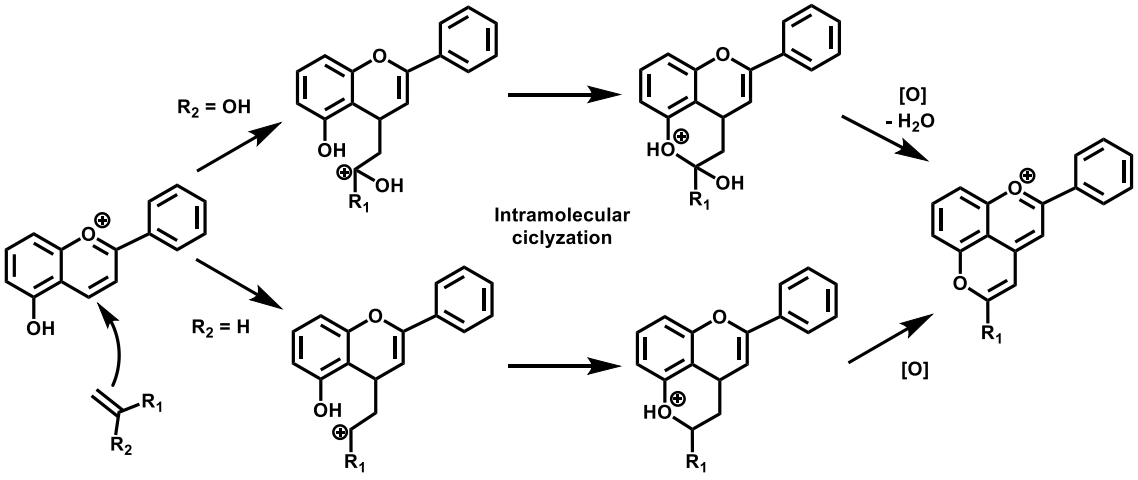


Figure 1.5. General mechanism for the formation of pyranoflavylium pigments.

The synthesis yield of pyranoflavylium pigments in wine-like solutions that follow a similar formation pathway to that occurring in the red wine aging is higher when compared to what is obtained if isolated directly from the red wine matrix. Nevertheless, this approach is still associated with some limitations, such as high-dilution conditions required to minimize side reactions and very moderate to low efficiency [37].

Regarding this, some studies have been carried out to improve yields. Changing the reactional conditions, such as pH, temperature, stoichiometry, or using more reactive molecules, have been studied. Work of Araújo *et al.* is an example of this, who compared the yields of the 10-carboxypyranomalvidin-3-*O*-glucoside (A-type vitisin) formation by the previously described reaction with pyruvic acid with the reaction with oxaloacetic acid (also found in musts and wines, but in lower quantities than pyruvic acid) and at different pH values (1.5, 2.6 and 3.5). The reaction with both acids showed better yields at pH 2.6; however, the oxaloacetic acid was more reactive, with yields of 59 % compared to 44 % of pyruvic acid (both at pH 2.6) [15]. Lu *et al.* also discovered serendipitously a methodology for obtaining 10-methylpyranoanthocyanins after extracting anthocyanin-based pigments from black currant seeds with acetone as a solvent, as already mentioned above. 10-methylpyranoanthocyanins were found in aged red wine but not as a consequence of the reaction between anthocyanins and acetone. Their presence in red wines was later postulated to result from a reaction with acetoacetic acid produced by yeast during fermentation. However, obtaining pyranoanthocyanins by reacting with acetone is cheaper and more efficient. B-type vitisin pigments (the simplest pyranoanthocyanin), usually originating from the reaction between anthocyanins and acetaldehyde during the red wine aging, have also been synthesized by the reaction with vinyloxy-trimethylsilane with higher yields (around 30%) [38].

Among the existing anthocyanins, some are more predisposed to form pyrano-derivatives than others. The reactivity may be related to the type of aglycone or the glycosidic substitution patterns. In terms of aglycones, malvidin was demonstrated to be the most efficient for pyranoanthocyanins formation, followed by cyanidin [39].

Although high glycosidic substitution was initially described as a hindrance to the formation of pyranoanthocyanins, Farr *et al*. reported that the saccharide number on substitution of the anthocyanin did not affect its efficiency in a linear trend [40]. They studied the influence of different glycosidic substitutions on C-3 of cyanidin on the 10-carboxypyranoanthocyanin formation and observed higher conversion rates with anthocyanins containing substitutions with disaccharides and 1→6 glycosidic bonds, comparatively to monosaccharides and disaccharides with 1→2 glycosidic bonds [40]. A possible explanation for these results may be related to the greater degree of rotation

that the disaccharides with 1→6 glycosidic bonds exhibit in solution (as free molecules), which might increase collision between molecules and attract pyruvic acid to the chromophore [40].

Although pyranoflavylium pigments had frequently been obtained by direct condensation of a 5-hydroxyflavylium cation with compounds containing an enolizable group, Roehri-Stoeckel *et al.* have developed a new methodology [41]. This methodology consists of the condensation reaction between 5-hydroxy-4-methylflavylium cations and aldehydes in methanol/ethanol as solvent under reflux. The 5-hydroxy-4-methylflavylium cations can be prepared using flavones and the methylmagnesium bromide as a Grignard reagent [41] or by acid-mediated condensation between a phenolic derivative and aroylacetones [42]. A series of pyranoflavylium cations were synthesized following this methodology with different aldehydes, and some of them were successfully obtained with good yields. Curiously, the formation of some of them was not observed, which the authors attributed to the nature of the aldehydes used, namely when they possess electron-withdrawing substituents, such as fluor, cyano, and nitro groups. Only aromatic aldehydes with electron-donating groups were reactive, which constituted a limitation of this synthetic pathway [41]. The exigence of having an aldehyde-rich electron-donating group led the authors to suppose that a charge-transfer complex formation is responsible for initiating the condensation between the two molecules instead of a nucleophilic attack of aldehyde by the vinylogous enol ether.

Later, C. da Silva *et al.* reported an improved procedure to the methodology described above, which allowed obtaining a wide variety of substituted pyranoflavylium cations with good to excellent yields (64 – 89 %). Modifications were made to the method of Chassaing and co-workers, including using excess aromatic aldehydes in an inert atmosphere during the first hours and using trifluoroacetic acid as an acid catalyst. These modifications allowed synthesize of pyranoflavylium cations with electron-withdrawing substituents that were not possible before and with a heterocyclic or polycyclic aromatic ring attached [43]. Based on those results, the authors do not exclude a charge-transfer interaction for the reactivity of electronic-rich aldehydes; however, they do not consider it as the dominant factor for the condensation reaction [41,43].

1.3. Properties of pyranoflavylium pigments

1.3.1. Chromatic features and chemical equilibria

As flavylium compounds, the chromatic features of pyranoflavylium pigments depend on the medium conditions, especially pH. However, their chromatic features differ from their respective flavylium precursors. The first evidence of this difference was the UV-Vis spectrum of the first pigments discovered by Camera-dos-Santos *et al.*, which underwent a hypsochromic shift in λ_{max} compared to original malvidins [9]. Most pyranoflavylium cations have a hypsochromic shift in λ_{max}, showing a more orange-yellowish color than the corresponding flavylium under the same pH conditions. This behavior was unexpected since the common conjugation rules dictate that a chromophore more π-conjugated electronically leads to an increase in the λ_{max} value. However, there are exceptions to the first behavior observed. Second-generation pyranoanthocyanins, such as portisins [24,27,44], dimers [22], and amino-based pyranoflavylium compounds [41,45,46] show a bathochromic shift, displaying a bluish to green hues. In 2010, Carvalho *et al.* presented an explanation for different deviations in the λ_{max} of the pyranoanthocyanins based on quantum theoretical studies. According to the authors, the changes in the λ_{max} were due to the combination of three factors: (i) the deviation from the planarity of the ubiquitous B ring; (ii) the reduction of delocalization capability with the B ring; and (iii) the extension of the remainder of the π-conjugated system [47]. Thus, in the case of simpler pyranoflavylium salts, it is the first two factors that prevail, leading to a hypsochromic shift. On the other hand, the extension of the π-conjugated system is predominant in the case of more complex pyranoflavylium salts or with amino groups, leading to a bathochromic shifting.

The intensity of the color of pyranoflavylium pigments can also differ from the original flavylium. For instance, anthocyanins have a high molar extinction coefficient (ε) at a very acidic pH (~1), which drastically decreases when the pH increase until the wine pH (~3.6) in a model wine solution. In contrast, pyranoanthocyanins do not show this drastic behavior, decreasing the molar extinction coefficient only slightly when pH increases from ~1 to 3.6. In some cases, it was even possible to observe a slight to a substantial increase of the molar extinction coefficient at pH 3.6, namely in oligomeric pyranoanthocyanin-flavan-3-ol pigments, as a result of intramolecular copigmentation [48]. The difference in color intensity at pH 3.6 between anthocyanins and pyranoanthocyanins is mainly related to their different chemical equilibria in an aqueous solution. The color intensity of anthocyanins decreases when pH increases from acid to

slightly acid or neutral, mainly due to the hydration equilibrium, which yields the colorless hemiketal species. Oppositely, pyranoflavylium compounds showed more resistance to hydration. The presence of the new pyranic ring in the skeleton protects the flavylium core against the nucleophilic attack by water, avoiding completely the hydration reaction or to a large extent. More specifically, the protection against the nucleophilic attack by water is ensured by the substitution at C-4 of flavylium chromophore since other flavylium compounds with C-4 substituted, such as a 7-hydroxy-4-methyl-flavylium, display the same behavior in aqueous solution [49]. Thus, the formation of colorless species can be neglectable, and the color changes in the entire pH range arise exclusively from the proton transfer reactions (Figure 1.6). The remarkable stability of these structures, namely the color intensity at different pH values, makes them more suitable for pigment applications in food and cosmetics.

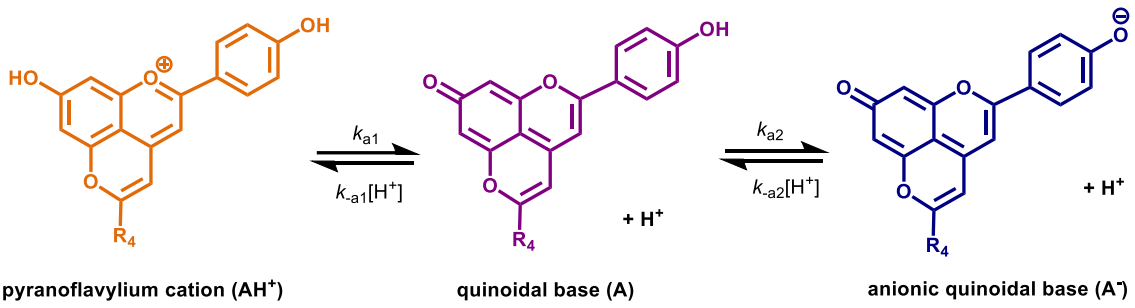


Figure 1.6. Equilibrium forms of pyranoflavylium in aqueous solutions.

The chemical equilibria of several pyranoflavylium pigments, such as pyranoanthocyanins, pyrano-3-deoxyanthocyanidins, among others, have been studied and acidity constants determined by UV-Vis and NMR spectroscopic techniques. Cruz *et al.* summarized the equilibrium constants of several pyranoflavylium pigments reported in the literature [1].

1.3.2. Color stabilization or modulation

Although pyranoflavylium-based pigments have shown to be more stable than flavylium precursors, their color can also be stabilized, modulated, or tuned for a specific application by modification of the substituents of the pyranoflavylium chromophore by non-covalent-interactions with macromolecules.

Oliveira *et al.* also studied the influence of the extent of π-conjugation of dimethylamino-based pyranoanthocyanins on their chromatic features. The extent of π-conjugation was

made by introducing one and two double bonds between the pyranic D ring and the aminophenyl unit (Figure 1.7) [50]. Although the presence of one double bond produced a significant bathochromic effect on the λ_{max} of the pyranoflavylium cation (from 557 nm to 633 nm), the presence of a second double bond has no significant effect on this value, which is similar to the λ_{max} of the dye-containing one double bond. In terms of chemical equilibria, the increase of the electronic delocalization promoted the protonation at the amino group, with a higher pK_{a1} value for the dye with extended π-conjugation. The first deprotonation of hydroxyl groups was also influenced, which diminished with the increase of the electronic delocalization, yielding the neutral quinoidal base at lower pH values [50].

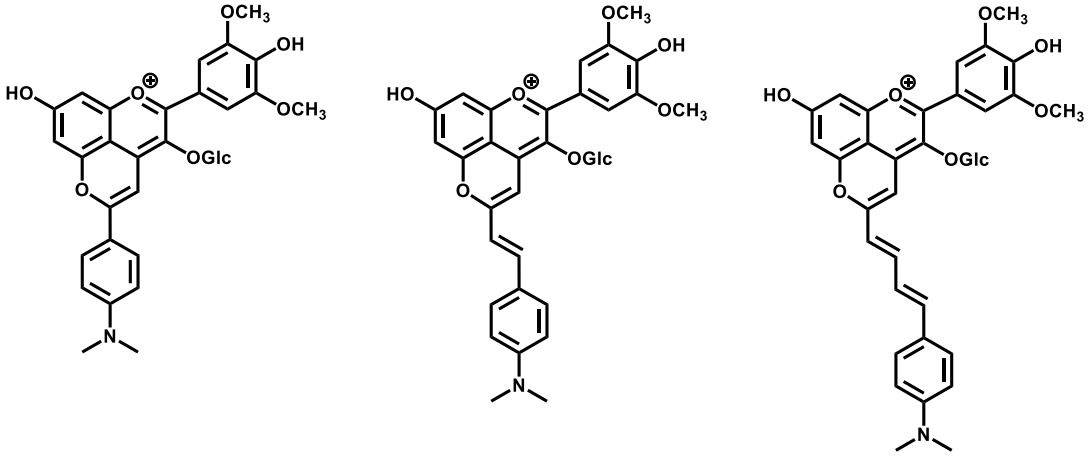


Figure 1.7. Structure of the three amino-derived pyranoanthocyanins [50].

Pyranoflavylium-based pigments with modifications in the chromophore were also developed, as is the case of a symmetrical pyrano-2-styrylbenzopyrylium salt, which has an extra double bond linking the benzopyrylium and the phenyl system, leading to an extension of π-conjugation [51] (Figure 1.8). As expected, introducing the double bond between the benzopyrylium core and ring B results in hyper and bathochromic shifts on the λ_{max} [51], from 496 nm to 556 nm, compared to similar pyranoflavylium without π-conjugation in C-2 and C-10 [52].

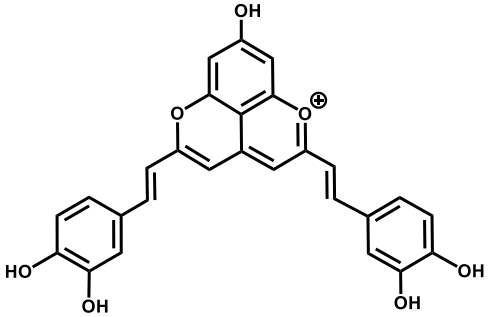


Figure 1.8. Structure of symmetrical 2,10-Bis-Styryl-1-Benzopyrylium Dye[51]

Araújo and co-workers studied the interactions of second-generation pyranoanthocyanins, namely Portisins and pyranoanthocyanins dimers, with lignin, the second most abundant natural macromolecule after cellulose. The interaction with this macromolecule was made through two different approaches: first with lignosulfonates, a water-soluble lignin-derived compound [53], and second with nanoparticles of Kraft lignin [54]. Lignosulfonates promoted a strong stabilization of pyranoflavylium cation form revealed by the considerable increase of the pK_{a1} (around two pH units) for both pyranoanthocyanins in the presence of this macromolecule when compared to the values obtained in its absence. In addition, the lignosulfonate improved the solubility of the dyes in aqueous systems over time, as shown in the example of Portisin in Figure 1.9 [53]. Moreover, for a higher concentration of lignin, the aggregation of dyes decreases, and each molecule is bound to a different site of lignin, resulting in a copigmentation phenomenon (charge-transfer complex). Nanoparticle systems of Kraft lignin and second-generation pyranoanthocyanins also showed good color stability toward pH change after 8 days of incubation at 37°C, compared to the pure bluish pigments [54].

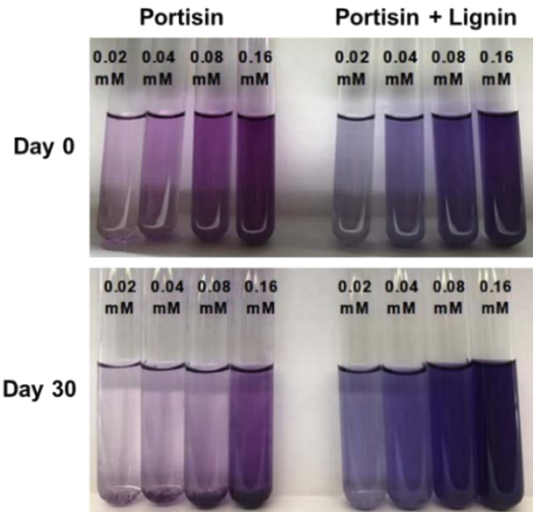


Figure 1.9. Color of the solutions of Portisin at different concentrations (20, 40, 80, and 160 μM) in the absence and presence of lignin (19 μM) in citrate buffer pH 3.5 at day 0 and after 30 days in the dark. Adapted from [53].

Recently, the color stabilization of pyranoanthocyanins by host−guest interaction mechanisms with anionic dendrimers was investigated. In contrast to previous results with simpler anthocyanins, the encapsulation becomes dominant as the dendrimer-to-dye concentration increases, promoted by the more hydrophobic nature of pyranoanthocyanins [55] (Figure 1.10).

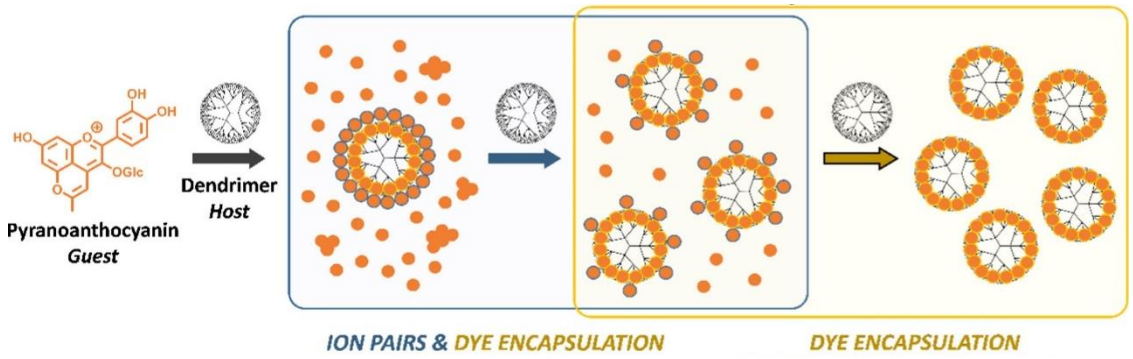


Figure 1.10. Host−guest interaction between pyranoanthocyanin and dendrimer. On increasing the dendrimer concentration, dye encapsulation becomes the dominant interaction. Adapted from [55].

1.3.3. Fluorescence Properties

Photochemical and photophysical studies have been conducted on pyranoflavylium compounds to evaluate their potential use as chromophores photosensitizers in solar cells (DSSC) and photodynamic therapy (PDT), as fluorescent probes in optical imaging, among other applications.

Similarly to flavylium, pyranoflavylium salts exhibit excited state proton transfer (ESPT). When in the excited state by absorption of light, proton transfer reactions of the excited species occur very fast compared to the decay process to the ground state (Figure 1.11). In addition to ESPT, these molecules usually display photoacidity. In other words, while they are weak acids in the ground state (pK_a typically in the range of 4–5), they exhibit a relatively strong photoacidity in the first excited singlet state, with pK^*_a between 0.2-0.7 [56]. However, their photoacidity is significantly less prominent than flavylium cations, and proton loss from the excited acid form is approximately two orders of magnitude slower. Consequently, the excited state life-times of pyranoflavylium singlet states are typically much longer than those of analogous flavylium cations [56–58].

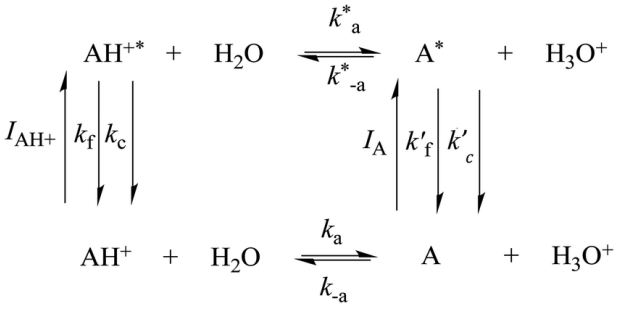


Figure 1.11. General scheme for excited state proton transfer: I_{AH+} is the absorbed light, k_f the fluorescence emission rate constant and k_c the sum of the rate constants of all non-radiative decays for the acid and mutatis mutandis for the base[59].

Freitas *et al.* investigated the effects of substituents on the ground- and excited-state acidity of a series of homologous pyranoflavylium cations [57]. The authors verified that the effects of substituents on the excited-state pK_a* of the pyranoflavylium cations were much more pronounced and systematic than those on the ground-state pK_a. Moreover, electron-donating groups reduce, and electron-withdrawing groups enhance the electronic redistribution in the excited acid, resulting in fast ESPT to water. In addition, the decay rate constants of the excited acid and base forms in the absence of ESPT also increase in a similar and systematic trend as the substituent on the pyranoflavylium chromophore changes from electron-donating to electron-withdrawing one [57].

Interestingly, and opposite to flavylium, pyranoflavylium dyes showed phosphorescence in a rigid TFA-acidified isopropanol glass and formed triplet states in an acidic acetonitrile solution [58]. These behaviors were detectable by nanosecond laser photolysis and quenched by molecular oxygen with the consequent formation of singlet oxygen. The strong visible light absorption, the relatively small singlet-triplet energy differences, the excited state redox potentials, and the reasonably long life times of pyranoflavylium triplet states in the absence of molecular oxygen suggest that they might be used as triplet sensitizers and cationic redox initiators in a polar aprotic solvent [58].

Moreover, theoretical studies were developed to predict photochemical and photophysical properties and, therefore, be a tool for designing new pyranoflavylium chromophores with the desired colors and photophysical properties, as well as for understanding the analogous properties of pyranoanthocyanins of red wine [60–62].

The first pyranoflavylium compounds to be studied as sensitizers for dye solar cells (DSSCs) were pyranoanthocyanins derived from an extract of red wine. More specifically, these pyranoanthocyanins were malvidin-3-*O*-glucoside and cyanidin-3-*O*-glucoside pyruvic acid adducts [63]. In contrast to the authors' expectations, the presence of pyruvic acid adducts decreased the effectiveness of the DSSCs relative to the corresponding anthocyanins. However, it has been shown that the presence of the catechol group in the structure of pigments (cyanidin derivatives) is advantageous for producing DSSCs. Despite their low efficiency (0.006% for Cy-Py and 0.003% for Mv-Py), these natural wine dyes created a new window of possibilities for environmentally friendly dye solar cells [63]. Pinto *et al*. investigated the effect of carboxylic and catechol units in pyranoflavylium structure on the efficiency of DSSCs [64]. They observed that the presence of catechol units clearly increases the efficacy of cells. The best performance was obtained for a symmetrical pyranoflavylium with two catechol units (10-catecholpyrano-5,7,3′,4′-tetrahydroxyflavylium), with an efficiency of 1.15%. Furthermore, the DSSC efficiency based on pyranoflavylium not only depends on the

linker units (carboxylate, catechol) but also on electron-donor groups (methoxy, hydroxyl, methyl), as well as the presence of sugar moieties. 10-methylpyranocyanidin-3-*O*-glucoside showed an improved efficiency of 1.57% [65]. However, higher efficiency was observed for dimethylamino-derived pyranoflavylium dye with 2.34 to 2.55 % [66]. The performance of DSSCs was improved by the stronger donor character of the dialkylamine unit, which participates effectively in the conjugation leading to a more rigid sensitizer chromophore [66].

1.3.4. Biological Properties

The biological properties of pyrano-derivatives have also been studied, with a more considerable emphasis on the pyranoanthocyanins. Antioxidant activity is the most studied, and the values are usually compared to the precursor anthocyanin. The first approach to the antioxidant properties was reported in a study of blueberry extract and two anthocyanin-derived extracts containing anthocyanins and first and second-generation pyranoanthocyanins, respectively [67]. The anthocyanin-derived blueberry extracts revealed a higher antioxidant and antiradical capacity than the original blueberry extract by DPPH and FRAP methods, and the results were corroborated by the *in vitro* lipidic oxidation assay. Furthermore, the extract rich in second-generation pyranoanthocyanins, namely Portisins, showed a higher capacity to inhibit lipid peroxidation of soybean PC liposomes [67]. When Portisins derived from Cy-3-glc (Cy-pt), Dp-3-glc (Dp-pt), and Mv-3-glc (Mv-pt) were tested as isolated compounds by Azevedo *et al*., they generally showed a significant increase of antioxidant capacity than respective anthocyanidins and anthocyanins [68]. The presence of a catechol group (*ortho*-dihydroxyl) in the flavanol moiety and the increase of the hydrophobicity of Portisins seemed to be the main factors for this effect. The increase of the number of hydroxyl groups leads to the extent of conjugation of π-electrons which could stabilize the radical scavenged throughout the whole structure and, consequently, increases the antiradical capacity (results obtained by DPPH) [68]. According to the results of the antioxidation evaluation in soybean PC liposomes, the higher hydrophilic character of Portisins allows them to strategically place themselves at the surface of the liposome membrane system, providing antioxidant protection against lipidic peroxidation [69].
First-generation pyranoanthocyanins, such as Mv-3-glc pyran-derivatives, also exhibited greater radical scavenging ability than the Mv-3-glc (by DPPH assay), mainly the pinotin-A with the catechol group in E ring. Only methylpyrano and oxovitisin derivatives were exceptions to this trend [68,70]. Therefore, the authors might conclude that the changes

that occur to anthocyanins during the age of red wine do not diminish their antioxidant potential [68]. In addition to the most common, rarer pyranoanthocyanins isolated from the staghorn sumac *R. hirta* extract [71], which had previously shown a strong antioxidant activity [72], were studied individually using an *in vitro* model with Caco-2 cells [73]. Among all sumac polyphenols evaluated, the two rare pyranoanthocyanins derived from Cy and Dp with the extra D ring showed the most interesting antioxidant properties for developing functional foods or beverages. Therefore, similar to flavonoids in general, the antioxidant activity of pyranoanthocyanins rises with the number of aromatic hydroxyl groups, especially *ortho*-dihydroxyl groups, in the molecule structure [68,70].

Recently, Correia *et al*. investigated the antioxidant activity of methyl and carboxypyran-derived from Mv and Cy (as well as other features described in the following subsections), focusing on their potential use as skin protectors for cosmeceutical applications [74]. The overproduction of reactive oxygen species (ROS) in the skin cells and, subsequently, oxidative stress is one of the most significant contributors to the age-related decline of the structural integrity and function of the skin. Antioxidants have been incorporated into skin care products as a strategy to delay this process. The antioxidant effect of the referred pyranoanthocyanins was evaluated by *in vitro* model in human skin cell lines: epidermal keratinocytes (HaCat) and dermal fibroblasts (HFF-1). As expected, Cy and related compounds proved a more pronounced influence on the reduction of ROS than Mv-derived structures. Even though Cy-3-glc and 10-carboxypyCy-3-glc had similar and the highest antioxidant efficacy, the authors deemed 10-carboxypyCy-3-glc the most promising molecule to use as a skin protector in cosmetic formulations due to its superior color stability compared to its anthocyanin counterpart [74].

The application of pyranoflavylium compounds in food or biological fields inevitably requires the assessment of their cell viability, such as the cytotoxicity activity. The effect of compounds on cell proliferation is usually investigated when the aim of their application is anticancer therapies. In addition to anthocyanins, which had previously demonstrated antiproliferative activity, Faria *et al*. found in 2010 that a 10-carboxypyranoanthocyanins-rich extract derived from a blueberry extract at noncytotoxic concentrations (<500 μg/ mL) was also able to inhibit cell growth in breast cancer cell lines (MDA-MB-231 and MCF7) via Sulforhodamine B (SRB) and methyl-[^{3}H]-thymidine incorporation methods [75]. Similar to the original blueberry extract, the 10-carboxypyranoanthocyanin-containing extract showed cell invasion inhibition and no inhibition of chemotaxis. Furthermore, this extract was the only one that interfered with the apoptosis pathway in the MCF7 cell line by observation of the increase of caspase-3 activity [75]. In the same year, the antiproliferative effect of isolated Portisins derived

from Cy-3-glc and Dp-3-glc was also studied on breast cancer cells (MCF7) [76]. Both exhibited significant antiproliferative activity, with identical values (about 70%) at the highest concentration tested (100 μM) and using the SRB assay. An opposite effect was observed when these values were compared to those obtained for the corresponding anthocyanins. While Cy-3-glc exhibited no antiproliferative activity at 100 mM, Dp-3-glc had a substantial growth inhibitory effect (about 40 %) and was superior to its respective Portisin at the same concentration. The authors verified that the inhibitory effect on cell proliferation was related to the hydroxylation pattern of ring B in the flavylium structure. They also evaluated the antiproliferation activity of simpler analogous compounds (flavonoids, phenolic acids, and phenols) with catechol and pyrogallol groups and concluded that anthocyanins and derivatives with pyrogallol group were more effective in preventing MCF-7 cell proliferation [76]. Pyrano-derivatives of Mv-3-glc, such as A-type vitisin, 10-methylpyranoantocyanin (Me-py), and 10-oxovitisin, were also studied in terms of antiproliferative capacity in breast cancer MCF-7 cells by the SRB method [77]. Although all compounds have shown the ability to inhibit cell growth, the values were inferior to those obtained for Mv-3-glc. However, 10-oxovitisin was the most effective in inhibiting proliferation among the derivatives. The authors attribute this result to the higher reactivity of the carbonyl group on pyranone, in comparison to the carboxylic acid group on A-type Vitisin and the methyl group on Me-py [77].

Contrary to pyranoanthocyanins, the biological studies of other pyranoflavylium compounds have been poorly documented in the literature. Pan *et al.* studied the cytotoxicity of a mixture of 10-methylpyranoanthocyanidins derived from a blueberry extract in human cervical cancer HeLa cells and their mechanisms [78]. 10-methylpyranoanthocyanidins were produced using acid hydrolysis of blueberry anthocyanins to remove the sugar, giving rise to the anthocyanidins, followed by the reaction with acetone. The blend was composed of 10-methylpyranoanthocyanidins generated mostly from delphinidin, petunidin, and malvidin, with smaller contributions from cyanidin and peonidin. Unlike the previously mentioned studies, the effectiveness of the compounds against cancer was made by evaluating the cellular inhibition for concentrations below the cytotoxicity values. In this case, the authors evaluate the efficacy through the cytotoxicity of the compounds. 10-methylpyranoanthocyanidins showed a cytotoxic effect on the HeLa cells and a dose-dependent decrease in cell viability. Furthermore, its inhibition on HeLa cells was higher than the anthocyanins precursors; however, anthocyanidins had the strongest inhibition [78].

2. pH-indicators for food freshness monitoring

2.1. Food Packaging

"Food safety" and "food waste" are growing concerns in actual society. The World Health Organization (WHO) estimated 600 million cases of illness due to contaminated food supplies, and 420,000 people die every year as they are affected by foodborne contamination [79]. On the other hand, the Food and Agriculture Organization of the United Nations (FAO) estimated that the total food waste for the edible part is around 1.3 billion tons [80]. Food packaging has played a crucial role in maintaining the quality and safety of foods during storage, transportation, and sale. In addition, new packaging systems have been extensively studied to improve food preservation and give information on food quality, increasing food safety across the entire supply chain until the final consumer [81]. Innovation in food packaging systems aims to extend the food shelf-life – active packaging – and provide information on food quality or freshness – intelligent packaging [82].

2.1.1. Intelligent food packaging

The European Union defines intelligent packaging as "materials and articles that monitor the condition of packaged food or the environment surrounding the food" [83]. Its principal purpose is to detect and provide real-time information regarding food quality [82], hence ensuring food safety across the entire supply chain until the final consumer [81]. In addition, intelligent packaging can play an essential role in reducing food waste by replacing static "best before" or "use by" dates with the "dynamic shelf-life" concept, even among products of the same lot [84].

The real-time food control in a package can be made by monitoring the different food quality markers or parameters, such as pH changes, oxygen, temperature, or specific compounds. Particularly, pH changes in the food environment have been described as an effective method of identifying food spoilage [85]. Behind the technologies applied in intelligent packaging, colorimetric pH-indicators are the most studied in research since they provide immediate visual and qualitative (or semi-quantitative) information about the packaged food through a color change [86].

2.2. Food spoilage and pH variations

pH variations during spoilage of animal-origin foodstuffs, namely fish and meat products and their derivatives, are very characteristic. Muscle-based foods are an excellent source of biologically available proteins and essential nutrients; however, they are highly perishable and readily susceptible to spoilage [87]. Their initial physical-chemical properties like pH (5.5 – 6.5), a_w (0.98 – 0.99) values, and chemical composition (proteins, sugar, fat, vitamins, etc.) are favorable parameters to fast post-mortem degradation by endogenous and exogenous microorganisms. The degradation begins when the oxygen of the muscles is depleted, and the anaerobic glycolysis starts, producing organic acids and decreasing the pH. After glycolysis, proteolysis is induced by endogenous enzymes activated by the lower pH. The degradation of protein and nonproteic nitrogen (NPN) molecules produces short-chain peptides, amino acids, and nitrogen-based compounds. These molecules represent an ideal substrate for microorganisms, leading to bacterial growth [88]. The degradation process continues with the predominance of microbial enzyme activity, which leads to the formation of different compounds responsible for off-odors and off-flavor of food spoilage.

Amino acids are decomposed by decarboxylation by decarboxylase enzyme activities, which are mainly of microbial origin, producing amines designed as biogenic amines (BAs). The most relevant BAs found in food are histamine, tyramine, putrescine, cadaverine, *β*-phenylethylamine, agmatine, tryptamine, serotonin, spermidine, and spermine [89]. Trimethylamine-*N*-oxide is an NPN molecule present in muscles, mainly in fishes, which is demethylated to dimethylamine (DMA) by endogenous enzymes and reduced to trimethylamine (TMA) by bacterial enzymes. Other NPN compounds, such as urea (i.e., present in elasmobranchs blood of fishes), are decomposed to ammonia (NH_3). These compounds are responsible for strong ammonia-like off-odors in spoiled food [88]. The set of these compounds is called total volatile basic-nitrogen (TVB-N) and describes the sum of primary, secondary, and tertiary volatile amines found in animal muscle that shows toxicity at a certain level in food.

The quality of perishable food and the spoilage process is influenced by numerous factors that can be divided into three groups: raw materials (composition, pH, ion strength, etc.), microorganisms (endogenous and exogenous microflora), and processing and storage conditions (fresh, cured, fermented, refrigerated, modified atmosphere, etc.). Volatile basic nitrogen compounds are naturally formed in live animals (as also in humans) in the gut and other organs, and they are used for vital functions or transported for storage in the muscle. Therefore, the TVB-N content post-mortem is also

influenced by TVB-N content in muscles in live animals [90]. In turn, its accumulation in the muscles depends on several factors, such as the specie type and the intake of precursors in the diet [87]. Furthermore, endogenous and exogenous microflora also has great variations. For example, the fish microflora depends on many factors, such as the environment in which the animal lives, the fishing season and the water temperature, the method of capture, the handling on the ship, and the technological and sale processes [88].

TVB-N is often applied as a biomarker for muscle foods' freshness and safety and to determine suitability for human consumption [87]. The limit values depend on the animal and species type. The European Community Regulation No 2074/2005/Annex II provided guidelines for the freshness of unprocessed fishery products depending on the fish species and final use [91]. Specifically, a threshold of 25 mg N/100 g muscle for Sebastes spp, 30 mg N/100 g muscle for members of the Pleuronectidae family (except for Hippoglossusspp.), and 35 mg N/100 g muscle for Salmo salar, and members of the Merlucciidae and Gadidae families. Several studies reported different limit values for meat depending of their animal origin. For example, a threshold of 29 mg N/100 g muscle for chicken and 42 mg N/100 g muscle for beef[92].

Summing up, the basic character of these N-based compounds leads to a pH increase in the product. Besides that, since they are volatile, they can accumulate in the inner packaged atmosphere and be detected by monitoring the pH inside the packaging.

2.3. pH-indicators for food freshness monitoring

A colorimetric freshness indicator can be defined as a material placed in the package and ideally should change its color according to the different stages of the food's freshness (i.e., super fresh, fresh, and spoiled) during storage. In a colorimetric pH-indicator, color is correlated to a specific pH value (or to a small pH range), which is directly related to the product's freshness. The color variation between the different freshness stages should be very noticeable to avoid ambiguity regarding the product's condition. Indicator components should be non-hazardous compounds, mainly due to the possibility of leaching into the food product during storage. The indicator should also be resistant and stable to environmental conditions (light, moisture, temperature, and oxygen) in order to maintain its integrity and desirable functional condition throughout the product's life-time [93]. Furthermore, for successful application in the food industry, the development of an indicator must meet some criteria that include: (i) a suitable performance that allows a sensitive and fast monitoring of alterations in the selected

substances and a good correlation between the detected changes and the quality of the food product; (ii) an easy implementation in the food industry driven by low prices and the need of simple technology for their inclusion in the packaging material and; (iii) a simple reading and interpretation by consumers [94].

Generally, a pH-indicator comprises a pH-responsive dye and a solid support [95]. The dye can be immobilized by physical adsorption on a solid support, covalently bonded to a support, or physically entrapped into a polymeric matrix [96].

Firstly, colorimetric pH-indicators were developed with synthetic dyes such as methyl red, cresol red, bromocresol green, bromocresol purple, chlorophenol, bromine thymol blue, and xylenol. However, most synthetic dyes are toxic, leading to unsafe indicators [93]. Therefore, synthetic dyes have been substituted by natural pH-sensitive dyes, such as anthocyanins, curcumin, alizarin, and betalains, owing to their inherent low toxicity, availability, and low environmental impacts [84,97,98]. Among these pigments, anthocyanins are the most widely studied ones [94,99–102] due to their color change from red to blue with pH increases and valuable features such as antimicrobial and antioxidant activities.

The most common technique for immobilizing a dye on support is physical entrapment in a polymeric matrix. The polymer should compromise some characteristics: (1) no/low toxicity to human health; (2) structurally and chemically compatible with dye to provide its uniform diffusion; (3) film-forming property; (4) adequate barrier properties; (5) relatively low water sensitivity[84,98].

In contrast to food packaging materials, which must be very resistant (e.g., high barrier properties and mechanical resistance) since their primary function is to protect the food, indicator materials must comprehend other physical properties. For example, the polymeric matrix of a pH-indicator must be semi-permeable to water to promote the penetration of H^+ and OH^- ions present in water droplets in the packaging atmosphere. High water permeability increases the contact surface area between dye and ions and volatile compounds, increasing the efficacy of the indicator. In addition, the matrix should be hydrophobic to prevent the disintegration of the film in contact with water and to avoid pigment leaching.

Polymeric matrices are usually made from biopolymers since synthetic polymers, namely petroleum-derived polymers, raise global concerns due to the associated environmental problems. Biopolymers are natural polymers from plant and animal sources, which are non-toxic, biocompatible, biodegradable, and with film-forming properties, making them suitable for intelligent packaging development. Besides, many valuable biopolymers can be obtained from agricultural and industrial by-products, an added benefit to the zero-

waste principle. Among several biopolymers, polysaccharide-based biopolymers are the most widely studied ones due to their excellent film formability, and suitable structure as solid support materials for dye immobilization in which chitosan, starch, agar, carrageenan, pectin, and cellulose derivatives are polysaccharide-based biopolymers have been commonly used for blending with pH-indicators [84][97]. Particularly, cellulose and its derivatives are gaining attention in the food packaging industry [103].

2.3.1. Cellulose acetate films as a solid support for pH-indicators

Cellulose is the most abundant polysaccharide in nature, mainly derived from various plants and microorganisms, divided into plant cellulose and bacterial cellulose [98]. Cellulose is composed of thousands of repeating D-glucose units linked by *β*-1,4 glycosidic bonds, characterized by its hydrophilicity and chemically modifying capacity [104]. Cellulose and its derivatives exhibit remarkable biocompatibility, biodegradability, and environmental sustainability. In terms of physical properties, they have mechanical and thermal resistance, water absorbance, porosity, and the ability to carry antioxidant and antibacterial agents; moreover, they are low-cost materials. The cellulose derivatives include several esters and ethers, such as cellulose acetate, carboxymethyl cellulose, methylcellulose, ethyl cellulose, cellulose nitrate, cellulose sulfate, hydroxyethyl cellulose, hydroxypropyl cellulose, and hydroxypropyl methylcellulose[103].

In this work, cellulose acetate (CA) was chosen as solid support for dye immobilization. CA is an ester present in green plant cell walls and can be synthesized by the reaction of cellulose with acetic anhydride and acetic acid in the presence of sulfuric acid (Figure 2.1). CA is soluble in acetone, dioxane, methyl acetate, and acetic acid; however, it is insoluble in water. The degree of substitution plays a crucial role in its solubility and biodegradability. It presents a relatively low cost, is nontoxic, heat resistant, shows excellent film-forming properties, and has high chemical and mechanical stability [103][104]. Previous studies already showed that CA-based films have promising properties for food packaging applications [105–111].

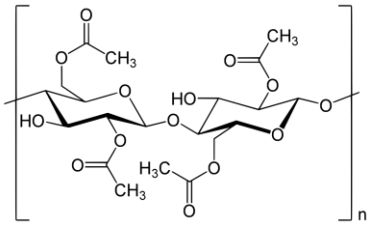


Figure 2.1. General structure of biopolymer cellulose acetate (CA).

Beyond the polymer matrix, which can be made up of one or a mixture of biopolymers, other compounds can be added to the formulation to improve the properties of the indicator film. Generally, plasticizers are low molecular weight and non-volatile molecules usually added to the film's formulation to improve its physical properties, such as flexibility, workability, distensibility, or water vapor permeability (WVP) [112,113]. Among the plasticizers, glycerol (Gly) is one of the most studied biodegradable compounds (Figure 2.2.) [112]. Although using glycerol as a plasticizer for CA-based films is not very commonly found in the literature, some recent works have studied its incorporation in the formulation [114–117].

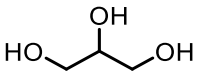


Figure 2.2. Structure of glycerol widely used as a plasticizer.

2.3.2. Film production, characterization, and test as pH-indicator

Indicator films can be obtained through various methods, such as solvent casting, extrusion, electrospinning, and layer-by-layer (LbL) assembly, with the last two techniques being the most innovative. For example, electrospinning produces films with enhanced surface area, high porosity, small pore size, and high absorbance capacity, which make films with a higher potential to be applied as pH-sensitive indicators [103]. However, solvent casting is the technique most used in developing pH-sensitive films due to its simplicity and low costs (Figure 2.3). In this method, polymer/s and pH-sensitive dye (and plasticizer, if necessary) are blended in a solution and cast in a plate for further drying [95]. In the case of CA films, the formulation is usually blended using an acetone solution.

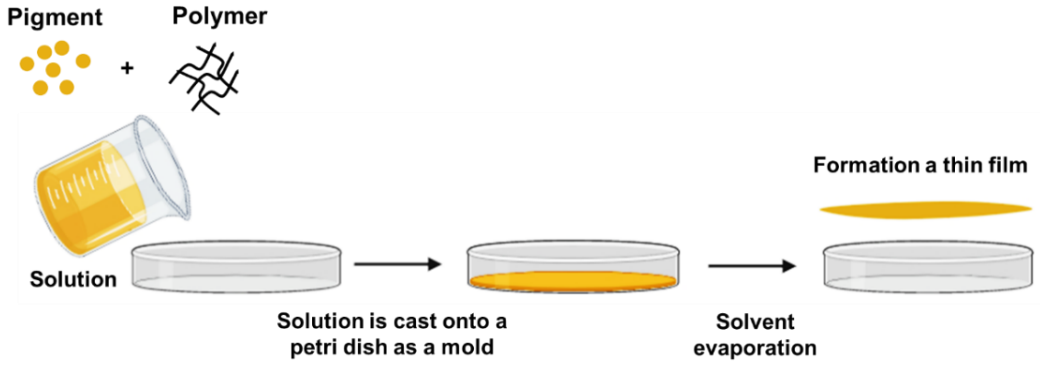


Figure 2.3. Solvent casting methodology for film formation.

After obtaining the films and before testing their performance as pH-indicator, they are subjected to various characterization techniques. Generally, film indicators are characterized in terms of structure and physical properties. Thickness, color, water solubility, moisture content, thermal, barrier, and mechanical properties are the most physical properties studied [98]. Thermal properties, namely, decomposition temperature and glass transition temperature (Tg) of films, are achieved by differential scanning calorimetry (DSC) and thermogravimetric analysis (TGA) [98]. Water vapor permeability (WVP), oxygen permeability (OP), and opacity (or transparency) are determined to obtain information on barrier properties. The mechanical properties of pH-responsive indicator films include tensile properties: tensile strength (TS), Young's modulus (YM), and elongation at break (EB) [98]. In addition, these techniques are crucial to understanding small variations in the film's final formulation (e.g., different pigment concentrations). Structural characterization can provide information on the arrangement of different film components and allow a better understanding of the films' physical properties. The structure of the films depends on the compatibility, miscibility, and intermolecular interactions between different film components, which directly affects their mechanical and barrier properties. Morphological and structural characterization can be may through scanning electron microscopy (SEM) of surface and cross-section, atomic force microscopy (AFM), Fourier transform infrared (FT-IR), and X-ray diffractometer [118].

The indicator performance concerning pH changes is usually first tested in buffer solutions at different pH values. Most of the works show the color variation of the film in pH solutions from 1 to 12. However, this pH range is too broad and useless to study food freshness stages. A significant color variation between 5 to 7 is required for a successful pH-indicator for freshness monitoring of perishable foods such as meat and fish. Other works tested a color response of the indicator to volatile ammonia. Nevertheless, a volatile ammonia-rich atmosphere may be an extreme and unrealistic condition for food spoilage simulation.

Finally, pH-indicator films are tested on real samples by submitting them to monitor the freshness of mainly protein-rich food products, such as fish, shrimp, chicken, pork, milk, and cheese [118]. On real samples assays, pH-indicators and food samples are usually placed in improvised and home-made packages. So far, none of the studies has shown to test the pH-indicators in more realistic retail conditions, such as, for example, in a modified atmosphere packaging (MAP). Also, the temperature conditions studied are around 3 and 25 ºC; however, using 25 ºC is incorrect since it does not represent the reality for such perishable products. Other degradation processes may occur at this

temperature, interfering with spoilage detection. Color variations of the pH-indicator should be correlated with the food sample's pH, TVB-N content, and microbiological profile.

2.4. Anthocyanin-based indicators

As already mentioned in section 2.3, and due to the interesting pH-sensitive color properties described in the first part of the introduction, ANCs have been widely studied as colorimetric indicators for application in intelligent food packaging [119–127]. Furthermore, as widely distributed in nature, ANCs are easy to obtain, making them inexpensive and good candidates for creating pH-indicators. Furthermore, ANCs are not related to toxicity issues, and according to the last re-evaluation of the Scientific Panel on Food Additives and Nutrient Sources Added to Food of the European Food Safety Authority, they have been considered unlikely to be a security concern (mainly the ones from grape skin extracts and black currants) [94,128].

ANCs are composed of aglycone moiety – anthocyanidin – and glycoside moiety. The most common ANCs are cyanidin, pelargonidin, peonidin, delphinidin, malvidin, and petunidin. The glycosylation of anthocyanidins as 3-glycosides or 3,5-diglycosides is the most common. Since the discovery of the first ANC, more than 700 related chemical structures have been identified in nature with different glycosylation and acylation patterns [1].

For the development of ANC-based indicators, ANCs are obtained from plant extracts. Although some extracts have been purified, the material used never consisted of pure-form ANCs. Instead, the material used is an ANC-rich extract containing different ANCs and other compounds. Extracts from different plants have different ANC profiles, which greatly influence extracts' functional and physical properties. Consequently, selecting the source of ANCs plays an essential role in the effectiveness of the pH-indicator. Determinant factors in choosing the plant source are the color variation of the extract and the content of chemically more stable ANCs. For example, acylated ANCs exhibit higher color stability when compared with non-acylated ones due to the intramolecular copigmentation effect. In addition, they have higher resistance to degradation and display an extension of the pH domain of the flavylium cation and a stabilization of the purple and blue colors at higher pH values [1]. Thus, red cabbage, purple sweet potato, and black carrot are extensively used as sources of ANCs because of their high contents of acylated ANCs [94]. Traditional sources of ANCs, such as blackberries and grapes,

are also being used as well as other more uncommon sources such as black soybean seed coat extracts, purple and black eggplant peels, or jambolan fruits [129].

2.4.1. Problems related to ANCs pH-indicators

Developing functional ANC-based freshness indicators is a very challenging process, where ANC extract should be compatible with the polymer and able to respond to the freshness alterations suffered by the food product during its storage and distribution. Additionally, color changes must be unequivocal and easily readable by the consumers/retailers and should always be related to quality changes in the packaged food product.

The main drawbacks of ANCs and, in general, of natural pigments are their instability in other environmental conditions, such as light and temperature. Even though they display an interesting color change from red to blue with pH increasing, ANCs have a complex multistate equilibrium that leads to color fading over time, mainly in neutral to basic pH values [2,130,131]. ANC's instability and color fading limit their use in the food industry [97].

The number of works published about ANCs applications as pH-indicators for food freshness monitoring is extensive in the literature. Although some works have shown their high potential, they only described issues related to 1) color variation of the extract in solution, 2) color variation of the film indicator in solution, 3) transparency or low-intensity colors of the indicator, and 4) conditions of trials with real samples.

Problems with the extract selected regarding color variation in the relevant pH range for food spoilage (pH ≈ 4.5 to 7.5) are common. Several studies used extracts with an attractive color change in the solution across a wide pH range (pH from 1 to 12); however, the color variation within the relevant pH range is barely noticeable [110,132,133]. For example, a red cabbage extract used to build a CA-based indicator changed color from pink to blue to green to yellow as the pH of the solution increased, as shown in Figure 2.4a [110]. However, there was practically no color difference between pH 5 and 8. In addition, the film indicator was tested for the visual detection of volatile ammonia and its reversibility with volatile acetic acid instead of the response to different and controlled pH solutions. Figure 2.4b demonstrates that ANC-based film is sensitive to those compounds, and its color is reversible. Nevertheless, the atmosphere generated by volatile ammonia and acid acetic represents extreme conditions that do not correspond to the reality of food spoilage [110].

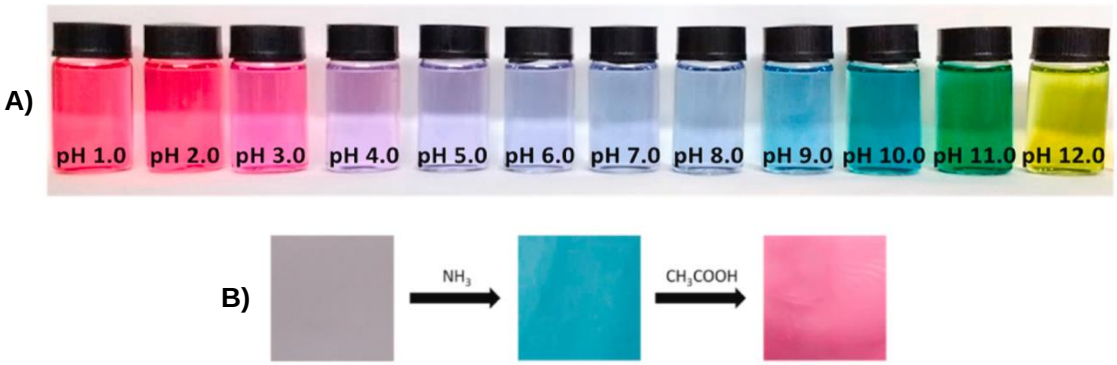


Figure 2.4. A) Color variation of a red cabbage extract in pH solutions between 1 and 12. B) Color response of the indicator based on purple sweet potato extract and cellulose acetate to volatile ammonia and its reversibility to volatile acetic acid. Adapted from [110].

Other works showed extracts with remarkable color variation in solutions at relevant pH values; however, when the indicator is immersed in a solution with a variable pH, the color change is not coincident. Therefore, the indicator may lose the interesting color variation of the extract. Choi *et al*. reported the color variation of an extract from a purple sweet potato, which changed from pink to purple to blue between pH 5 and 8 (Figure 2.5a) [134]. The extract was immobilized in agar, giving rise to the indicator film. When the film was exposed to different pH solutions, the color practically did not change between pH 5 and 7 (Figure 2.5b). Furthermore, indicator colors at different pH values lost chromaticity compared to extract color in solution, becoming more grayish. Authors attributed the color intensity decrease from pH 5 to 6 to hydration of the flavylium cation, which gives rise to the colorless hemiketal and yellow chalcones. However, this decrease is not pronounced in color variations of the extract in solution, and the authors did not discuss the differences between the indicator and the extract [134]. A low concentration of the extract in the film or some interactions with the polymer may lead to color fading. The intermolecular interactions between ANCs and biopolymers can restrict the structural changes of ANCs [118].



B)

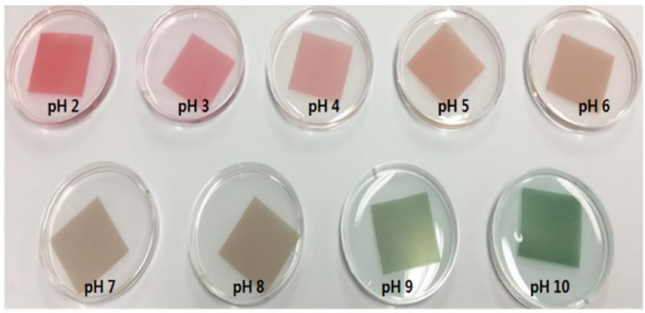


Figure 2.5. A) Color variation of an extract from a purple sweet potato in pH solutions between 2 and 10. B) Color variation of the indicator based on purple sweet potato extract and agar in pH solutions between 2 and 10. Adapted from [134].

Other authors tried to produce a multifunctional material to act simultaneously as a protecting material for packaging and to monitor food spoilage during storage (indicator material) [135,136]. Since packaging and indicator materials must have different properties, putting both functionalities together is a big challenge. While packaging materials must be impermeable to water and other gases to protect foods, pH-indicators' effectiveness is enhanced by permeability or semi-permeability. In addition, transparency is an essential feature of packaging since it influences consumers' acceptance of food products. However, transparency in indicator films becomes a disadvantage since it leads to barely perceptible colors. Figure 2.6 shows the performance of an indicator based on ANCs from petals in a chitosan nanofiber/methyl cellulose matrix [135]. The indicator is almost invisible inside the packaging used in the experiment. The authors refer to a color variation from violet (fresh product) to grey/green (spoilage product). However, no color variation of the indicator is observed [135].

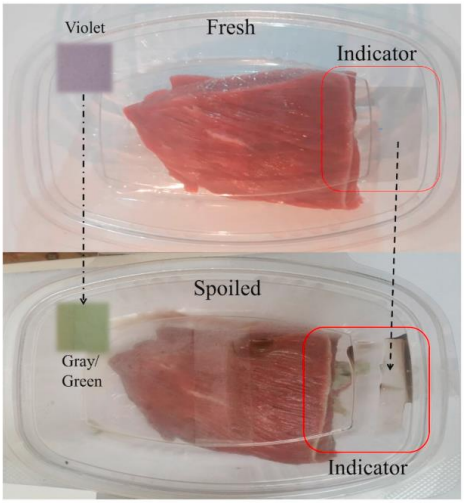


Figure 2.6. pH-indicator based on petal ANCs in a chitosan nanofiber/methyl cellulose matrix tested in the freshness of lamb meat. Adapted from [135].

Another typical problem is the experimental setup in real samples. For example, an indicator based on black carrot ANCs and bacterial cellulose nanofibers exhibit a remarkable color change during fish (rainbow trout (B) and common carp (C)) spoilage (Figure 2.7); however, the spoilage monitoring is done for 15 days at 5-day intervals. [124].

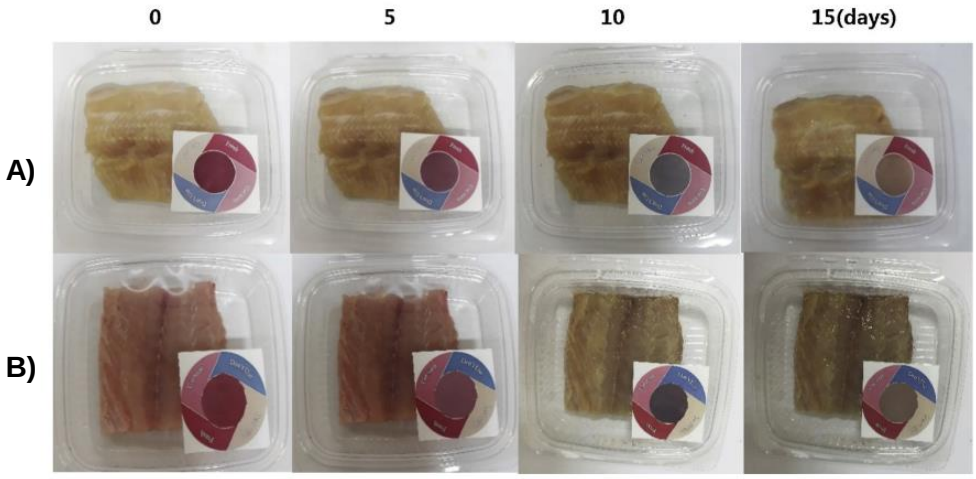


Figure 2.7. pH-indicator based on black carrot anthocyanins and bacterial cellulose nanofibers tested in the freshness of rainbow trout (B) and common carp (C) fillets. Adapted from [124]

A crucial feature of a colorimetric pH-indicator is detecting the exact moment the product becomes unsafe for human consumption. For that, daily monitoring is required, and the experimental time must be adequate for each sample type. Unfortunately, the shelf-life of fish products without MAP is not superior to 8 days, which makes the experimental time setup of 15 days inadequate for fish freshness monitoring.

3. Project Purpose

The main goal of this project was the rationale design and synthesis of new pyranoflavylium-based dyes with remarkable pH-responsive optical properties towards developing a smart label for food freshness monitoring. The incorporation of food freshness indicators in food packaging will allow real-time control of food quality, ensuring food safety across the entire supply chain until the final consumer. In addition, replacing the static expiration dates with a dynamic labeling system will greatly contribute to food waste reduction. Regarding this, the objective of this work meets 2 of the 17 goals of the 2030 Agenda for Sustainable Development, namely, goal 2 - End hunger, achieve food security and improved nutrition and promote sustainable agriculture, and goal 12 - Ensure sustainable consumption and production patterns.

Despite not being an entirely new concept, since several works have been published about this type of technology, its transition to the industry has not been successful so far. On the one hand, using efficient but synthetic pigments makes their application unfeasible due to the cytotoxicity problems associated with pigments. On the other hand, using natural pigments such as anthocyanins solves the cytotoxicity problems; however, these are associated with stability problems over time, which is also a limitation for this kind of application. Hereupon, a possible solution involves the development of anthocyanin-inspired derivatives with improved properties in terms of chemical stability and color variation, among others. Thus, the specific aims of this project involved the following steps:

a) Design and synthesis of new pyranoflavylium-based compounds and structural characterization;

b) Determination of chemical equilibria as a function of pH. Modulation or tuning their equilibrium constants by structural modifications or interaction with micellar systems;

c) Evaluation of the cytotoxicity of the new compounds obtained;

d) Building cellulose acetate-based films (smart label) containing the most promising pyranoflavylium pH-responsive dye by solvent casting method.

e) Physico-chemical characterization of the smart label and validation of the chromatic performance in simulated spoilage conditions and in real food samples.

References

[1] Cruz L, Basílio N, Mateus N, de Freitas V, Pina F. Natural and Synthetic Flavylium-Based Dyes: The Chemistry Behind the Color. Chem Rev 2022;122:1416–81. https://doi.org/10.1021/acs.chemrev.1c00399.

[2] Pina F, Melo MJ, Laia C a. T, Parola a. J, Lima JC. Chemistry and applications of flavylium compounds: a handful of colours. Chem Soc Rev 2012;41:869. https://doi.org/10.1039/c1cs15126f.

[3] Oliveira J, Mateus N, De Freitas V. Wine-Inspired Chemistry: Anthocyanin Transformations for a Portfolio of Natural Colors. Synlett 2017;28:898–906. https://doi.org/10.1055/s-0036-1589937.

[4] Pina F, Oliveira J, De Freitas V. Anthocyanins and derivatives are more than flavylium cations. Tetrahedron 2015;71:3107–14. https://doi.org/10.1016/j.tet.2014.09.051.

[5] Brockmann H, Haase R. Über Dracorubin, den roten Farbstoff des „Drachenblutes" (I. Mitteil.). Berichte Der Dtsch Chem Gesellschaft (A B Ser 1936;69:1950–4. https://doi.org/10.1002/cber.19360690828.

[6] Brockmann H, Haase R. Über das Dracorubin (II. Mitteil.). Berichte Der Dtsch Chem Gesellschaft (A B Ser 1937;70:1733–8. https://doi.org/10.1002/cber.19370700818.

[7] Collins (née Jones) DA, Haworth F, Isarasena K, Robertson A. The pigments of "dragon's blood" resin. Part I. Dracorubin. J Chem Soc 1950:1876–81. https://doi.org/10.1039/JR9500001876.

[8] Agbakwuru EOP, Whalley WB. The pigments of 'dragon's blood' resin. Part VIII. Synthesis of (±)-dracorubin and of (±)-nordracorubin. J Chem Soc, Perkin Trans 1 1976:1392–4. https://doi.org/10.1039/P19760001392.

[9] Cameira-dos-Santos P, Brillouet J, Cheynier V, Moutounet M. Detection and Partial Characterisation of New AnthocyaninDerived Pigments in Wine. J Sci Food Agric 1996;70:204–8. https://doi.org/10.1002/(SICI)1097-0010(199602)70:2<204::AID-JSFA484>3.3.CO;2-6.

[10] Fulcrand H, dos Santos P-JC, Sarni-Manchado P, Cheynier V, Favre-Bonvin J. Structure of new anthocyanin-derived wine pigments. J Chem Soc Perkin Trans 1 1996;69:735. https://doi.org/10.1039/p19960000735.

[11] Bakker J, Timberlake CF. Isolation, Identification, and Characterization of New Color-Stable Anthocyanins Occurring in Some Red Wines. J Agric Food Chem 1997;45:35–43. https://doi.org/10.1021/jf960252c.

[12] Fulcrand H, Benabdeljalil C, Rigaud J, Cheynier V, Moutounet M. A new class of wine pigments generated by reaction between pyruvic acid and grape anthocyanins. Phytochemistry 1998;47:1401–7. https://doi.org/10.1016/S0031-9422(97)00772-3.

[13] Jingren HE, Santos-Buelga C, Silva AMS, Mateus N, De Freitas V. Isolation and structural characterization of new anthocyanin-derived yellow pigments in aged red wines. J Agric Food Chem 2006;54:9598–603. https://doi.org/10.1021/jf062325q.

[14] Gómez-Alonso S, Blanco-Vega D, Gómez MV, Hermosín-Gutiérrez I. Synthesis, isolation, structure elucidation, and color properties of 10-Acetyl-pyranoanthocyanins. J Agric Food Chem 2012;60:12210–23. https://doi.org/10.1021/jf303854u.

[15] Araújo P, Fernandes A, De Freitas V, Oliveira J. A new chemical pathway yielding A-type vitisins in red wines. Int J Mol Sci 2017;18. https://doi.org/10.3390/ijms18040762.

[16] Hayasaka Y, Asenstorfer RE. Screening for Potential Pigments Derived from Anthocyanins in Red Wine Using Nanoelectrospray Tandem Mass Spectrometry. J Agric Food Chem 2002;50:756–61. https://doi.org/10.1021/jf010943v.

[17] Schwarz M, Wabnitz TC, Winterhalter P. Pathway Leading to the Formation of Anthocyanin−Vinylphenol Adducts and Related Pigments in Red Wines. J Agric Food Chem 2003;51:3682–7. https://doi.org/10.1021/jf0340963.

[18] Håkansson AE, Pardon K, Hayasaka Y, De Sa M, Herderich M. Structures and colour properties of new red wine pigments. Tetrahedron Lett 2003;44:4887–91. https://doi.org/10.1016/S0040-4039(03)01090-6.

[19] Lu Y, Foo L, Sun Y. New pyranoanthocyanins from blackcurrant seeds. Tetrahedron Lett 2002;43:7341–4. https://doi.org/10.1016/S0040-4039(02)01721-5.

[20] Rentzsch M, Schwarz M, Winterhalter P, Hermosín-Gutiérrez I. Formation of hydroxyphenyl-pyranoanthocyanins in Grenache wines: Precursor levels and evolution during aging. J Agric Food Chem 2007;55:4883–8. https://doi.org/10.1021/jf0702491.

[21] Mateus N, Silva AMS, Santos-Buelga C, Rivas-Gonzalo JC, de Freitas V. Identification of Anthocyanin-Flavanol Pigments in Red Wines by NMR and Mass Spectrometry. J Agric Food Chem 2002;50:2110–6. https://doi.org/10.1021/jf0111561.

[22] Oliveira J, Azevedo J, Silva AMS, Teixeira N, Cruz L, Mateus N, et al. Pyranoanthocyanin dimers: A new family of turquoise blue anthocyanin-derived pigments found in port wine. J Agric Food Chem 2010;58:5154–9. https://doi.org/10.1021/jf9044414.

[23] Mateus N, Silva AMS, Rivas-Gonzalo JC, Santos-Buelga C, de Freitas V. A New Class of Blue Anthocyanin-Derived Pigments Isolated from Red Wines. J Agric Food Chem 2003;51:1919–23. https://doi.org/10.1021/jf020943a.

[24] Mateus N, Oliveira J, Santos-Buelga C, Silva AMS, De Freitas V. NMR structure characterization of a new vinylpyranoanthocyanin-catechin pigment (a portisin). Tetrahedron Lett 2004;45:3455–7. https://doi.org/10.1016/j.tetlet.2004.03.007.

[25] Mateus N, Oliveira J, González-Paramás AM, Santos-Buelga C, De Freitas V. Screening of portisins (vinylpyranoanthocyanin pigments) in Port wine by LC/DAD-MS. Food Sci Technol Int 2005;11:353–8. https://doi.org/10.1177/1082013205057940.

[26] Mateus N, Oliveira J, Pissarra J, González-Paramás AM, Rivas-Gonzalo JC, Santos-Buelga C, et al. A new vinylpyranoanthocyanin pigment occurring in aged red wine. Food Chem 2006;97:689–95. https://doi.org/10.1016/j.foodchem.2005.05.051.

[27] Oliveira J, De Freitas V, Silva AMS, Mateus N. Reaction between hydroxycinnamic acids and anthocyanin-pyruvic acid adducts yielding new portisins. J Agric Food Chem 2007;55:6349–56. https://doi.org/10.1021/jf070968f.

[28] Nave F, Teixeira N, Mateus N, de Freitas V. Hemisynthesis and structural characterization of flavanol-(4,8)-vitisins by mass spectrometry. Rapid Commun Mass Spectrom 2010;24:1964–70. https://doi.org/10.1002/rcm.4599.

[29] Rein MJ, Ollilainen V, Vahermo M, Yli-Kauhaluoma J, Heinonen M. Identification of novel pyranoanthocyanins in berry juices. Eur Food Res Technol 2005;220:239–44. https://doi.org/10.1007/s00217-004-1063-6.

[30] Fossen T, Andersen ØM. Anthocyanins from red onion, Allium cepa, with novel aglycone. Phytochemistry 2003;62:1217–20. https://doi.org/10.1016/S0031-9422(02)00746-X.

[31] Andersen ØM, Fossen T, Torskangerpoll K, Fossen A, Hauge U. Anthocyanin from strawberry (Fragaria ananassa) with the novel aglycone, 5-carboxypyranopelargonidin. Phytochemistry 2004;65:405–10. https://doi.org/10.1016/j.phytochem.2003.10.014.

[32] Fukui Y, Kusumi T, Masuda K, Iwashita T, Nomoto K. Structure of rosacyanin B, a novel pigment from the petals of Rosa hybrida. Tetrahedron Lett 2002;43:2637–9. https://doi.org/10.1016/S0040-4039(02)00305-2.

[33] Khalil A, Baltenweck-Guyot R, Ocampo-Torres R, Albrecht P. A novel symmetrical pyrano-3-deoxyanthocyanidin from a Sorghum species. Phytochem Lett 2010;3:93–5. https://doi.org/10.1016/j.phytol.2010.02.003.

[34] Bai Y, Findlay B, Sanchez Maldonado AF, Schieber A, Vederas JC, Gänzle MG. Novel pyrano and vinylphenol adducts of Deoxyanthocyanidins in sorghum sourdough. J Agric Food Chem 2014;62:11536–46. https://doi.org/10.1021/jf503330b.

[35] Lu Y, Sun Y, Foo LY. Novel pyranoanthocyanins from black currant seed. Tetrahedron Lett 2000;41:5975–8. https://doi.org/10.1016/S0040-4039(00)00954-0.

[36] Lu Y, Foo LY. Unusual anthocyanin reaction with acetone leading to pyranoanthocyanin formation. Tetrahedron Lett 2001;42:1371–3.

[37] Chassaing S, Isorez-Mahler G, Kueny-Stotz M, Brouillard R. Aged red wine pigments as a source of inspiration for organic synthesis - The cases of the color-stable pyranoflavylium and flavylium-(4???8)-flavan chromophores. Tetrahedron 2015;71:3066–78. https://doi.org/10.1016/j.tet.2014.10.058.

[38] Oliveira J, de Freitas V, Mateus N. A novel synthetic pathway to vitisin B compounds. Tetrahedron Lett 2009;50:3933–5. https://doi.org/10.1016/j.tetlet.2009.04.072.

[39] Miyagusuku-Cruzado G, Voss DM, Giusti MM. Influence of the Anthocyanin and Cofactor Structure on the Formation Efficiency of Naturally Derived Pyranoanthocyanins. Int J Mol Sci 2021;22:6708. https://doi.org/10.3390/ijms22136708.

[40] Farr JE, Sigurdson GT, Giusti MM. Influence of cyanidin glycosylation patterns on carboxypyranoanthocyanin formation. Food Chem 2018;259:261–9. https://doi.org/10.1016/j.foodchem.2018.03.117.

[41] Roehri-Stoeckel C, Gonzalez E, Fougerousse A, Brouillard R. Synthetic dyes: simple and original ways to 4-substituted flavylium salts and their corresponding vitisin derivatives. Can J Chem 2001;79:1173–8. https://doi.org/10.1139/v01-089.

[42] Chassaing S, Isorez G, Kueny-Stotz M, Brouillard R. En route to color-stable pyranoflavylium pigments-a systematic study of the reaction between 5-hydroxy-4-methylflavylium salts and aldehydes. Tetrahedron Lett 2008;49:6999–7004. https://doi.org/10.1016/j.tetlet.2008.09.139.

[43] da Silva CP, Pioli RM, Liu L, Zheng S, Zhang M, Silva GTDM, et al. Improved Synthesis of Analogues of Red Wine Pyranoanthocyanin Pigments. ACS Omega 2018;3:954–60. https://doi.org/10.1021/acsomega.7b01955.

[44] Oliveira J, Mateus N, Freitas V De. Synthesis of a new bluish pigment from the reaction of a methylpyranoanthocyanin with sinapaldehyde. Tetrahedron Lett 2011;52:1996–2000. https://doi.org/10.1016/j.tetlet.2011.02.079.

[45] Oliveira J, Araújo P, Fernandes A, Mateus N, de Freitas V. Synthesis and Structural Characterization of Amino-Based Pyranoanthocyanins with Extended Electronic Delocalization. Synlett 2016;27:2459–62. https://doi.org/10.1055/s-0035-1562471.

[46] Oliveira J, Fernandes A, De Freitas V. Synthesis and structural characterization by LC-MS and NMR of a new semi-natural blue amino-based pyranoanthocyanin compound. Tetrahedron Lett 2016;57:1277–81. https://doi.org/10.1016/j.tetlet.2016.02.026.

[47] Carvalho ARF, Oliveira J, Freitas V de, Mateus N, Melo A. A theoretical interpretation of the color of two classes of pyranoanthocyanins. J Mol Struct THEOCHEM 2010;948:61–4. https://doi.org/10.1016/j.theochem.2010.02.020.

[48] He J, Carvalho ARF, Mateus N, De Freitas V. Spectral features and stability of oligomeric pyranoanthocyanin-flavanol pigments isolated from red wines. J Agric Food Chem 2010;58:9249–58. https://doi.org/10.1021/jf102085e.

[49] Lima JC, Abreu I, Brouillard R, Mac L. Kinetics of ultra-fast excited state proton transfer from 7-hydroxy-4-methylflavylium chloride to water. Chem Phys Lett 1998;298:189–95.

[50] Oliveira J, Araújo P, Fernandes A, Pina F, Freitas V De. Influence of the structural features of amino-based pyranoanthocyanins on their acid-base equilibria in aqueous solutions. Dye Pigment 2017;141:479–86. https://doi.org/10.1016/j.dyepig.2017.03.005.

[51] Gomes V, Mateus N, Freitas V, Cruz L. Synthesis and Structural Characterization of a Novel Symmetrical 2,10-Bis-Styryl-1-Benzopyrylium Dye. Synlett 2018;29:1390–4. https://doi.org/10.1055/s-0036-1591978.

[52] Cruz L, Sousa JLC, Marinho A, Mateus N, de Freitas V. Synthesis and structural characterization of novel pyranoluteolinidin dyes. Tetrahedron Lett 2017;58:159–62. https://doi.org/10.1016/j.tetlet.2016.11.123.

[53] Araújo P, Basílio N, Azevedo J, Fernandes A, Mateus N, Pina F, et al. Colour modulation of blue anthocyanin-derivatives. Lignosulfonates as a tool to improve the water solubility of natural blue dyes. Dye Pigment 2018;153:150–9. https://doi.org/10.1016/j.dyepig.2018.02.019.

[54] Araújo P, Costa A, Fernandes I, Mateus N, de Freitas V, Sarmento B, et al.

Stabilization of bluish pyranoanthocyanin pigments in aqueous systems using lignin nanoparticles. Dye Pigment 2019;166:367–74. https://doi.org/10.1016/j.dyepig.2019.03.020.

[55] Cruz L, Correa J, Mateus N, De Freitas V, Tawara MH, Fernandez-Megia E. Dendrimers as Color-Stabilizers of Pyranoanthocyanins: The Dye Concentration Governs the Host-Guest Interaction Mechanisms. ACS Appl Polym Mater 2021;3:1457–64. https://doi.org/10.1021/acsapm.0c01321.

[56] Freitas AA, Silva CP, Silva GTM, Maçanita AL, Quina FH. From vine to wine: Photophysics of a pyranoflavylium analog of red wine pyranoanthocyanins. Pure Appl. Chem., vol. 89, 2017, p. 1761–7. https://doi.org/10.1515/pac-2017-0411.

[57] Freitas AA, Silva CP, Silva GTM, Maçanita AL, Quina FH. Ground- and Excited-State Acidity of Analogs of Red Wine Pyranoanthocyanins,. Photochem Photobiol 2018;94:1086–91. https://doi.org/10.1111/php.12944.

[58] Silva GTM, Thomas SS, Silva CP, Schlothauer JC, Baptista MS, Freitas AA, et al. Triplet Excited States and Singlet Oxygen Production by Analogs of Red Wine Pyranoanthocyanins. Photochem Photobiol 2019;95:176–82. https://doi.org/10.1111/php.12973.

[59] Alejo-Armijo A, Basílio N, Freitas AA, MaçAnita AL, Lima JC, Jorge Parola A, et al. Ground and excited state properties of furanoflavylium derivatives. Phys Chem Chem Phys 2019;21:21651–62. https://doi.org/10.1039/c9cp04917g.

[60] Siddique F, Silva CP, Medeiros Silva GT, Lischka H, Quina FH, Aquino AJA. The electronic transitions of analogs of red wine pyranoanthocyanin pigments. Photochem Photobiol Sci 2019;18:45–53. https://doi.org/10.1039/C8PP00391B.

[61] Silva CP, Silva GTM, Costa TDS, Carneiro VMT, Siddique F, Aquino AJA, et al. Chromophores inspired by the colors of fruit, flowers and wine. Pure Appl Chem 2020;92:255–63. https://doi.org/10.1515/pac-2019-0226.

[62] Wang J, Siddique F, Freitas AA, Silva CP, Silva GTM, Quina FH, et al. A computational study of the ground and excited state acidities of synthetic analogs of red wine pyranoanthocyanins. Theor Chem Acc 2020;139:1–11. https://doi.org/10.1007/s00214-020-02633-9.

[63] Santos CM, Oliveira J, Rocha S, Coelho M, Freitas V, Aguilar H. Pyranoflavylium Derivatives Extracted from Wine Grape as Photosensitizers in Solar Cells. J Braz Chem Soc 2014;25:1029–35. https://doi.org/10.5935/0103-5053.20140075.

[64] Pinto AL, Cruz L, Gomes V, Cruz H, Calogero G, de Freitas V, et al. Catechol versus carboxyl linkage impact on DSSC performance of synthetic pyranoflavylium salts. Dye Pigment 2019;170:107577. https://doi.org/10.1016/j.dyepig.2019.107577.

[65] Pinto AL, Oliveira J, Araújo P, Calogero G, de Freitas V, Pina F, et al. Study of the multi-equilibria of red wine colorants pyranoanthocyanins and evaluation of their potential in dye-sensitized solar cells. Sol Energy 2019;191:100–8. https://doi.org/10.1016/j.solener.2019.08.050.

[66] Pinto AL, Cruz H, Oliveira J, Araújo P, Cruz L, Gomes V, et al. Dye-sensitized solar cells based on dimethylamino-π-bridge-pyranoanthocyanin dyes. Sol Energy 2020;206:188–99. https://doi.org/10.1016/j.solener.2020.05.101.

[67] Faria A, Oliveira J, Neves P, Gameiro P, Santos-Buelga C, De Freitas V, et al.

Antioxidant properties of prepared blueberry (Vaccinium myrtillus) extracts. J Agric Food Chem 2005;53:6896–902. https://doi.org/10.1021/jf0511300.

[68] Azevedo J, Oliveira J, Cruz L, Teixeira N, Brás NF, De Freitas V, et al. Antioxidant features of red wine pyranoanthocyanins: Experimental and theoretical approaches. J Agric Food Chem 2014;62:7002–9. https://doi.org/10.1021/jf404735j.

[69] Azevedo J, Fernandes I, Faria A, Oliveira J, Fernandes A, Freitas V de, et al. Antioxidant properties of anthocyanidins, anthocyanidin-3-glucosides and respective portisins. Food Chem 2010;119:518–23. https://doi.org/10.1016/j.foodchem.2009.06.050.

[70] Sun J, Li X, Luo H, Ding L, Jiang X, Li X, et al. Comparative Study on the Stability and Antioxidant Activity of Six Pyranoanthocyanins Based on Malvidin-3-glucoside. J Agric Food Chem 2020;68:2783–94. https://doi.org/10.1021/acs.jafc.9b06734.

[71] Kirby CW, Wu T, Tsao R, McCallum JL. Isolation and structural characterization of unusual pyranoanthocyanins and related anthocyanins from Staghorn sumac (Rhus typhina L.) via UPLC-ESI-MS, 1H, 13C, and 2D NMR spectroscopy. Phytochemistry 2013;94:284–93. https://doi.org/10.1016/j.phytochem.2013.06.017.

[72] Wu T, McCallum JL, Wang S, Liu R, Zhu H, Tsao R. Evaluation of antioxidant activities and chemical characterisation of staghorn sumac fruit (Rhus hirta L.). Food Chem 2013;138:1333–40. https://doi.org/10.1016/j.foodchem.2012.10.086.

[73] Peng Y, Zhang H, Liu R, Mine Y, McCallum J, Kirby C, et al. Antioxidant and anti-inflammatory activities of pyranoanthocyanins and other polyphenols from staghorn sumac (Rhus hirta L.) in Caco-2 cell models. J Funct Foods 2016;20:139–47. https://doi.org/10.1016/j.jff.2015.10.026.

[74] Correia P, Araújo P, Ribeiro C, Oliveira H, Pereira AR, Mateus N, et al. Anthocyanin-related pigments: Natural allies for skin health maintenance and protection. Antioxidants 2021;10. https://doi.org/10.3390/antiox10071038.

[75] Faria A, Pestana D, Teixeira D, De Freitas V, Mateus N, Calhau C. Blueberry anthocyanins and pyruvic acid adducts: Anticancer properties in breast cancer cell lines. Phyther Res 2010;24:1862–9. https://doi.org/10.1002/ptr.3213.

[76] Fernandes I, Faria A, Azevedo J, Soares S, Calhau C, De Freitas V, et al. Influence of anthocyanins, derivative pigments and other catechol and pyrogallol-type phenolics on breast cancer cell proliferation. J Agric Food Chem 2010;58:3785–92. https://doi.org/10.1021/jf903714z.

[77] Oliveira H, Wu N, Zhang Q, Wang J, Oliveira J, De Freitas V, et al. Bioavailability studies and anticancer properties of malvidin based anthocyanins, pyranoanthocyanins and non-oxonium derivatives. Food Funct 2016;7:2462–8. https://doi.org/10.1039/c6fo00445h.

[78] Pan F, Liu Y, Liu J, Wang E. Stability of blueberry anthocyanin, anthocyanidin and pyranoanthocyanidin pigments and their inhibitory effects and mechanisms in human cervical cancer HeLa cells. RSC Adv 2019;9:10842–53. https://doi.org/10.1039/c9ra01772k.

[79] World Health Organization. Food safety 2020. https://www.who.int/news-room/fact-sheets/detail/food-safety.

[80] FAO. Food wastage footprint. 2013.

[81] Heising JK, Claassen GDH, Dekker M. Options for reducing food waste by quality-controlled logistics using intelligent packaging along the supply chain. Food Addit Contam - Part A Chem Anal Control Expo Risk Assess 2017;34:1672–80. https://doi.org/10.1080/19440049.2017.1315776.

[82] Drago E, Campardelli R, Pettinato M, Perego P. Innovations in Smart Packaging Concepts for Food: An Extensive Review. Foods 2020;9:1628. https://doi.org/10.3390/foods9111628.

[83] European Commision. Commission Regulation (EC) No. 450/2009 of on active and intelligent materials and articles intended to come into contact with food. Off J Eur Union 2009:3–11.

[84] Priyadarshi R, Ezati P, Rhim J-W. Recent Advances in Intelligent Food Packaging Applications Using Natural Food Colorants. ACS Food Sci Technol 2021;1:124–38. https://doi.org/10.1021/acsfoodscitech.0c00039.

[85] Yousefi H, Su HM, Imani SM, Alkhaldi K, Filipe CD, Didar TF. Intelligent Food Packaging: A Review of Smart Sensing Technologies for Monitoring Food Quality. ACS Sensors 2019;4:808–21. https://doi.org/10.1021/acssensors.9b00440.

[86] Vanderroost M, Ragaert P, Devlieghere F, De Meulenaer B. Intelligent food packaging: The next generation. Trends Food Sci Technol 2014;39:47–62. https://doi.org/10.1016/j.tifs.2014.06.009.

[87] Bekhit AEDA, Giteru SG, Holman BWB, Hopkins DL. Total volatile basic nitrogen and trimethylamine in muscle foods: Potential formation pathways and effects on human health. Compr Rev Food Sci Food Saf 2021;20:3620–66. https://doi.org/10.1111/1541-4337.12764.

[88] Comi G. Spoilage of Meat and Fish. Elsevier Ltd; 2017. https://doi.org/10.1016/B978-0-08-100502-6.00011-X.

[89] Ruiz-Capillas C, Herrero AM. Impact of biogenic amines on food quality and safety. Foods 2019;8. https://doi.org/10.3390/foods8020062.

[90] Triki M, Herrero A, Jiménez-Colmenero F, Ruiz-Capillas C. Quality Assessment of Fresh Meat from Several Species Based on Free Amino Acid and Biogenic Amine Contents during Chilled Storage. Foods 2018;7:132. https://doi.org/10.3390/foods7090132.

[91] EC. Determination of the concentration of TVB-N in fish and fishery products. Commission Regulation, Chapter III. (EC) No 2074/2005. Off J Eur Union 2005:L338/37-39.

[92] Bekhit AEDA, Holman BWB, Giteru SG, Hopkins DL. Total volatile basic nitrogen (TVB-N) and its role in meat spoilage: A review. Trends Food Sci Technol 2021;109:280–302. https://doi.org/10.1016/j.tifs.2021.01.006.

[93] Cheng H, Xu H, Julian McClements D, Chen L, Jiao A, Tian Y, et al. Recent advances in intelligent food packaging materials: Principles, preparation and applications. Food Chem 2022;375:131738. https://doi.org/10.1016/j.foodchem.2021.131738.

[94] Becerril R, Nerín C, Silva F. Bring some colour to your package: Freshness indicators based on anthocyanin extracts. Trends Food Sci Technol

2021;111:495–505. https://doi.org/10.1016/j.tifs.2021.02.042.

[95] Luo Q, Hossen A, Sameen DE, Ahmed S, Dai J, Li S, et al. Recent advances in the fabrication of pH-sensitive indicators films and their application for food quality evaluation. Crit Rev Food Sci Nutr 2021;0:1–17. https://doi.org/10.1080/10408398.2021.1959296.

[96] Abolghasemi MM, Sobhi M, Piryaei M. Preparation of a novel green optical pH sensor based on immobilization of red grape extract on bioorganic agarose membrane. Sensors Actuators, B Chem 2016;224:391–5. https://doi.org/10.1016/j.snb.2015.10.038.

[97] Alizadeh-Sani M, Mohammadian E, Rhim JW, Jafari SM. pH-sensitive (halochromic) smart packaging films based on natural food colorants for the monitoring of food quality and safety. Trends Food Sci Technol 2020;105:93–144. https://doi.org/10.1016/j.tifs.2020.08.014.

[98] Zheng L, Liu L, Yu J, Shao P. Novel trends and applications of natural pH-responsive indicator film in food packaging for improved quality monitoring. Food Control 2021;134:108769. https://doi.org/10.1016/j.foodcont.2021.108769.

[99] Yong H, Liu J. Recent advances in the preparation, physical and functional properties, and applications of anthocyanins-based active and intelligent packaging films. Food Packag Shelf Life 2020;26:100550. https://doi.org/10.1016/j.fpsl.2020.100550.

[100] Oliveira Filho JG de, Braga ARC, Oliveira BR de, Gomes FP, Moreira VL, Pereira VAC, et al. The potential of anthocyanins in smart, active, and bioactive eco-friendly polymer-based films: A review. Food Res Int 2021;142:110202. https://doi.org/10.1016/j.foodres.2021.110202.

[101] Ghareaghajlou N, Hallaj-Nezhadi S, Ghasempour Z. Red cabbage anthocyanins: Stability, extraction, biological activities and applications in food systems. Food Chem 2021;365:130482. https://doi.org/10.1016/j.foodchem.2021.130482.

[102] Roy S, Rhim JW. Anthocyanin food colorant and its application in pH-responsive color change indicator films. Crit Rev Food Sci Nutr 2021;61:2297–325. https://doi.org/10.1080/10408398.2020.1776211.

[103] Liu Y, Ahmed S, Sameen DE, Wang Y, Lu R, Dai J, et al. A review of cellulose and its derivatives in biopolymer-based for food packaging application. Trends Food Sci Technol 2021;112:532–46. https://doi.org/10.1016/j.tifs.2021.04.016.

[104] Romão S, Bettencourt A, Ribeiro IAC. Novel Features of Cellulose-Based Films as Sustainable Alternatives for Food Packaging. Polymers (Basel) 2022;14:4968.

[105] Gemili S, Yemenicioğlu A, Altinkaya SA. Development of cellulose acetate based antimicrobial food packaging materials for controlled release of lysozyme. J Food Eng 2009;90:453–62. https://doi.org/10.1016/j.jfoodeng.2008.07.014.

[106] Rajeswari A, Christy EJS, Swathi E, Pius A. Fabrication of improved cellulose acetate-based biodegradable films for food packaging applications. Environ Chem Ecotoxicol 2020;2:107–14. https://doi.org/10.1016/j.enceco.2020.07.003.

[107] Assis RQ, Rios PDA, Rios A de O, Olivera FC. Biodegradable packaging of cellulose acetate incorporated with norbixin, lycopene or zeaxanthin. Ind Crops Prod 2020;147:112212. https://doi.org/10.1016/j.indcrop.2020.112212.

[108] Ardila-Diaz LD, de Oliveira T V., Soares N de FF. Development and evaluation of the chromatic behavior of an intelligent packaging material based on cellulose acetate incorporated with polydiacetylene for an efficient packaging. Biosensors 2020;10. https://doi.org/10.3390/BIOS10060059.

[109] Saha NR, Sarkar G, Roy I, Bhattacharyya A, Rana D, Dhanarajan G, et al. Nanocomposite films based on cellulose acetate/polyethylene glycol/modified montmorillonite as nontoxic active packaging material. RSC Adv 2016;6:92569–78. https://doi.org/10.1039/c6ra17300d.

[110] Freitas PAV, Silva RRA, de Oliveira T V., Soares RRA, Junior NS, Moraes ARF, et al. Development and characterization of intelligent cellulose acetate-based films using red cabbage extract for visual detection of volatile bases. Lwt 2020;132:109780. https://doi.org/10.1016/j.lwt.2020.109780.

[111] Aghaei Z, Emadzadeh B, Ghorani B, Kadkhodaee R. Cellulose Acetate Nanofibres Containing Alizarin as a Halochromic Sensor for the Qualitative Assessment of Rainbow Trout Fish Spoilage. Food Bioprocess Technol 2018;11:1087–95. https://doi.org/10.1007/s11947-017-2046-5.

[112] Vieira MGA, Da Silva MA, Dos Santos LO, Beppu MM. Natural-based plasticizers and biopolymer films: A review. Eur Polym J 2011;47:254–63. https://doi.org/10.1016/j.eurpolymj.2010.12.011.

[113] Mekonnen T, Mussone P, Khalil H, Bressler D. Progress in bio-based plastics and plasticizing modifications. J Mater Chem A 2013;1:13379–98. https://doi.org/10.1039/c3ta12555f.

[114] de Melo PG, Fornazier Borges M, Afonso Ferreira J, Vicente Barbosa Silva M, Ruggiero R. Bio-based cellulose acetate films reinforced with lignin and glycerol. Int J Mol Sci 2018;19:1–13. https://doi.org/10.3390/ijms19041143.

[115] Gonçalves SM, dos Santos DC, Motta JFG, Santos RR dos, Chávez DWH, Melo NR de. Structure and functional properties of cellulose acetate films incorporated with glycerol. Carbohydr Polym 2019;209:190–7. https://doi.org/10.1016/j.carbpol.2019.01.031.

[116] Moreira Gonçalves S, Gomes Motta JF, Ribeiro-Santos R, Hidalgo Chávez DW, Ramos de Melo N. Functional and antimicrobial properties of cellulose acetate films incorporated with sweet fennel essential oil and plasticizers. Curr Res Food Sci 2020;3:1–8. https://doi.org/10.1016/j.crfs.2020.01.001.

[117] Teixeira SC, Silva RRA, de Oliveira TV, Stringheta PC, Pinto MRMR, Soares N de FF. Glycerol and triethyl citrate plasticizer effects on molecular, thermal, mechanical, and barrier properties of cellulose acetate films. Food Biosci 2021;42. https://doi.org/10.1016/j.fbio.2021.101202.

[118] Yong H, Liu J. Recent advances in the preparation, physical and functional properties, and applications of anthocyanins-based active and intelligent packaging films. Food Packag Shelf Life 2020;26:100550. https://doi.org/10.1016/j.fpsl.2020.100550.

[119] Veiga-Santos P, Ditchfield C, Tadini CC. Development and Evaluation of a Novel pH Indicator Biodegradable Film Based on Cassava Starch. J Appl Polym Sci 2010;120:1069–1079. https://doi.org/doi.org/10.1002/app.33255.

[120] Shukla V, Kandeepan G, Vishnuraj MR, Soni A. Anthocyanins based indicator sensor for intelligent packaging application. Agric Res 2016;5:205–9.

https://doi.org/10.1007/s40003-016-0211-0.

[121] Luchese CL, Sperotto N, Spada JC, Tessaro IC. Effect of blueberry agro-industrial waste addition to corn starch-based films for the production of a pH-indicator film. Int J Biol Macromol 2017;104:11–8. https://doi.org/10.1016/j.ijbiomac.2017.05.149.

[122] Wei YC, Cheng CH, Ho YC, Tsai ML, Mi FL. Active gellan gum/purple sweet potato composite films capable of monitoring pH variations. Food Hydrocoll 2017;69:491–502. https://doi.org/10.1016/j.foodhyd.2017.03.010.

[123] Zhang J, Zou X, Zhai X, Huang XW, Jiang C, Holmes M. Preparation of an intelligent pH film based on biodegradable polymers and roselle anthocyanins for monitoring pork freshness. Food Chem 2019;272:306–12. https://doi.org/10.1016/j.foodchem.2018.08.041.

[124] Moradi M, Tajik H, Almasi H, Forough M, Ezati P. A novel pH-sensing indicator based on bacterial cellulose nanofibers and black carrot anthocyanins for monitoring fish freshness. Carbohydr Polym 2019;222:115030. https://doi.org/10.1016/j.carbpol.2019.115030.

[125] Liang T, Sun G, Cao L, Li J, Wang L. A pH and NH3 sensing intelligent film based on Artemisia sphaerocephala Krasch. gum and red cabbage anthocyanins anchored by carboxymethyl cellulose sodium added as a host complex. Food Hydrocoll 2019;87:858–68. https://doi.org/10.1016/j.foodhyd.2018.08.028.

[126] Andretta R, Luchese CL, Tessaro IC, Spada JC. Development and characterization of pH-indicator films based on cassava starch and blueberry residue by thermocompression. Food Hydrocoll 2019;93:317–24. https://doi.org/10.1016/j.foodhyd.2019.02.019.

[127] Chen H zhi, Zhang M, Bhandari B, Yang C hui. Novel pH-sensitive films containing curcumin and anthocyanins to monitor fish freshness. Food Hydrocoll 2020;100:105438. https://doi.org/10.1016/j.foodhyd.2019.105438.

[128] Opinion S, Panel E, Additives F, Sources N, Food E, Authority S. Scientific Opinion on the re-evaluation of anthocyanins (E 163) as a food additive. EFSA J 2013;11:1649. https://doi.org/10.2903/j.efsa.2013.3145.

[129] da Silva Filipini G, Romani VP, Guimarães Martins V. Biodegradable and active-intelligent films based on methylcellulose and jambolão (Syzygium cumini) skins extract for food packaging. Food Hydrocoll 2020;109. https://doi.org/10.1016/j.foodhyd.2020.106139.

[130] Brouillard R, Chassaing S, Isorez G, Kueny-Stotz M, Figueiredo P. The Visible Flavonoids or Anthocyanins: From Research to Applications. Recent Adv. Polyphen. Res., Oxford, UK: Wiley-Blackwell; 2010, p. 1–22. https://doi.org/10.1002/9781444323375.ch1.

[131] Pina F. Chemical applications of anthocyanins and related compounds. A source of bioinspiration. J Agric Food Chem 2014;62:6885–97. https://doi.org/10.1021/jf404869m.

[132] Wu C, Sun J, Zheng P, Kang X, Chen M, Li Y, et al. Preparation of an intelligent film based on chitosan/oxidized chitin nanocrystals incorporating black rice bran anthocyanins for seafood spoilage monitoring. Carbohydr Polym 2019;222:115006. https://doi.org/10.1016/j.carbpol.2019.115006.

[133] Jiang G, Hou X, Zeng X, Zhang C, Wu H, Shen G, et al. Preparation and characterization of indicator films from carboxymethyl-cellulose/starch and purple sweet potato (Ipomoea batatas (L.) lam) anthocyanins for monitoring fish freshness. Int J Biol Macromol 2020;143:359–72. https://doi.org/10.1016/j.ijbiomac.2019.12.024.

[134] Choi I, Lee JY, Lacroix M, Han J. Intelligent pH indicator film composed of agar/potato starch and anthocyanin extracts from purple sweet potato. Food Chem 2017;218:122–8. https://doi.org/10.1016/j.foodchem.2016.09.050.

[135] Alizadeh-Sani M, Tavassoli M, McClements DJ, Hamishehkar H. Multifunctional halochromic packaging materials: Saffron petal anthocyanin loaded-chitosan nanofiber/methyl cellulose matrices. Food Hydrocoll 2021;111:106237. https://doi.org/10.1016/j.foodhyd.2020.106237.

[136] Sani MA, Tavassoli M, Hamishehkar H, McClements DJ. Carbohydrate-based films containing pH-sensitive red barberry anthocyanins: Application as biodegradable smart food packaging materials. Carbohydr Polym 2021;255:117488. https://doi.org/10.1016/j.carbpol.2020.117488.

Chapter I

Novel pyranoflavylium and related dyes: synthesis and physicochemical characterization

Article I

Synthesis and chemical equilibria of a new 10-methylpyrano-2-styrylbenzopyrylium pigment in aqueous solution and its modulation by different micellar systems

Vânia Gomes, Nuno Mateus, Victor de Freitas, Luís Cruz

REQUIMTE/LAQV, Departamento de Química e Bioquímica, Faculdade de Ciências, Universidade do Porto, Rua Do Campo Alegre, 687, 4169-007, Porto, Portugal

---

Gomes, V., Cruz, L., Mateus, N., de Freitas, V., Synthesis and chemical equilibria of a new 10-methylpyrano-2-styrylbenzopyrylium pigment in aqueous solution and its modulation by different micellar systems, *Dyes and Pigments*, **2019**, 167, 60–67.

DOI https://doi.org/10.1016/j.dyepig.2019.04.004

Dyes and Pigments 167 (2019) 60–67

Contents lists available at ScienceDirect

Dyes and Pigments

journal homepage: www.elsevier.com/locate/dyepig

Synthesis and chemical equilibria of a new 10-methylpyrano-2-styrylbenzopyrylium pigment in aqueous solution and its modulation by different micellar systems

Vânia Gomes, Nuno Mateus, Victor de Freitas, Luís Cruz*

REQUIMTE/LAQV, Departamento de Química e Bioquímica, Faculdade de Ciências, Universidade Do Porto, Rua Do Campo Alegre, 687, 4169-007, Porto, Portugal

ARTICLE INFO

Keywords:
Pyranostyrylbenzopyrylium
pK_a
UV–Vis
Micelles
Color stability

ABSTRACT

The pyranostyrylbenzopyrylium moiety is a new type of benzopyrylium derivative, which has an extra double bond between the benzopyrylium and the phenyl ring B and an additional pyranic ring between C-5 and C-4. In this work, the synthesis and the chemical equilibrium of a new 10-methylpyrano-2-styrylbenzopyrylium in aqueous solutions by UV–Vis spectrophotometry are reported. The introduction of the double bond leads to changes in its chromatic properties, making the pigment exhibit a higher colorant capacity, when comparing with traditional pyranoanthocyanins. There is a stabilization of the color mainly due to the value of the second pK_a that increase from 6.5 to 7.3. The modulation of its equilibria network by different micellar systems with different charges (SDS, Triton x-100 and CTAB) was studied. SDS and CTAB had opposite effects on the variation of pK_a values, whereas Triton X-100 showed only a slight influence. The stability of each species (AH^+, A or A^-) in different systems in solution was also studied over 48 h. Overall, the best color stabilization of each species was achieved for the SDS micellar system.

1. Introduction

Pyranoanthocyanins are a class of anthocyanin-derived pigments that are found in processed foodstuffs based on fruits and vegetables such as juices and red wines [1]. These pigments result from cycloaddition reactions between anthocyanins and other compounds present in the food matrix during processing (fermentation, maturation, etc.), forming a new pyranic ring. More specifically, the cycloaddition reaction occurs between the C4/C5—OH of anthocyanins and a double bond (enolic form) of another molecule such as acetaldehyde, pyruvic acid, vinylcatechin and vinylcatechol, etc [1–3]. Over the last years, several pyranoanthocyanins have been isolated from these food products such as A- and B-type vitisins [4,5], oxovitisins [6], methylpyranoanthocyanins [7], portisins [8], pyranoanthocyanins, dimers [9], among others [10–12], as recently reviewed in Oliveira et al. [13]. The mechanisms of formation of these molecules, as well as other synthesis methodologies [14–16] have been studied in order to obtain these pyranoanthocyanins and pyrano-3-deoxyanthocyanins [17–20]. Several studies of their physicochemical, chromatic and antioxidant properties have demonstrated that these molecules differ from anthocyanins in various aspects [21,22]. One of the most important features is their greater stability to pH variations and bleaching by SO_2 in comparison to anthocyanins. In fact, the presence of the new pyranic ring avoids the hydration reaction of the anthocyanins and, therefore, the formation of hemiketal colorless species [2,22,23].

Pyranoanthocyanins and their derivatives have been studied for numerous applications such as dyes for hair and textiles, photosensitizers for solar cell applications [24], photochromic and pH-sensors for food packaging, photodynamic therapy, amongst others.

This study follows a previous work [25] and reports a new pigment from a new class of pyrano-3-deoxyanthocyanins: pyrano-2-styrylbenzopyrylium. These compounds have the same basic skeleton than pyrano-3-deoxyanthocyanins with an extra double bond linking the benzopyrylium (A and C ring) and the phenyl system (B ring). The addition of this double bond is already described in the literature but only for flavylium compounds, resulting in 2-styrylbenzopyrylium salts. Studies on 2-styrylbenzopyrylium salts reported that the introduction of the double bond between B and C rings have profound effects in the color and reaction network which is very important for food colorant applications [26,27]. Pina and co-workers described a series of these 2-styrylbenzopyrylium salts and studied their reaction network and photochromic properties in the absence and presence of CTAB micelles [28–30].

Bearing this, this work reports the synthesis of the a new pyrano-2-

* Corresponding author.
E-mail address: luis.cruz@fc.up.pt (L. Cruz).

https://doi.org/10.1016/j.dyepig.2019.04.004
Received 14 February 2019; Received in revised form 28 March 2019; Accepted 2 April 2019
Available online 06 April 2019
0143-7208/ © 2019 Elsevier Ltd. All rights reserved.

styrylbenzopyrylium with a methyl group attached to C10 and their chemical equilibria in aqueous solutions was study. Furthermore, the influence of three different micellar systems (anionic SDS, neutral TRITON X-100 and cationic CTAB) in the pK_a values was also studied aiming to tune/modulate its chromatic properties for potential colorant applications.

2. Material and methods

2.1. General methods

2.1.1. Reagents

All chemicals were obtained from Sigma-Aldrich (Madrid, Spain), with exception of the 3,4-dihy-droxybenzylideneacetone which was obtained from Alfa Aesar (Heysham, England). A universal buffer of Theorell and Stenhagen [31] was made by dissolving phosphoric acid 85% (w/w) (2.25 mL, 3.23 g, 0.03 mol), citric acid monohydrate (7.00 g, 0.03 mol), boric acid (3.54 g, 0.06 mol) and NaOH 1M (343 mL, 13.7 g, 0.343 mol) solution in millipore water until 1 L. Solutions were made using millipore water.

2.1.2. NMR spectroscopy

^{1}H NMR (600.13 MHz) and ^{13}C NMR (125.77 MHz) spectra were recorded in DMSO-d_6/TFA (90:10) and MeOD-d4/TFA (90:10) on a Bruker-Avance 600 spectrometer at 303 K and with TMS as an internal standard [chemical shifts (d) in parts per million, coupling constants (J) in Hertz]. Multiplicities are recorded as singlets (s), doublets (d) and double doublets (dd). ^{1}H chemical shifts were assigned using 2D NMR (COSY, NOESY) experiments while ^{13}C resonances were assigned using 2D NMR techniques (gHMBC and gHSQC). The delay for the long-range C/H coupling constant was optimized to 7 Hz.

2.1.3. High resolution mass spectrometry (HRMS)

Analysis were done on an LTQ Orbitrap™ XL hybrid mass spectrometer (Thermo Fischer Scientific, Bremen, Germany) controlled by *LTQ Tune Plus 2.5.5* and *Xcalibur 2.1.0*. Positive mode: The capillary voltage of the electrospray ionization source (ESI) was set to 3.1 kV. The capillary temperature was 275 °C. The sheath gas was at 5 (arbitrary unit as provided by the software settings). The capillary voltage was 49 V and the tube lens voltage 80 V.

2.1.4. Absorption spectroscopy

UV–Vis absorption spectra were recorded in a Varian-Cary 100 Bio spectrophotometer. Spectroscopic absorbance curves were recorded at 25 °C for all the solutions from 200 to 800 nm with a 1 nm sampling interval using a quartz cell cuvette of 3.5 mL capacity and 1 cm of optical path.

2.2. Synthesis

2.2.1. Synthesis of 2-(3′,4′-dihydroxystyryl)-5,7-dihydroxy-1-benzopyrylium **3**

The synthesis and all characterization of the 2-(3,4-dihydroxystyryl)-5,7-dihydroxy-1-benzopyrylium **3** has been reported [25].

2.2.2. Synthesis of 2-(3′,4′-dihydroxystyryl)-10-methylpyrano-7-hydroxy-1-benzopyrylium chloride **4**

Compound **3** (47.0 mg, 0.14 mmol) was dissolved in 50 mL of aqueous EtOH 20% and acetone 20% solution. The reaction mixture was stirred at 37 °C and pH 2.5 for 4 d. The crude product was purified by column chromatography using C18 silica gel with acidified aqueous solution of 30–40% of MeOH. After lyophilization, a dark orange powder (8.1 mg) was obtained with 16% of yield. ^{1}H NMR (600.13 MHz, DMSO-d_6:TFA 9:1), δ (ppm): 7.92 (d, J = 15.7 Hz, 1H, Hβ) 7.23 (d, J = 1.7 Hz, 1H, H2′), 7.17 (dd, J = 8.1, 1.2 Hz, 1H, H6′), 7.15 (s, 1H, H6 or H8), 7.09 (d, J = 15.8 Hz, 1H, Hα), 7.06 (s, 1H, H3), 7.03 (s, 1H, H6 or H8), 6.95 (s, 1H, H9), 6.86 (d, J = 8.2 Hz, 1H, H5′), 2.54 (s, 3H, CH_3). ^{13}C NMR (125.77 MHz, DMSO-d_6:TFA 9:1), δ (ppm): 172.08 (C10), 168.33 (C2), 153.91 (C5 or C8a), 153.37 (C5 or C8a), 150.85 (C4′), 146.35 (C3′), 144.92 (Cβ), 126.55 (C1′), 123.71 (C6′),116.48 (C5′), 115.70 (C2′), 115.46 (Cα), 107.60 (C4a), 105.22 (C9), 104.65 (C3), 100.55 (C6 or C8), 100.26 (C6 or C8), 21.18 (CH_3). HRMS (ESI) molecular formula $C_{20}H_{15}O_5^+$ requires $[M]^+$ 335.0914; Found, 335.0916. UV/VIS data λ_{max} (0.01 M HCl in MeOH) 536 nm and molar extinction coefficient ε_{max} = 17499 $mol^{-1}dm^3cm^{-1}$.

2.3. Titrations

The acidic thermodynamic constants were determined by spectrophotometric titrations. It was subsequently added to the cell cuvette 1 mL of NaOH solution (0.1 M), 1 mL of universal buffer solution at pH 1 and 1 mL of stock solution of the pigment 0.03 M (with 75% ethanol), where the final concentration was 0.01 mM and 25% ethanol. In case of the micellar solutions, the stock solutions of pigments at 0.03 mM was prepared with 0.3 M of the surfactants (SDS, Triton X-100 and CTAB) for the final concentration of 0.01 mM and 0.1 M to pigment and surfactant, respectively. The first UV–Vis spectrum was immediately recorded. Increasing amounts of NaOH solution (1 M) were added to the cell cuvette achieving a pH range between 1 and 12. After each addition, the mixture was rapidly shacked, a UV–Vis spectrum was recorded, and the pH was measured. Final volumes were appropriately corrected. All pH measurements were made in a Radiometer Copenhagen PHM240 pH/ion meter. The fitting for pK_a determination was carried out using Solver program from Microsoft Excel.

3. Results and discussion

3.1. Synthesis of the 2-(3′,4′-dihydroxystyryl)-10-methylpyrano-7-hydroxybenzopyrylium chloride **4**

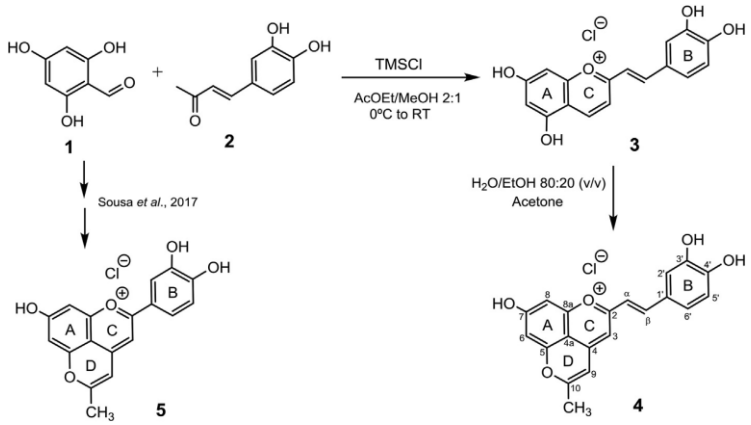
Compound **4** was synthesized according to the conditions described in Scheme 1. The synthesis of 2-styrylbenzopyrylium **3** was previously described in the literature [25] through an acidic aldol condensation between 2,4,6-trihydroxybenzaldehyde **1** and acetophenone **2,** according to a procedure adapted either from Katritzky [32] or Robinson [33], both frequently used in the synthesis of 2-phenyl-1-benzopyrylium salts. The next step consisted in the cycloaddition reactions between 2-styrylbenzopyrylium **3** and acetone (enolic form) in a hydroalcoholic solution. After the purification steps, the pigment was analyzed by LC-DAD/ESI-MS in the positive ion mode and its structure was fully elucidated by ^{1}H and ^{13}C NMR using 1D and 2D techniques (see supporting information). Scheme 1 also presents the structure of compound **5** (without double bond between B and C rings) previously developed [19].

3.2. Chromatic properties

Two chromatic properties, namely the maximum absorption wavelength (λ_{max}) and the molar absorptivity coefficient in MeOH HCl 0.01 M were determined for the pigments **4** and **5** (Fig. 1 and Table 1). Comparing the values obtained for both pigments, it could be observed that there was a significant redshift of the maximum absorption wavelength of **4** relatively to **5**. In the case of the extinction molar coefficients, the new pigment presented a value considerably higher in relation to its analogue **5**. Thus, these results confirmed that the presence of the double bond between ring B and C of the flavylium core has a great influence on its properties, making the pigments to exhibit a higher colorant capacity (see Table 1).

3.3. Determination of pK_a values

The pK_a values for the novel pigment were determined by titrations



Scheme 1. Synthesis strategy to obtain compounds **4** and **5** [19].

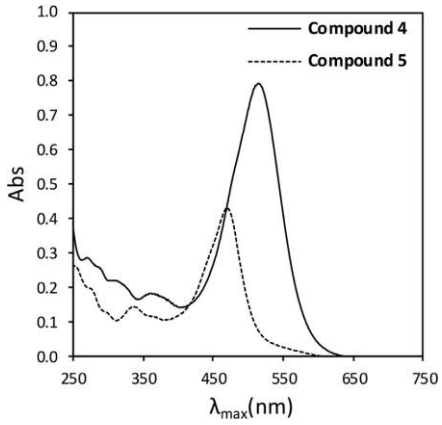


Fig. 1. UV–Vis spectra of **4** and **5** at 0.1 mM in MeOH HCl 0.01 M.

Table 1
Maximum absorption wavelengths and the molar absorptivity coefficients determined of the pigments at 0.1 mM in MeOH HCl 0.01 M.

Pigment	Wavelength, λ (nm)	Molar Absortivity, ε ($mol^{-1}.L.cm^{-1}$)
4	536	17499
5	469	10519

in the absence and presence of micellar systems. In the absence of any micellar system, the titrations were made in a water/ethanol mixture (75:25 (v/v)) because the pigment is not completely water-soluble. The experiments with the micellar systems were made with three different types of surfactants, based on their charge, namely with SDS (anionic), Triton X-100 (non-ionic) and CTAB (cationic) at concentrations above of their critical micelle concentration (0.1 M). The titration was fast enough to avoid significant precipitation (which is a relatively slow process). The UV–Vis spectra of the pigment were obtained for the pH range between 1 and 12. All pK_a values were defined as apparent pK_a values because these they were calculated using the apparent pH values. In case of the hydroalcoholic solution, the pH values are approximate due to presence of ethanol in solution which can induce some variations. However, it was verified that these variations not influenced significantly the pK_a values since they are within the standard deviation range. In micellar solution, the measured pH values correspond to the pH of the intermicellar aqueous phase (pH_w). It is known that the pH values at the intermicellar aqueous phase and the micellar surface are different, however, this study was done based on the pH_w as reported by other works elsewhere [34,35].

3.3.1. Hydroalcoholic solution (water/ethanol 75:25 (v/v))

The equilibrium forms of **4** were studied in an aqueous solution with 25% of ethanol (75:25 (v/v)) at different pH values and its apparent pK_a values determined through UV–visible spectroscopy. Fig. 2 showed the evolution of the UV–vis spectra of the solution of the pigment at different pH values measured immediately after the pH jump.

The UV–vis spectra were divided into 3 different pH ranges to display some important isosbestic points for the determination of the different species in equilibrium. The first information that can be drawn from the UV–Vis spectra is that there is no apparent hydration reaction occurs for this compound with increasing pH, which is in agreement with the literature available for pyranoanthocyanins [22,36–38]. Therefore, the multistate reactions in solution of this pigment depend only on acid-base equilibria (AH^+, A, A^-, A^{2-}). In the first spectrum (Fig. 2a), at pH between 1.83 and 6.50, the isosbestic point at 440 nm determines the equilibrium between AH^+ and A. In the second spectrum (Fig. 2b), from 6.50 to 9.88, the isosbestic point at 496 nm represents the equilibrium between A and A^-, and, finally, in the third spectrum (Fig. 2c), the 561 nm point determines the equilibrium between A^- and A^{2-}. On this basis, the flavylium cation can undergo protonation/deprotonation reactions. The global process can be accounted for by equations (1)–(3):

$$AH^+ + H_2O \leftrightarrow A + H_3O^+ \; K_{a1} \text{ First proton transfer} \quad (1)$$

$$A + H_2O \leftrightarrow A^- + H_3O^+ \; K_{a2} \text{ Second proton transfer} \quad (2)$$

$$A^- + H_2O \leftrightarrow A^{2-} + H_3O^+ \; K_{a3} \text{ Third proton transfer} \quad (3)$$

where

$$K_{a1} = \frac{[A]\,[H_3O^+]}{[AH^+]} \quad K_{a2} = \frac{[A^-]\,[H_3O^+]}{[A]} \quad K_{a3} = \frac{[A^{2-}]\,[H_3O^+]}{[A^-]} \quad (4)$$

The total concentration of individual species, C_0, is given by equation (5):

$$C_0 = [AH^+] + [A] + [A^-] + [A^{2-}] \quad (5)$$

and the mole fraction distribution of the different species χ_i, was calculated as follows:

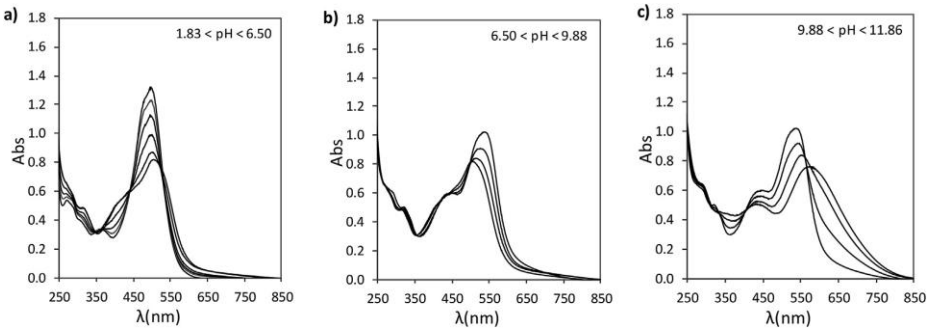


Fig. 2. (a) Spectral variations as a function of pH of pigment in the pH range 1.83 < pH < 6.50; (b) the same for 6.50 < pH < 9.88; (c) the same in the pH region 9.88 < pH < 11.86.

$$\chi_{AH^+} = \frac{[AH^+]}{C_0} = \frac{[H_3O^+]^3}{[H_3O^+]^3 + K_{a1}.[H_3O^+]^2 + K_{a1}.K_{a2}.[H_3O^+] + K_{a1}.K_{a2}.K_{a3}} \quad (6)$$

$$\chi_A = \frac{[A]}{C_0} = \frac{K_{a1}.[H_3O^+]^2}{[H_3O^+]^3 + K_{a1}.[H_3O^+]^2 + K_{a1}.K_{a2}.[H_3O^+] + K_{a1}.K_{a2}.K_{a3}} \quad (7)$$

$$\chi_{A^-} = \frac{[A^-]}{C_0} = \frac{K_{a1}.K_{a2}.[H_3O^+]}{[H_3O^+]^3 + K_{a1}.[H_3O^+]^2 + K_{a1}.K_{a2}.[H_3O^+] + K_{a1}.K_{a2}.K_{a3}} \quad (8)$$

$$\chi_{A^{2-}} = \frac{[A^{2-}]}{C_0} = \frac{K_{a1}.K_{a2}.K_{a3}}{[H_3O^+]^3 + K_{a1}.[H_3O^+]^2 + K_{a1}.K_{a2}.[H_3O^+] + K_{a1}.K_{a2}.K_{a3}} \quad (9)$$

These equations could be simplified to the following ones:

$$\chi_{AH^+} = \frac{1}{1 + \frac{K_{a1}}{[H^+]} + \frac{K_{a2}.K_{a1}}{[H^+]^2} + \frac{K_{a3}.K_{a2}.K_{a1}}{[H^+]^3}} \quad (6.1)$$

$$\chi_A = \frac{K_{a1}.\chi_{AH^+}}{[H^+]} \quad (7.1)$$

$$\chi_{A^-} = \frac{K_{a2}.\chi_A}{[H^+]} \quad (8.1)$$

$$\chi_{A^{2-}} = \frac{K_{a3}.\chi_{A^-}}{[H^+]} \quad (9.1)$$

The absorbance at a given wavelength shows a pH dependence which is given by the following equation:

$$A_{calc} = \varepsilon_{AH^+}.\chi_{AH^+} + \varepsilon_A.\chi_A + \varepsilon_{A^-}.\chi_{A^-} + \varepsilon_{A^{2-}}.\chi_{A^{2-}} \quad (10)$$

where ε_{AH^+}, ε_A, ε_{A^-}, $\varepsilon_{A^{2-}}$ are the mole absorption coefficients of the individual species or components at the considered wavelength.

The apparent pK_a values were determined by fitting the experimental absorbance values as a function of pH through equation (10). Solver function was then used to minimize the sum of the difference between theoretical and experimental values squared.

An excellent fitting was obtained between the experimental absorbance values and the theoretical ones at 496, 536, and 600 nm as a function of pH (Fig. 3) for the values of pK_{a1} = 5.1 ± 0.1, pK_{a2} = 7.3 ± 0.2 and pK_{a3} = 11.3 ± 0.1. Fig. 3 also showed the values of the mole fractions of each species as a function of pH (2–12).

The first pK_a refers to the deprotonation of the 7-OH group and the second one to deprotonation of the 4′—OH group, as described for

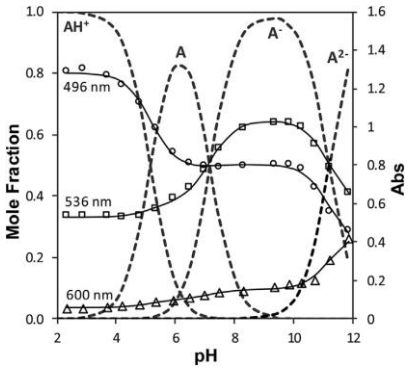


Fig. 3. Fitting was achieved for pK_{a1} = 5.1 ± 0.1, pK_{a2} = 7.3 ± 0.2 and pK_{a3} = 11.3 ± 0.1 for hydroalcoholic solution.

analogue compounds [39–42]. It was assumed that the third deprotonation occurred in the methyl group, and thereafter a delocalization of the charge should happen, as it was observed in a similar compound by Oliveira et al. [38] (see Fig. 4).

The multistate equilibrium for this pigment in the pH range studied is essentially characterized by the species AH^+ (λ_{max} = 496 nm) and A^- (λ_{max} = 536 nm). The A^{2-} (λ_{max} = 574 nm) species had low expression, once pK_{a3} was only determined at pH = 11.3. The species A also has little expression at this equilibrium, being only between pH values 5 and 7 and its maximum wavelength (λ_{max} = 505 nm) is very close to the AH^+ value. For this reason, this species is not very distinguishable in the UV–Vis spectrum.

Comparing the pK_a values obtained for this pigment with the similar compound **5** (pK_{a1} = 5.0 ± 0.1 and pK_{a2} = 6.5 ± 0.1) [19], it was verified that there was no significant variation of the value of the first deprotonation. However, there was a slight increase in the value of pK_{a2} which showed that the presence of the double bond between rings B and C stabilizes the nonionic quinoidal base, shifting the 7-OH deprotonation to higher pH values. This may be a consequence of the increase in electronic delocalization provided by the presence of the new double bond. It was not possible to compare the value of pK_{a3} since it could not be determined for methylpyranoflavylium due to the occurrence of precipitation at higher pH values, not observed for of pigment **5**.

3.3.2. Micellar solutions

Fig. 5 showed the absorption spectra of pigment **4** in equilibrated 0.1 M aqueous micellar solutions of the anionic surfactant SDS, the cationic surfactant CTAB and the nonionic surfactant Triton X-100, as a

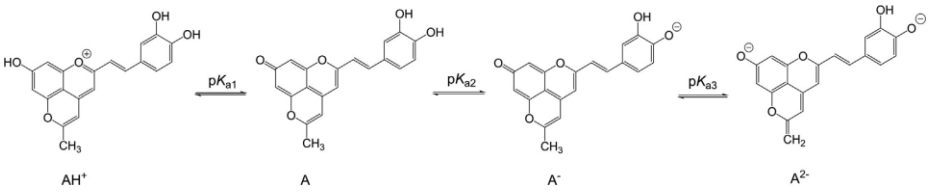


Fig. 4. Chemical equilibria of compound **4** in water/ethanol 75:25 (v/v) between pH 2 and 12.

function of pH of the intermicellar aqueous phase (pH_w). The absorption maxima of the acid form AH^+ is very similar for all micellar systems (511, 512 and 515 nm to SDS, CTAB and Triton X-100, respectively). A slight difference was observed for species A, with λ_{max} = 520, 525 and 529 nm for CTAB, SDS and Triton X-100, respectively. The largest difference in absorption maxima was observed for species A^-, which in SDS is 582 nm, in CTAB is 604 nm and in Triton X-100 is 620 nm. A^{2-} species was only observed in solution of CTAB with λ_{max} = 668 nm at the pH range studied.

In comparison to the hydroalcoholic solution, the presence of surfactants promotes a bathochromic effect in the spectra since it induces a redshift of maximum absorption wavelength of each species in all micellar system. The bathochromic effect observed resulted from the interaction that are establish between the different micellar aggregates and the pigment [43]. In general, SDS is the only one that has a hyperchromic effect at the absorption maxima for all species in solution at different pH with the same pigment concentration. Conversely, in Triton X-100 and CTAB micelles the species revealed a lower absorbance (hypochromic effect) on their maximum wavelengths for all, except for the A^{2-} species in CTAB solution. The destabilization/stabilization of the different species in solution could be attributed mainly to two factors: micellar surface charge and structural differences on the surfactants used. In the case of SDS, the greater stabilization observed should result from the strong interaction between anionic charge of micelle and the cationic form of the pigment. On the other hand, the structural compatibility of the surfactant with the pigment could explain the stabilization of other forms. In CTAB, electrostatic repulsion of cationic micelle charge and cationic flavylium form contribute to the decrease of the absorbance. In the case of nonionic Triton X-100, the effect of charge is not considered, and the structure of the surfactant should not be compatible with the pigment resulting in the color destabilization.

The apparent pK_a values were determined for the three micellar systems according to the equations previously described. Figs. 6–8 showed the fitting obtained to the experimental absorbance values at different wavelengths as a function of pH_w as well as the values of the molar fractions of each species as a function of pH_w (2–11).

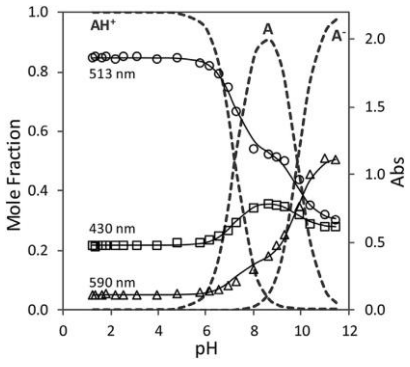


Fig. 6. Fitting was achieved for pK_{a1} = 6.8 ± 0.2 and pK_{a2} = 9.5 ± 0.2 for SDS micellar solution.

The apparent pKa values obtained in this work are resumed in Table 2. Analyzing the results obtained and comparing the apparent pK_a values of the micellar systems with those of the hydroalcoholic solution, it was observed that the pK_{a1} value is the same to the one determined in non-ionic surfactant, which means that this system has no effect in terms of the stabilization the AH^+ species, but the same did not occur for the SDS and CTAB micellar systems. Due to the negative charge character of SDS micelles, this system establishes electrostatic interactions with the positive charge of the AH^+ species, shifting its pK_a to much higher pH values. In contrast, CTAB, which possesses the same surface charge as the flavylium cation, destabilizes this species at lower pH values that results in a lower pK_{a1} value.

Both SDS and Triton X-100 had similar pK_{a2} values and higher to those obtained in hydroalcoholic solution. So, apparently Triton X-100 in solution makes the pigment retain a higher pK_{a2} value because of its neutral character and therefore tends to stabilize the non-ionic quinoidal base. On the other hand, SDS also tends to stabilize the non-ionic

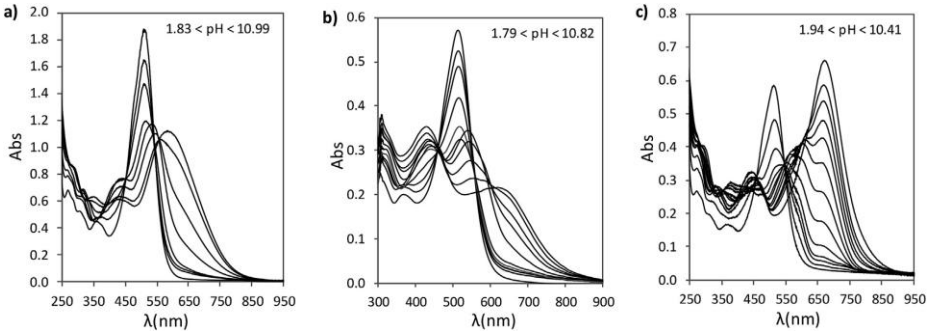


Fig. 5. Spectral variations as a function of pH of pigment in different micellar solution: (a) SDS in the pH range 1.83 < pH_w < 10.99; (b) Triton X-100 for 1.79 < pH_w < 10.82; (c) CTAB in the pH region 1.94 < pH_w < 10.41.

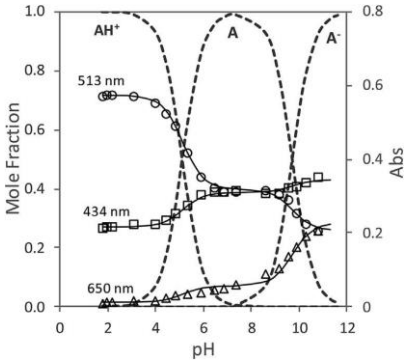


Fig. 7. Fitting was achieved for pK_{a1} = 5.1 ± 0.1 and pK_{a2} = 9.7 ± 0.1 for Triton X-100 micellar solution.

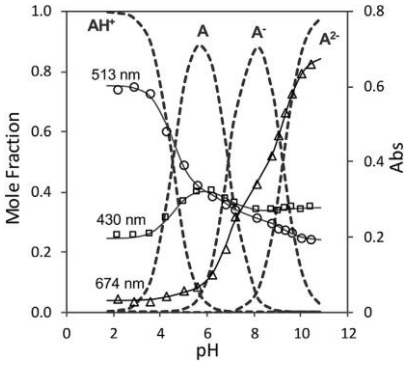


Fig. 8. Fitting was achieved for pK_{a1} = 4.5 ± 0.1, pK_{a2} = 6.9 ± 0.1 and pK_{a3} = 9.2 ± 0.1 for CTAB micellar solution.

Table 2
Summary of the apparent pK_a values obtained for compound **4** in presence and absence of surfactants.

		pK_{a1}	pK_{a2}	pK_{a3}
H_2O/EtOH (75:25)		5.1 ± 0.1	7.3 ± 0.2	11.3 ± 0.1
Micellar system	**SDS**	6.8 ± 0.2	9.5 ± 0.2	–
	TRITON X-100	5.1 ± 0.1	9.7 ± 0.1	–
	CTAB	4.5 ± 0.1	6.9 ± 0.1	9.2 ± 0.1

species instead of an anionic species due to electrostatic repulsion between the charges with the same signal for both (SDS and anionic species). The value of pK_{a2} for the CTAB solution was far below the values obtained in the other systems as well as the value obtained in hydroalcoholic solution. As expected, the surface positive charge of this micellar system stabilizes the oppositely charged species, namely A^- and A^2. Therefore, the third deprotonation was only observed in this system, since it is the only system that stabilizes the anionic species. The value of pK_{a3} was also lower in comparation with obtained in the absence of micellar system. Thus, it can be concluded that it was possible to modulate the reaction network of this pigment through the different micellar systems used in this work.

3.4. Study of the color stability of the species in solution with different micellar systems

The study of the color stability of the different species was performed in the presence and absence of the micellar system and the UV–Vis spectra were taken only after the system reach the thermodynamic equilibrium. This study did not include A^{2-} species because of its low relevance in the chemical equilibria in the systems used. The pH values were chosen based on the pH in which each species had major expression (X_i equal or close to 1) as it can be observed in the representation of the mole fractions as a function of pH (Figs. 3 and 6–8). The absorbance spectrum for all pH values were obtained over time from 0 to 48 h. The absorbance values taken at the maximum wavelength of each species in the different solution system were represented as a function of time (t = 0, 0.5, 1, 24, 48 h) (Figs. 9–11).

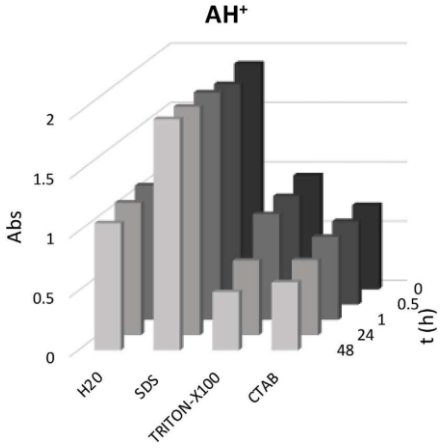


Fig. 9. Absorbance values obtained for species AH^+ over time for each system: H_2O/EtOH (75:25 (v/v)), λ_{max} = 496 nm, pH = 3.0; SDS, λ_{max} = 511 nm, pH_w = 3.2; Triton X-100, λ_{max} = 515 nm, pH_w = 3.0; CTAB, λ_{max} = 512 nm, pH_w = 2.6.

Fig. 9 showed the color behavior of the AH^+ species over time for the different systems. The color of this species is stable for the hydroalcoholic and SDS systems, remaining with the same absorbance over the studied time. In fact, this stability is expectable since the compound is stable at the lower pH values. In case of the SDS solution, in addition

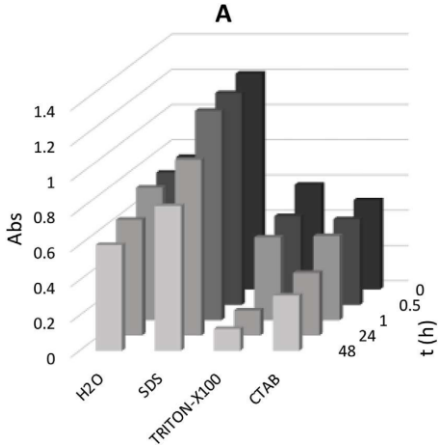


Fig. 10. Absorbance values obtained for species A over time for each system: H_2O/EtOH (75:25 (v/v)), λ_{max} = 505 nm, pH = 6.4; SDS, λ_{max} = 525 nm, pH_w = 8.5; Triton X-100, λ_{max} = 529 nm, pH_w = 7.0; CTAB, λ_{max} = 520 nm, pH_w = 5.4.

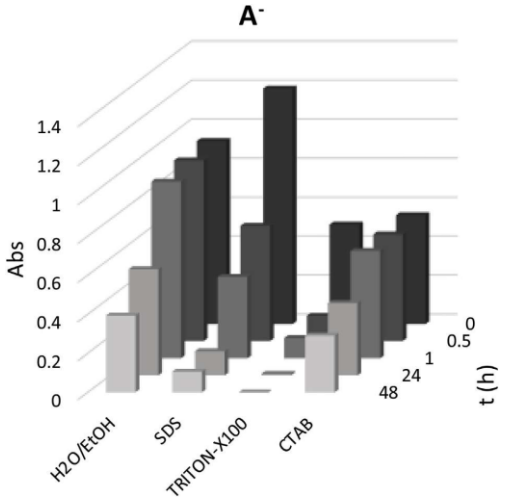


Fig. 11. Absorbance values obtained for species A^- over time for each system: H_2O/EtOH (75:25 (v/v)), λ_{max} = 536 nm, pH = 9.2; SDS, λ_{max} = 582 nm, pH_w = 10.9; Triton X-100, λ_{max} = 620 nm, pH_w = 10.5; CTAB, λ_{max} = 604 nm, pH_w = 8.1.

to this intrinsic stability, it is clearly the strong interaction of the cationic form of the compound with the anionic micelles by the increase of color intensity observed (Fig. 9). The largest color fade was observed for Triton X-100 which decreased its intensity to half after 48 h. CTAB was the micellar system that induces a lower color intensity of the AH^+ species but had only a slight fading after 48 h. This result was surprising because it would be expected that CTAB could cause a greater color loss with respect to Triton X-100, since CTAB tends to destabilize the AH^+ species, as it had previously seen.

The greatest stabilization of the non-ionic quinoidal base A over time was found to be in the hydroalcoholic solution (Fig. 10). The micellar solutions of SDS and CTAB induced a slight color fading, about 30%, due to their different surface charge with respect to the neutral A species. Contrary to expectations, the greatest color loss was observed for the Triton X-100 solution.

In relation to anionic quinoidal base, in general, there is a color fading in all systems (Fig. 11). This loss was practically total for SDS and Triton X-100 and more than 50% for the hydroalcoholic solution in 48 h. On the other hand, CTAB micellar system, could stabilize this species in relation to the others, although there was a decrease in 50% of its color after two days.

The behavior of the pigment in its different equilibrium forms in the SDS micellar system was very similar to the hydroalcoholic system during the studied period. It is known that for a long period of time, SDS tends to stabilize the acid form of anthocyanins [35,44,45]. CTAB was shown to have a more constant behavior for the different species, but the resulting color was less intense than in SDS and hydroalcoholic systems. Triton X-100 was shown to be the poorest system in terms of stabilization, leading to significant color losses of all species in solution after 48 h. This result showed that the structural compatibility of the Triton X-100 with the pigment should be low, as had already been seen above. This behavior might be probably due to the type of micellar aggregates that this surfactant could adopt in solution, since the polar region (responsible for the interaction with pyranoanthocyanins) is a long ethoxylated chain, unlike SDS and CTAB in which the polar head are small charged groups ($-SO_4^-$ and $-N(CH_3)_3^+$). The structure of the Triton X-100 micelles could not favor the immobilization of the pigment within the intermicellar phase.

4. Conclusions

A new pyrano-2-styrylbenzopyrylium compound with an extra double bond between the benzopyrylium and the phenyl system was synthesized, structurally characterized and its chromatic properties towards pH variation was studied in the presence and absence of model surfactants. In fact, the extension of the π conjugation makes the pigment to display a higher colorant capacity comparing with compound **5** already reported. The equilibrium multistate also changed, mainly in the value of the second deprotonation providing an extra color stabilization of the neutral quinoidal species.

The presence of the different micellar model-systems had also a significant influence in its equilibrium multistate. In fact, SDS revealed a greater increase of both pK_{a1} and pK_{a2}, CTAB had the opposite effects and Triton X-100 showed no significant effect on the color variation. This study allowed to conclude that the same pigment could have a greater color variation within a wide pH range. The modulation of the color might be very important for application of this kind of compounds as pH-colorimetric sensors in several disciplines.

Declarations of interest

None.

Conflicts of interest

The authors declare that they have no conflicts of interest.

Acknowledgments

The authors thank to Dr. Silvia Maia for the MS analysis and to Dr. Mariana Andrade for the NMR analysis. This research was supported by a research project grant (PTDC/OCE-ETA/31250/2017) with financial support from FCT/MEC through national funds and co-financed by FEDER, under the Partnership Agreement PT2020 (UID/QUI/50006/2013 – POCI/01/0145/FEDER/007265). Luís Cruz gratefully acknowledges FCT for his research contract. Vânia Gomes gratefully acknowledges the Ph.D. grant from FCT (SFRH/BD/136556/2018).

Appendix A. Supplementary data

Supplementary data to this article can be found online at https://doi.org/10.1016/j.dyepig.2019.04.004.



References

[1] Rentzsch M, Schwarz M, Winterhalter P. Pyranoanthocyanins - an overview on structures, occurrence, and pathways of formation. Trends Food Sci Technol 2007;18(10):526–34.
[2] Oliveira J, Mateus N, De Freitas V. Previous and recent advances in pyranoanthocyanins equilibria in aqueous solution. Dyes Pigments 2014;100(1):190–200.
[3] Cruz L, Borges E, Silva AMS, Mateus N, De Freitas V. Synthesis of a new (+)-catechin-derived compound: 8-vinylcatechin. Lett Org Chem 2008;5(7):530–6.
[4] Fulcrand H, Benabdeljalil C, Rigaud J, Cheynier V, Moutounet M. A new class of

wine pigments generated by reaction between pyruvic acid and grape anthocyanins. Phytochemistry 1998;47:1401–7.
[5] Bakker J, Bridle P, Honda T, Kuwano H, Saito N, Terahara N, et al. Identification of an anthocyanin occurring in some red wines. Phytochemistry 1997;44(7):1375–82.
[6] He J, Oliveira J, Silva AMS, Mateus N, De Freitas V. Oxovitisins: a new class of neutral pyranone-anthocyanin derivatives in red wines. J Agric Food Chem 2010;58(15):8814–9.
[7] He J, Santos-Buelga C, Silva AMS, Mateus N, De Freitas V. Isolation and structural characterization of new anthocyanin-derived yellow pigments in aged red wines. J Agric Food Chem 2006;54(25):9598–603.
[8] Mateus N, Silva AMS, Rivas-Gonzalo JC, Santos-Buelga C, De Freitas V. A new class of blue anthocyanin-derived pigments isolated from red wines. J Agric Food Chem 2003;51(7):1919–23.
[9] Oliveira J, Azevedo J, Silva AMS, Teixeira N, Cruz L, Mateus N, et al. Pyranoanthocyanin dimers: a new family of turquoise blue anthocyanin-derived pigments found in port wine. J Agric Food Chem 2010;58(8):5154–9.
[10] Cruz L, Teixeira N, Silva AMS, Mateus N, Borges J, De Freitas V. Role of vinylcatechin in the formation of pyranomalvidin-3-glucoside-(+)-catechin. J Agric Food Chem 2008;56(22):10980–7.
[11] Gómez-Alonso S, Blanco-Vega D, Gómez MV, Hermosín-Gutiérrez I. Synthesis, isolation, structure elucidation, and color properties of 10-Acetyl-pyranoanthocyanins. J Agric Food Chem 2012;60(49):12210–23.
[12] He J, Santos-Buelga C, Mateus N, De Freitas V. Isolation and quantification of oligomeric pyranoanthocyanin-flavanol pigments from red wines by combination of column chromatographic techniques. J Chromatogr A 2006;1134(1–2):215–25.
[13] Oliveira J, Mateus N, De Freitas V. Wine-inspired chemistry: anthocyanin transformations for a portfolio of natural colors. Synlett 2017;28(8):898–906.
[14] Chassaing S, Isorez G, Kueny-Stotz M, Brouillard R. En route to color-stable pyranoflavylium pigments—a systematic study of the reaction between 5-hydroxy-4-methylflavylium salts and aldehydes. Tetrahedron Lett 2008;49(49):6999–7004.
[15] Chassaing S, Isorez-Mahler G, Kueny-Stotz M, Brouillard R. Aged red wine pigments as a source of inspiration for organic synthesis - the cases of the color-stable pyranoflavylium and flavylium-(4- > 8)-flavan chromophores. Tetrahedron 2015;71(20):3066–78.
[16] Schwarz M, Winterhalter P. A novel synthetic route to substituted pyranoanthocyanins with unique colour properties. Tetrahedron Lett 2003;44(41):7583–7.
[17] Cruz L, Sousa JLC, Marinho A, Mateus N, de Freitas V. Synthesis and structural characterization of novel pyranoluteolinidin dyes. Tetrahedron Lett 2017;58:159–62.
[18] Sousa A, Araujo P, Mateus N, de Freitas V. Deoxyvitisins: a new set of pyrano-3-deoxyanthocyanidins. Tetrahedron Lett 2013;54(35):4785–8.
[19] Sousa JLC, Gomes V, Mateus N, Pina F, de Freitas V, Cruz L. Synthesis and equilibrium multistate of new pyrano-3-deoxyanthocyanin-type pigments in aqueous solutions. Tetrahedron 2017;73(41):6021–30.
[20] Oliveira J, Araújo P, Fernandes A, Mateus N, de Freitas V. Synthesis and structural characterization of amino-based pyranoanthocyanins with extended electronic delocalization. Synlett 2016;27(17):2459–62.
[21] Azevedo J, Oliveira J, Cruz L, Teixeira N, Brás NF, De Freitas V, et al. Antioxidant features of red wine pyranoanthocyanins: experimental and theoretical approaches. J Agric Food Chem 2014;62(29):7002–9.
[22] Cruz L, Petrov V, Teixeira N, Mateus N, Pina F, De Freitas V. Establishment of the chemical equilibria of different types of pyranoanthocyanins in aqueous solutions: evidence for the formation of aggregation in pyranomalvidin-3-O-coumaroylglucoside-(+)-catechin. J Phys Chem B 2010;114(41):13232–40.
[23] Sarni-Manchado P, Fulcrand H, Souquet JM, Cheynier V, Moutounet M. Stability and color of unreported wine anthocyanin-derived pigments. J Food Sci 1996;61(5):938–41.
[24] Santos CM, Oliveira J, Rocha S, Coelho M, Freitas V, Aguilar H. Pyranoflavylium derivatives extracted from wine grape as photosensitizers in solar cells. J Braz Chem Soc 2014;25(6):1029–35.
[25] Gomes V, Mateus N, de Freitas V, Cruz L. Synthesis and structural characterization of a novel symmetrical 2,10-bis-styryl-1-benzopyrylium dye. Synlett 2018;14(10):1390–4.
[26] Buck JS, Heilbron IM. CXLIV.-Benzopyrylium salts of distyryl ketones. Part I. J Chem Soc Trans 1922;121(0):1198–212.
[27] Amic D, Trinajstic N, Davidovic-Amic D. Experimental and theoretical study of the styrylbenzopyrylium chromophore. J. Chem. Soc. Perkin Trans. 1992;2(11):1933–8.
[28] Diniz AM, Gomes R, Parola AJ, Laia CAT, Pina F. Photochemistry of 7-Hydroxy-2-(4-hydroxystyryl)-1-benzopyrylium and related compounds. J Phys Chem B 2009;113(3):719–27.
[29] Gomes R, Diniz AM, Jesus A, Parola AJ, Pina F. The synthesis and reaction network of 2-styryl-1-benzopyrylium salts: an unexploited class of potential colorants. Dyes Pigments 2009;81(1):69–79.
[30] Petrov V, Jorge Parola A, Pina F. Isomerization between 2-(2,4-dihydroxystyryl)-1-benzopyrylium and 7-hydroxy-2-(4-hydroxystyryl)-1-benzopyrylium. J. Phys. Chem., A 2012;116(31):8107–18.
[31] Küster WF, Thiel A. Tabelle per le analisi chimiche e chimico-fisiche. 12 ed. 1982. Hoepli: Milano.
[32] Katritzky AR, Czerney P, Levell JR, Du W. Molecular engineering of benzo[b]pyrylium salts by indirect electrophilic substitution. Eur J Org Chem 1998;1998(11):2623–9.
[33] Pratt DD, Robinson R. CLXXXVIII.-A synthesis of pyrylium salts of anthocyanidin type. J Chem Soc Trans 1922;121(0):1577–85.
[34] Lima JC, Vautier-Giongo C, Lopes A, Melo E, Quina FH, Macanita AL. Color stabilization of anthocyanins: effect of SDS micelles on the acid-base and hydration kinetics of malvidin 3-glucoside (Oenin). J Phys Chem, A 2002;106(24):5851–9.
[35] Vautier-Giongo C, Yihwa C, Moreira PF, Lima JC, Freitas AA, Alves M, et al. Manipulation of the reactivity of a synthetic anthocyanin analogue in aqueous micellar media. Langmuir 2002;18(26):10109–15.
[36] Oliveira J, Mateus N, de Freitas V. Network of carboxypyranomalvidin-3-O-glucoside (vitisin A) equilibrium forms in aqueous solution. Tetrahedron Lett 2013;54(37):5106–10.
[37] Oliveira J, Mateus N, Silva AMS, De Freitas V. Equilibrium forms of vitisin B pigments in an aqueous system studied by NMR and visible spectroscopy. J Phys Chem B 2009;113(32):11352–8.
[38] Oliveira J, Petrov V, Parola AJ, Pina F, Azevedo J, Teixeira N, et al. Chemical behavior of methylpyranomalvidin-3-O-glucoside in aqueous solution studied by NMR and UV-Visible spectroscopy. J Phys Chem B 2011;115(6):1538–45.
[39] McClelland RA, McGall GH. Hydration of the flavylium ion. 2. The 4'-hydroxyflavylium ion. J Org Chem 1982;47(19):3730–6.
[40] Pina F, Melo MJ, Ballardini R, Flamigni L, Maestri M. Flash photolysis of 4',7-dihydroxyflavylium perchlorate. New J Chem 1997;21(9):969–76.
[41] Pina F, Melo MJ, Parola AJ, Maestri M, Balzani V. pH-controlled photochromism of hydroxyflavylium ions. Chem Eur J 1998;4(10):2001–7.
[42] Pina F, Roque A, Melo MJ, Maestri I, Belladelli L, Balzani V. Multistate/multifunctional molecular-level systems: light and pH switching between the various forms of a synthetic flavylium salt. Chem Eur J 1998;4(7):1184–91.
[43] Cruz LsM, Basílio NM, de Freitas VA, Lima JoC, Pina FJ. Extending the study of the 6,8 rearrangement in flavylium compounds to higher pH values: interconversion between 6-bromo and 8-Bromo-apigeninidin. ChemistryOpen 2016;5(3):236–46.
[44] Mendoza J, Pina F, Basílio N, Guimarães M, de Freitas V, Cruz L. Extending the stability of red and blue colors of malvidin-3-glucoside-lipophilic derivatives in the presence of SDS micelles. Dyes Pigments 2018;151:321–6.
[45] Lima JC, Vautier-Giongo C, Lopes A, Melo E, Quina FH, Maçanita AL. Color stabilization of anthocyanins: effect of SDS micelles on the acid-base and hydration kinetics of malvidin 3-glucoside (Oenin). J Phys Chem A 2002;106(24):5851–9.

Supporting Information

Synthesis and chemical equilibria of a new 10-methylpyrano-2-styryl-1-benzopyrylium pigment in aqueous solution and its modulation by different micellar systems

Vânia Gomes, Nuno Mateus, Victor de Freitas, Luís Cruz*

REQUIMTE/LAQV, Department of Chemistry and Biochemistry, Faculty of Sciences, University of Porto, Rua do Campo Alegre, 4169-007 Porto, Portugal

*luis.cruz@fc.up.pt

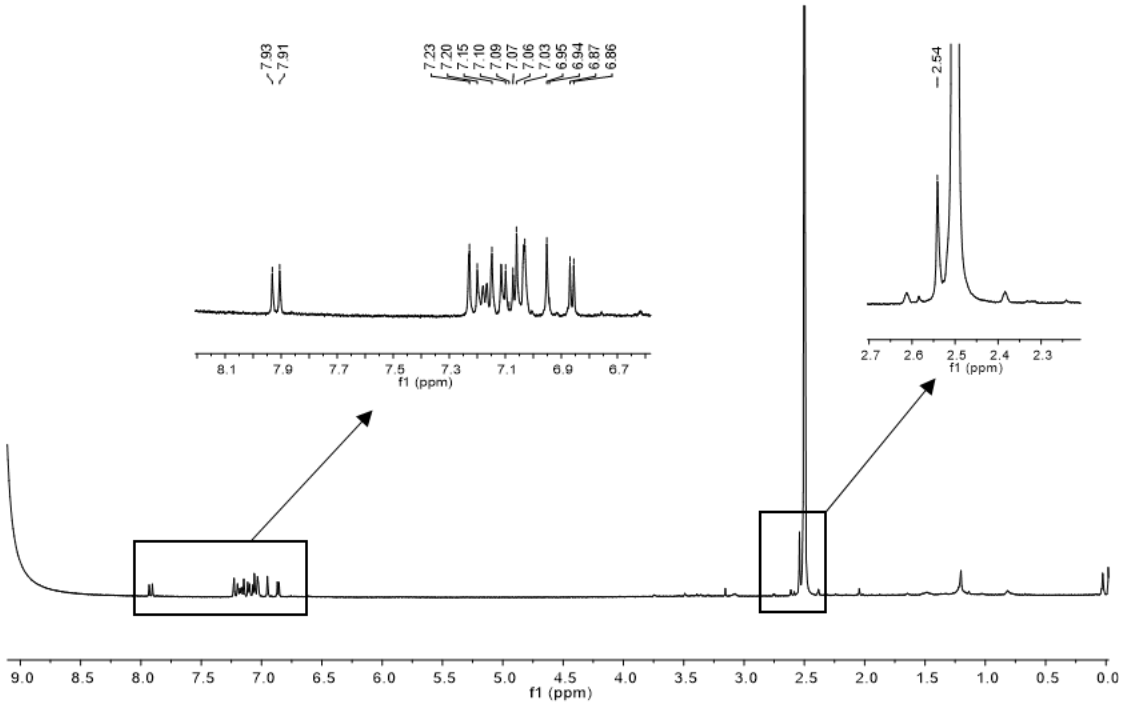


Figure 1. ^{1}H NMR (600 MHz) spectrum of the compound **4** in DMSO/TFA (9:1).

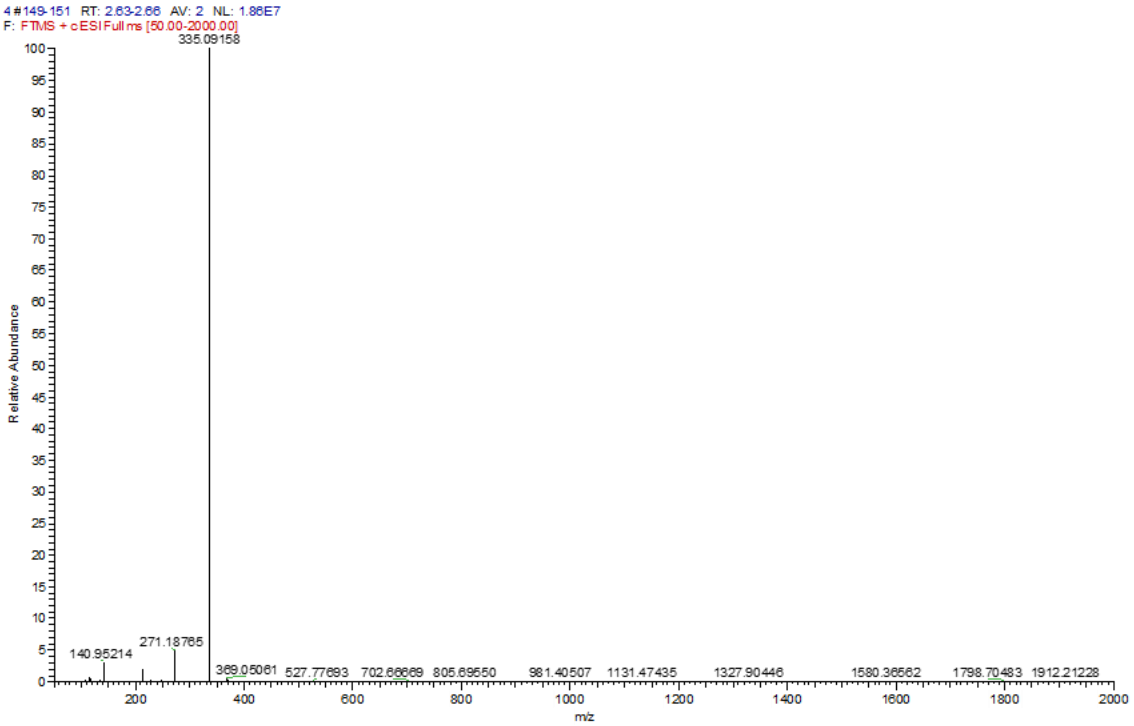


Figure 2. The HRMS (ESI) of compound **4.**

Article II

A pH-responsive fluorescent sensor based on a new pyranoxanthylium salt

Vânia Gomes, Nuno Mateus, Victor de Freitas, Luís Cruz

REQUIMTE/LAQV, Departamento de Química e Bioquímica, Faculdade de Ciências, Universidade do Porto, Rua Do Campo Alegre, 687, 4169-007, Porto, Portugal

---

Gomes V., Mateus N., de Freitas V., Cruz L., A pH-responsive fluorescent sensor based on a new pyranoxanthylium salt. *Photochemical and Photobiological Sciences*, **2021**, 20(4), 513-521.

DOI https://doi.org/10.1007/s43630-021-00033-x

Photochemical & Photobiological Sciences (2021) 20:513–521
https://doi.org/10.1007/s43630-021-00033-x

ORIGINAL PAPERS

A pH-responsive fluorescent sensor based on a new pyranoxanthylium salt

Vânia Gomes[1] · Nuno Mateus[1] · Victor de Freitas[1] · Luís Cruz[1]

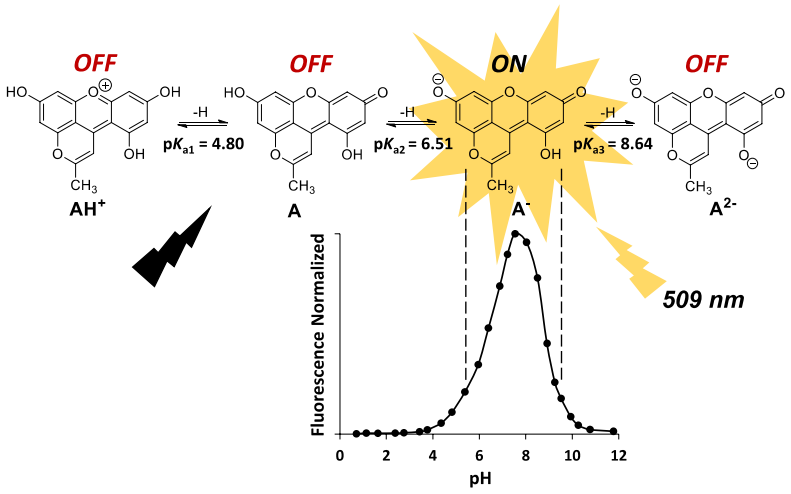
Received: 30 November 2020 / Accepted: 2 March 2021 / Published online: 10 March 2021
© The Author(s), under exclusive licence to European Photochemistry Association,European Society for Photobiology 2021

Abstract

Stimuli-responsive pigments are very interesting for several technological applications, such as food and cosmetic colorants, color-based sensors and fluorescence probes, among others. In this work, the synthesis of a new xanthylium-derived pigment was developed and the chemical and photophysical properties in hydroalcoholic solution at different pH values were investigated by UV–Vis and fluorescence spectroscopy. The UV–Vis titration of 3,6,8-trihydroxy-11-methylpyranoxanthylium has shown four different colored chemical species (AH^+, A, A^- and A^{2-}) in hydroalcoholic solution in a pH range between 1 and 12 with the thermodynamic acidic constants of $pK_{a1} = 4.80 \pm 0.03$, $pK_{a2} = 6.51 \pm 0.05$ and $pK_{a3} = 8.64 \pm 0.01$. Regarding fluorescence properties, this dye revealed an interesting pH-dependent emission behavior. In fact, the anionic quinoidal base A^- predominant at pH range between 5 and 9 should be mainly responsible for the pronounced fluorescence intensity observed at λ_{ex} 467 nm/λ_{em} 510 nm pair (maximum at pH 7.5). This set of new insights make this dye useful as a potential "off-on-off" pH-responsive fluorescent probe for biological applications.

Graphic abstract

A pyranoxanthylium dye was developed and revealed a selective fluorescence emission between $5 < pH < 9$, being maximum at pH 7.5, which make it very interesting as a pH-responsive "off-on-off" fluorescent probe for biomedical applications.



Keywords Fluorescent probes · pH-stimuli · Sensors · Thermodynamics · UV–Vis spectroscopy · Yellow dye

✉ Luís Cruz
luis.cruz@fc.up.pt

Extended author information available on the last page of the article

1 Introduction

For several decades, the scientific community has been dedicated to the study of natural or bioinspired pigments and dyes. This interest is obviously due to their fascinating chromatic properties which make them excellent candidates for several applications such as food and cosmetic colorants, color-based sensors and fluorescence probes, among others.

Xanthylium salts are yellow to brownish pigments that could be present in grape-derived foods, like juices and wines. In 1976, Timberlake and Bridle suggested for the first time the eventual formation of yellow xanthylium salts by the direct reaction between anthocyanins and phenolic compounds present in wine [1, 2]. Years later, a new xanthylium compound was discovered in a model wine solution during a wine color variation storage study [3, 4]. It is well known that the phenolic compounds present in wine undergo progressive transformations that affect sensorial properties like color, taste, and colloidal stability during conservation. One of these changes is the appearance of pigments that have high absorbance in the 400–500 nm visible region. A study from Es-Safi et al. showed that the formation of xanthylium salts could be responsible for this color variation [5]. Results from a study reported by Bührle et al. demonstrated that xanthylium derivatives play only a secondary role in coloration of white wine, as intermediate products in polymerization and browning [6].

In terms of structure–reactivity relationship, Dangles and Brouillard demonstrated that highly hydroxylated xanthylium salts (1,3,6,8-tetrahydroxylxanthylium cation) are more resistant towards nucleophiles than flavylium ions, and no significant xanthenol formation was verified from covalent hydration [7, 8]. Therefore, in contrast to anthocyanins (flavylium cation), the equilibrium multistate of this kind of xanthylium salts only depends on proton transfer reactions. The chemical equilibrium of a xanthylium salt towards pH variation was studied by Es-Safi (2004), and it showed that in relatively acidic pH, the pigment displayed an intense yellow color and a pink-reddish coloration for higher pH values [9].

On the other hand, xanthylium salts are cationic derivatives of xanthenes that have been extensively studied as fluorophores such as fluoresceins, rhodols and rhodamines. These compounds show interesting fluorescence properties, like high fluorescence quantum yields (close to 100%) and high molar absorption coefficients in the order of 100,000 $M^{-1}.cm^{-1}$ [10]. They are also well known for their pH-dependent emission spectra with pK_a values around the physiological pH, making them the most widely fluorescent indicators used for applications in molecular imaging and clinical diagnostics [11].

In the present work, the synthesis of a new pyranoxanthylium salt was achieved, and its chemical equilibrium and fluorescence properties in solution at different pH values were investigated. This new family of pigments could be potentially explored for different applications such as pH-sensors for food intelligent packaging, biomedical, and energy fields (e.g., dye-sensitive solar cells, fluorescent probes).

2 Material and methods

2.1 Reagents

All chemicals were obtained from Sigma-Aldrich (Madrid, Spain). Theorell and Stenhagen universal buffer was prepared by dissolving phosphoric acid (2.25 mL, 85% w/w), boric acid (3.54 g), monohydrated citric acid (7.00 g), and NaOH (343 mL, 1 M) solution diluted in distilled water until 1 L [12].

2.2 Synthesis

2.2.1 Synthesis of 1,3,6,8-tetrahydroxyxanthylium chloride (2)

2,4,6-dihydroxybenzaldehyde **1** (100 mg, 0.65 mmol) was dissolved in 3 mL of AcOEt/MeOH (2:1), and TMSCl (20 eq.) was added slowly to the solution. After one hour of stirring, 20 mL of the AcOEt was added to promote the precipitation of the desired compound. Dark orange solid (90 mg, 0.32 mmol) was obtained with a quantitative yield (98%). ^{1}H NMR (600.13 MHz, MeOD-d_4/TFA 9:1) δ 9.44 (s, 1H), 6.61 (s, 2H), 6.50 (s, 2H). ^{13}C NMR (125.77 MHz, MeOD-d_4/TFA 9:1) δ 174.49, 162.91, 159.94, 144.60, 110.83, 101.03, 96.14. The characterization of the compound is in agreement with data reported in literature [7, 13, 14].

2.2.2 Synthesis of 3,6,8-trihydroxy-11-methylpyranoxanthylium chloride (3)

Xanthylium compound **2** (90 mg, 0.32 mmol, 1 eq.) was dissolved in 100 mL (approximately 1 mg/mL) of hydroalcoholic solution (EtOH/H_2O 20:80 (v/v)) and a large excess of acetone (10 mL) was added to reaction. The reaction mixture was stirred at 37 °C for 24 h and the formation of the product was monitored by HPLC–DAD. The organic solvents were evaporated, and the reaction product was pre-purified by liquid–liquid extraction with acidified H_2O (200 mL) and AcOEt (4 × 50 mL). The organic phase was discarded, and the aqueous phase was concentrated for the chromatography purification.

The purification was carried out by column chromatography using C18 silica gel and acidified H_2O (with HCl 2%) with increasing percentages of methanol as eluent. The final product was isolated with MeOH 20–30% and a dark yellow solid (42 mg, 0.13 mmol) was obtained after lyophilization with 41% of yield. ^{1}H NMR (600.13 MHz, MeOD-d_4/TFA 9:1) δ 8.19 (s, 1H), 6.95 (d, J = 1.9 Hz, 1H), 6.92 (d, J = 2.0 Hz, 1H), 6.45 (d, J = 2.2 Hz, 1H), 6.41 (d, J = 2.2 Hz, 1H), 2.66 (s, 3H). ^{13}C NMR (125.77 MHz, MeOD-d_4/TFA 9:1) δ 174.29, 170.78, 168.79, 164.74, 159.72, 156.74, 153.94, 150.93, 107.03, 106.44, 101.54, 101.33, 101.30, 99.78, 97.37, 21.87. ESI–MS (MeOH) molecular formula $C_{16}H_{11}O_5^+$ requires $[M]^+$ 283.06; found, 283.33.

2.3 NMR spectroscopy

^{1}H NMR (600.13 MHz) and ^{13}C NMR (125.77 MHz) spectra were recorded on a Bruker-Avance 600 spectrometer at 303 K. The sample was prepared in MeOD-d_4/TFA (9:1). Chemical shifts were assigned using 2D NMR experiments (COSY, NOESY, *g*HMBC and *g*HSQC).

2.4 Mass spectrometry (ESI–MS)

Analyses were performed on a Finnigan LCQ (Finnigan Corp., San Jose, Calif., USA) mass detector and an API source using an electron spray ionization (ESI) interface. The capillary voltage was 4 V and the capillary temperature 275 °C. Spectra were recorded in positive ion mode between *m/z* 200 and 2000. The mass spectrometer was programmed to do a full scan mass (MS) and also a zoom scan of the most intense ion in the first scan (MS^2).

2.5 UV–Vis spectroscopy

Varian-Cary 100 Bio spectrophotometer was used to record all UV–Vis absorption spectra in the range of 200–800 nm with a 1-nm sampling interval. UV–Vis absorption spectra were recorded of pigment solutions at 25 °C using a quartz cell cuvette of 3.5 mL capacity and 1 cm of optical path.

2.6 Fluorescence spectroscopy

Fluorescence studies were carried out by a spectrofluorometer FluoroMax®-4 (HORIBA Scientific) in a QS high-precision cell made of quartz SUPRASIL with a length path of 3 mm (Hellma Analytics). The concentration of pigment solutions was defined to have absorbances equal or less than 0.1 at the excitation wavelength. All fluorescence spectra were corrected for the spectral response of the spectrofluorometer emission and excitation units. For all experiments, both excitation and emission slits consisted of a 4-nm bandpass. For the different experiments, a specific range of wavelengths was used for excitation and emission and reported in the results section. Fluorescence quantum yields (Φ_F) were determined using acridine orange in basic ethanol as a standard reference [15], according to the following equation:

$$\Phi_{fl,s} = \Phi_{fl,r} \times \frac{n_s^2}{n_r^2}\left(\frac{K_s}{K_r}\right), \quad (1)$$

where subscripts *r* and *s* denote reference and test sample, respectively,

Φ_{fl} is the fluorescence quantum yield, K is the slope of the integrated fluorescence intensity vs. absorbance plot, and n is the refractive index of the solvent. Measurements were performed by exciting all dye solutions at 385 nm.

2.7 pH measurements

All pH measurements were made in a Radiometer Copenhagen PHM240 pH/ion meter. pH values obtained in the hydroalcoholic solutions were defined as apparent pH values due to the presence of ethanol in solution.

2.8 Equilibrium constants

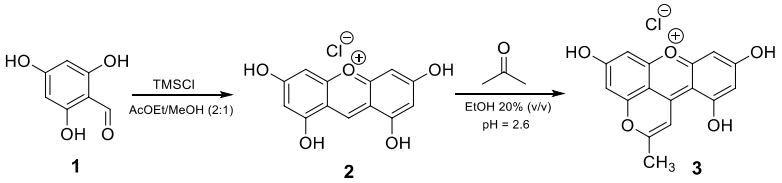
2.8.1 Determination by UV–Vis spectroscopy

The equilibrium constants (pK_a values) were determined by spectrophotometric titrations. Firstly, a stock solution of the pigment at 300 μM in EtOH:H_2O 75:25 (v/v) at HCl 0.1 M was prepared. In a quartz cuvette, it was subsequently added: 1 mL of NaOH solution (0.1 M), 1 mL of Theorell and Stenhagen universal buffer solution at pH 1, and 1 mL of stock solution of the pigment. The final concentration of pigment was 100 μM in EtOH:H_2O 25:75 (v/v). Increasing volumes of a NaOH solution (1 M) were added to the cell cuvette achieving different pH values. After each addition of the base, a UV–Vis spectrum was taken, and the final pH was measured. The final volumes were appropriately corrected. The pK_a values were fitted using the least-squares method and the Solver program from Microsoft Excel.

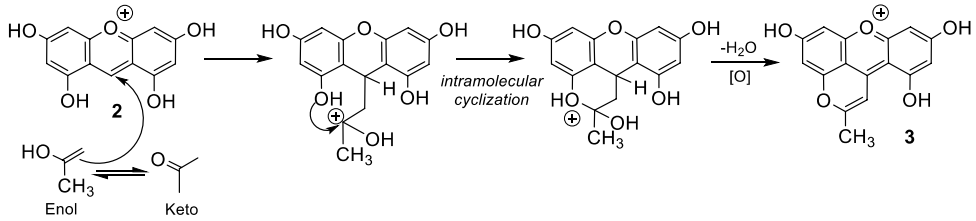
2.8.2 Determination by fluorescence spectroscopy

The equilibrium constants were also determined by fluorescence spectroscopy at different pH values (from 1 to 12). The experiment was carried out by adding a stock solution of pigment (15 μM) in EtOH:H_2O 75:25 (v/v) and HCl 0.1 M (0.3 mL) to a microtube containing a solution of NaOH 0.1 M (0.3 mL) and universal buffer of Theorell and Stenhagen (0.3 mL) at the desired pH. The final pH of the solutions of pigment (5 μM) in EtOH:H_2O 75:25 (v/v) was measured by pH meter. Emission spectra were obtained

Scheme 1 Strategy followed to obtain the pyranoxanthylium salt (**3**)



Scheme 2 A proposed mechanism for the formation of pyranoxanthylium (**3**)



for all solutions (0.1 mL) in a 3-mm fluorescence quartz cuvette, following the parameters presented in *1.5*. Different excitation/emission wavelength pairs were used for different experiments, which are described in the results section. The pK_a values were determined by fluorescence measurements at moderate acidic to neutral pH regions by regression analysis of the fluorescence data to fit Eq. (2) [16]:

$$\text{pH - p}Ka' = \log \frac{(F_{max} - F)}{(F - F_{min})}, \quad (2)$$

where F is the area under the corrected emission curve, F_{max} and F_{min} are maximum and minimum limiting values of F, respectively.

3 Results and discussion

3.1 Synthesis

The synthesis of the pyranoxanthylium salt (**3**) followed the procedure that is usually used for the synthesis of methylpyranoflavylium salts [17–20]. Primarily, the xanthylium compound (**2**) was obtained with a quantitative yield through an acid-catalyzed dimerization reaction of 2,4,6-trihydroxybenzaldehyde (**1**) in the presence of TMS-Cl to generate HCl in situ (Scheme 1). Compound (**2**) has been described already by Dangles and Brouillard [7, 14]. The pyranoxanthylium (**3**) resulted from the annelation reaction between the xanthylium salt and excess of acetone, involving C-5 and one of the hydroxyl groups of C-4 or C-6 of the xanthylium (**2**) and acetone in enolic form. The proposed mechanism for this reaction is similar to the one described for the formation of pyranoflavylium salts and is shown in Scheme 2 [21]. Product (**3**) was obtained with a yield of ca. 40%.

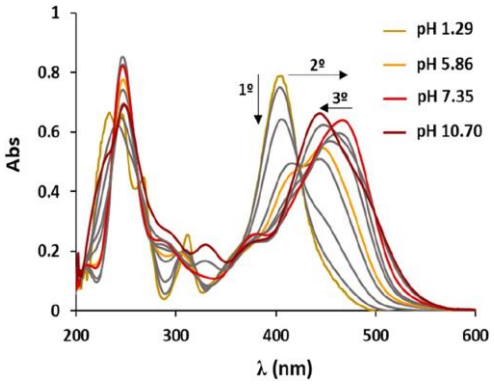


Fig. 1 UV–Vis spectra as a function of pH for pigment **3** at 100 µM in EtOH:H_2O 25:75 (v/v) in the pH range 1.29 < pH < 10.70. The first arrow indicates the decrease in absorbance at 404 nm. The second arrow indicates the bathochromic shift from 404 to 467 nm. The third arrow indicates the hypsochromic shift from 467 to 442 nm

3.2 Determination of equilibrium constants

3.2.1 UV–Vis spectroscopy

The chemical equilibrium constants (pK_a values) for compound **3** were determined by UV–Vis spectroscopic titrations. Problems with the total dissolution of the pigment in water have been overcome using a hydroethanolic solution (EtOH:H_2O 25:75 (v/v)). The UV–Vis spectra (Fig. 1) were obtained for the pH range between 1 and 12 by adding small volumes of NaOH. All pK_a values were defined as apparent

pK_a values because they were calculated using the apparent pH values. Actually, it was verified that these variations not influenced significantly the pK_a values since they were within the standard deviation range.

As previously mentioned, Dangles and Brouillard demonstrated that no significant xanthenol formation by hydration of xanthylium salts in an aqueous solution. Moreover, the presence of the new pyranic ring in the structure will also prevent the hydration as described for pyranoflavylium salts [22]. Therefore, it will be considered that the equilibria multistate of the pigment **3** in aqueous solution are based only on acid–base reactions. The first spectrum obtained at pH 1.29 shows a maximum absorption wavelength at 404 nm that corresponds to the xanthylium cation (AH^+). As the pH increases, the absorption at 404 nm decreases, and a new absorption maximum at 447 nm was observed at pH 5.86, with a bathochromic shift of 43 nm. Then, a bathochromic effect continues to occur until pH 7.35, with a new maximum absorbance at 467 nm. For even higher pH values, there is a hypsochromic shift of 25 nm and a new absorption maximum at 442 nm. Since the pigment has three hydroxyl groups, it is known that it can have four different species in solution depending on the pH, namely: xanthylium cation (AH^+), nonionic quinoidal base (A), and two anionic quinoidal bases (A^- and A^{2-}). Consequently, three pK_a values were achieved according to the fitting of the experimental absorbance values as a function of pH.

The global process can be accounted for by Eqs. (3) to (8) [23]:

$$AH^+ + H_2O \leftrightarrow A + H_3O^+ \quad K_{a1}, \tag{3}$$

$$A + H_2O \leftrightarrow A^- + H_3O^+ \quad K_{a2}, \tag{4}$$

$$A^- + H_2O \leftrightarrow A^{2-} + H_3O^+ \quad K_{a3}, \tag{5}$$

where

$$K_{a1} = \frac{[A] \cdot [H_3O^+]}{[AH^+]}, \tag{6}$$

$$K_{a2} = \frac{[A^-] \cdot [H_3O^+]}{[A]}, \tag{7}$$

$$K_{a3} = \frac{[A^{2-}] \cdot [H_3O^+]}{[A^-]}. \tag{8}$$

The total concentration of individual species, C_0, is given by Eq. (9):

$$C_0 = [AH^+]+[A]+[A^-]+[A^{2-}], \tag{9}$$

and the mole fraction distribution of the different species, χ_i, was calculated as follows:

$$\chi_{AH^+} = \frac{[AH^+]}{C_0} = \frac{1}{1+\frac{K_{a1}}{[H^+]}+\frac{K_{a2}K_{a1}}{[H^+]^2}+\frac{K_{a3}K_{a2}K_{a1}}{[H^+]^3}}, \tag{10}$$

$$\chi_{A} = \frac{[A]}{C_0} = \frac{K_{a1} \cdot \chi_{AH^+}}{[H^+]} \tag{11}$$

$$\chi_{A^{2-}} = \frac{[A^{2-}]}{C_0} = \frac{K_{a3} \cdot \chi_{A^-}}{[H^+]} \tag{12}$$

The fitting of the experimental data (absorbance in the function of pH) at a given wavelength by Eq. (14) allowed the achievement of the pK_a values.

$$Abs = \varepsilon_{AH^+} \cdot \chi_{AH^+} + \varepsilon_{A} \cdot \chi_{A} + \varepsilon_{A^-} \cdot \chi_{A^-} + \varepsilon_{A^{2-}} \cdot \chi_{A^{2-}}, \tag{14}$$

where $\varepsilon_{AH^+}, \varepsilon_{A}, \varepsilon_{A^-}, \varepsilon_{A^{2-}}$ are the mole absorption coefficients of the individual species or components at the considered wavelength.

The excellent fitting obtained for the experimental absorbance values at different wavelengths (404, 447, and 467 nm) as a function of pH confirming the presence of four different species in solution (Fig. 2). Thus, three equilibrium constants were determined with the following values: pK_{a1} = 4.80 ± 0.03, pK_{a2} = 6.51 ± 0.05 and pK_{a3} = 8.64 ± 0.01. Figure 2 also shows the values of the mole fractions of each species as a function of pH (2–11).

The first deprotonation of the AH^+ species (λ_{max} = 404 nm) gives rise to the neutral quinoidal base A (λ_{max} = 547 nm). The second and third deprotonations lead to the formation of the anionic A^- (λ_{max} = 467 nm) and dianionic A^{2-} (λ_{max} = 447 nm) quinoidal bases, respectively. Scheme 3 shows the proposed chemical equilibrium network of the four species with pH variation. The location

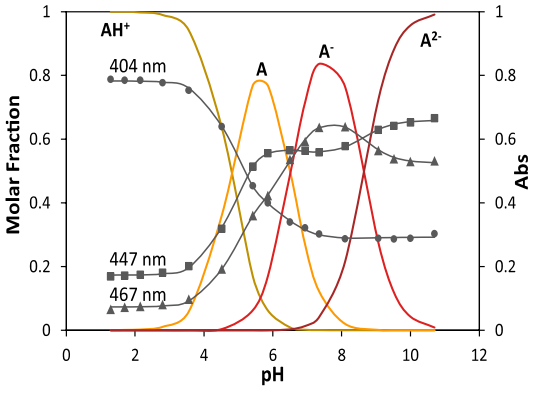
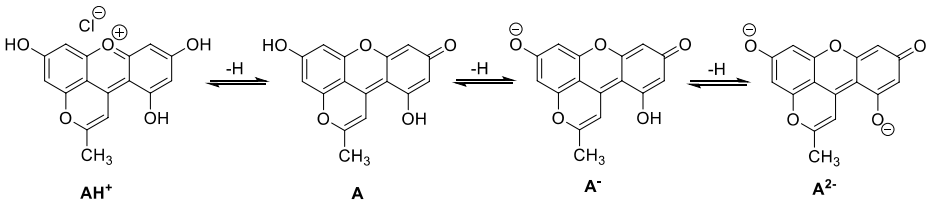


Fig. 2 Fitting achieved for pK_{a1} = 4.80 ± 0.03, pK_{a2} = 6.51 ± 0.05 and pK_{a3} = 8.64 ± 0.01 for pigment 3 at 100 µM in hydroalcoholic solution



Scheme 3 Hypothetical chemical equilibrium for species AH^+, A, A^- and A^{2-} of xanthylium salt (**3**) in solution

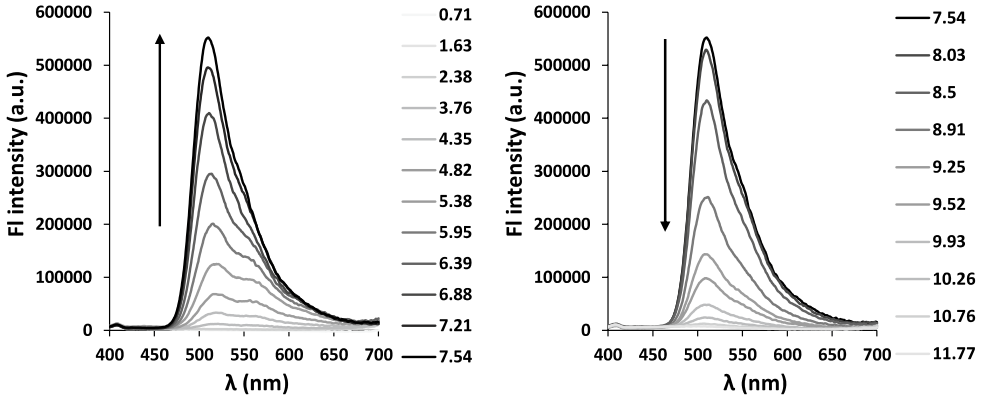


Fig. 3 Fluorescence emission spectra as a function of pH of the pigment **3** (5 μM) in the pH range 0.71 < pH < 11.77 at λ_{exc} = 360 nm in hydroalcoholic solution

(hydroxylic group) where each deprotonation occurred is still unknown.

3.3 Fluorescence study

Similarly to absorption spectroscopy, the determination of pK_a values by fluorescence was also done in 25% (v/v) ethanolic solutions of pigment **3** (5 μM) at different pH values. Fluorescence emission spectra were obtained by excitation at isosbestic point wavelength, $\lambda_{exc} = \lambda_{isosbestic} = 360$ nm. A single maximum emission at 510 nm was observed in the entire pH range studied (Fig. 3), and the higher intensity of emission spectra was around pH 7.54 (Fig. 4).

The pK'_a value obtained by regression analysis of the fluorescence data (Eq. (2)) was 6.37 ± 0.05, which corresponds to the pK_{a2} value determined by absorption spectroscopy (pK_{a2} = 6.51 ± 0.05). These values are similar, although the slightly different between them could be related with the different fitting methods used in each technique.

By analyzing the absorption and emission spectra at pH 7.5 (where fluorescence intensity is highest) (Fig. 5), the excitation/emission pair found was λ_{ex} 467 nm/λ_{em} 510 nm. The λ_{ex} 467 nm corresponds to the maximum wavelength of

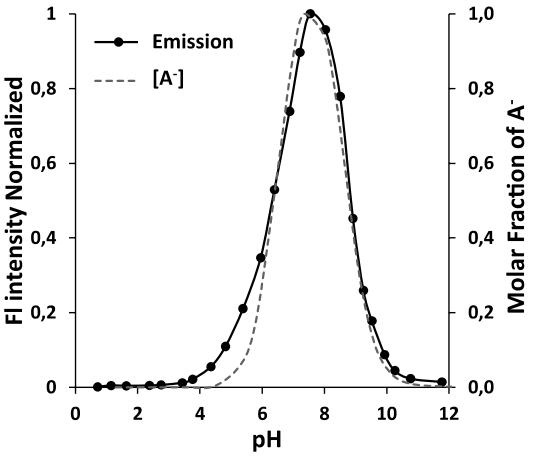


Fig. 4 Fluorescence intensity normalized as a function of pH of the **3** (5 μM) in the pH range 0.71 < pH < 11.77 at λ_{exc} = 360 nm in hydroalcoholic solution, and the molar fraction of A^- species determined by UV–Vis spectroscopy

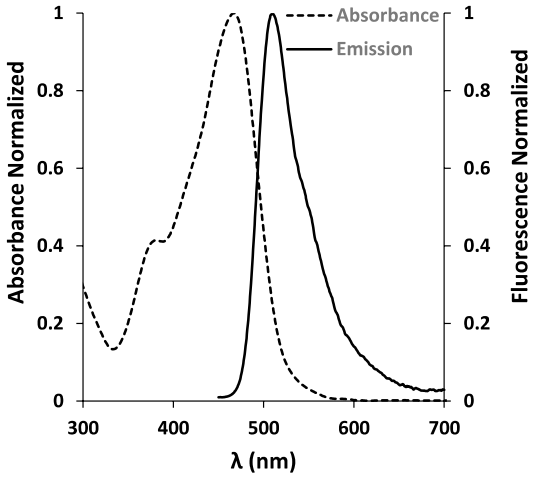


Fig. 5 Absorption and emission spectrum of pigment **3** at pH 7.5 in a hydroalcoholic solution (25% EtOH)

the monoanionic species (A^-) observed by UV–Vis spectroscopy (Fig. 2). Comparing the fluorescence emission curve at λ_{em} 509 nm and the molar fraction distribution of A^- species as a function of pH (Fig. 4), it is possible to observe that they perfectly fit. Therefore, it seems that the monoanionic species is the one in solution at the ground state responsible for the fluorescence.

In fact, A^- species showed intense fluorescence while AH^+, A and A^{2-} species do not, which is very interesting to act as switch-on and switch-off fluorescence sensor to different pH environment changes. This property makes pigment **3** an attractive fluorophore for use as "off-on-off" pH probe in biomedical applications. Indeed, physiological pH is generally between 4.5 and 7.4 (intracellular pH ~ 6.8, cytosol pH ~ 7.4, cell's acidic organelles pH ~ 4.5 and 6.0) [24], this pigment can be useful as a fluorescence probe to sensing pH changes within these ranges.

3.4 Photophysical properties

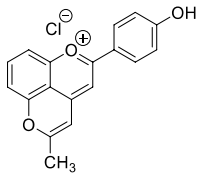
Fluorescence properties of the pigment were studied in hydroethanolic solution [EtOH:H_2O 25:75 (v/v)] at pH 7.5, namely stokes shifts ($\Delta\nu$), quantum yields (Φ_F) and absorption coefficient (ε). The last two parameters can be combined into a brightness/quantum efficient value ($QE_{max} = \varepsilon\Phi_F$) [25]. Figure 5 shows the absorption and emission spectra of pigment **3**, and photophysical parameters are presented in Table 1.

In terms of fluorescence quantum yields, $\boldsymbol{\Phi_F}$, this pigment does not show an impressively high value compared to conventional xanthene-derived fluorophores. However, when compared with a pyranoflavylium-type pigment studied in a previous work (Fig. 6, $\boldsymbol{\Phi_F} = 0.5\%$ at pH ≈ 3) [26], it reveals a tenfold higher fluorescence quantum yield. The main difference is the flavylium core instead of xanthylium. Moreover, the pyranoflavylium salt showed fluorescence at acidic pH values. This result confirmed that the structure, namely the presence of three conjugated aromatic rings, is very important for their fluorescence properties.

Table 1 Photophysical characterization of pigment **3** at pH 7.5 in EtOH 25% (v/v)

$\lambda_{max,abs}$ [nm]	ε (λ_{max}) [M^{-1} cm^{-1}]	$\lambda_{max,em}$ [nm]	Φ_F [%]	$\Delta\nu$ [cm^{-1}]	QE_{max} [M^{-1} cm^{-1}]
467	15,575	510	6	1767	779

Fig. 6 Structure of 4′-hydroxy-10-methylpyranoflavylium [22]



4 Conclusions

In this work, a new class of unexplored xanthylium derivatives was developed, and its chemical equilibrium constants and fluorescence properties were studied. The synthesis was successful following the usual procedure in the synthesis of pyranoflavylium salts. Three equilibrium constants of 3,6,8-trihydroxy-11-methylpyranoxanthylium in hydroalcoholic solution were achieved by absorption spectroscopy: $pK_{a1} = 4.80 \pm 0.03$, $pK_{a2} = 6.51 \pm 0.05$ and $pK_{a3} = 8.64 \pm 0.01$. By the fluorescence study, a single emission was observed entire pH range, with λ_{ex} 467 nm/λ_{em} 510 nm pair. The pK_a obtained from fluorescence was 6.37 ± 0.05, indicating the A^- species as the fluorescence species. The "off-on-off" fluorescence behavior and the pK'_a within neutral range make this pigment an interesting candidate as a pH-responsive fluorescent probe for several applications, namely in the biomedical field.

Supplementary Information The online version contains supplementary material available at https://doi.org/10.1007/s43630-021-00033-x.

Acknowledgements The authors thank Dr. Zélia Azevedo for the MS analysis and Dr. Mariana Andrade for the NMR analysis. This work was supported by the Associate Laboratory for Sustainable Chemistry, Clean Processes and Technologies LAQV. The latter is financed by national funds from UIDB/50006/2020. This research is supported by AgriFood XXI I&D&I project (NORTE-01-0145-FEDER-000041) cofinanced by European Regional Development Fund (ERDF), through the NORTE 2020 (Pro-grama Operacional Regional do Norte 2014/2020). This work was also supported by the project

PTDC/OCE-ETA/31250/2017 funded by FCT and FEDER. Luís Cruz acknowledges the FCT research contract and Vânia Gomes acknowledges the Ph.D. grant from FCT (SFRH/BD/136556/2018).

Author contributions VG: conceptualization, methodology, investigation, writing—original draft. NM: writing—review and editing. VF: writing—review and editing, project administration, funding acquisition. LC: conceptualization, methodology, investigation, writing—review and editing, project administration, funding acquisition.

Data availability All data generated or analyzed during this study are included in this published article [and its supplementary information files].

Declarations

Conflict of interest The authors declare no conflict of interest.

References

1. Timberlake, C. F., & Bridle, P. (1976). Interactions between anthocyanins, phenolic compounds, and acetaldehyde and their significance in red wines. *American Journal of Enology and Viticulture, 27*(3), 97–105.
2. Bakker, J., & Timberlake, C. F. (1997). Isolation, identification, and characterization of new color-stable anthocyanins occurring in some red wines. *Journal of Agricultural and Food Chemistry, 45*(1), 35–43. https://doi.org/10.1021/jf960252c
3. Es-Safi, N. E., Guernevé, C. L., Labarbe, B., Fulcrand, H., Cheynier, V., & Moutounet, M. (1999). Structure of a new xanthylium salt derivative. *Tetrahedron Letters, 40*(32), 5869–5872. https://doi.org/10.1016/S0040-4039(99)01156-9
4. Es-Safi, N. E., Le Guernevé, C., Fulcrand, H., Cheynier, V., & Moutounet, M. (1999). New polyphenolic compounds with xanthylium skeletons formed through reaction between (+)-catechin and glyoxylic acid. *Journal of Agricultural and Food Chemistry, 47*(12), 5211–5217. https://doi.org/10.1021/jf990424g
5. Es-Safi, N. E., Le Guernevé, C., Fulcrand, H., Cheynier, V., & Moutounet, M. (2000). Xanthylium salts formation involved in wine colour changes. *International Journal of Food Science and Technology, 35*(1), 63–74. https://doi.org/10.1046/j.1365-2621.2000.00339.x
6. Bührle, F., Gohl, A., & Weber, F. (2017). Impact of xanthylium derivatives on the color of white wine. *Molecules (Basel, Switzerland)*. https://doi.org/10.3390/molecules22081376
7. Dangles, O., & Brouillard, R. (1994). UV-visible spectroscopic investigation of the 1,3,6,8-tetrahydroxyxanthylium ion in aqueous solution: structural transformations and molecular complexation with cyclodextrins and caffeine. *New Journal of Chemistry, 18*(2), 288–296.
8. Brouillard, R., & Dangles, O. (1994). Anthocyanin molecular interactions: the first step in the formation of new pigments during wine aging? *Food Chemistry, 51*(4), 365–371. https://doi.org/10.1016/0308-8146(94)90187-2
9. Es-Safi, N. E. (2004). Colour of a xanthylium pigment in aqueous solutions at different pH values. *Food Chemistry, 88*(3), 367–372. https://doi.org/10.1016/j.foodchem.2004.01.049
10. Licha, K., & Resch-Genger, U. (2014). *Fluorescent Reporters and Optical Probes. Comprehensive Biomedical Physics* (Vol. 4). Elsevier B.V. https://doi.org/https://doi.org/10.1016/B978-0-444-53632-7.00402-0
11. Yin, J., Hu, Y., & Yoon, J. (2015). Fluorescent probes and bioimaging: Alkali metals, alkaline earth metals and pH. *Chemical Society Reviews. Royal Society of Chemistry*. https://doi.org/10.1039/c4cs00275j
12. Küster, F. W., Thiel, A., & Brückner, E. (1985). *Tabelle per le analisi chimiche e chimicofisiche*. Retrieved from https://books.google.co.uk/books?id=GWmOAAAACAAJ
13. Mora-Soumille, N., Al Bittar, S., Rosa, M., & Dangles, O. (2013). Analogs of anthocyanins with a 3′,4′-dihydroxy substitution: Synthesis and investigation of their acid-base, hydration, metal binding and hydrogen-donating properties in aqueous solution. *Dyes and Pigments*. https://doi.org/10.1016/j.dyepig.2012.07.006
14. Al Bittar, S., Mora, N., Loonis, M., & Dangles, O. (2016). A simple synthesis of 3-deoxyanthocyanidins and their O-glucosides. *Tetrahedron, 72*(29), 4294–4302. https://doi.org/10.1016/j.tet.2016.05.076
15. Taniguchi, M., & Lindsey, J. S. (2018). Database of absorption and fluorescence spectra of > 300 common compounds for use in PhotochemCAD. *Photochemistry and Photobiology, 94*(2), 290–327. https://doi.org/10.1111/php.12860
16. Chen, H., Lin, W., Jiang, W., Dong, B., Cui, H., & Tang, Y. (2015). Locked-flavylium fluorescent dyes with tunable emission wavelengths based on intramolecular charge transfer for multi-color ratiometric fluorescence imaging. *Chemical Communications, 51*(32), 6968–6971. https://doi.org/10.1039/c5cc01242b
17. Cruz, L., Sousa, J. L. C., Marinho, A., Maeteus, N., & de Freitas, V. (2017). Synthesis and structural characterization of novel pyranoluteolinidin dyes. *Tetrahedron Letters, 58,* 159–162. https://doi.org/10.3390/molecules181013111
18. Sousa, J. L. C., Gomes, V., Mateus, N., Pina, F., de Freitas, V., & Cruz, L. (2017). Synthesis and equilibrium multistate of new pyrano-3-deoxyanthocyanin-type pigments in aqueous solutions. *Tetrahedron, 73*(41), 6021–6030. https://doi.org/10.1016/j.tet.2017.08.051
19. Gomes, V., Mateus, N., Freitas, V. D., & Cruz, L. (2019). Synthesis and chemical equilibria of a new 10-methylpyrano-2-styrylbenzopyrylium pigment in aqueous solution and its modulation by different micellar systems. *Dyes and Pigments, 167,* 60–67. https://doi.org/10.1016/j.dyepig.2019.04.004
20. Gomes, V., & Gomes, V. (2019). Bioinspired synthesis and physical-chemical properties of a new 10-methylpyrano-4′-hydroxyflavylium chloride salt. *Synlett*. https://doi.org/10.1055/s-0039-1690744
21. De Freitas, V., & Mateus, N. (2011). Formation of pyranoanthocyanins in red wines: A new and diverse class of anthocyanin derivatives. *Analytical and Bioanalytical Chemistry, 401*(5), 1467–1477. https://doi.org/10.1007/s00216-010-4479-9
22. Oliveira, J., Mateus, N., & Freitas, V. D. (2014). Previous and recent advances in pyranoanthocyanins equilibria in aqueous solution. *Dyes and Pigments, 100,* 190–200. https://doi.org/10.1016/j.dyepig.2013.09.009
23. Cruz, L., Petrov, V., Teixeira, N., Mateus, N., Pina, F., & Freitas, V. D. (2010). Establishment of the chemical equilibria of different types of pyranoanthocyanins in aqueous solutions: Evidence for the formation of aggregation in pyranomalvidin-3-O-coumaroylglucoside-(+)-catechin. *Journal of Physical Chemistry B, 114*(41), 13232–13240. https://doi.org/10.1021/jp1045673
24. Johnson, I., & Spence, M. (Eds.). (2011). pH indicators. In *The Molecular Probes handbook. A guide to fluorescent probes and labeling technologies* (11th ed., pp. 882–902). https://doi.org/https://doi.org/10.1134/s0006297911110101
25. Cosco, E. D., Caram, J. R., Bruns, O. T., Franke, D., Day, R. A., Farr, E. P., Bawendi, M. G., & Sletten, E. M. (2017). Flavylium polymethine fluorophores for near- and shortwave infrared

imaging. *Angewandte Chemie International Edition, 56*(42), 13126–13129. https://doi.org/10.1002/anie.201706974
26. Gomes, V., Pires, A. S., Fernandes, I., Mateus, N., de Freitas, V., & Cruz, L. (2020). Synthesis of novel pyrano-3,7-deoxyanthocyanin derivatives and study of their thermodynamic, photophysical and cytotoxicity properties. *Photochemistry & Photobiology, A: Chemistry*, *Submitted*

Authors and Affiliations

Vânia Gomes[1] · Nuno Mateus[1] · Victor de Freitas[1] · Luís Cruz[1]

[1] REQUIMTE/LAQV, Departamento de Química e Bioquímica, Faculdade de Ciências, Universidade Do Porto, Rua Do Campo Alegre, 687, 4169-007 Porto, Portugal

Supporting Information

A pH-responsive fluorescent sensor based on a new pyranoxanthylium salt

Vânia Gomes, Nuno Mateus, Victor de Freitas, Luís Cruz*

REQUIMTE/LAQV, Departamento de Química e Bioquímica, Faculdade de Ciências, Universidade do Porto, Rua Do Campo Alegre, 687, 4169-007, Porto, Portugal

*Corresponding author: Luís Cruz: Tel.: +351 220402558; fax: +351 220402658.

Email address: luis.cruz@fc.up.pt

Characterization

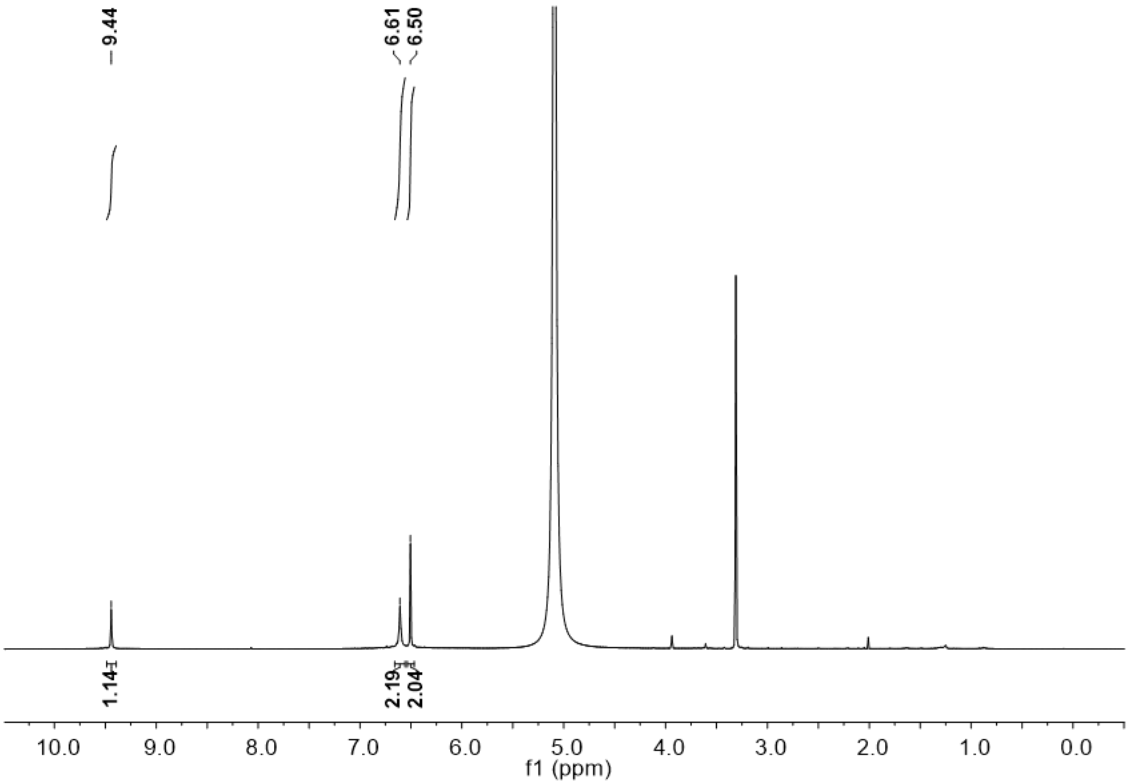


Figure 1. ^{1}H NMR (600.13 MHz) spectrum of 1,3,6,8-tetrahydroxyxanthylium chloride (**2**) in MeOD-d_4/TFA (9:1).

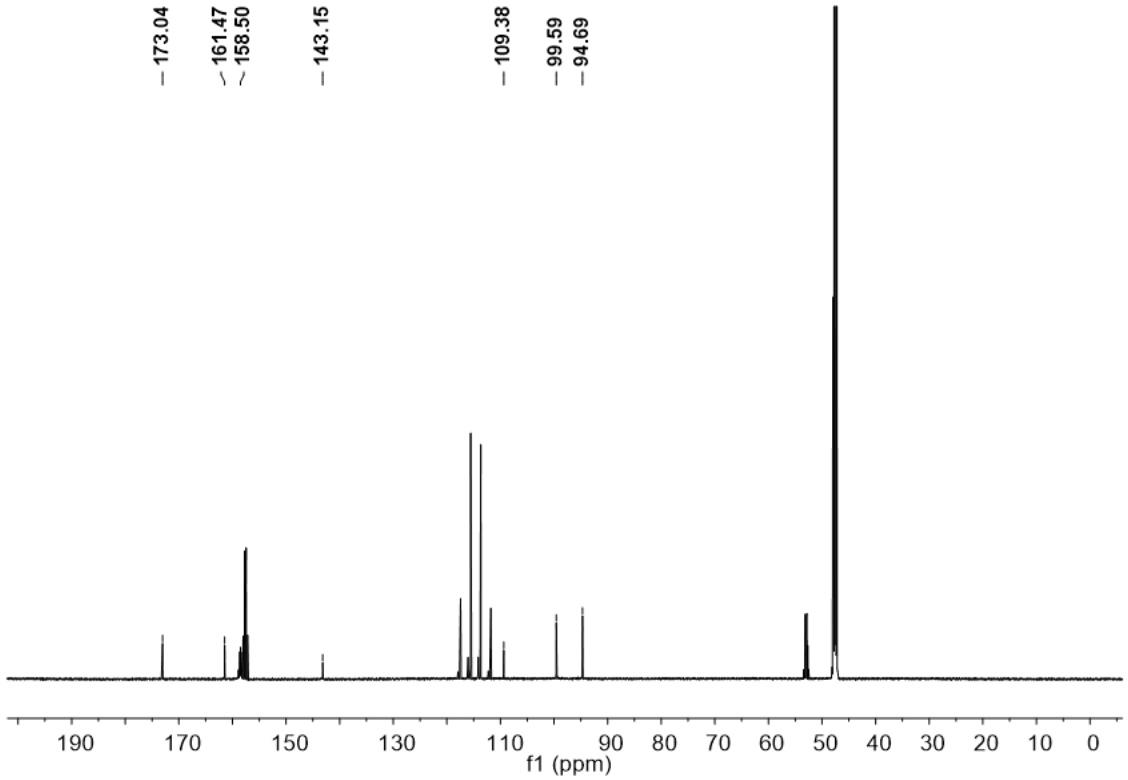


Figure 2. ^{13}C NMR (125.77 MHz) spectrum of 1,3,6,8-tetrahydroxyxanthylium chloride (**2**) in MeOD-*d*$_4$/TFA (9:1).

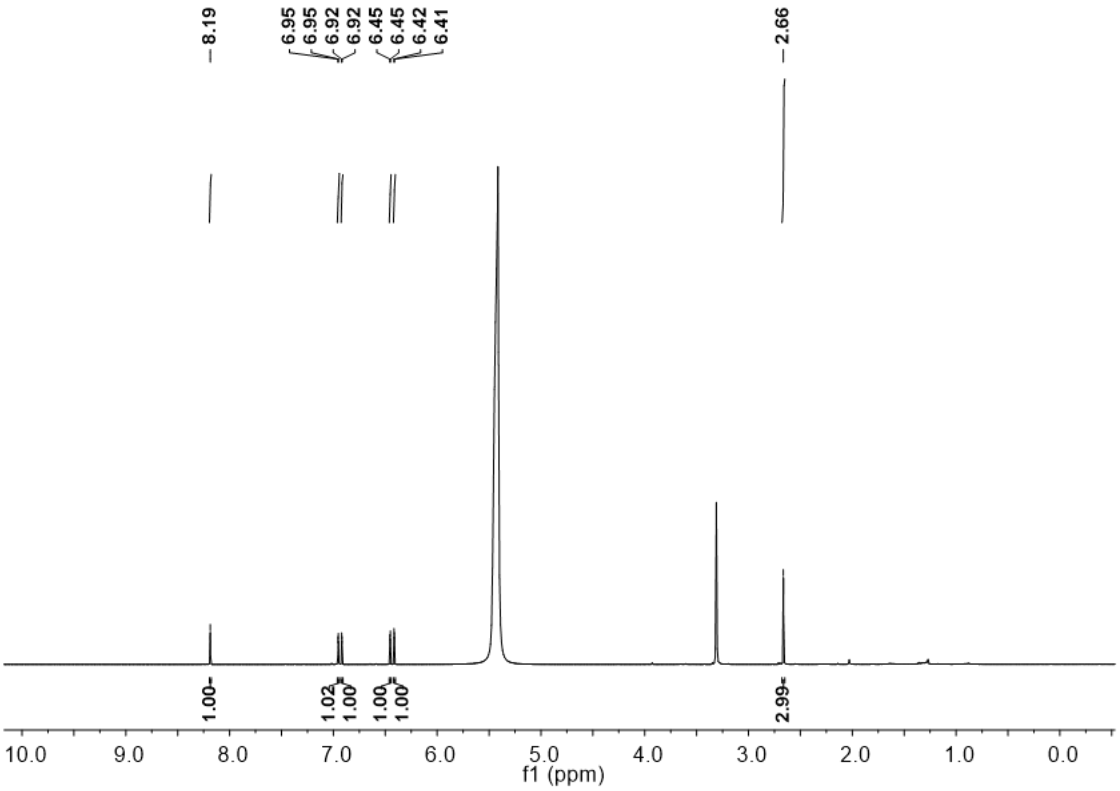


Figure 3. ^{1}H NMR (600.13 MHz) spectrum of 3,6,8-trihydroxy-11-methylpyranoxanthylium (**3**) in MeOD-*d*$_4$/TFA (9:1).

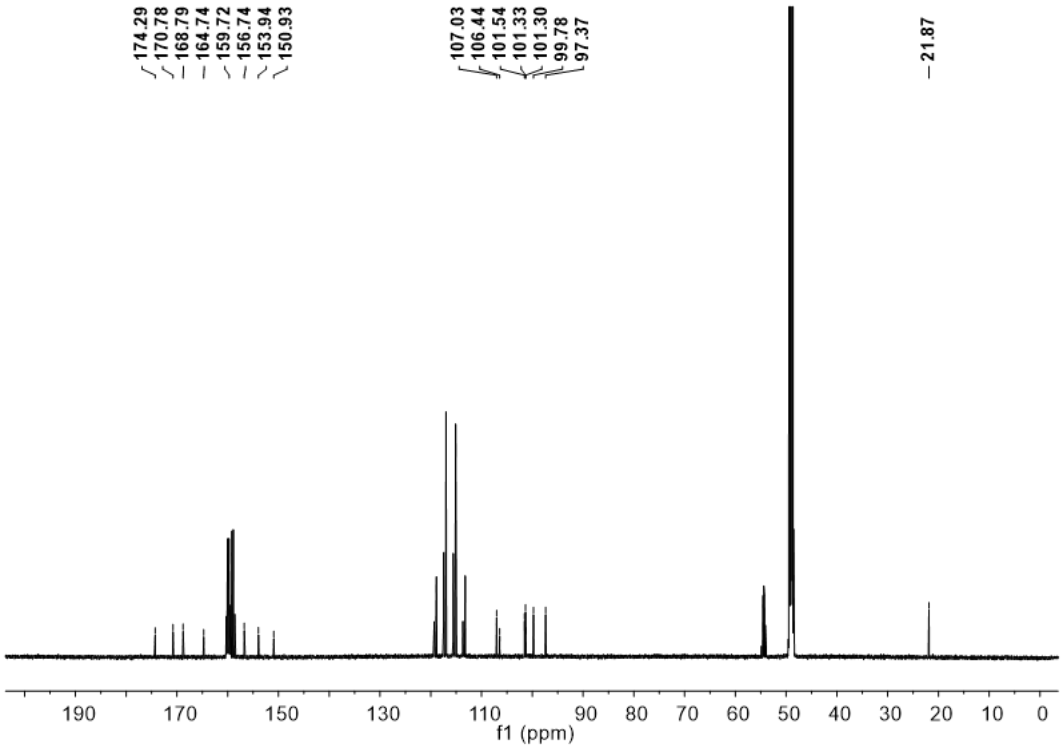


Figure 4. ^{13}C NMR (125.77 MHz) spectrum of 3,6,8-trihydroxy-11-methylpyranoxanthylium (**3**) in MeOD-*d*$_4$/TFA (9:1).

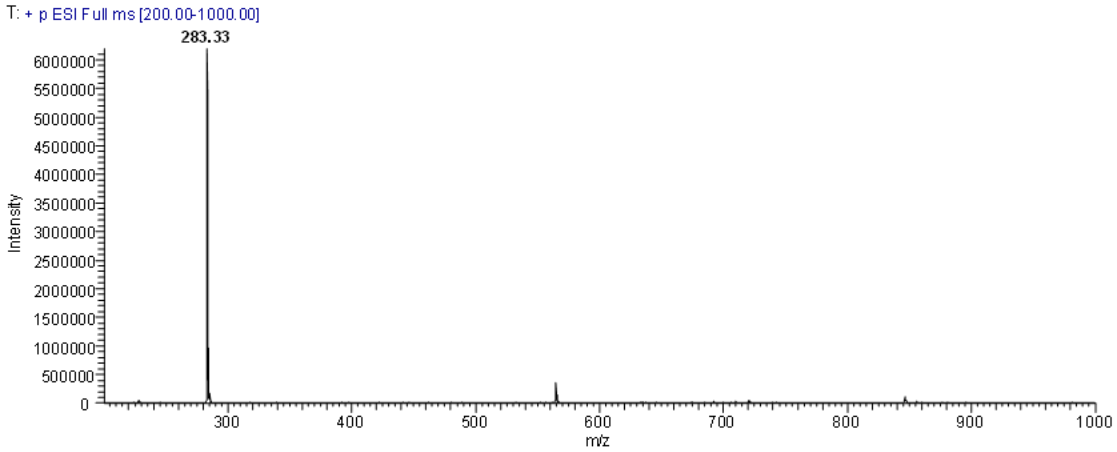


Figure 5. Full ESI-MS (MeOH) spectrum in positive ion mode of 3,6,8-trihydroxy-11-methylpyranoxanthylium (**3**).

Article III

Bio-inspired synthesis and physical-chemical properties of a new 10-methylpyrano-4'-hydroxyflavylium chloride salt

Vânia Gomes, Marta Guimarães, Gabriela Gonçalves, Victor de Freitas, and Luís Cruz

REQUIMTE/LAQV, Departamento de Química e Bioquímica, Faculdade de Ciências, Universidade do Porto, Rua Do Campo Alegre, 687, 4169-007, Porto, Portugal

Gomes, V., Guimarães, M., Gonçalves, G., de Freitas, V., Cruz, L., Bioinspired Synthesis and Physical-Chemical Properties of a New 10-Methylpyrano-4′-hydroxyflavylium Chloride Salt, *Synlett*, **2020**, 31(04), 334-338.

DOI 10.1055/s-0039-1690744

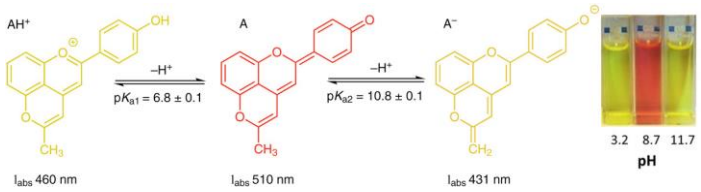
Synlett V. Gomes et al. Letter

Bioinspired Synthesis and Physical-Chemical Properties of a New 10-Methylpyrano-4′-hydroxyflavylium Chloride Salt

Vânia Gomes
Marta Guimarães
Gabriela Gonçalves
Victor de Freitas
Luís Cruz*

REQUIMTE/LAQV, Department of Chemistry and Biochemistry, Faculty of Sciences, University of Porto, Rua do Campo Alegre, 4169-007 Porto, Portugal
luis.cruz@fc.up.pt

Published as part of the Special Section
11th EuCheMS Organic Division Young Investigator Workshop



Received: 04.10.2019
Accepted after revision: 24.10.2019
Published online: 07.11.2019
DOI: 10.1055/s-0039-1690744; Art ID: st-2019-d0531-l

Abstract A novel bioinspired 10-methylpyranoflavylium dye was synthesized. The dye was fully characterized by LC-DAD/ESI-MS and NMR 1D and 2D techniques, and its equilibrium constants towards pH variations were determined by UV–vis titration. These studies revealed the presence of three species (a flavylium cation AH^+, a neutral quinoidal base A, and an anionic quinoidal base A^-) in the pH range 1–12, driven by the two pK_a values of the dye: pK_{a1} = 6.8 ± 0.1 and pK_{a2} = 10.8 ± 0.1. The first deprotonation of the dye occurs within the pH range for spoilage of many packed-food products, making the dye an excellent candidate for use as a pH sensor for real-time monitoring of the quality and freshness of foods.

Key words methylpyranohydroxyflavylium, dye, pH sensor, food chemistry

Flavylium-based dyes are a huge family of natural and synthetic pigments that include anthocyanins, 3-deoxyanthocyanins, and their derivatives, such as pyranoanthocyanins. Beyond their important biological properties (e.g., antioxidant and antiproliferative activities),[1] these dyes are responsible for the coloration of many flowers, vegetables, and fruits in shades ranging from yellow to violet. One of the most fascinating properties of all flavylium dyes is their pH-dependent chemical equilibrium network in aqueous solutions (Figure 1). At low pH values, the dyes are essentially present in a red cationic form **AH⁺** but, as the pH increases, the flavylium immediately undergoes a proton-transfer reaction leading to the formation of a violet quinoidal base **A** and, within a short timescale, the flavylium cation hydrates to give a colorless hemiketal $\mathbf{B_2}$. This species is in rapid equilibrium with a pale yellow *cis*-chalcone $\mathbf{C_c}$, which isomerizes slowly to a *trans*-chalcone $\mathbf{C_t}$.[2–4]

This amazing pH dependence makes flavylium dyes suitable for use as smart pH sensors in various fields; for example, in food packaging, they can be used to monitor food freshness and shelf life, since changes in pH are an important factor in the detection of spoilage of many food products. However, the use of the dyes in their native forms is somewhat limited because their color changes in the pH range for food spoilage (pH 5–7) are not very noticeable. To

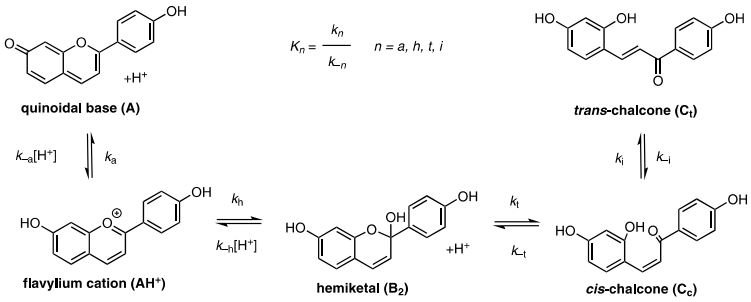


Figure 1 Equilibrium forms of flavylium-type compounds in aqueous solution

© 2019. Thieme. All rights reserved.
Georg Thieme Verlag KG, Rüdigerstraße 14, 70469 Stuttgart, Germany

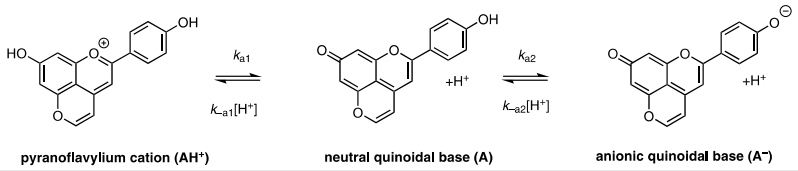
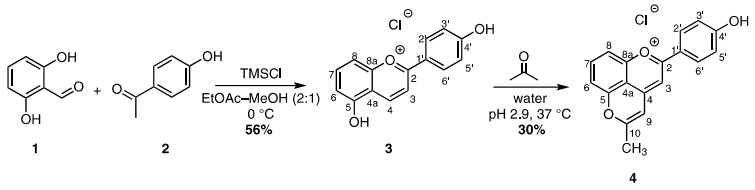


Figure 2 pH-dependent equilibria of pyranoflavylium salts



Scheme 1 Strategy for the synthesis of the 10-methylpyrano-4′-hydroxyflavylium chloride **4**

produce efficient pH sensors, the use of other flavylium derivatives, such as pyranoflavylium dyes, appears to be a promising alternative. In the last decade, the efforts of our research group have been dedicated to the synthesis, isolation, and characterization of natural and bioinspired pyranoflavylium-type dyes.[5–10] These pigments have much greater color stability over a wide pH range than their precursors, because the C-4 position of the C ring is blocked by the additional pyran ring. This prevents the hydration reaction and, thereby, the appearance of a colorless hemiketal form. Consequently, only acid–base reactions can take place,[11] giving rise to species that display various colors on changing the pH (Figure 2).

In this work, a novel bioinspired 10-methylpyrano-4′-hydroxyflavylium salt **4** (Scheme 1) was synthesized and structurally characterized, and its chromatic properties towards pH variations were evaluated. First, the flavylium precursor **3** was obtained by the acid-catalyzed aldol condensation of compounds **1** and **2**, using an excess of TMSCl to generate HCl *in situ*.[12,13] When pigment **3** was added to acetone–water (10:90 v:v) at pH 2.9 and 37 °C,[14] the pyranoflavylium salt **4** was formed through an annelation reaction involving the C-4 atom of the flavylium moiety, the hydroxy group at C-5, and the enolic form of acetone.[7,8,15–18] All compounds were analyzed by HPLC-DAD,[19] and fully characterized by LC-DAD/ESI-MS[20] in positive-ion mode (m/z = 239 and 277 for [M⁺] of pigments **3** and **4**, respectively) and by 1D- and 2D-NMR spectroscopy[21] (see Supporting Information).

To determine the thermodynamic constants of the pyranoflavylium salt **4**, we performed a UV–vis titration in a water–ethanol (75:25) mixture to avoid insolubility of the pigment, and a series of spectra were obtained in the pH range 1–12 by adding small volumes of 1 M aqueous NaOH.[22,23] As the pH increased, no clear evidence of the formation of hemiketal B_2 species was observed (no appearance of a band with an absorption at 280 nm). This does not exclude the formation of residual amounts of the hemiketal; however, this process can be neglected due to its small contribution, as already reported for similar pyranoanthocyanins.[7] Bearing this in mind, only protonation–deprotonation reactions need be included in the global process, through the Equations 1–3:

$$AH^+ + H_2O \leftrightarrow A + H_3O^+ \qquad K_{a1}$$

Equation 1

$$A + H_2O \leftrightarrow A^- + H_3O^+ \qquad K_{a2}$$

Equation 2

where

$$K_{a1} = \frac{[A].[H_3O^+]}{[AH^+]} \qquad K_{a2} = \frac{[A^-].[H_3O^+]}{[A]}$$

Equation 3

The total concentration of individual species, C_0, is given by Equation 4:

$$C_0 = [AH^+] + [A] + [A^-]$$

Equation 4

The mole-fraction distribution of the various species X_i was calculated as shown in Equations 5–7.

$$X_{AH^+} = \frac{[AH^+]}{C_0} = \frac{1}{1 + \frac{K_{a1}}{[H^+]} + \frac{K_{a2}K_{a1}}{[H^+]^2}}$$

Equation 5

© 2019. Thieme. All rights reserved.

C

$$\chi_{A}=\frac{[A]}{c_0}=\frac{K_{a1}\cdot\chi_{AH^+}}{[H^+]}$$

Equation 6

$$\chi_{A^-}=\frac{[A^-]}{c_0}=\frac{K_{a2}\cdot\chi_{A}}{[H^+]}$$

Equation 7

The experimental data (absorbance as a function of pH) at a given wavelength were fitted by using Equation 8.

$$A_{calc}=\varepsilon_{AH^+}\chi_{AH^+}+\varepsilon_{A}\cdot\chi_{A}+\varepsilon_{A^-}\cdot\chi_{A^-}$$

Equation 8

Here, ε_{AH}^{+}, ε_{A}, and ε_{A}^{-} are the molar absorption coefficients of the individual species or components at the specific wavelength.

The pK_a values were determined by fitting the experimental absorbance values as a function of pH with Equation 8 by using the Solver add-in program for Microsoft *Excel*. The difference between the squares of the theoretical and the experimental values was then minimized. Figure 3a shows the various spectra obtained for the pigment during titration from pH 1.5 to pH 12, and Figure 3b shows the fittings obtained by using three wavelengths (460, 478, and 510 nm), as well as the mole-fraction distributions of the species present, as functions of the pH. An optimized fitting between the experimental absorbance values and the theoretical values was obtained as a function of pH for the values pK_{a1} = 6.8 ± 0.1 and pK_{a2} = 10.8 ± 0.1.

Deprotonation of the AH^+ species (λ_{max} = 460 nm) occurred at the 4′-hydroxy group, giving rise to the neutral quinoidal base A (λ_{max} = 510 nm), whereas the second deprotonation was ascribed to loss of a proton from the methyl group at C-10, leading to the formation of the anionic quinoidal base A^- (λ_{max} = 431 nm), with consequential electron delocalization across the chromophore[17,24] (Figure 4).

Because of its structure, compound **4** shows excellent chromatic characteristics, rendering it suitable for use as a pH sensor for food packaging. In fact, because of the absence of a hydroxy group at C-7, a remarkable color change from yellow to red, driven by the first pK_a, occurs within the pH window of for spoilage of several packed-food products, such as meat or fish.[25,26] This dye is therefore potentially suitable for real-time monitoring and detection of spoilage in these types of foods.

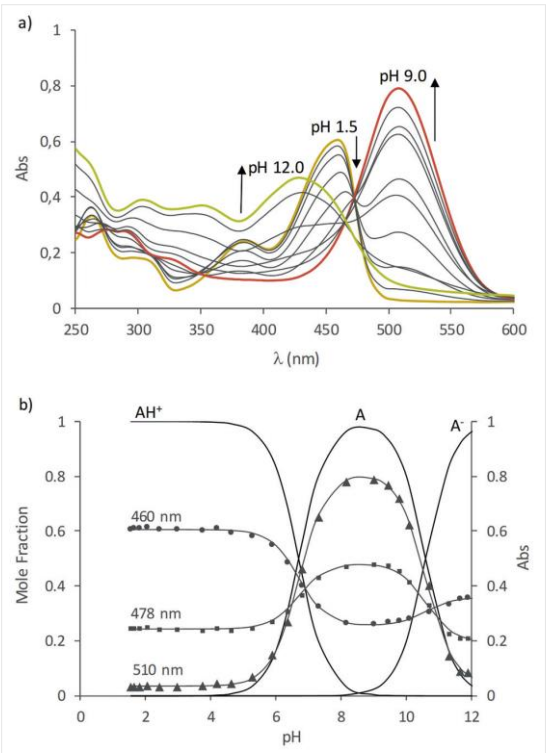


Figure 3 (a) Spectroscopic variations as a function of pH for pigment **4** in the pH range 1.55 < pH < 12.08. (b) Fitting achieved for pK_{a1} = 6.8 ± 0.1 and pK_{a2} = 10.8 ± 0.1 for an aqueous alcoholic solution.

Funding Information

This research was supported by a research project grant (PTDC/OCE-ETA/31250/2017) with financial support from FCT/MEC through national funds and was co-financed by FEDER under the Partnership

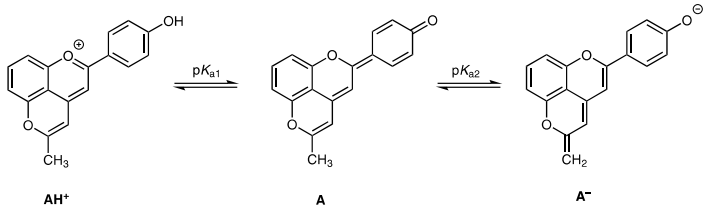


Figure 4 Equilibrium species of pigment **4** at pH values between 1.5 and 12

© 2019. Thieme. All rights reserved.

Agreement PT2020 (UID/QUI/50006/2019-POCI/01/0145/FERDER/007265, 2017). L.C. acknowledges an FCT research contract and V. G. acknowledges receipt of a Ph.D. grant from FCT (SFRH/BD/136556/2018).

Acknowledgment

The authors thank Dr. Zélia Azevedo for the MS analyses and Dr. Mariana Andrade for the NMR analyses.

Supporting Information

Supporting information for this article is available online at https://doi.org/10.1055/s-0039-1690744.

References and Notes

(1) Sousa, A.; Araújo, P.; Azevedo, J.; Cruz, L.; Fernandes, I.; Mateus, N.; de Freitas, V. *Food Chem.* **2016**, *192*, 142.
(2) Pina, F. *Recent Adv. Polyphenol Res.* **2014**, *4*, 341.
(3) Pina, F.; Melo, M. J.; Laia, C. A. T.; Parola, A. J.; Lima, J. C. *Chem. Soc. Rev.* **2012**, *41*, 869.
(4) Mendoza, J.; Basílio, N.; de Freitas, V.; Pina, F. *ACS Omega* **2019**, *4*, 12058.
(5) de Freitas, V.; Mateus, N. *Anal. Bioanal. Chem.* **2011**, *401*, 1463.
(6) Oliveira, J.; Azevedo, J.; Silva, A. M. S.; Teixeira, N.; Cruz, L.; Mateus, N.; de Freitas, V. *J. Agric. Food Chem.* **2010**, *58*, 5154.
(7) Cruz, L.; Petrov, V.; Teixeira, N.; Mateus, N.; Pina, F.; de Freitas, V. *J. Phys. Chem. B* **2010**, *114*, 13232.
(8) Cruz, L.; Sousa, J. L. C.; Marinho, A.; Mateus, N.; de Freitas, V. *Tetrahedron Lett.* **2017**, *58*, 159.
(9) Gomes, V.; Mateus, N.; de Freitas, V.; Cruz, L. *Synlett* **2018**, *29*, 1390.
(10) Pinto, A. L.; Cruz, L.; Gomes, V.; Cruz, H.; Calogero, G.; de Freitas, V.; Pina, F.; Parola, A. J.; Carlos Lima, J. *Dyes Pigm.* **2019**, *170*, 107577.
(11) Oliveira, J.; Mateus, N.; de Freitas, V. *Dyes Pigm.* **2014**, *100*, 190.
(12) Al Bittar, S.; Mora, N.; Loonis, M.; Dangles, O. *Tetrahedron* **2016**, *72*, 4294.
(13) **5-Hydroxy-2-(4-hydroxyphenyl)chromenium Chloride (3)**
2,6-Dihydroxybenzaldehyde (**1**; 204 mg, 1.48 mmol) and 4-hydroxyacetophenone (**2**; 1 equiv) were dissolved in 2:1 EtOAc–MeOH (5 mL), and the solution was cooled to 0 °C. TMSCl (20 equiv) was added, and the mixture was stirred for 60 min. The product was precipitated by addition of EtOAc, and the solid was collected by filtration and washed with Et_2O to give a dark-orange powder; yield: 227 mg (56%).
^{1}H NMR (600.13 MHz, 9:1 DMSO-d_6–TFA): δ = 9.29 (d, *J* = 9.1 Hz, 1 H, H4), 8.53 (d, *J* = 9.1 Hz, 1 H, H3), 8.50 (d, *J* = 8.8 Hz, 2 H, H2′, H6′), 8.00 (t, *J* = 8.3 Hz, 1 H, H7), 7.61 (d, *J* = 8.5 Hz, 1 H, H6 or H8), 7.20 (d, *J* = 8.1 Hz, 1 H, H6 or H8), 7.11 (d, *J* = 8.8 Hz, 2 H, H3′, H6′). ^{13}C NMR (125.77 MHz, 9:1 DMSO-d_6–TFA): δ = 174.3 (C2), 168.2 (C4′), 157.5 (C5 or C8a), 155.9 (C5 or C8a), 150.2 (C4), 140.2 (C7), 134.6 (C2′, C6′), 119.9 (C3′, C5′), 118.3 (C1′), 115.5 (C4a), 115.1 (C3), 113.3 (C6 or C8), 108.6 (C6 or C8). LC-DAD/ESI-MS: *m/z* = 239 [M]$^+$. UV–vis: λ_{max} = 440 nm.
(14) **2-(4-Hydroxyphenyl)-5-methylpyrano[4,3,2-*de*]chromen-1-ium Chloride (4)**
The dihydroxyflavylium chloride **3** (50 mg, 0.18 mmol) was dissolved in 10:90 acetone–H_2O, and the mixture was stirred at 37 °C and pH 2.9 for 3 d. The mixture was then extracted with Et_2O, and the aqueous fraction was purified by reverse-phase column chromatography [C_{18} silica gel, MeOH–H_2O (10:90) acidified with 2% HCl]. The solvent was evaporated, and the product was freeze dried to give a dark-orange powder; yield: 17 mg (30%).
^{1}H NMR (600.13 MHz, 9:1 DMSO-d_6–TFA): δ = 8.24 (d, *J* = 8.93 Hz, 2 H, H2′, H6′), 8.21 (t, *J* = 8.42 Hz, 1 H, H7), 7.88 (s, 1 H, H3), 7.87 or 7.73 (d, *J* = 4.21 Hz, 1 H, H8), 7.73 or 7.87 (d, *J* = 4.21 Hz, 1 H, H6), 7.09 (s, 1 H, H9), 7.06 (d, *J* = 8.90 Hz, 2 H, H3′, H5′), 2.65 (s, 3 H, CH_3). ^{13}C NMR (125.77 MHz, 9:1 DMSO-d_6–TFA): δ = 174.0 (C10), 170.0 (C2), 165.4 (C4′), 153.4 (C8a), 152.7 (C5), 137.4 (C7), 131.8 (C2′,C6′), 120.0 (C1′), 117.3 (C3′,C5′), 113.0 (C4a), 106.5 (C9), 102.4 (C3), 21.5 (CH_3). LC-DAD/ESI-MS: *m/z* = 277 [M$^+$]. UV–vis: λ_{max} = 460 nm.
(15) Cruz, L.; Teixeira, N.; Silva, A. M. S.; Mateus, N.; Borges, J.; de Freitas, V. *J. Agric. Food Chem.* **2008**, *56*, 10980.
(16) Oliveira, J.; de Freitas, V.; Mateus, N. *Tetrahedron Lett.* **2009**, *50*, 3933.
(17) Sousa, J. L. C.; Gomes, V.; Mateus, N.; Pina, F.; de Freitas, V.; Cruz, L. *Tetrahedron* **2017**, *73*, 6021.
(18) Cruz, L.; Borges, E.; Silva, A. M. S.; Mateus, N.; de Freitas, V. *Lett. Org. Chem.* **2008**, *5*, 530.
(19) HPLC-DAD analyses were performed on a Merck-Hitachi L-7100 apparatus with a 150 × 4.6 mm i.d. reverse-phase ODS C18 column (Merck, Darmstadt) at 25 °C. Detection was carried out using a L-7450A diode array detector (DAD). The eluents were A: H_2O–HCO_2H (9:1) and B: CH_3CN. The gradient consisted of 0–35% B for 50 min at a flow rate of 0.5 mL/min. The column was washed with 100% B over 10 min and then stabilized to the initial conditions during another 10 min.
(20) LC-DAD/ESI-MS: LC-DAD/ESI/MS analyses were performed on a Finnigan Surveyor series liquid chromatograph equipped with a Finnigan LCQ mass detector and an API source using an ESI interface. The samples were analyzed on a reverse-phase column (150 × 4.6 mm, 5 µm, C18) at 25 °C using the same eluents, gradients and flow rates as used for HPLC analysis (see Ref. 19). The capillary voltage was 4 V and the capillary temperature was 275 °C. Spectra were recorded in positive- and negative-ion modes between *m/z* = 120 and *m/z* = 1500. The mass spectrometer was programmed to carry out a series of three scans: a full mass scan, a zoom scan of the most intense ion in the first scan, and an MS–MS of the most intense ion using a relative collision energy of 30 and 60.
(21) The ^{1}H NMR (600.13 MHz) and ^{13}C NMR (125.77 MHz) spectra were recorded in 95:5 DMSO–TFA on a Bruker-Avance 600 spectrometer at 303 K, with TMS as an internal standard. ^{1}H chemical shifts were assigned by using 2D NMR (COSY, NOESY) experiments, whereas ^{13}C resonances were assigned by using 2D NMR techniques (gHMBC and gHSQC). The delay for the long-range C–H coupling constant was optimized to 7 Hz.
(22) **UV-Vis Titration**
A 0.3 mM pigment stock solution was prepared in 0.1 M HCl in 75:25 EtOH–H_2O. A quartz cell was charged with Teorell and Stenhagen universal buffer[23] at pH 1 (1 mL), 0.1 M aq NaOH (1 mL), and the pigment stock solution (1 mL). The final concentration of the pigment was 0.1 mM in 25% EtOH. Titrations were performed up to pH 12 by the addition of small volumes of 1 M aq NaOH. Successive spectra were recorded immediately after the addition of the base in a Thermo Scientific Evolution Array UV–Visible spectrophotometer at 25 °C. All titrations were performed in triplicate. Final volumes were appropriately corrected. All pH measurements were made with a Radiometer

© 2019. Thieme. All rights reserved.

Copenhagen PHM240 pH/ion meter. The fitting for pK_a determinations was carried out by using the Solver add-in program for Microsoft Excel.

(23) Teorell and Stenhagen universal buffer was prepared by dissolving phosphoric acid (2.25 mL, 85% w/w), boric acid (3.54 g), monohydrated citric acid (7.00 g), and 1 M aq NaOH (343 mL) in distilled water to a volume of 1 L.

(24) Gomes, V.; Mateus, N.; de Freitas, V.; Cruz, L. *Dyes Pigm.* **2019**, *167*, 60.

(25) Pacquit, A.; Frisby, J.; Diamond, D.; Lau, K. T.; Farrell, A.; Quilty, B.; Diamond, D. *Food Chem.* **2007**, *102*, 466.

(26) Zhang, X.; Lu, S.; Chen, X. *Sensors Actuators B: Chem.* **2014**, *198*, 268.

© 2019. Thieme. All rights reserved.

Supporting Information

Bio-inspired synthesis and physical-chemical properties of a new 10-methylpyrano-4'-hydroxyflavylium chloride salt

Vânia Gomes, Marta Guimarães, Gabriela Gonçalves, Victor de Freitas, Luís Cruz*

REQUIMTE/LAQV, Department of Chemistry and Biochemistry, Faculty of Sciences, University of Porto, Rua do Campo Alegre, 4169-007 Porto, Portugal

*luis.cruz@fc.up.pt

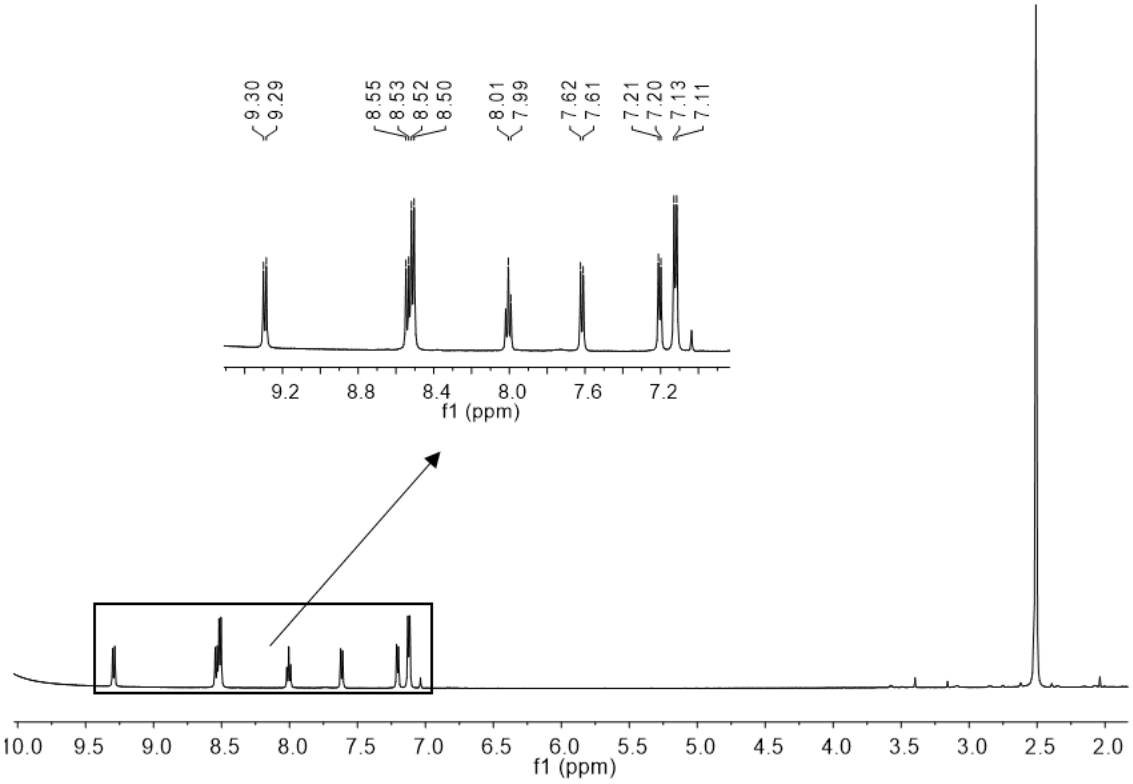


Figure 1. ^{1}H NMR (600 MHz) spectrum of the compound **3** in DMSO/TFA (9:1).

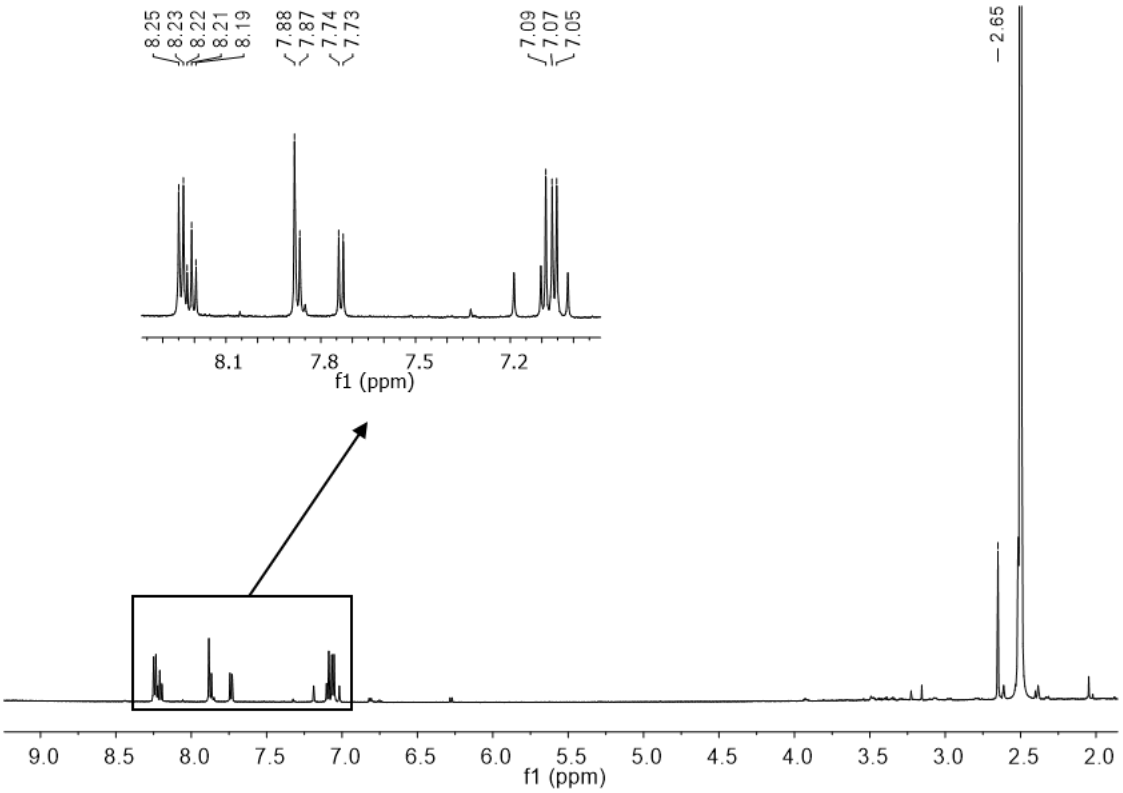


Figure 2. ^{1}H NMR (600 MHz) spectrum of the compound **4** in DMSO/TFA (9:1).

Article IV

Synthesis of novel pyrano-3,7-deoxyanthocyanin derivatives and study of their thermodynamic, photophysical and cytotoxicity properties

Vânia Gomes, Ana Sofia Pires, Iva Fernandes, Nuno Mateus, Victor de Freitas, Luís Cruz

REQUIMTE/LAQV, Departamento de Química e Bioquímica, Faculdade de Ciências, Universidade do Porto, Rua Do Campo Alegre, 687, 4169-007, Porto, Portugal

---

Gomes, V., Pires, A. P., Fernandes, I., Mateus, N., de Freitas, V, Cruz, L., Synthesis of novel pyrano-3,7-deoxyanthocyanin derivatives and study of their thermodynamic, photophysical and cytotoxicity properties, *Journal of Photochemistry and Photobiology A: Chemistry*, **2021**, 415, 113313.

DOI https://doi.org/10.1016/j.jphotochem.2021.113313

Journal of Photochemistry & Photobiology, A: Chemistry 415 (2021) 113313

Contents lists available at ScienceDirect

Journal of Photochemistry & Photobiology, A: Chemistry

journal homepage: www.elsevier.com/locate/jphotochem

Synthesis of novel pyrano-3,7-deoxyanthocyanin derivatives and study of their thermodynamic, photophysical and cytotoxicity properties

Vânia Gomes, Ana Sofia Pires, Iva Fernandes, Nuno Mateus, Victor de Freitas, Luís Cruz *

REQUIMTE/LAQV, Departamento de Química e Bioquímica, Faculdade de Ciências, Universidade do Porto, Rua Do Campo Alegre, 687, 4169-007, Porto, Portugal

ARTICLE INFO

Keywords:
Pyranoflavylium dyes
Fluorescence
UV-Vis
Acid dissociation constants
pH-sensors
Food packaging

ABSTRACT

Pyranoflavylium-derived compounds have been shown to have improved properties over the corresponding flavylium precursors, such as chemical and photochemical stability. In addition, they have the characteristic of responding to stimuli like pH due to the proton transfer reactions leading to different colored quinoidal bases. Thus, these dyes can be used as powerful pH-indicators for several sensing applications. In this work, the thermodynamic constants and photophysical properties of novel pyrano-3,7-deoxyanthocyanin dyes bearing phenol and catechol groups were studied by UV–vis absorbance and fluorescence measurements as a function of pH. The cytotoxicity properties of these compounds were also evaluated. Overall, the symmetrical phenol-based pyranoflavylium dye showed the greatest color variation within pH range of food spoilage process, remarkable fluorescence properties, and reduced cytotoxicity, which make it a promising candidate as a pH-dependent colorimetric and fluorescence sensor for food intelligent packaging.

1. Introduction

Flavylium (2-phenylbenzopyrylium) salts (Fig. 1) are an important class of natural and seminatural dyes that includes anthocyanins, anthocyanidins, and 3-deoxyanthocyanins. They are well known for their remarkable colors, antioxidant activity, photochemical properties, among others [1]. In general, they are composed of the same basic chromophore structure of 7-hydroxyflavylium cation, they can have hydroxyl substituents at C3 and C5 (some of them glycosylated), and the B-ring (2-phenyl) has one or more hydroxy or methoxy substituents [2]. Most natural flavylium compounds have a complex chemical equilibria network in an aqueous solution that involves proton transfer, hydration, tautomerization, and isomerization reactions, which have been well-described in the literature [3,4]. The proton transfer reaction plays a very important role in the chemical characteristics of these pigments, namely in color variation. This color variation results from the deprotonation of hydroxyl groups in the flavylium structure, leading to the formation of the quinoidal bases that exhibit a chromatic redshift relatively to the flavylium cation. The hydroxyl group at position C7 found in anthocyanins is responsible for the first color variation because it is the most acidic group ($pK_{a1} \approx 4$), followed by the hydroxyl group at position C4′ ($pK_{a2} \approx 7$) [5,6].

Flavylium-based pigments (natural, semi-synthetic, or synthetic) have been studied for a wide range of applications like cosmetic dyes, food colorants, colorimetric pH-sensors for smart food packaging [7–11], dye-sensitized solar cells [12–14], fluorescence probes [15–19], among others. Most of these studies use anthocyanin extracts, but it is known that they constitute a complex mixture of compounds, and therefore the reproducibility of the results can often be compromised. On the other hand, the characteristic multistate equilibrium of anthocyanins leads to a color loss of these pigments with the increase of pH due to hydration, tautomerization, and isomerization reactions, limiting their use as a color sensor for certain applications. Moreover, some synthetic flavylium-based fluorophores have been investigated for imaging applications; however, in these cases, all compounds were designed in order to limit the equilibrium multistate to the proton transfer reactions, preventing nonradiative decay [17,18].

Pyranoflavylium salts are flavylium derivatives composed of the same chromophore structure with an additional pyranic ring between C5-OH and C4 (Fig. 1). This kind of pigment can be found in natural matrices such as in resin of dragon's blood trees [20], strawberry, and black currant [21,22]. They could also be found in processed beverages, mainly in red wine, due to the reaction between anthocyanins and other molecules released to the medium during the yeast fermentation process (e.g., pyruvic acid, acetaldehyde, acetoacetic acid) [23–27]. The new pyranic ring is crucial for the equilibrium multistate of these compounds

* Corresponding author.
E-mail address: luis.cruz@fc.up.pt (L. Cruz).

https://doi.org/10.1016/j.jphotochem.2021.113313
Received 25 August 2020; Received in revised form 15 April 2021; Accepted 17 April 2021
Available online 22 April 2021
1010-6030/© 2021 Elsevier B.V. All rights reserved.

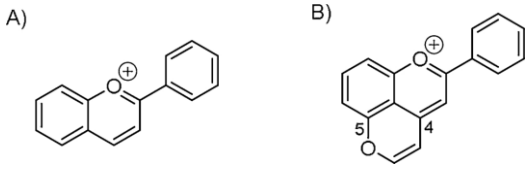


Fig. 1. Basic structure of flavylium cation (A) and pyranoflavylium cation (B).

since the substitution in position C4 prevents the typical anthocyanin reactions, namely hydration, tautomerization, and isomerization. Therefore, the equilibrium multistate of pyranoanthocyanins only depends on the proton-transfer reactions [28]. Consequently, these kind of pigments has been shown to display higher color intensity and stability at a wider pH range compared to their flavylium precursors, which makes them better for diverse applications [29]. Furthermore, pyranoflavylium salts exhibit excited-state proton transfer (ESPT) such as flavylium cations and other phenols. Recent studies on the photophysics of synthetic pyranoflavylium salts showed that, like flavylium salts, these compounds display an interesting photoacidity property with the first acidity constant at excited state (pK^*_a) between 0.2−0.7 [30,31]. Bearing this, several works have been dedicated to the synthesis, isolation, and characterization of natural and bioinspired pyranoflavylium-type dyes [32–43].

In the present work, a new family of pyranoflavylium dyes without the presence of the hydroxyl group at position C7 was synthesized and characterized by spectroscopy techniques. Thus, the aim of this work was to correlate the number of hydroxyl substituents present in the pigments with their chromatic properties as a function of pH. The acidic equilibrium constants and photophysical properties were studied by UV–vis spectrophotometry and by steady-state fluorescence measurements. The cytotoxicity properties of the pigments were evaluated to assess their potential as pH-responsive dyes for food packaging applications.

2. Material and methods

2.1. Reagents

All chemicals were obtained from Sigma-Aldrich (Madrid, Spain), except for 2,6-dihydroxybenzaldehyde, which was obtained from Alfa Aesar (Heysham, England). Theorell and Stenhagen universal buffer was prepared by dissolving phosphoric acid (2.25 mL, 85 % w/w), boric acid (3.54 g), monohydrated citric acid (7.00 g), and NaOH (343 mL, 1 M) solution diluted in distilled water until 1 L [44].

2.2. Synthesis

2.2.1. Synthesis of 5-hydroxyflavylium salts *4* and *5*

Equimolar amounts of 2,6-dihydroxybenzaldehyde (**1**) and 3,4-dihydroxyacetophenone (**2**) or 4-hydroxyacetophenone (**3**) were dissolved in 3 mL of AcOEt/MeOH (2:1), and TMSCl (20 eq.) was added slowly to the reaction at 0 °C. After one hour of stirring, 20 mL of the AcOEt was added to promote the precipitation of the desired compound. Precipitated solid was purified by column chromatography using C18 silica gel with an acidified aqueous solution of 20–40 % of MeOH and lyophilized.

*2.2.1.1. 3′,4′,5-trihydroxyflavylium chloride (**4**).* Dark orange solid. Yield 62 %. ^{1}H NMR (600.13 MHz, MeOD-d$_4$/TFA 9:1) δ (ppm) 8.46 (d, J =9.1 Hz, 1H, H4), 7.54 (d, J =9.1 Hz, 1H, H3), 7.27 (dd, J = 8.6, 2.2 Hz, 1H, H6′), 7.18 (t, J =8.4 Hz, 1H, H7), 7.09 (d, J =2.2 Hz, 1H, H2′), 6.75 (d, J =8.4 Hz, 1H, H6 or H8), 6.35 (d, J =8.4 Hz, 1H, H6 or H8), 6.29 (d, J =8.6 Hz, 1H, H5′). ^{13}C NMR (125.77 MHz, MeOD-d_4/TFA 9:1) δ (ppm) 166.33 (C2), 149.59 (C4′), 149.06 (C5 or C8a), 147.66 (C5 or C8a), 140.67 (C4), 139.35 (C3′), 131.36 (C7), 118.55 (C6′), 112.03 (C1′), 108.84 (C5′), 107.23 (C4a), 106.04 (C3), 104.27 (C6 or C8), 99.82 (C6 or C8). MS (ESI, positive ion mode) molecular formula $C_{23}H_{15}O_6^+$ requires $[M]^+$ 255.0652; Found, 255.0647.

*2.2.1.2. 4′,5-Dihydroxyflavylium chloride (**5**).* Characterization has already been reported [45].

2.2.2. Synthesis of pyranoflavylium salts *6* to *8*

Flavylium compounds **4** and **5** (1 eq.) were dissolved in 50 mL (approximately 1 mg/mL) of hydroalcoholic solution (EtOH 20 % (v/v)) and acetone (10 % (v/v)), caffeic acid (5 eq.) or vinylphenol (5 eq.) were added to the respective reaction. The pH was set to 2.6 for the reaction with acetone and 3.5 for the reaction of caffeic acid and vinylphenol. The reaction mixtures were stirred at 37 °C for 2 h with vinylphenol, 24 h with acetone, and 6 days with caffeic acid. The reaction products were pre-purified by liquid-liquid extraction. The final products were isolated by column chromatography using C18 silica gel with an acidified aqueous solution of MeOH 10–20 % (for compounds **6** and **7**) and 40–50 % (for compounds **8** and **9**) and further lyophilized.

*2.2.2.1. 3′,4′-dihydroxy-10-methylpyranoflavylium chloride (**6**).* Dark orange solid. Yield 16 %. ^{1}H NMR (600.13 MHz, MeOD-d_4/TFA 9:1) δ (ppm) 8.18 (t, J = 8.4 Hz, 1H, H7), 7.78–7.80 (m, 2H, H6 or H8 and H6′), 7.69 (s, 1H, H2′), 7.66 (d, J = 8.4 Hz, 1H, H6 or H8), 7.62 (s, 1H, H3), 7.05 – 6.98 (m, 2H, H9 and H5′), 2.66 (s, 3 H). ^{13}C NMR (125.77 MHz, MeOD-d_4/TFA 9:1) δ (ppm) 175.23 (C10), 172.54 (C2), 155.55 (C4′), 154.42 (C4), 153.88 (C5 or C8a), 153.52 (C5 or C8a), 147.98 (C3′), 138.45 (C7), 124.38 (C6′), 122.10 (C1′), 117.57 (C5′), 115.83 (C2′), 11.41 (C4a), 113.73 (C6 or C8), 113.59 (C6 or C8), 107.35 (C9), 103.26 (C3), 21.63 (CH_3). HRMS (ESI, positive ion mode) molecular formula $C_{18}H_{13}O_4^+$ requires $[M]^+$ 293.0808; Found, 293.0822.

*2.2.2.2. 2,10-Bis-(3′,4′,3′′,4′′-dihydroxyphenyl)pyranobenzopyrylium chloride (**7**).* Orange solid. Yield 15 %. ^{1}H NMR (600.13 MHz, MeOD-d_4/TFA 9:1) δ (ppm) 8.12 (t, J =8.4 Hz, 1H, H7), 7.68 (m, 4H, H5, H8, H6′ and H6′′), 7.60 (d, J =1.7 Hz, 2H, H2′ and H2′′), 7.55 (s, 2H, H3 and H9), 6.96 (d, J =8.4 Hz, 2H, H5′ and H5′′). ^{13}C NMR (125.77 MHz, MeOD-d_4/TFA 9:1) δ (ppm): 170.21 (C2 and C10), 154.60 (C4′ and C4′′), 153.13 (C5 and C8a), 152.79 (C4), 147.77 (C3′ and C3′′), 137.93 (C7), 123.50 (C6′ and C6′′), 122.38 (C1′ and C1′′), 117.38 (C5′ and C5′′), 115.44 (C2′ and C2′′), 113.85 (C4a), 113.55 (C6 and C8), 103.03 (C3 and C9). HRMS (ESI, positive ion mode) molecular formula $C_{23}H_{15}O_6^+$ requires $[M]^+$ 387.0863; Found, 387.0863.

*2.2.2.3. 4′-hydroxy-10-methylpyranoflavylium chloride (**8**).* All characterization has been reported elsewhere [45].

*2.2.2.4. 2,10-Bis-(4′,4′′-hydroxyphenyl)pyranobenzopyrylium chloride (**9**).* Dark orange solid. Yield 33 %. UV/Vis data λ_{max} (0.01 % HCl in MeOH) =500.60 nm and molar extinction coefficient ε =44.61 mol^{-1} dm^3 cm^{-1}. ^{1}H NMR (600.13 MHz, DMSO-d_6/TFA 9:1) δ (ppm): 8.16–8.20 (m, 5H, H7, H2′, H6′, H2′′ and H6′′), 7.82 (d, J = 8.4 Hz, 2H, H6 and H8), 7.75 (s, 2H, H3 and H9), 7.06 (d, J = 8.7 Hz, 4H, H3′, H5′, H3′′ and H5′′). ^{13}C NMR (125.77 MHz, DMSO-d_6/TFA 9:1), δ (ppm): 168.30 (C2 and C10), 164.65 (C4′ and C4′′), 152.05 (C4), 151.72 (C5 and C8a), 137.27 (C7), 131.07 (C2′, C6′, C2′′ and C6′′), 120.47 (C1′ and C1′′), 117.23 (C3′, C5′, C3′′ and C5′′), 112.90 (C4a), 112.81 (C6 and C8), 102.29 (C3 and C9). HRMS (ESI, positive ion mode) molecular formula $C_{23}H_{15}O_4^+$ requires $[M]^+$ 355.0965; Found 355.0969.

2.3. NMR spectroscopy

^{1}H NMR (600.13 MHz) and ^{13}C NMR (125.77 MHz) spectra were recorded on a Bruker-Avance 600 spectrometer at 303 K. The sample

was prepared in DMSO-d_6/TFA (9:1) or MeOD-d_4/TFA (9:1). Chemical shifts were assigned using 2D NMR experiments (COSY, NOESY, *g*HMBC, and *g*HSQC).

2.4. High-resolution mass spectrometry (HRMS)

Analyzes were made on an LTQ Orbitrap™ XL hybrid mass spectrometer (Thermo Fischer Scientific, Bremen, Germany) controlled by *LTQ Tune Plus 2.5.5* and *Xcalibur 2.1.0.* Positive ion mode: The capillary voltage of the electrospray ionization source (ESI) was set to 3.1 kV. The capillary temperature was 275 °C. The sheath gas was at 5 (arbitrary unit as provided by the software settings). The capillary voltage was 49 V, and the tube lens voltage 80 V.

2.5. Absorption spectroscopy

Varian-Cary 100 Bio spectrophotometer was used to record all UV–vis absorption spectra in the range of 200–800 nm with a 1 nm sampling interval. UV–vis absorption spectra were recorded of pigment solutions at 25 °C using a quartz cell cuvette of 3.5 mL capacity and 1 cm of the optical path.

2.6. Fluorescence spectroscopy

Fluorescence studies were carried out by a spectrofluorometer FluoroMax®-4 (HORIBA Scientific) in a QS high-precision cell made of quartz SUPRASIL with a length path of 3 mm (Hellma Analytics). The concentration of pigment solutions was defined to have absorbances equal or less than 0.1 at the excitation wavelength. All fluorescence spectra were corrected for the spectral response of the spectrofluorometer emission and excitation units. For all experiments, both the front and exit entrance slits consisted of a 4-nm bandpass. For the different experiments, a specific range of wavelengths was used for excitation and emission and reported in the results section. Fluorescence quantum yields (Φ_F) were determined using acridine orange in basic ethanol as standard reference ($\Phi_{fl,r} = 0.2$) [46], according to the following Eq. (1) and the procedure described elsewhere [47]:

$$\Phi_{fl,s} = \Phi_{fl,r} \times \frac{n_s^2}{n_r^2} \left(\frac{K_s}{K_r}\right) \quad (1)$$

where subscripts r and s denote reference and test sample, respectively, Φ_{fl} is the fluorescence quantum yield, K is the slope of the integrated fluorescence intensity vs. absorbance plot, and n is the refractive index of the solvent. Measurements were performed with the absorbance at 385 nm of all dye solutions.

2.7. pH measurements

All pH measurements were made in a Radiometer Copenhagen PHM240 pH/ion meter. The measured pH values in the ethanolic solutions were corrected by the Eq. (2): [48]

$$pH = pH_{app} - \delta \quad (2)$$

where pH is the corrected value, pH_{app} is the pH measured by pH meter calibrated with aqueous buffer solutions, and δ is the correction factor in a function of percent of ethanol. For 25 % EtOH/H_2O (v/v), the average correction factor is $\delta = 0.075$ at 25 °C [48].

2.8. Equilibrium constants

2.8.1. Determination by absorption spectroscopy

The equilibrium constants (pK_a values) were determined by spectrophotometric titrations. Firstly, different stock solutions of the pigments at 300 μM in EtOH:H_2O 75:25 (v/v) with HCl 0.1 M were prepared. In a quartz cuvette, it was subsequently added: 1 mL of NaOH solution (0.1 M), 1 mL of Theorell and Stenhagen [38] universal buffer solution at pH 1, and 1 mL of stock solution of the pigment. The final concentrations of pigments were 100 μM in EtOH:H_2O 25:75 (v/v). Increasing volumes of a NaOH solution (1 M) were added to the cell cuvette achieving different pH values. After each addition of base, a UV–vis spectrum was taken and the final pH was measured. The final volumes were appropriately corrected. The pK_a values were fitted using the least-squares method and the Solver program from Microsoft Excel.

2.8.2. Determination by fluorescence spectroscopy

The equilibrium constants were also determined by fluorescence spectroscopy at different pH values (from 1 to 12). The experiments were carried out by adding a stock solution of pigment (30 μM) in EtOH 75 % (v/v) and HCl 0.1 M (0.3 mL) to a microtube containing a solution of NaOH 0.1 M (0.3 mL) and universal buffer of Theorell and Stenhagen (0.3 mL) at the desired pH. The final pH of the solutions of pigment (10 μM) in EtOH 25 % (v/v) was measured by pH meter. Emission spectra were obtained for all solutions (0.1 mL) in a 3 mm fluorescence quartz cuvette, following the parameters presented in *2.7*. Different excitation/emission wavelength pairs were used for different experiments, which are described in the results section. The pK_a values were fitted using the least-squares method and the Solver program from Microsoft Excel.

2.9. Cell culture conditions

Caco-2 cells were grown in Minimum Essential Medium Eagle supplemented with 15 % of fetal bovine serum, 100 U/mL penicillin, 100 mg/mL streptomycin, and 0.25 mg/mL amphotericin B (all from Sigma-Aldrich) at 37 °C in a humidified atmosphere containing 5 % CO_2. For the experiments, cells were plated on 96-well plates at 1.5×10^5 cells/mL in a final volume of 100 μL/ well.

2.10. Cell viability assay

The cell viability was quantified using resazurin, the active ingredient of Alamar Blue assay. In this assay, living cells will reduce the nonfluorescent dye resazurin to the strongly-fluorescent dye resorufin. 24 h after the initial seeding, the compounds were incubated for a 48 h period, in a range of concentration [6.3–100 μM], prepared by dilution of the original stocks (100 mM in DMSO 10 % TFA). The solvent alone was also evaluated. At the end of the incubation time, a fresh medium with 10 % (v/v) of resazurin was added to the cells, which were incubated at 37 °C in a humidified atmosphere of 95 % air and 5 % CO_2 for 3 h. Then, 100 μL were transferred to a 96-well plate, and the fluorescence was recorded in a flex (FlexStation®3 Multi-Mode Microplate Reader, California, USA) using a 560 nm excitation / 590 nm emission filter set.

2.11. Data analysis

Results from cytotoxicity were subjected to solvent effect subtraction in each assay. Results are expressed as % proliferation of compounds comparatively to another (mean ± SEM). Data from cytotoxicity were analyzed in GraphPad Prism 8.0.1 Software using two-way analysis of variance (ANOVA) followed by Tukey's multiple comparison test. Statistical significance was considered when $P < 0.0001$.

3. Results and discussion

3.1. Synthesis

The synthesis of the pyranoflavylium salts followed the procedures that are usually used to obtain these kinds of compounds. Firstly, the flavylium compounds (**4**, **5**) were synthesized through the acid-catalyzed aldol condensation between benzaldehyde and acetophenone derivatives using an excess of TMS-Cl to generate HCl *in situ*

(Scheme 1), following the procedure described by Al Bittar et al. [49], with yields around 60 %. The next step consisted of the reactions of flavylium salts with acetone to give compounds **6** and **8**, with caffeic acid to give compound **7**, and with vinylphenol to give compound **9**. The synthesis of pyranoflavylium dyes **6** to **9** occurred via annelation reaction involving carbon 4 of flavylium cation, the hydroxyl group of C5, and the enolic form of acetone, caffeic acid, or vinylphenol reagents following the mechanism pathway already described [24,41,50–53]. Products **6**, **7**, and **9** were obtained with yields between 16 and 33 %.

3.2. Determination of equilibrium constants

Firstly, the chemical equilibrium constants (pK_a values) for pigments **6**, **7**, and **9** were determined by UV–vis titrations in a hydroethanolic solution of 25 % (v/v) because the pigments were not completely water-soluble. UV–vis spectra were obtained for the pH range between 1 and 12 for different dyes by adding small volumes of NaOH. From the UV–vis spectra (SI) obtained, there is no evidence for the formation of hemiketal (B_2) species (appearance of a band with absorption at 280 nm) with increasing pH. This does not exclude the formation of residual amounts of hemiketal; however, this process could be neglected due to its small contribution as already reported for similar pyranoanthocyanins [54]. Therefore, the chemical equilibrium network of these pigments in solution is simplified, having only acid-base reactions. The obtained UV–vis spectra (SI) also suggested that there are three different species (AH^+, A, and A^-) in solution for all studied pigments, and, consequently, two pK_a values were achieved. The global process can be accounted for Eqs. (3) and (4):

$$AH^+ + H_2O \leftrightarrow A + H_3O^+ \; K_{a1} \text{ First proton transfer} \quad (3)$$

$$A + H_2O \leftrightarrow A^- + H_3O^+ \; K_{a2} \text{ Second proton transfer} \quad (4)$$

where

$$K_{a1} = \frac{[A][H_3O^+]}{[AH^+]} \quad (5)$$

$$K_{a2} = \frac{[A^-][H_3O^+]}{[A]} \quad (6)$$

The total concentration of individual species, C_0, is given by Eq. (7):

$$C_0 = [AH^+] + [A] + [A^-] \quad (7)$$

and the mole fraction distribution of the different species, χ_i, was calculated by simplified equations as follows (8–10):

$$\chi_{AH^+} = \frac{[AH^+]}{C_0} = \frac{1}{1 + \frac{K_{a1}}{[H^+]} + \frac{K_{a2}K_{a1}}{[H^+]^2}} \quad (8)$$

$$\chi_A = \frac{[A]}{C_0} = \frac{K_{a1}\chi_{AH^+}}{[H^+]} \quad (9)$$

$$\chi_{A^-} = \frac{[A^-]}{C_0} = \frac{K_{a2}\chi_A}{[H^+]} \quad (10)$$

The fittings of the experimental data (absorbance as a function of pH) at a given wavelength by Eq. (11) allowed the achievement of the pK_a values.

$$A_{calc} = \varepsilon_{AH^+}\chi_{AH^+} + \varepsilon_A\chi_A + \varepsilon_{A^-}\chi_{A^-} \quad (11)$$

where ε_{AH^+}, ε_A and ε_{A^-} are the mole absorption coefficients of the individual species or components at the considered wavelength.

Excellent fittings for the experimental absorbance values at different wavelengths as a function of pH were obtained, confirming the presence of different species in solution for each pigment (Figs. 2–4).

Table 1 summarizes all equilibrium constants determined in this work for pigments **6-9** (Fig. 5) as well as for the analogs of **6** and **7** (pigments **6a** and **7a**, respectively) (Fig. 5), which were already reported [40].

Analyzing the first equilibrium constants (pK_{a1}) obtained for pigments **6** to **9** and comparing with the natural-occurring analogs **6a** and **7a**, it can be observed that the absence of the hydroxyl group at position 7 (C7-OH) leads to an increase of pK_{a1}. Although there is no study in the literature regarding the first deprotonation position at the

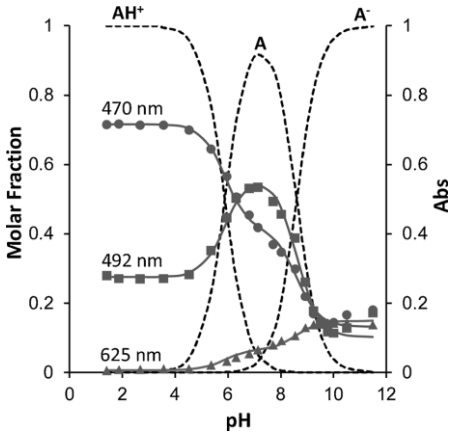
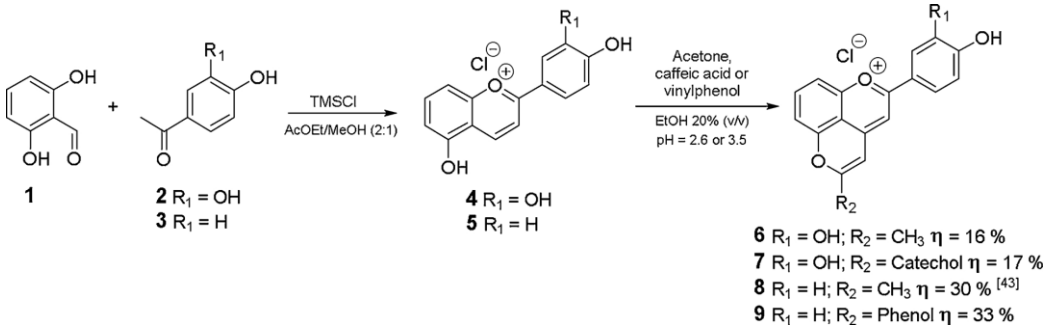


Fig. 2. Absorbance values of compound **6** taken at different wavelengths as a function of pH. Fitting was achieved for pK_{a1} = 5.80 ± 0.02 and pK_{a2} = 8.68 ± 0.12 in EtOH 25 % (v/v).



Scheme 1. Strategy for the synthesis of the pigments **6**, **7**, **8** [45] and **9**.

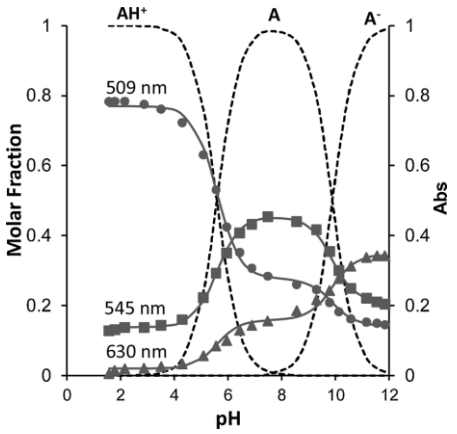


Fig. 3. Absorbance values of compound **7** taken at different wavelengths as a function of pH. Fitting was achieved for pK_{a1} = 5.50 ± 0.08 and pK_{a2} = 9.77 ± 0.02 in EtOH 25 % (v/v).

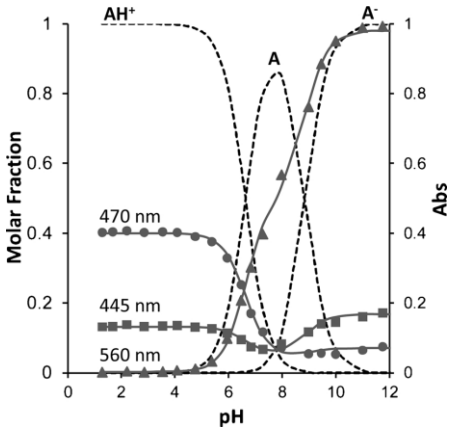


Fig. 4. Absorbance values of compound **9** taken at different wavelengths as a function of pH. Fitting was achieved for pK_{a1} = 6.47 ± 0.07 and pK_{a2} = 8.86 ± 0.11 in EtOH 25 % (v/v).

pyranoflavylium structure (either at C7-OH of A ring or in —OH groups of B ring), this is well defined for flavylium salts. The phenolic groups of the flavylium cation at C4′, C5 and C7 are fairly acidic, but there is consensus among several authors that the C7-OH is the most acidic group, and therefore, the corresponding neutral quinoidal base can be considered to be the predominant tautomer [1,6,55,56]. Considering that pyranoflavylium salts behave in the same way, it was expectable that the absence of the hydroxyl group at position C7 of ring A lead to an increase of pK_{a1}. Besides, a recent study reported pK_{a1} values between 3.4 and 4.4 for pyranoflavylium salts with a single hydroxyl group at position C7 [30,31]. This confirms that the hydroxyl group in A ring in pyranoflavylium salts also has a higher acid character than the hydroxyl groups in the B or E rings. On the other hand, the number of hydroxyl groups present in B ring (or E) also influences pK_{a1} values. Overall, the fewer hydroxyl groups at pyranoflavylium structure, the higher pK_{a1} values (compounds **8** and **9**). The largest variation was observed between pigment **7a** and pigment **8** with a difference of more than two pH units. For the second equilibrium constant (pK_{a2}), the comparison between the values obtained is more complex because it also depends on the substituents of the pyranic ring (E). In the case of compound **8**, this value cannot be compared because it does not correspond to the deprotonation of a hydroxyl group but to the loss of the proton from the methyl group, which occurs at high hydroxide concentration as already described elsewhere [45,57]. For the other pigments, it was not observed any trend for the pK_{a2} values. For example, it was not expected that the pK_{a2} value of pigment **7** would be higher than the pigment **9,** taking into account the number of hydroxyl groups of both pigments.

In general, the first pK_a values (5.80–6.47) of these pigments lead to a remarkable color changing which make them powerful candidates as pH-freshness indicators for food packaging applications. In fact, the pH window variation during the spoilage of several packed perishable foods such as meat or fish is between 5 and 7 [9,58,59]. Therefore, these dyes are very suitable for sensing and spoilage monitoring of these types of foods in real-time.

3.3. Fluorescence study

The fluorescence properties of the four synthesized pigments were studied at different pH values with the same solvent (EtOH 25 % (v/v)) as the one used in the study for thermodynamic constants determination by UV–vis spectrophotometry for further comparison. Initially, a screening of emission capacity of compounds **6** to **9** was performed at different pH values. For this preliminary study, all dyes were studied at pH around 3, 6, and 10, and the excitation wavelength chosen corresponded to the maximum absorption wavelength of each species of each pigment (data not shown). We observed that pigments **6** and **7** showed no relevant results of fluorescence for any pH value. Oppositely, dyes **8** and **9** presented fluorescence emission, mainly for pH 3 in both cases (see SI), which suggests that the flavylium cation species is the main responsible that contributes to this behavior. This result is very interesting since all pigments are structurally similar, but only pigments **8** and **9** showed remarkable fluorescence properties. Apparently, the presence of an additional hydroxyl group in *ortho*-position in B ring (catechol group) may avoid/annul the emission when pigments **6** and **7** are excited. Furthermore, it also was observed that the excitation spectrum obtained by the maximum emission wavelength of each species was very similar to the absorption spectrum (data not shown). For this reason, the acid equilibrium constants were determined by fluorescence spectroscopy only for **8** and **9** pigments. First, a wavelength for excitation was chosen for each pigment. This value corresponds to an

Table 1
The pK_a values obtained for the different pigments by absorbance and fluorescence experiments.

		Compound					
		6a	**6**	**7a**	**7**	**8**	**9**
Absorbance	**pK_{a1}**	5.0 ± 0.1[a]	5.80 ± 0.02	4.7 ± 0.1[a]	5.50 ± 0.08	6.8 ± 0.1[b]	6.47 ± 0.07
	pK_{a2}	6.5 ± 0.1[a]	8.68 ± 0.12	7.9 ± 0.1[a]	9.77 ± 0.02	10.8 ± 0.1[b]	8.9 ± 0.1
Fluorescence	**pK_{a1}**	–	–	–	–	6.8 ± 0.1	6.4 ± 0.1
	pK_{a2}	–	–	–	–	9.9 ± 0.2	8.1 ± 0.2

[a] Results from [40].
[b] Results from [45].

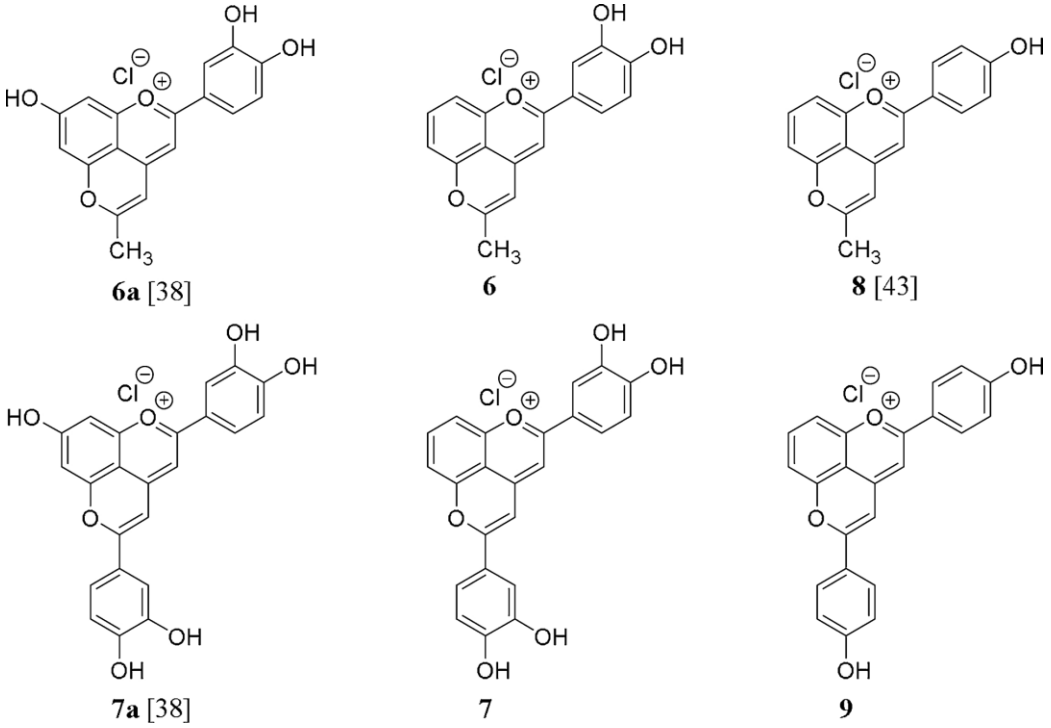


Fig. 5. Structures of synthesized pigments in this work (**6**, **7,** and **9**) and pigments **6a**, **7a,** and **8** already studied.

absorbance wavelength that had a similar absorbance intensity across the entire pH range, such as isosbestic points. In this case, 355 and 445 nm were set as the excitation wavelengths for dyes **8** and **9**, respectively. Emission spectra were obtained for the pH range between 1 and 12 for the two pigments. The global process followed the same equations presented in the absorbance spectrometry study (Eqs. 3–11). The pK_a values were determined by fitting the experimental normalized fluorescence intensity values as a function of pH (Figs. 6 and 7), and the values are presented in Table 1.

For pigment **8**, the first pK_a = 6.7 ± 0.1 was obtained through an excellent fitting for the maximum emission wavelength at 490 nm. For higher pH values, no significant emission was observed for any wavelength, which indicates that the species present is not fluorescent in these conditions. For this reason, although the pK_{a2} = 9.9 ± 0.2 has been determined through the fitting obtained at λ_{em} =490 nm, the associated error can be slightly higher. Pigment **9** showed two emission wavelengths between the pH values of 1.61 and 11.05. The first emission value at 512 nm is observed for lower pH values (1.61–7.06) and corresponds to AH^+ species. The second at 630 nm has low intensity than the first one and appears for higher pH values (8.74–11.05). For intermediate pH values (7.06–8.74), no maximum emission wavelength was observed, which indicates that the species present (A) does not emit fluorescence. The pK_a values determined by fitting were pK_{a1} = 6.4 ± 0.1 and pK_{a2} = 8.1 ± 0.2 (Fig. 7).

Comparing the chemical equilibria data obtained through fluorescence with the ones obtained by the UV–vis absorption (Table 1), it can be observed that the pK_{a1} values are concordant. In contrast, pK_{a2} values obtained are slightly different, with pigment **8** recording the largest difference (10.8 to 9.9). This main difference might be associated with the lower fluorescent intensity of A and A^- species compared to AH^+, which could lead to less sensitive pKa determinations. Thus, it can be concluded that steady-state fluorescence is not the best technique to study chemical equilibrium in the fundamental state as a function of pH, namely when all species in solution do not display fluorescence emission.

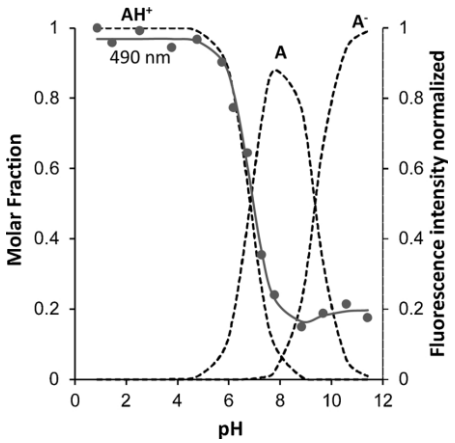


Fig. 6. Fluorescence emission of compound **8** as a function of pH, λ_{exc} =355 nm for λ_{em} =491 nm. Fitting was achieved for pK_{a1} = 6.8 ± 0.1 and pK_{a2} = 9.9 ± 0.2 in EtOH 25 % (v/v).

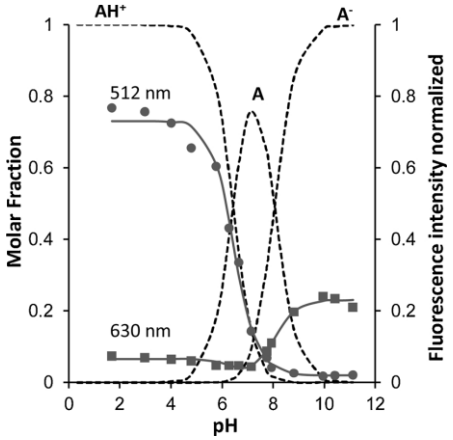


Fig. 7. Fluorescence emission of compound **9** as a function of pH, λ_{exc} =445 nm for λ_{em} =512 nm and for λ_{em} =630 nm. Fitting was achieved for $pK_{a1} = 6.4 \pm 0.1$ and $pK_{a2} = 8.1 \pm 0.2$ in EtOH 25 % (v/v).

3.3.1. *Photophysical properties of pigments **8** and **9***

Pigments **8** and **9** were studied in relation to their fluorescence properties, namely stokes shifts (Δν), quantum yields (Φ_F) and absorption coefficient (ε), where the last two parameters can be combined into a single quantum efficiency value ($QE_{max} = \varepsilon\Phi_F$). In the case of pigments **8** and **9**, and for the absorption maxima of each species, it was observed that the pyranoflavylium cation was the species with higher fluorescence intensity (SI). Furthermore, fluorescence decay measurements were also studied for both pigments which lifetime revealed to be in the picoseconds time scale (< 120 ps). Their values were not considered accurate for their characterization since they were within the experimental error of the equipment (see SI). Figs. 8 and 9 showed the absorption and emission spectra of pigments **8** and **9** at pH ≈ 3, respectively, and photophysical parameters are presented in Table 2.

Both pigments have similar photophysical properties, with slight differences among them. Compound **9** demonstrated a slightly higher maximum absorption and emission wavelengths, molar absorptivity coefficient, as well quantum yield than compound 8, resulting in a higher QE value. These emission properties make these pigments

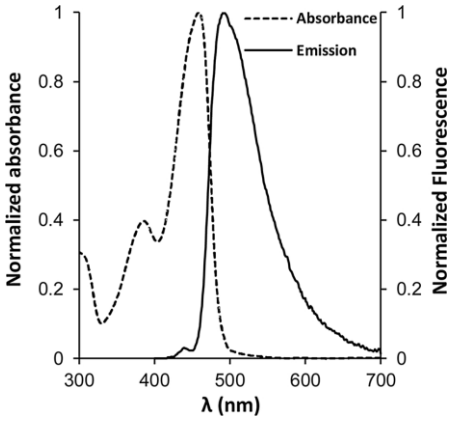


Fig. 8. Absorption and emission spectrum of pigment **8** at pH ≈ 3 in a hydroalcoholic solution in EtOH 25 % (v/v).

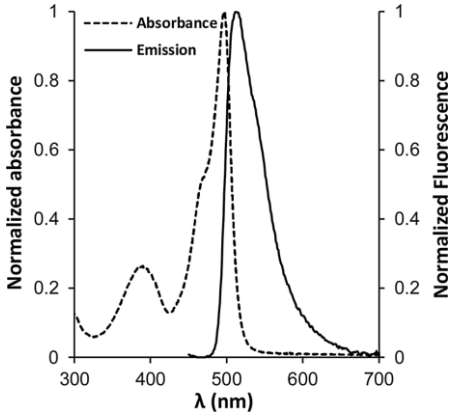


Fig. 9. Absorption and emission spectrum of pigment **9** at pH ≈ 3 in a in EtOH 25 % (v/v).

potential optical pH sensors for food packaging, both by colorimetric and fluorescence response. [60,61]

3.4. *Cell viability evaluation*

Cytotoxicity properties of the compounds were evaluated in caco-2 cells by alamar blue assay. The four compounds were initially intended to be evaluated in terms of their toxicity using caco-2 cell line, a human epithelial colorectal adenocarcinoma as a model of the gastrointestinal tract. However, due to the precipitation effect of compound **7** in the cellular medium (MEME), it was discarded. The presence of two *ortho*-catechol groups may render this compound's ability to interact with the protein content of the medium, resulting in the formation of huge insoluble complexes.

According to the results obtained (Fig. 10), none of the three compounds tested were able to reduce to 50 % the amount of living cells. Nevertheless, at 100 μM, compounds can be ordered by inhibitory capacity, as followed: compound **9** (89.86 % ± 2.13), compound **6** (77.94 % ± 2.57), and compound **8** (58.35 % ± 2.16) (Fig. 10). Compound **8,** which contains a phenol group, and one methyl group is the one that presents the higher cytotoxicity, so the replacement of a phenol group by a catechol group seems to be associated with a protective effect as observed in compound **6**. The protective effect of catechol groups associated with antioxidant activity was already reported. [62] Comparing compound **8** with compound **9**, the substitution of the methyl group by a second phenol is associated with a reduction in the inhibitory effect possible related to the larger size of the molecule and also a higher LogP, which may reduce the ability to enter or interact with the cell membrane. Considering the putative applications of the compounds as sensors for food packaging and fluorescent probes for biological field, it is expected to observe a reduction or even absence of inhibitory effect in normal human cells due to their lower proliferation rates. However, compound **9** is noteworthy for its less inhibitory capacity and, therefore, the least cytotoxicity.

3.5. *Conclusions*

In this work, novel pyrano-3,7-deoxyanthocyanin-based pigments (**6-9**) were synthesized and studied in terms of chromatic, photophysical, and cytotoxicity properties with pH variation by spectrophotometry and by steady-state fluorescence measurements. Oppositely to natural compounds, these pyranoflavylium derivatives are characterized by the absence of a hydroxyl group at position C7, which promoted the increase of their pK_a values. The fluorescence study showed that

Table 2
Photophysical characterization of pigments **8** and **9** in EtOH 25 % (v/v).

Compound	$\lambda_{max,abs}$ [nm]	ε (λ_{max}) [M^{-1} cm^{-1}]	$\lambda_{max,em}$ [nm]	Φ_F	$\Delta\nu$ [cm^{-1}]	QE_{max} [M^{-1} cm^{-1}]
8	463	13691	491	$0.005 \pm 6\times10^{-4}$	1232	69
9	494	18969	512	$0.006 \pm 3\times10^{-4}$	712	114

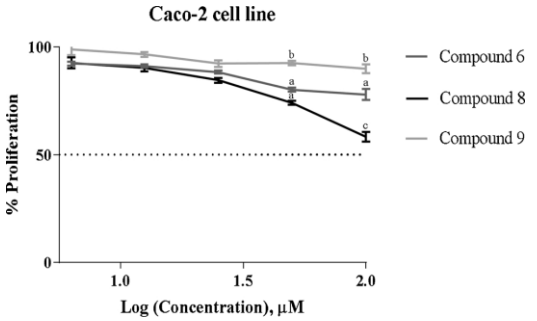


Fig. 10. Percentage of reduction of Alamar Blue® as a function of concentration for compounds **6**, **8,** and **9**, after 48 h of incubation. Data are reported as % control of two independent experiments (n = 6). Values are expressed as mean ± SEM. Statistical significance, between compounds for the same concentration was considered when $P < 0.0001$ and is indicated by different letters.

dyes **6** and **7** with two hydroxyl groups in *ortho*-position in rings B and E (catechol) do not exhibit fluorescence properties. On the other hand, pigments **8** and **9,** which have linked phenol groups at B and E rings, showed fluorescence emission mainly at lower pH values (pyranoflavylium cation), with maximum emission wavelengths of 490 nm for **8**, and 512 nm for **9**. The thermodynamic constants determined by fluorescence agree with the values obtained by absorbance for the first pK_a value. The second pK_a value revealed high significant variations due to the lack of fluorescence of the species present at higher pH values (quinoidal bases).

Overall, in terms of cytotoxicity, none of the compounds studied (**6**, **8,** and **9**) showed significant cytotoxicity in caco-2 cells; however, the best results were obtained for compound **9**. In fact, compound **9** showed the most remarkable and promising properties, which makes it an interesting candidate for pH-responsive applications such as colorimetric and fluorescence sensors for food intelligent packaging.

CRediT authorship contribution statement

Vânia Gomes: Conceptualization, Methodology, Investigation, Writing - original draft. **Ana Sofia Pires:** Methodology, Investigation. **Iva Fernandes:** Methodology, Investigation. **Nuno Mateus:** Writing - review & editing. **Victor de Freitas:** Writing - review & editing, Project administration, Funding acquisition. **Luís Cruz:** Conceptualization, Methodology, Investigation, Writing - review & editing, Funding acquisition.

Declaration of Competing Interest

The authors declare that they have no known competing financial interests or personal relationships that could have appeared to influence the work reported in this paper.

Acknowledgments

The authors thank Dr. Silvia Maia for the MS analysis and Dr. Mariana Andrade for the NMR analysis. We grateful acknowledge to Prof. João Carlos Lima and Dr Artur Moro from FCT-UNL for the fluorescence decay measurements. This work was supported by the Associate Laboratory for Sustainable Chemistry, Clean Processes, and Technologies LAQV. The latter is financed by national funds from UIDB/50006/2020. This work was also supported by the project PTDC/OCE-ETA/31250/2017 funded by FCT and FEDER. Luís Cruz and Iva Fernandes acknowledge the FCT research contract, and Vânia Gomes acknowledges the Ph.D. grant from FCT (SFRH/BD/136556/2018).

Appendix A. Supplementary data

Supplementary material related to this article can be found, in the online version, at doi:https://doi.org/10.1016/j.jphotochem.2021.113313.

References

[1] F. Pina, M.J. Melo, C.A.T. Laia, A.J. Parola, J.C. Lima, Chemistry and applications of flavylium compounds: a handful of colours, Chem. Soc. Rev. 41 (2012) 869–908.
[2] F.H. Quina, P.F. Moreira, C. Vautier-Giongo, D. Rettori, R.F. Rodrigues, A. A. Freitas, P.F. Silva, A.L. Maçanita, Photochemistry of anthocyanins and their biological role in plant tissues, Pure Appl. Chem. 81 (2009) 1687–1694.
[3] A. Castañeda-Ovando, Md.L. Pacheco-Hernández, M.E. Páez-Hernández, J. A. Rodríguez, C.A. Galán-Vidal, Chemical studies of anthocyanins: a review, Food Chem. 113 (2009) 859–871.
[4] F. Pina, Chemical applications of anthocyanins and related compounds. A source of bioinspiration, J. Agric. Food Chem. 62 (2014) 6885–6897.
[5] R. Brouillard, S. Chassaing, G. Isorez, M. Kueny-Stotz, P. Figueiredo, The visible flavonoids or anthocyanins: from research to applications. Recent Advances in Polyphenol Research, Wiley-Blackwell, 2010, pp. 1–22.
[6] O. Dangles, J.A. Fenger, The chemical reactivity of anthocyanins and its consequences in food science and nutrition, Molecules 23 (2018).
[7] V.A. Pereira Jr, I.N.Q. de Arruda, R. Stefani, Active chitosan/PVA films with anthocyanins from Brassica oleraceae (Red Cabbage) as Time–Temperature Indicators for application in intelligent food packaging, Food Hydrocoll. 43 (2015) 180–188.
[8] Y.-C. Wei, C.-H. Cheng, Y.-C. Ho, M.-L. Tsai, F.-L. Mi, Active gellan gum/purple sweet potato composite films capable of monitoring pH variations, Food Hydrocoll. 69 (2017) 491–502.
[9] I. Choi, J.Y. Lee, M. Lacroix, J. Han, Intelligent pH indicator film composed of agar/potato starch and anthocyanin extracts from purple sweet potato, Food Chem. 218 (2017) 122–128.
[10] J. Zhang, X. Zou, X. Zhai, X. Huang, C. Jiang, M. Holmes, Preparation of an intelligent pH film based on biodegradable polymers and roselle anthocyanins for monitoring pork freshness, Food Chem. 272 (2019) 306–312.
[11] S. Kang, H. Wang, L. Xia, M. Chen, L. Li, J. Cheng, X. Li, S. Jiang, Colorimetric film based on polyvinyl alcohol/okra mucilage polysaccharide incorporated with rose anthocyanins for shrimp freshness monitoring, Carbohydr. Polym. 229 (2020), 115402.
[12] G. Calogero, A. Sinopoli, I. Citro, G. Di Marco, V. Petrov, A.M. Diniz, a.J. Parola, F. Pina, Synthetic analogues of anthocyanins as sensitizers for dye-sensitized solar cells, Photochem. Photobiol. Sci. 12 (2013) 883–894.
[13] C.M. Santos, J. Oliveira, S. Rocha, M. Coelho, V. Freitas, H. Aguilar, Pyranoflavylium derivatives extracted from wine grape as photosensitizers in solar cells, J. Braz. Chem. Soc. 25 (2014) 1029–1035.
[14] A.L. Pinto, L. Cruz, V. Gomes, H. Cruz, G. Calogero, V. de Freitas, F. Pina, A. J. Parola, J. Carlos Lima, Catechol versus carboxyl linkage impact on DSSC performance of synthetic pyranoflavylium salts, Dye. Pigment. 170 (2019).
[15] P. Veiga-Santos, C. Ditchfield, C.C. Tadini, Development and evaluation of a novel pH indicator biodegradable film based on cassava starch, J. Appl. Polym. Sci. 120 (2011) 1069–1079.
[16] C.M.P. Yoshida, V.B.V. Maciel, M.E.D. Mendonça, T.T. Franco, Chitosan biobased and intelligent films: monitoring pH variations, Lwt - Food Sci. Technol. 55 (2014) 83–89.
[17] H. Chen, W. Lin, W. Jiang, B. Dong, H. Cui, Y. Tang, Locked-flavylium fluorescent dyes with tunable emission wavelengths based on intramolecular charge transfer for multi-color ratiometric fluorescence imaging, Chem. Commun. 51 (2015) 6968–6971.
[18] E.D. Cosco, J.R. Caram, O.T. Bruns, D. Franke, R.A. Day, E.P. Farr, M.G. Bawendi, E.M. Sletten, Flavylium polymethine fluorophores for near- and shortwave infrared imaging, Angew. Chem. Int. Ed. Engl. 56 (2017) 13126–13129.

[19] S. Wang, Y. Fan, D. Li, C. Sun, Z. Lei, L. Lu, T. Wang, F. Zhang, Anti-quenching NIR-II molecular fluorophores for in vivo high-contrast imaging and pH sensing, Nat. Commun. 10 (2019) 1058.
[20] A. Robertson, W.B. Whalley, J. Yates, 606. The pigments of "dragon's blood" resins. Part III. The constitution of dracorubin, J. Chem. Soc. (Resumed) (1950) 3117–3123.
[21] Y. Lu, Y. Sun, L.Y. Foo, Novel pyranoanthocyanins from black currant seed, Tetrahedron Lett. 41 (2000) 5975–5978.
[22] Ø.M. Andersen, T. Fossen, K. Torskangerpoll, A. Fossen, U. Hauge, Anthocyanin from strawberry (Fragaria ananassa) with the novel aglycone, 5-carboxypyranopelargonidin, Phytochemistry 65 (2004) 405–410.
[23] J. Bakker, P. Bridle, T. Honda, H. Kuwano, N. Saito, N. Terahara, C.F. Timberlake, Identification of an anthocyanin occurring in some red wines, Phytochemistry 44 (1997) 1375–1382.
[24] H. Fulcrand, C. Benabdeljalil, J. Rigaud, V. Cheynier, M. Moutounet, A new class of wine pigments generated by reaction between pyruvic acid and grape anthocyanins, Phytochemistry 47 (1998) 1401–1407.
[25] A.E. Hakansson, K. Pardon, Y. Hayasaka, M. de Sa, M. Herderich, Structures and colour properties of new red wine pigments, Tetrahedron Lett. 44 (2003) 4887–4891.
[26] N. Mateus, A.M.S. Silva, J.C. Rivas-Gonzalo, C. Santos-Buelga, V. de Freitas, A new class of blue anthocyanin-derived pigments isolated from red wines, J. Agric. Food Chem. 51 (2003) 1919–1923.
[27] N. Mateus, J. Oliveira, J. Pissarra, A.M. González-Paramás, J.C. Rivas-Gonzalo, C. Santos-Buelga, A.M.S. Silva, V. De Freitas, A new vinylpyranoanthocyanin pigment occurring in aged red wine, Food Chem. 97 (2006) 689–695.
[28] M. Rentzsch, M. Schwarz, P. Winterhalter, Pyranoanthocyanins - an overview on structures, occurrence, and pathways of formation, Trends Food Sci. Technol. 18 (2007) 526–534.
[29] J. Oliveira, N. Mateus, V. De Freitas, Previous and recent advances in pyranoanthocyanins equilibria in aqueous solution, Dyes Pigm. 100 (2014) 190–200.
[30] A.A. Freitas, C.P. Silva, G.T.M. Silva, A.L. Macanita, F.H. Quina, From vine to wine: photophysics of a pyranoflavylium analog of red wine pyranoanthocyanins, Pure Appl. Chem. 89 (2017) 1761–1767.
[31] A.A. Freitas, C.P. Silva, G.T.M. Silva, A.L. Macanita, F.H. Quina, Ground- and excited-state acidity of analogs of red wine pyranoanthocyanins, Photochem. Photobiol. 94 (2018) 1086–1091.
[32] J. Oliveira, V. De Freitas, A.M.S. Silva, N. Mateus, Reaction between hydroxycinnamic acids and anthocyanin-pyruvic acid adducts yielding new portisins, J. Agric. Food Chem. 55 (2007) 6349–6356.
[33] J. Oliveira, N. Mateus, A.M.S. Silva, V. De Freitas, Equilibrium forms of vitisin B pigments in an aqueous system studied by NMR and visible spectroscopy, J. Phys. Chem. B 113 (2009) 11352–11358.
[34] L. Cruz, V. Petrov, N. Teixeira, N. Mateus, F. Pina, V.D. Freitas, Establishment of the chemical equilibria of different types of pyranoanthocyanins in aqueous solutions: evidence for the formation of aggregation in pyranomalvidin-3- O -coumaroylglucoside-(+)-catechin, J. Phys. Chem. B 114 (2010) 13232–13240.
[35] J. Oliveira, J. Azevedo, A.M.S. Silva, N. Teixeira, L. Cruz, N. Mateus, V. De Freitas, Pyranoanthocyanin dimers: a new family of turquoise blue anthocyanin-derived pigments found in port wine, J. Agric. Food Chem. 58 (2010) 5154–5159.
[36] A. Sousa, P. Araujo, N. Mateus, V. de Freitas, Deoxyvitisins: a new set of pyrano-3-deoxyanthocyanidins, Tetrahedron Lett. 54 (2013) 4785–4788.
[37] J. Azevedo, J. Oliveira, L. Cruz, N. Teixeira, N.F. Brás, V. De Freitas, N. Mateus, Antioxidant features of red wine pyranoanthocyanins: experimental and theoretical approaches, J. Agric. Food Chem. 62 (2014) 7002–7009.
[38] J. Oliveira, P. Araújo, A. Fernandes, N. Mateus, V. de Freitas, Synthesis and structural characterization of amino-based pyranoanthocyanins with extended electronic delocalization, Synlett 27 (2016) 2459–2462.
[39] L. Cruz, J.L.C. Sousa, A. Marinho, N. Mateus, V. de Freitas, Synthesis and structural characterization of novel pyranoluteolinidin dyes, Tetrahedron Lett. 58 (2017) 159–162.
[40] J.L.C. Sousa, V. Gomes, N. Mateus, F. Pina, V. de Freitas, L. Cruz, Synthesis and equilibrium multistate of new pyrano-3-deoxyanthocyanin-type pigments in aqueous solutions, Tetrahedron 73 (2017) 6021–6030.
[41] V. Gomes, N. Mateus, V. de Freitas, L. Cruz, Synthesis and structural characterization of a novel symmetrical 2,10-Bis-Styryl-1-Benzopyrylium dye, Synlett 14 (2018) 1390–1394.
[42] C.P. da Silva, R.M. Pioli, L. Liu, S. Zheng, M. Zhang, G.Td.M. Silva, V.M. T. Carneiro, F.H. Quina, Improved synthesis of analogues of red wine pyranoanthocyanin pigments, ACS Omega 3 (2018) 954–960.
[43] V. Gomes, N. Mateus, V.D. Freitas, L. Cruz, Synthesis and chemical equilibria of a new 10-methylpyrano-2- styrylbenzopyrylium pigment in aqueous solution and its modulation by di ff erent micellar systems, Dye. Pigment. 167 (2019) 60–67.
[44] W.F. Küster, A. Thiel, Tabelle per le analisi chimiche e chimico-fisiche, 12 ed., Hoepli, Milano, 1982.
[45] V. Gomes, M. Guimarães, G. Gonçalves, V. de Freitas, L. Cruz, Bioinspired synthesis and physical-chemical properties of a new 10-Methylpyrano-4′-hydroxyflavylium chloride salt, Synlett 31 (2020) 334–338.
[46] M. Taniguchi, J.S. Lindsey, Database of absorption and fluorescence spectra of &300 common compounds for use in PhotochemCAD, Photochem. Photobiol. 94 (2018) 290–327.
[47] A Guide to Recording Fluorescence Quantum Yields, HORIBA UK Limited, 2020. https://static.horiba.com/fileadmin/Horiba/Application/Materials/Material_Research/Quantum_Dots/quantumyieldstrad.pdf.
[48] W.J. Gelsema, C.L. de Ligny, A.G. Remijnse, H.A. Blijleven, pH-Measurements in alcohol-water mixtures, using aqueous standard buffer solutions for calibration, Recl. Des Trav. Chim. Des Pays-Bas 85 (1966) 647–660.
[49] S. Al Bittar, N. Mora, M. Loonis, O. Dangles, A simple synthesis of 3-deoxyanthocyanidins and their O-glucosides, Tetrahedron 72 (2016) 4294–4302.
[50] H. Fulcrand, P. dos Santos, P. Sarni-Manchado, V. Cheynier, J. Bonvin, Structure of new anthocyanin-derived pigments, J. Chem. Soc. Perkin Trans. I 1 (1996) 735.
[51] Y. Lu, L.Y. Foo, Unusual anthocyanin reaction with acetone leading to pyranoanthocyanin formation, Tetrahedron Lett. 42 (2001) 1371–1373.
[52] M. Schwarz, P. Winterhalter, A novel synthetic route to substituted pyranoanthocyanins with unique colour properties, Tetrahedron Lett. 44 (2003) 7583–7587.
[53] L. Cruz, N. Teixeira, A.M.S. Silva, N. Mateus, J. Borges, V. De Freitas, Role of vinylcatechin in the formation of pyranomalvidin-3-glucoside-(+)-catechin, J. Agric. Food Chem. 56 (2008) 10980–10987.
[54] L. Cruz, V. Petrov, N. Teixeira, N. Mateus, F. Pina, V. De Freitas, Establishment of the chemical equilibria of different types of pyranoanthocyanins in aqueous solutions: evidence for the formation of aggregation in Pyranomalvidin-3-O-coumaroylglucoside-(+)-catechin, J. Phys. Chem. B 114 (2010) 13232–13240.
[55] P. Figueiredo, J.C. Lima, H. Santos, M.C. Wigand, R. Brouillard, A.L. Macanita, F. Pina, Photochromism of the synthetic 4′,7-Dihydroxyflavylium chloride, J. Am. Chem. Soc. 116 (1994) 1249–1254.
[56] F. Pina, Chemical applications of anthocyanins and related compounds. A source of bioinspiration, J. Agric. Food Chem. 62 (2014) 6885–6897.
[57] J. Oliveira, V. Petrov, A.J. Parola, F. Pina, J. Azevedo, N. Teixeira, N.F. Bras, P. A. Fernandes, N. Mateus, M.J. Ramos, V. de Freitas, Chemical behavior of methylpyranomalvidin-3-O-glucoside in aqueous solution studied by NMR and UV-Visible spectroscopy, J. Phys. Chem. B 115 (2011) 1538–1545.
[58] A. Pacquit, J. Frisby, D. Diamond, K.T. Lau, A. Farrell, B. Quilty, D. Diamond, Development of a smart packaging for the monitoring of fish spoilage, Food Chem. 102 (2007) 466–470.
[59] X. Zhang, S. Lu, X. Chen, A visual pH sensing film using natural dyes from Bauhinia blakeana Dunn, Sens. Actuators B Chem. 198 (2014) 268–273.
[60] E. Drago, R. Campardelli, M. Pettinato, P. Perego, Innovations in smart packaging concepts for food: an extensive review, Foods 9 (2020) 1628.
[61] E. Mohebi, L. Marquez, Intelligent packaging in meat industry: an overview of existing solutions, J. Food Sci. Technol. 52 (2015) 3947–3964.
[62] I. Fernandes, A. Faria, J. Azevedo, S. Soares, C. Calhau, V. De Freitas, N. Mateus, Influence of anthocyanins, derivative pigments and other catechol and pyrogallol-type phenolics on breast Cancer cell proliferation, J. Agric. Food Chem. 58 (2010) 3785–3792.

Article V

Colorimetric pH-responsive Biomaterials Based on Pyranoflavylium-Biopolymer Hybrid Conjugates

Ana Sofia Pires, Vânia Gomes, Dina Neves, Nuno Mateus, Victor de Freitas, Luís Cruz

REQUIMTE/LAQV, Departamento de Química e Bioquímica, Faculdade de Ciências, Universidade do Porto, Rua Do Campo Alegre, 687, 4169-007, Porto, Portugal

---

Pires, A. P., Gomes, V., Neves, D., Mateus, N., de Freitas, V, Cruz, L., Colorimetric pH-Responsive Biomaterials Based on Pyranoflavylium-Biopolymer Hybrid Conjugates, *ACS Applied Polymer Materials*, **2022**, 4, 7, 4961–4971.
DOI https://doi.org/10.1021/acsapm.2c00514

ACS APPLIED POLYMER MATERIALS

pubs.acs.org/acsapm Article

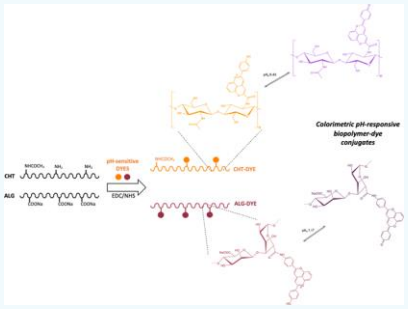
Colorimetric pH-Responsive Biomaterials Based on Pyranoflavylium-Biopolymer Hybrid Conjugates

Ana Sofia Pires, Vânia Gomes, Dina Neves, Nuno Mateus, Victor de Freitas, and Luís Cruz*

Cite This: ACS Appl. Polym. Mater. 2022, 4, 4961−4971 Read Online

ACCESS | Metrics & More | Article Recommendations | Supporting Information

ABSTRACT: The conjugation of functional molecules into marine-origin biopolymers has been extensively used toward the creation of new (bio)materials for applications in food and biomedical areas. Herein, two chitosan (CHT) and alginate (ALG) biobased conjugates functionalized with pH-dyes were successfully developed to be integrated as smart labels and tags in biocompatible packaging materials for food spoilage sensing. For that, two pyranoflavylium-based pH-indicator dyes, Pyflav (**4**) and Pyflav (**5**), were designed, synthesized, and then grafted onto CHT and ALG scaffolds via EDC/NHS carbodiimide coupling chemistry with substitution degrees of 14 and 1.2%, respectively. Afterward, the conjugates were fully characterized by Fourier transform infrared, ^{1}H NMR, and dynamic light scattering techniques, and their acidity constants were determined by UV−vis spectroscopy, yielding a great color variation (from orange to purple, pK_a 6.43 ± 0.04, for Pyflav-CHT (**6**) and from pink to purple, pK_a 7.17 ± 0.02, for Pyflav-ALG (**7**) and compatible with the food spoilage pH range of many perishable foods (pH between 5.8 and 7.4).



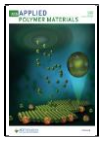
KEYWORDS: *pyranoflavylium salts, acidic constants, pH-indicators, dyes, alginate, chitosan, pH-responsive materials, food intelligent packaging*

1. INTRODUCTION

The expansion of advanced functional systems or smart devices in the food industry is emerging and gaining attention nowadays as a solution to combat huge economic and environmental losses due to food waste problems. Currently, there is a huge interest in the design and fabrication of nanostructured functional materials with tunable compositions, precise layered structures, and well-defined control of properties and functions, which found many applications in a wide range of research fields including sensing technologies for food packaging industry.[1−4]

Intelligent packaging is defined as a smart system that can monitor the food shelf-life allowing to inform the consumers about the food status in real-time.[5] This includes the incorporation of sensors/indicators within food packaging with responsiveness to a stimulus (pH, O_2, CO_2, humidity, temperature, etc.), usually related to changes in physical and chemical properties of foods, thus allowing to monitor the state of food product, either quantitatively or qualitatively. One of the approaches that has been widely used to identify spoilage in many perishable foods is the colorimetric pH-based freshness indicators. For example, during the deterioration process of meat and fish products, the pH increases due to the microbial growth that releases volatile nitrogen-based compounds.[6] Flavylium-based dyes, which comprehend a large family of pigments including natural anthocyanins, 3-deoxyanthocyanins, and pyranoanthocyanins, display different colored species in solution because of their pH-dependent chemical network.[7] This feature makes them suitable for application in food intelligent packaging as pH-sensors to ensure food quality, safety, monitoring or to detect spoilage at early stages.[6] Furthermore, the use of natural-inspired pH sensitive dyes is currently of great interest for food packaging applications because of their intrinsic lower toxicity and higher biocompatibility compared with synthetic ones.[8−10] In fact, anthocyanins are currently being explored as potential pH-sensors of perishable foods (milk, meat, fish).[8,11−14] However, in the spoilage pH range (4.6−7.5), these molecules are not only chemically unstable but also highly reactive. These factors contribute to an overall poor color variation, mainly due to the formation in high extension and thermodynamically stable colorless hemiketals, which decrease the efficiency as an optical sensor.[15] On the other hand, the chromatic properties with pH variation of natural and bio-inspired pyranoflavylium-based dyes have been studied over the last years.[16] Oppositely to anthocyanins, their pH-dependent equilibrium forms are only due to acid-base reactions yielding species with a great color

Received: March 25, 2022
Accepted: May 25, 2022
Published: June 7, 2022



ACS Publications © 2022 American Chemical Society

https://doi.org/10.1021/acsapm.2c00514
ACS Appl. Polym. Mater. 2022, 4, 4961−4971

variation between them, namely, from red-orange acidic flavylium cation to blue and purple neutral and anionic quinoidal bases.[17−20] Over the last years, new pyranoflavylium-based molecules with specific and suitable functional groups have been carefully designed to tune their pK_a values into the food spoilage pH window.[18−21] For these reasons, the use and application of these dyes as pH-indicators to develop smart labels and membranes to monitor food freshness in real-time and to detect food spoilage at early stages are much more promising. In our previous work, a suitable pyranoflavylium dye was designed and immobilized by conventional non-covalent interactions in cellulose acetate-based films produced by the classical solvent casting method.[22] Now, in this work, a different approach is given where two promising pyrano-flavylium-based dyes were covalently bounded at marine-origin polysaccharides [chitosan (CHT), alginate (ALG)] via EDC/NHS coupling chemistry, and further structural and physi-ochemically characterized. These conjugates constitute valuable building blocks to further build-up tick, flexible and robust free-standing multilayer membranes by powerful bottom-up layer-by-layer technology for application as pH-freshness sensors in food packaging.

2. EXPERIMENTAL SECTION

2.1. Materials. CHT powder from ChitoClear (M_w = 150−250 kDa, 78% degree of deacetylation) was purchased from Primex ehf (Siglufjordur, Iceland) and alginic acid sodium salt (ALG) with an α-L-guluronic acid (G) to β-D-mannuronic acid (M) (M/G) ratio of 1.56 and M_w = 120−190 kDa was obtained from Sigma-Aldrich (Madrid, Spain). *N*-(3-dimethylaminopropyl)-*N*′-carbodiimide hydrochloride (EDC·HCl), *N*-hydroxysuccinimide (NHS, 98%), 2,6-dihydroxybenzaldehyde, 4-hydroxyacetophenone, oxaloacetic acid, and 4-aminocinnamic acid were also purchased from Sigma-Aldrich. A dialysis cellulose membrane of 3.5 kDa molecular weight cutoff was purchased from Spectrum Laboratories, Inc. Theorell and Stenhagen universal buffer was obtained as described elsewhere.[23]

2.2. Synthesis of Pyranoflavylium-Based Dyes (4, 5). The synthesis and structural characterization of 4′,5-dihydroxyflavylium (**3**) was performed between 2,6-dihydroxybenzaldehyde (**1**) and 4-hydroxyacetophenone (**2**) as already reported in the literature.[21] Pyranoflavylium-based dyes (**4**) and (**5**) were synthesized according to the following procedures: 4′,5-dihydroxyflavylium chloride salt (**3**) (1 equiv) was dissolved in H_2O/EtOH 80:20 (v/v), 1 mg/mL) and oxaloacetic acid (10 equiv) or 4-aminocinnamic acid (5 equiv) were, respectively, added. The pH was adjusted to 2.6 for the reaction with oxaloacetic acid and 3.5 for the reaction of 4-aminocinnamic acid. The reactions were stirred at 37 °C for 1 day and then pre-purified by liquid−liquid extraction. The compounds were purified by column chromatography loaded with C18 silica gel and eluted with acid hydroalcoholic solutions containing MeOH 15−25% (compound **4**) and MeOH 35−45% (compound **5**) and further lyophilized.

2.2.1. 10-Carboxy-4′-hydroxypyranoflavylium (4). Orange solid. Yield 12%. ^{1}H NMR (600.13 MHz, DMSO-d_6/TFA 9:1): δ (ppm) 8.34 (m, H7, H2′ and H6′), 8.27 (s, 1H, H3), 8.02 (d, J = 8.4 Hz, 1H, H6 or H8), 7.89 (d, J = 8.4 Hz, 1H, H6 or H8), 7.81 (s, 1H, H9), 7.15 (d, J = 8.9 Hz, 2H, H3′ and H5′). ^{13}C NMR (125.77 MHz, DMSO-d_6/TFA 9:1): δ (ppm): 172.04 (C2), 166.58 (C4′), 160.13 (C10 or COOH), 155.69 (C10 or COOH), 152.21 (C5 or C8a), 136.94 (C7 or C2′ or C6′), 130.99 (C7 or C2′ or C6′), 119.86 (C1′), 116.02 (C3′ and C5′), 114.48 (C4a), 108.25 (C9), 105.39 (C4), 103.86 (C3). LC-DAD/ESI-MS $[M]^+$ m/z: 307.

2.2.2. 10-Aminophenyl-4′-hydroxypyranoflavylium (5). Dark purple solid. Yield 13%. ^{1}H NMR (600.13 MHz, DMSO-d_6/TFA 9:1): δ (ppm) 8.10 (m, 3H, H7, H2′ and H6′), 8.06 (d, J = 9.1 Hz, 2H, H2″ and H6″), 7.70−7.74 (d, J = 8.4 Hz, 2H, H6 and H8), 7.59 (s, 1H, H9), 7.55 (s, 1H, H3′), 7.05 (d, J = 9.8 Hz, 2H, H3′ and H5′), 6.81 (d, J = 8.9 Hz, 2H, H3″ and H5″). ^{13}C NMR (125.77 MHz, DMSO-d_6/TFA 9:1): δ (ppm) 168.56 (C10), 165.75 (C2), 163.88 (C4′), 156.86 (C4″), 156.39 (C7), 151.44 (C4), 151.40 (C5), 131.57 (C2″ and C6″), 129.93 (C2′ and C6′), 120.78 (C1′), 116.94 (C3′ and C5′), 115.48 (C1″), 114.71 (C3″ and C5″), 112.43 (C6 and C8), 111.97 (C4a), 101.03 (C3), 100.82 (C9). LC-DAD/ESI-MS $[M]^+$ m/z: 354.

2.3. Synthesis of Pyranoflavylium-Modified Biopolymers (6, 7). *2.3.1. Pyranoflavylium-Modified CHT (Pyflav-CHT) (6).* CHT (10 mg, 5 equiv) was solubilized in 5 mL of water at pH 5.5 (HCl 0.1 M) and stirred at room temperature overnight. 10-carboxy-4′-hydroxy-pyranoflavylium chloride (**4**) (3 mg, 1 equiv) was dissolved in 5 mL of DMF/H_2O 40:60 (v/v) and EDC·HCl (2.53 mg, 1.5 equiv) was added and stirred at room temperature. After 20 min, NHS (1.52 mg, 1.5 equiv) was added to the solution and the reaction was continued for 20 min, stirred at room temperature. Afterward, the previously prepared CS solution was then gradually added to reaction mixture and kept stirring for 24 h at room temperature. The final product was dialyzed against deionized water for 3 days replacing 3−4 times per day to eliminate free hydrochloride acid and the unreacted pigment molecules. Finally, the dialysates were lyophilized to provide Pyflav-CHT (**6**), a light orange powder. The grafting of pigment **4** onto CHT was analyzed by Fourier transform infrared (FTIR), dynamic light scattering (DLS), and ^{1}H NMR where the grafting ratio was determined based on the peak areas taken from ^{1}H NMR.

2.3.2. Pyranoflavylium-Modified ALG (Pyflav-ALG) (7). ALG (10 mg, 5 equiv) was solubilized in water (5 mL) at pH 5.5 and stirred at room temperature overnight. Then, EDC·HCl (10 mg, 1.5 equiv) was added to the ALG solution. After 20 min, NHS (7.5 mg, 1.5 equiv) was added, and after another 20 min, 10-aminophenyl-4′-hydroxy-pyranoflavylium chloride (**5**) (3 mg, 1 equiv) was added. The final pH was set to 5.5 and the reaction was kept stirring for 24 h at room temperature. The final product was dialyzed against deionized water for 3 days replacing 3−4 times per day to eliminate free hydrochloride acid and the unreacted pigment molecules. After lyophilization, a light purple powder was obtained. The successful conjugation of pigment **5** onto ALG was assigned by UV−vis, FTIR, and ^{1}H NMR where the grafting ratio was determined based on the peak areas taken from ^{1}H NMR.

2.4. Determination of pK_a Values by UV−Vis Spectroscopy. Spectrophotometric titrations of the free pigments and conjugates were performed to determine the respective pK_a values. First, stock solutions of free pigments and conjugates were prepared in EtOH/H_2O 75:25 (v/v) solution with 0.1 M HCl (pH ∼ 1) and 0.001 M HCl (pH ∼ 3), respectively. In a quartz cuvette, different solutions were added in the following order: 1 mL of NaOH (0.1 M), 1 mL of universal buffer at desired pH, and 1 mL of the stock solution of the free pigments or conjugates where the final solution was obtained with EtOH/H_2O 25:75 (v/v) and with following final concentrations: Pyflav (**4**) and Pyflav (**5**) at 40 and 46 μg/mL, and Pyflav-CHT (**6**) and Pyflav-ALG (**7**) at 160 and 94 μg/mL, respectively. Titration experiments were performed with NaOH solution (1 M) where increasing volumes were added to the cuvette achieving different pH values, covering the pH range between 1 and 12. After each addition of base, the mixture was shaken, a UV−vis spectrum was recorded, and the final pH was measured. The pK_a values were taken from the least-squares method using the Solver function of Microsoft Excel to fit the experimental values.

2.5. pH Measurements. A Radiometer Copenhagen PHM240 pH/ion meter was used to take all of pH measurements. The experimental pH values in the ethanolic solutions were adjusted using eq 1[24]

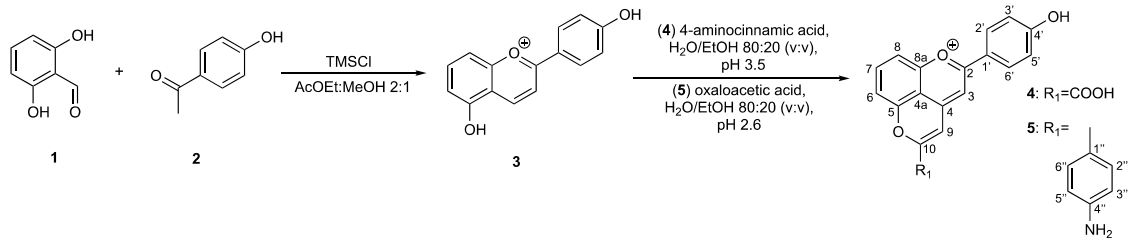
$$\mathrm{pH} = \mathrm{pH}_{app} - \delta \quad (1)$$

where pH is the corrected value, pH_{app} is the experimental pH measured by pH meter calibrated with aqueous buffer solutions, and δ represents the correction factor for the 25% EtOH/H_2O (v/v) solution (δ = 0.075 at 25 °C).

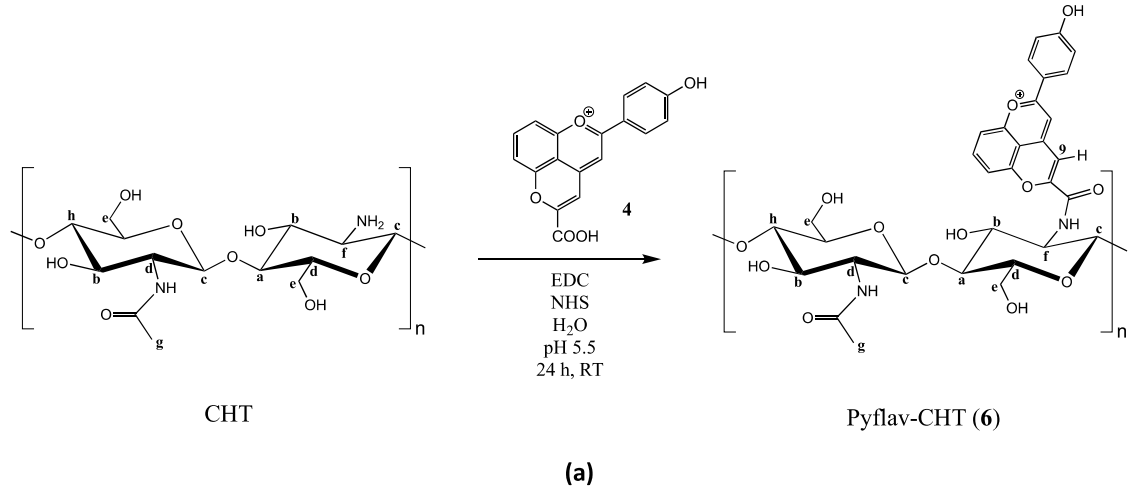
2.6. NMR. ^{1}H NMR (600.13 MHz) and ^{13}C NMR (125.77 MHz) spectra were recorded using a Bruker AVANCE 600 spectrometer working at 298.15 or 313.15 K and TMS was used as an internal

https://doi.org/10.1021/acsapm.2c00514
ACS Appl. Polym. Mater. 2022, 4, 4961−4971

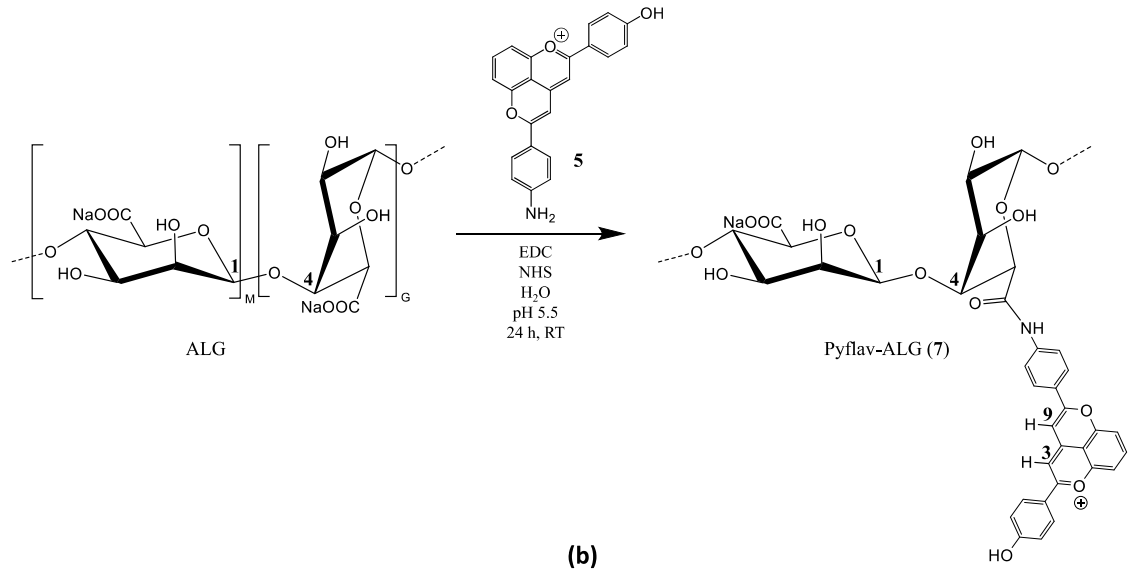
Scheme 1. Strategy for the Synthesis of the Pyranoflavylium-Based Dyes (4, 5)



Scheme 2. Coupling Reactions between 10-Carboxy-4′-hydroxypyranoflavylium (4) and CHT (a) and between 10-Aminophenyl-4′-hydroxypyranoflavylium (5) and ALG (b) by EDC/NHS Carbodiimide Chemistry



(a)



(b)

standard. The samples were prepared in D_2O and in DMSO-d_6 with different amounts of acid or base [trifluoroacetyl (TFA) or NaOD]. ^1H chemical shifts were assigned using two-dimensional (2D) NMR experiments [correlation spectroscopy (COSY), nuclear Overhauser

https://doi.org/10.1021/acsapm.2c00514
ACS Appl. Polym. Mater. 2022, 4, 4961−4971

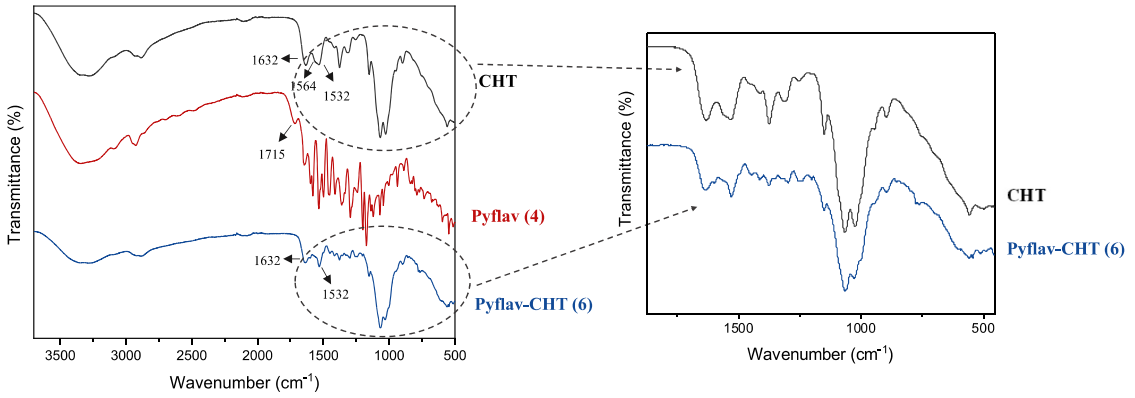


Figure 1. FTIR spectra of CHT, Pyflav (**4**), and Pyflav-CHT (**6**).

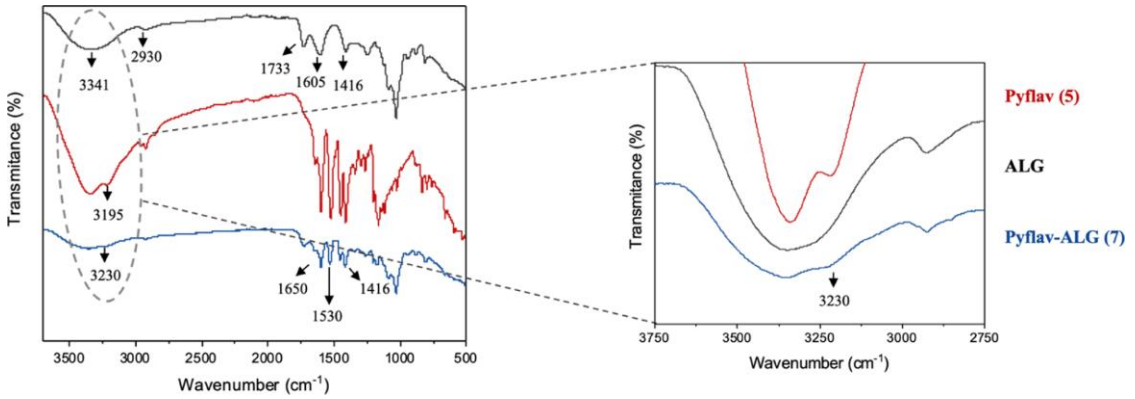


Figure 2. FTIR spectra of ALG, Pyflav (**5**), and Pyflav-ALG (**7**).

enhancement spectroscopy (NOESY)], while ^{13}C resonances were assigned using 2D NMR techniques (gHMBC and gHSQC). Multiplicities are expressed as singlet (s), doublet (d), and triplet (t), chemical shifts (δ) in parts per million, and coupling constants (J) in hertz.

2.7. LC-DAD/ESI-MS. LC-DAD/ESI/MS analyses were carried out using the equipment and experimental conditions described elsewhere.[25]

2.8. FTIR-ATR. The FTIR characterization was performed in a PerkinElmer (model Spectrum Two), in the frequency range of 4000−400 cm^{-1}, with four scans and a resolution of 4 cm^{-1}.

2.9. DLS. Stock solutions of native polymers and respective conjugates (1 mg/mL) were prepared in MilliQ water where the measurements were performed at a final concentration of 0.2 mg/mL. DLS analyses were carried out on a Litesizer500 (Anton Paar, ES), with Omega Cuvette, operating at 658 nm with automatic scattering angle, at 25 °C.

3. RESULTS AND DISCUSSION

3.1. Synthesis of Pyranoflavylium-Based Dyes and Conjugates. The synthesis of pH-sensitive pyranoflavylium dyes (**4**, **5**) followed the standard procedures: first, the 4′,5-dihydroxyflavylium dye (**3**) was synthesized by the classical aldol condensation between 2,6-dihydroxybenzaldehyde (**1**) and 4-hydroxyacetophenone (**2**) using a TMS-Cl reagent to produce HCl in situ.[26] Subsequently, pigments **4** and **5** were obtained by typical cycloaddition reactions following the mechanism of pyranoanthocyanins described elsewhere (Scheme 1)[7] with yields of 12 and 13%, respectively. Products **4** and **5** were structurally characterized by mass spectrometry and NMR spectroscopy using mono- and bidimensional techniques.

The Pyflav-CHT (**6**) and Pyflav-ALG (**7**) conjugates were prepared by grafting 10-carboxy-4′-hydroxypyranoflavylium (**4**) and 10-aminophenyl-4′-hydroxypyranoflavylium (**5**) onto CHT and ALG backbones, respectively, via EDC/NHS coupling chemistry following the mechanisms already reported (Scheme 2).[27,28]

Carbodiimide-based chemical coupling reagents such EDC have been successfully used for the synthesis of several kinds of CHT-polyphenol conjugates including CHT-caffeic acid,[29] CHT-ferulic acid,[30] and CHT-chlorogenic acid.[31] The synthesis of Pyflav-CHT (**6**) and Pyflav-ALG (**7**) using EDC/NHS activating coupling agents followed the typical mechanism described in the literature.[32−34]

3.2. FT-IR Spectroscopy. FT-IR spectroscopy technique was further used to characterize the functional groups and new chemical bonds formed on the pyranoflavylium-biopolymer conjugates.

3.2.1. Pyflav-CHT Conjugate (6). The FT-IR spectrum of CHT, as shown in Figure 1, exhibited characteristic absorption bands at 1632 cm^{-1} (C═O stretching of N-acetyl residues, amide I), 1532 cm^{-1} (N−H bending, amide II), and 1311

https://doi.org/10.1021/acsapm.2c00514
ACS Appl. Polym. Mater. 2022, 4, 4961−4971

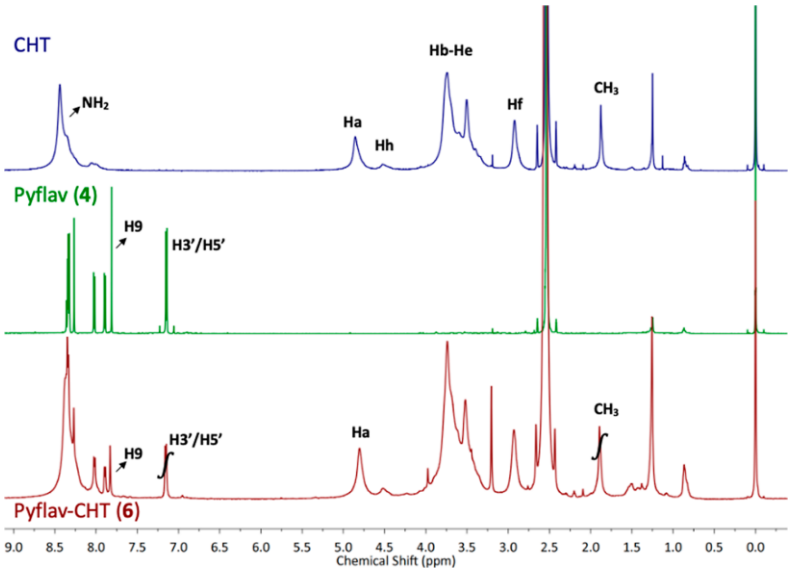


Figure 3. Nuclear magnetic resonance (^{1}H NMR) spectra of CHT, Pyflav **4**, and Pyflav-CHT **6** recorded in DMSO-d_6/TFA (90:10).

cm^{-1} (C−N stretching (amide III). The band at 1564 cm^{-1} was due to the N−H bending of the primary amine.[35] The bands at 1415 and 1376 cm^{-1} were attributed to $-CH_2$ bending and $-CH_3$ symmetrical deformation, respectively.[36]

As seen in Figure 1, for 10-carboxy-4′-hydroxypyranoflavylium, Pyflav (**4**), some typical C=C stretching bands on aromatic ring were observed within 1450−1600 cm^{-1} and a band at 1715 cm^{-1} that corresponds to the C=O stretching vibration.[37,38]

Analyzing the spectrum of Pyflav-CHT (**6**), as compared with CHT, the N−H bending of the primary amine (1564 cm^{-1}) seems to disappear (or at least its intensity is reduced). This could indicate the conversion of the primary into a secondary amine with the formation of an amide linkage between the amine groups of CHT and the carboxylic group of the pigment.[39]

3.2.2. Pyflav-ALG Conjugate (7). The FT-IR spectrum of ALG, Figure 2, showed some characteristic bands: a broad band at about 3341 cm^{-1}, assigned to the stretching of O−H group, a weak peak at 2930 cm^{-1} (C−H antisymmetrical stretching),[40] 1733 cm^{-1} (C=O stretching),[41] 1605 cm^{-1} (COO^- antisymmetric stretching), 1416 cm^{-1} (C−O symmetric stretching),[42] and 1245 cm^{-1} (C−O stretching). For 10-aminophenylpyrano-4′-hydroxyflavylium a band at 3335 cm^{-1} is assigned to the stretching of the O−H group and the presence of a second peak at 3195 cm^{-1} is attributed to the N−H stretching vibration mode.[43] The peak observed at 1450−1600 cm^{-1} is a typical band assigned to the C=C stretching vibration on an aromatic ring. Analyzing FTIR of Pyflav-ALG conjugate **7**, the spectrum showed the presence of the band about 3230 cm^{-1}, assigned to N−H stretching, already existing on the pigment spectrum and not in the ALG one. Three new peaks were also observed: 1650 cm^{-1} assigned to C=O amide stretching, 1530 cm^{-1} (N−H bend in plane), and at 1456 cm^{-1} assigned to the C−N stretching vibration mode.[44] The presence of these bands could indicate the successful formation of an amide chemical bond between the carboxylic groups of the ALG and the phenylamine group of pigment **6**.

3.3. NMR. The successful synthesis of pyranoflavylium-biopolymer conjugates was confirmed by NMR spectroscopy including 2D techniques (COSY, HSQC, HMBC, TOCSY, and NOESY), providing structural information. The different free pigments, conjugates, and native biopolymers were necessarily recorded in different solvent systems and temperatures to ensure total solubilization and enhancement of the peak resolution.

3.3.1. Pyflav-CHT Conjugate (6). As shown in Figure 3, CHT showed characteristic proton signals[45,46] at δ 8.44 ppm (H−N), δ 4.86 ppm (H-a), δ 4.53 ppm (H−h), multiplet peaks δ 3.90−3.28 ppm (H-b to H-e), δ 2.92 ppm (H-f), and a singlet peak at δ 1.88 ppm assigned to the protons of N-acetyl glucosamine units. Beside the proton signals of CHT, Pyflav-CHT conjugate **6** also showed new peaks in the region between 7.0 and 8.4 ppm, which can be assigned to the aromatic protons of 10-carboxypyrano-4′-hydroxyflavylium moieties.[47] In general, the proton chemical shifts assigned to the structure of 10-carboxypyrano-4′-hydroxyflavylium, remain at the same value except the one assigned to H-9. The chemical shift assigned to H-9 in the pigment analysis is located at 7.81 ppm and, in the conjugate, this proton is slight shifted to 7.83 ppm. This slight change can be explained by its proximity to the new amide bond, thus allowing the detection of the difference in the surrounding chemical environment. On the other hand, comparing the modified CHT with the native molecule the most significant difference is related with the chemical shift the H-a proton which changed from 4.86 (free CHT) to 4.80 (conjugated) ppm. These results suggested that 10-carboxy-4′-hydroxypyranoflavylium was successfully grafted onto CHT and confirm that the reaction occurs between the COOH group of the pigment and the amine group of CHT.

The acquired NMR spectra allowed the determination of the substitution degree (DS) of 10-carboxypyrano-4′-hydroxyflavylium in CHT according to eq 2[48] taking into consideration

https://doi.org/10.1021/acsapm.2c00514
ACS Appl. Polym. Mater. 2022, 4, 4961−4971

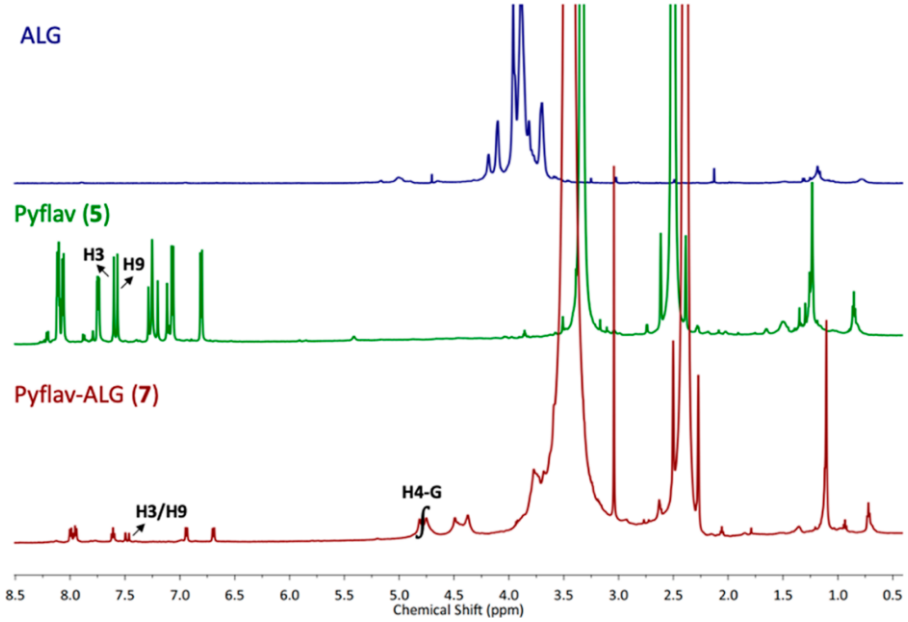


Figure 4. ^{1}H NMR spectra of ALG (recorded in D_2O with signal suppression), Pyflav **5** (in DMSO-d_6), and Pyflav-ALG **7** (in DMSO-d_6:NaOD 98:2 at 40 °C).

its acetylation degree. From the ratio between the peak integrals corresponding to H-3′ and H-5′ protons of the pigment (7.16 ppm) and CH_3 protons of CHT (1.89 ppm), DS was obtained to be 14%, similarly to values reported in the literature.[49]

$$\mathrm{DS} = \frac{\int H3'/5'(\mathrm{pigment})}{\int \mathrm{CH_3(chitosan)}} \times \frac{3}{2} \times \text{degree of acetylation} \quad (2)$$

3.3.2. Pyflav-ALG Conjugate 7. Due to solubility issues of ALG in DMSO-d_6, its NMR spectrum was acquired in D_2O and therefore it was not possible to carry out a direct comparison of the chemical shift values on the Pyflav-ALG **7** spectrum. To ensure the total solubility of the latter, NMR spectroscopy was performed with DMSO-d_6. As shown in Figure 4, Pyflav-ALG **7** spectrum showed new peaks in the aromatic region (between 6.7 and 8.2 ppm), which can be assigned to the characteristic protons of the Pyflav-CHT **6** residue. In general, for the conjugate and free pigment, the proton chemical shifts assigned to the structure of Pyflav-CHT **6** did not alter significantly except for the two singlets assigned to H-3 and H-9 which slightly undergo downfield shifts. The peaks with higher chemical shift (δ 4.83 ppm) in the sodium ALG region were assigned to the guluronic acid anomeric proton (H-4G) in agreement with data previously reported in the literature.[50,51] The acquired NMR spectra also allowed the determination of substitution of pigment **5** in ALG to be 1.2%, from the ratio between of the peak integrals corresponding to H-3″ and H-5″ protons of pigment (6.80 ppm) and the one at 4.83 ppm that corresponds to proton H-4G in ALG, as shown in eq 3[52]

$$\mathrm{DS} = \frac{\int H3''/5''(\mathrm{pigment})}{2.56 \int \mathrm{H4G(alginate)}} \times \frac{1}{2} \quad (3)$$

3.4. Dynamic Light Scattering. The DLS technique was used to assess the zeta potential of both native polymers and respective conjugates (Figure 5). The aim here was essentially

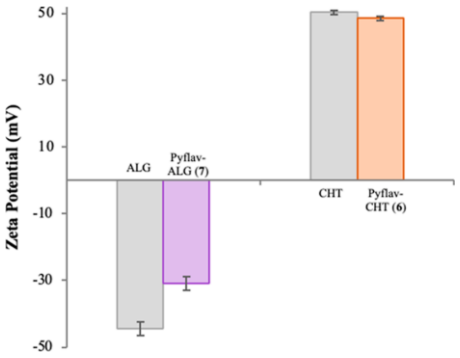


Figure 5. Zeta potential of ALG, Pyflav-ALG **7**, CHT, and Pyflav-CHT **6**.

to confirm that the pyranoflavylium dye functionalization did not alter significatively the charge of native polymers in order to produce multilayer membranes by electrostatic interactions.

The zeta potential measurements demonstrated that CHT has a positive average surface charge due to the protonation of the amino group ($-NH_2$) with an absolute value of ζ-potential, 50.4 ± 0.6 mV. Analyzing the charge of Pyflav-CHT **6**, the absolute value of ζ-potential was 48.6 ± 0.6 mV which indicates that there is no significant charge variation between

https://doi.org/10.1021/acsapm.2c00514
ACS Appl. Polym. Mater. 2022, 4, 4961−4971

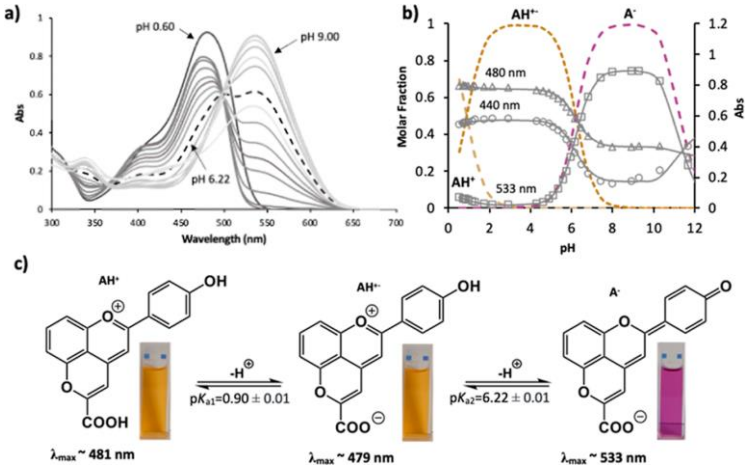


Figure 6. (**a**) Spectral variations of PyFlav **4** as a function of pH; (**b**) fitting was achieved for pK_{a1} = 0.90 ± 0.01 e pK_{a2} = 6.22 ± 0.01; and (**c**) chemical equilibria and species color displayed by PyFlav **4** in water/ethanol (75:25) (v/v).

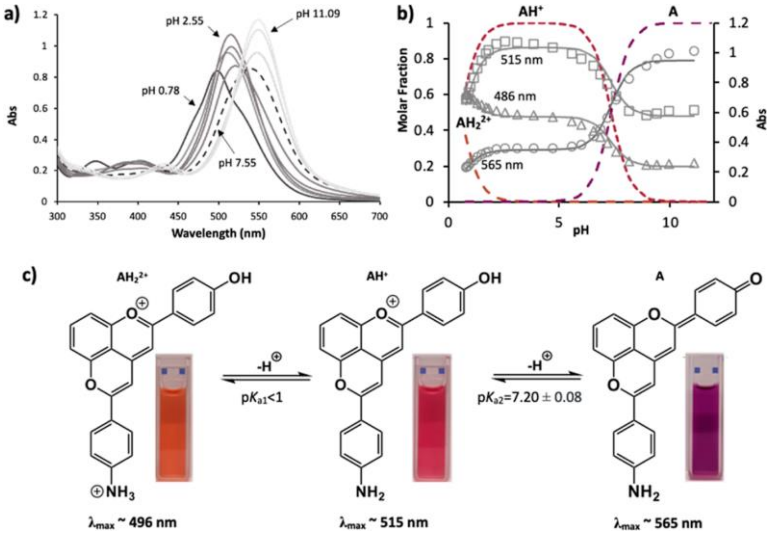


Figure 7. a) Spectral variations of PyFlav **5** as a function of pH; (**b**) fitting was achieved for pK_{a1} < 1 e pK_{a2} = 7.20 ± 0.08; and (**c**) chemical equilibria and species color displayed by Pyflav **5** in water/ethanol (75:25) (v/v).

the polymer and its conjugate. This result is expected because both CHT and pigment are positively charged which led to an insignificant charge variation. For ALG, due to the presence of carboxylic groups, the average surface charge gave −44.4 ± 2 mV, while for Pyflav-ALG **7**, a ζ-potential of −30.9 ± 2 mV was obtained. This result indicates the impact of a positively charge compound on ALG functionalization yielding in a decrease of the absolute charge average on the conjugate.

Therefore, the ζ-potential of both conjugates with well-defined oppositely charges revealed to be promising to ensure electrostatic−driven interactions by direct deposition on inert substrates (e.g., polypropylene), aiming the formation of pH-responsive multilayered membranes through layer-by-layer assembly technology.

3.5. UV−Vis Spectroscopy. Spectrophotometric titrations were conducted to determine equilibrium forms and respective acidity constants of the free pyranoflavylium dyes and respective conjugates (pK_a values).

The UV−vis spectra results showed that the hydration reaction do not occurs for these pigments because there is no evidence of a band with the absorption at 280 nm and color fading with the increase in pH. Actually, this is a similar behavior described for other pyranoanthocyanins already reported in the literature.[53,54] For that reason, the study of the chemical equilibria of these systems in solution only considered proton transfer reactions (acid-base equilibria). The global process is given by the following equations

$$AH^+ + H_2O \leftrightarrow A + H_3O^+ K_{a1} \text{ first proton transfer} \quad (4)$$

https://doi.org/10.1021/acsapm.2c00514
ACS Appl. Polym. Mater. 2022, 4, 4961−4971

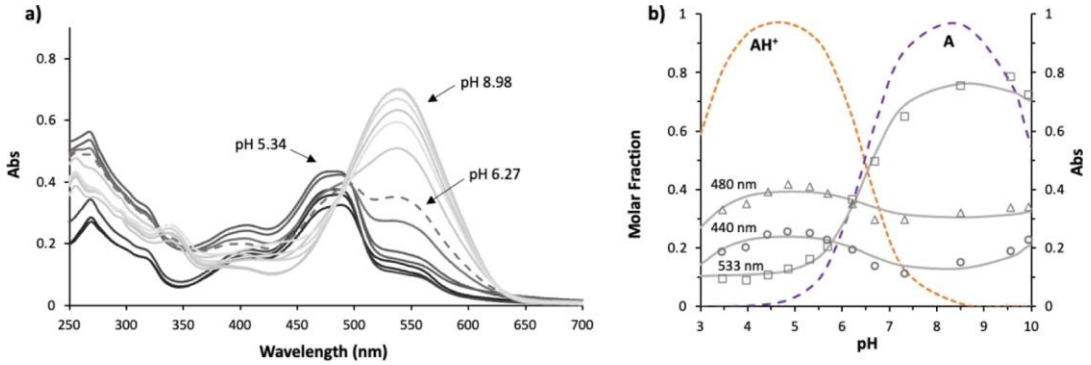


Figure 8. (a) Spectral variations of PyFlav-CHT **6** as a function of pH; (b) fitting was achieved for pK_a (4′OH) = 6.43 ± 0.04.

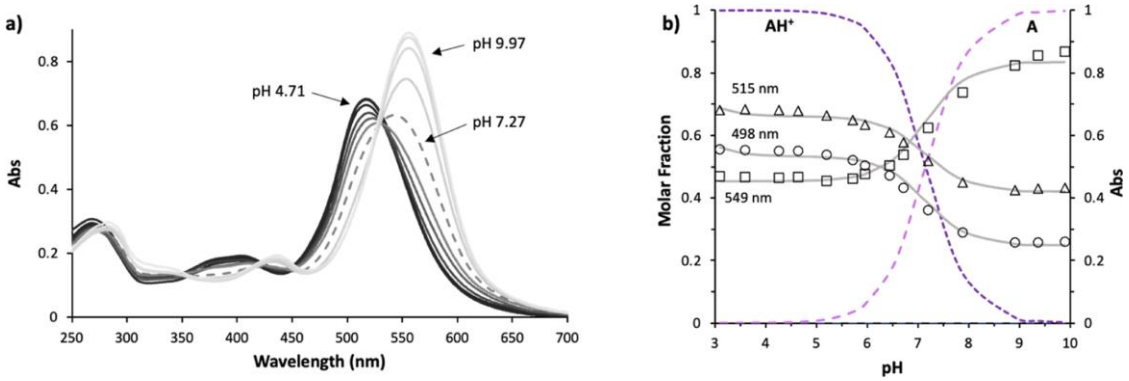


Figure 9. a) Spectral variations of PyFlav-ALG **7** as a function of pH; **b**) fitting was achieved for pK_a (4′OH) = 7.17 ± 0.02.

$$A + H_2O \leftrightarrow A^- + H_3O^+ K_{a2} \text{ second proton transfer} \quad (5)$$

$$\text{where: } K_{a1} = \frac{[A]\cdot[H_3O^+]}{[AH^+]} \qquad K_{a2} = \frac{[A^-]\cdot[H_3O^+]}{[A]} \quad (6)$$

Considering the total concentration, C_0 is the sum of the individual species

$$C_0 = [AH^+] + [A] + [A^-] + [A^{2-}] \quad (7)$$

their mole fraction distribution, χ_i, is calculated by the simplified equations

$$\chi_{AH^+} = \frac{[AH^+]}{C_0} = \frac{1}{1 + \frac{K_{a1}}{[H^+]} + \frac{K_{a2}\cdot K_{a1}}{[H^+]}} \quad (8)$$

$$\chi_A = \frac{[A]}{C_0} = \frac{K_{a1}\cdot\chi_{AH^+}}{[H^+]} \quad (9)$$

$$\chi_{A^-} = \frac{[A^-]}{C_0} = \frac{K_{a2}\cdot\chi_A}{[H^+]} \quad (10)$$

The fitting of experimental data at a given wavelength, λ, is given by the following equation

$$A_{calc} = \varepsilon_{AH^+}\cdot\chi_{AH^+} + \varepsilon_A\cdot\chi_A + \varepsilon_{A^-} + \chi_{A^-} \quad (11)$$

where ε_{AH^+}, ε_A, and ε_{A^-} represent the mole absorption coefficients of individual species.

The apparent pK_a values were obtained by simultaneously fitting the absorbance values, calculated using eq 11, to the ones obtained experimentally at several wavelengths using the solver function to minimize the sum of least-squares method. The fitting was successful indicating the presence of different species in solution.

The UV−vis spectral variations of hydroalcoholic solutions of pigments **4** and **5** at different pH values are shown in Figures 6 and 7, respectively. Similarly to the pyranoanthocyanin analogues already described, there is no evidence of the hydration process observed after the pH increase as well as no evidence of the formation of B hemiketal species, characterized by the appearance of a band with absorption at 280 nm. Such a behavior was observed for the two compounds studied throughout this work. The molar fractions of all species and respective absorbance values at chosen wavelengths were plotted as a function of pH together with the respective fittings.

For pigment **4**, the UV−vis spectra obtained allowed us to determine two equilibrium constants, and as the pH increases, one isosbestic point was observed, which is detected when the pK_a values are sufficiently separated, resulting in a good fitting, as shown in Figure 6.

The first pK_a around 0.90 caused by the deprotonation of the carboxylic group at C-10 of the flavylium cation only caused a very small spectral variation, generating the appearance of a zwitterion species, AH^{+-}. The second pK_a value was established between the zwitterion compound and

https://doi.org/10.1021/acsapm.2c00514
ACS Appl. Polym. Mater. 2022, 4, 4961−4971

Table 1. pK_a Values Obtained for Pyflav 4, Pyflav-CHT 6, Pyflav 5, and Pyflav-ALG 7

	Pyflav 4	Pyflav-CHT 6	Pyflav 5	Pyflav-ALG 7
pK_a (10-COOH/NH_2)	0.90 ± 0.01		<1	
pK_a (4′-OH)	6.22 ± 0.01	6.43 ± 0.04	7.20 ± 0.08	7.17 ± 0.02

the quinoidal base, assigned to the deprotonation of the C-4′OH group.

On the other hand, for compound **5**, shown in Figure 7, the first pK_a was assigned to the protonation of the aniline group attached at C-10 of the flavylium cation (AH^+), concomitantly with the increase in concentrations of HCl, yielding a dicationic species (AH_2^{2+}). The fitting allowed the determination of the first pK_a to be less than 1, as described recently for an analogous dye.[55]

The determination of pK_a value of Pyflav-biopolymer conjugates (**6**, **7**) through spectrophotometric titrations was conducted using the same experimental conditions as the ones of the free pigments to ensure direct comparison except for the initial pH that was set to 3 due to insolubility issues, mainly for Pyflav-ALG conjugate (Figures 8 and 9).

Moreover, due to the new chemical linkage between the pigments and biopolymers, the first equilibrium was not considered for the pK_a determination. Therefore, this method was used to determine the pK_a value related to the deprotonation of the OH group present at C4′ of the conjugates in order to understand if the covalent amide bond could or not tune/shift the pK_a value of the free pigments. In general, the conjugation to biopolymers did not significantly shift the absorption maximum wavelength of each species, as well as their pK_a values. Actually, the thermodynamic parameters obtained for the conjugates fits well in the pH sensing range (between 5 and 8) where they are pretended to yield a colorimetric response. As shown in Table 1, the difference between pigments and respective conjugates was slightly more evident for Pyflav-CHT **6** in comparison with respective Pyflav **4**. This can be attributed to the difference in the structure of the pigments, resulting in a higher proximity of the new amide bond formed on the conjugate (Pyflav-CHT **6**) to the C4′ of Pyflav **4**. This proximity can influence the deprotonation of the C4′-OH group more likely than in Pyflav-ALG **7**. Overall, the Pyflav-biobased conjugates (**6**, **7**) have great potential for monitoring pH alterations (between 5.8 and 7.4) of perishable foods such as meat or fish as a result of the formation of volatile basic nitrogen-based metabolites (e.g., biogenic amines) during the degradation process.

4. CONCLUSIONS

The strategy of chemical functionalization of biocompatible polymers with pyranoflavylium pH-sensitive pigments is a suitable tool for the development of novel functional materials. Overall, in this work, it was possible to achieve for the very first time new pyranoflavylium-biopolymer hybrid conjugates which are promising starting materials to build up colorimetric pH-responsive (bio)films. Future work will deal with the construction of thick, flexible, and robust free-standing multilayered membranes on inert low surface energy substrates (e.g., polypropylene) making use of electrostatic interactions between oppositely charged polyelectrolytes (e.g., ALG/Pyflav-CHT and Pyflav-ALG/CHT) through layer-by-layer assembly technology.

■ ASSOCIATED CONTENT

Supporting Information

The Supporting Information is available free of charge at https://pubs.acs.org/doi/10.1021/acsapm.2c00514.

2D NMR spectra (COSY, HSQC, HMBC, NOESY, and TOCSY) of both free dyes and biopolymer conjugates (PDF)

■ AUTHOR INFORMATION

Corresponding Author

Luís Cruz − *REQUIMTE/LAQV, Department of Chemistry and Biochemistry, Faculty of Sciences, University of Porto, Porto 4169-007, Portugal;* orcid.org/0000-0003-2226-0404; Phone: +351 220402558; Email: luis.cruz@fc.up.pt; Fax: +351 220402658

Authors

Ana Sofia Pires − *REQUIMTE/LAQV, Department of Chemistry and Biochemistry, Faculty of Sciences, University of Porto, Porto 4169-007, Portugal*

Vânia Gomes − *REQUIMTE/LAQV, Department of Chemistry and Biochemistry, Faculty of Sciences, University of Porto, Porto 4169-007, Portugal*

Dina Neves − *REQUIMTE/LAQV, Department of Chemistry and Biochemistry, Faculty of Sciences, University of Porto, Porto 4169-007, Portugal*

Nuno Mateus − *REQUIMTE/LAQV, Department of Chemistry and Biochemistry, Faculty of Sciences, University of Porto, Porto 4169-007, Portugal*

Victor de Freitas − *REQUIMTE/LAQV, Department of Chemistry and Biochemistry, Faculty of Sciences, University of Porto, Porto 4169-007, Portugal;* orcid.org/0000-0003-0586-2278

Complete contact information is available at: https://pubs.acs.org/10.1021/acsapm.2c00514

Author Contributions

A.S.P.: writing—original draft, conceptualization, methodology, and investigation. V.G.: conceptualization, methodology, investigation, and writing—review and editing. D.N.: methodology and investigation. N.M.: writing—review and editing. V.F.: writing—review and editing, project administration, and funding acquisition. L.C.: conceptualization, methodology, investigation, writing—original draft, writing—review and editing, project administration, and funding acquisition.

Notes

The authors declare no competing financial interest.

■ ACKNOWLEDGMENTS

The authors thank Dr. Silvia Maia for the MS analysis and Dr. Mariana Andrade for the NMR analysis. This work was supported by the Associate Laboratory for Sustainable Chemistry, Clean Processes and Technologies LAQV. The latter is financed by national funds from UIDB/50006/2020. This work was also supported by the project PTDC/OCE-

https://doi.org/10.1021/acsapm.2c00514
ACS Appl. Polym. Mater. 2022, 4, 4961−4971

ETA/31250/2017 funded by FCT and FEDER. Ana Pires acknowledges the research grant from the project PTDC/OCE-ETA/31250/2017. L.C. acknowledges the FCT research contract (DL 57/2016/CP1334/CT0008). A.S.P., V.G., and D.N. acknowledge the PhD grants from FCT (2021.08670.BD, SFRH/BD/136556/2018, and 2020.065.23.BD, respectively).

REFERENCES

(1) Borges, J.; Mano, J. F. Molecular Interactions Driving the Layer-by-Layer Assembly of Multilayers. *Chem. Rev.* **2014**, *114*, 8883−8942.
(2) Borges, J.; Sousa, M. P.; Cinar, G.; Caridade, S. G.; Guler, M. O.; Mano, J. F. Nanoengineering Hybrid Supramolecular Multilayered Biomaterials Using Polysaccharides and Self-Assembling Peptide Amphiphiles. *Adv. Funct. Mater.* **2017**, *27*, 1605122.
(3) Vargas, M.; Pastor, C.; Chiralt, A.; McClements, D. J.; González-Martínez, C. Recent Advances in Edible Coatings for Fresh and Minimally Processed Fruits. *Crit. Rev. Food Sci. Nutr.* **2008**, *48*, 496−511.
(4) Guzey, D.; McClements, D. J. Formation, stability and properties of multilayer emulsions for application in the food industry. *Adv. Colloid Interface Sci.* **2006**, *128-130*, 227−248.
(5) Biji, K. B.; Ravishankar, C. N.; Mohan, C. O.; Srinivasa Gopal, T. K. Smart packaging systems for food applications: a review. *J. Food Sci. Technol.* **2015**, *52*, 6125−6135.
(6) Yousefi, H.; Su, H.-M.; Imani, S. M.; Alkhaldi, K.; M. Filipe, C. D.; Didar, T. F. Intelligent Food Packaging: A Review of Smart Sensing Technologies for Monitoring Food Quality. *ACS Sens.* **2019**, *4*, 808−821.
(7) Cruz, L.; Basílio, N.; Mateus, N.; de Freitas, V.; Pina, F. Natural and Synthetic Flavylium-Based Dyes: The Chemistry Behind the Color. *Chem. Rev.* **2022**, *122*, 1416−1481.
(8) Choi, I.; Lee, J. Y.; Lacroix, M.; Han, J. Intelligent pH indicator film composed of agar/potato starch and anthocyanin extracts from purple sweet potato. *Food Chem.* **2017**, *218*, 122−128.
(9) Maciel, V. B. V.; Yoshida, C. M. P.; Franco, T. T. Chitosan/pectin polyelectrolyte complex as a pH indicator. *Carbohydr. Polym.* **2015**, *132*, 537−545.
(10) Pereira, V. A., Jr; de Arruda, I. N. Q.; Stefani, R. Active chitosan/PVA films with anthocyanins from Brassica oleraceae (Red Cabbage) as Time-Temperature Indicators for application in intelligent food packaging. *Food Hydrocolloids* **2015**, *43*, 180−188.
(11) Lu, M.; Shiau, Y.; Wong, J.; Lin, R.; Kravis, H.; Blackmon, T.; Pakzad, T.; Jen, T.; Cheng, A.; Chang, J.; Ong, E.; Sarfaraz, N.; Wang, N. S. Milk Spoilage: Methods and Practices of Detecting Milk Quality. *Food Nutr. Sci.* **2013**, *04*, 113.
(12) Weston, M.; Phan, M. A. T.; Arcot, J.; Chandrawati, R. Anthocyanin-based sensors derived from food waste as an active use-by date indicator for milk. *Food Chem.* **2020**, *326*, 127017.
(13) Dudnyk, I.; Janeček, E.-R.; Vaucher-Joset, J.; Stellacci, F. Edible sensors for meat and seafood freshness. *Sens. Actuators, B* **2018**, *259*, 1108−1112 Article.
(14) Zhai, X.; Li, Z.; Zhang, J.; Shi, J.; Zou, X.; Huang, X.; Zhang, D.; Sun, Y.; Yang, Z.; Holmes, M.; Gong, Y.; Povey, M. Natural Biomaterial-Based Edible and pH-Sensitive Films Combined with Electrochemical Writing for Intelligent Food Packaging. *J. Agric. Food Chem.* **2018**, *66*, 12836−12846 Article.
(15) Cruz, L.; Basílio, N.; Mendoza, J.; Mateus, N.; de Freitas, V.; Tawara, M. H.; Correa, J.; Fernandez-Megia, E. Impact of a Water-Soluble Gallic Acid-Based Dendrimer on the Color-Stabilizing Mechanisms of Anthocyanins. *Chem.—Eur. J.* **2019**, *25*, 11696−11706.
(16) Oliveira, J.; Mateus, N.; De Freitas, V. Previous and recent advances in pyranoanthocyanins equilibria in aqueous solution. *Dyes Pigm.* **2014**, *100*, 190−200.
(17) Sousa, J. L. C.; Gomes, V.; Mateus, N.; Pina, F.; de Freitas, V.; Cruz, L. Synthesis and equilibrium multistate of new pyrano-3-deoxyanthocyanin-type pigments in aqueous solutions. *Tetrahedron* **2017**, *73*, 6021−6030.
(18) Cruz, L.; Gomes, V.; Mateus, N.; de Freitas, V. Synthesis and Structural Characterization of a Novel Symmetrical 2,10-Bis-Styryl-1-Benzopyrylium Dye. *Synlett* **2018**, *29*, 1390−1394.
(19) Gomes, V.; Mateus, N.; de Freitas, V.; Cruz, L. Synthesis and chemical equilibria of a new 10-methylpyrano-2-styrylbenzopyrylium pigment in aqueous solution and its modulation by different micellar systems. *Dyes Pigm.* **2019**, *167*, 60−67.
(20) Cruz, L.; Gomes, V.; Guimarães, M.; Gonçalves, G.; de Freitas, V. Bioinspired Synthesis and Physical-Chemical Properties of a New 10-Methylpyrano-4′-hydroxyflavylium Chloride Salt. *Synlett* **2020**, *31*, 334−338.
(21) Gomes, V.; Pires, A. S.; Fernandes, I.; Mateus, N.; de Freitas, V.; Cruz, L. Synthesis of novel pyrano-3,7-deoxyanthocyanin derivatives and study of their thermodynamic, photophysical and cytotoxicity properties. *J. Photochem. Photobiol., A* **2021**, *415*, 113313.
(22) Gomes, V.; Pires, A. S.; Mateus, N.; de Freitas, V.; Cruz, L. Pyranoflavylium-cellulose acetate films and the glycerol effect towards the development of pH-freshness smart label for food packaging. *Food Hydrocolloids* **2022**, *127*, 107501.
(23) Küster, W. F.; Thiel, A. *Tabelle per le analisi chimiche e chimico-fisiche*, 12, ed.; Hoepli: Milano, 1982.
(24) Gelsema, W. J.; De Ligny, C.; Remijnse, A.; Blijleven, H. pH-Measurements in alcohol-water mixtures, using aqueous standard buffer solutions for calibration. *Recl. Trav. Chim. Pays-Bas* **1966**, *85*, 647−660.
(25) Cruz, L.; Basílio, N.; Mateus, N.; Pina, F.; de Freitas, V. Characterization of Kinetic and Thermodynamic Parameters of Cyanidin-3-glucoside Methyl and Glucuronyl Metabolite Conjugates. *J. Phys. Chem. B* **2015**, *119*, 2010−2018.
(26) Al Bittar, S.; Mora, N.; Loonis, M.; Dangles, O. A simple synthesis of 3-deoxyanthocyanidins and their O-glucosides. *Tetrahedron* **2016**, *72*, 4294−4302.
(27) Pettignano, A.; Grijalvo, S.; Häring, M.; Eritja, R.; Tanchoux, N.; Quignard, F.; Díaz Díaz, D. Boronic acid-modified alginate enables direct formation of injectable, self-healing and multistimuli-responsive hydrogels. *Chem. Commun.* **2017**, *53*, 3350−3353.
(28) An, H.; Bo, Y.; Chen, D.; Wang, Y.; Wang, H.; He, Y.; Qin, J. Cellulose-based self-healing hydrogel through boronic ester bonds with excellent biocompatibility and conductivity. *RSC Adv.* **2020**, *10*, 11300−11310.
(29) Aytekin, A. O.; Morimura, S.; Kida, K. Synthesis of chitosan-caffeic acid derivatives and evaluation of their antioxidant activities. *J. Biosci. Bioeng.* **2011**, *111*, 212−216.
(30) Woranuch, S.; Yoksan, R. Preparation, characterization and antioxidant property of water-soluble ferulic acid grafted chitosan. *Carbohydr. Polym.* **2013**, *96*, 495−502.
(31) Wei, Z.; Gao, Y. Evaluation of structural and functional properties of chitosan-chlorogenic acid complexes. *Int. J. Biol. Macromol.* **2016**, *86*, 376−382.
(32) Pasanphan, W.; Chirachanchai, S. Conjugation of gallic acid onto chitosan: An approach for green and water-based antioxidant. *Carbohydr. Polym.* **2008**, *72*, 169−177.
(33) Satheesha Babu, B. K.; Srinivasa Rao, K. Synthesis and characterization of sodium alginate conjugate: Preparation and evaluation of transdermal patches of losartan potassium using sodium alginate conjugate. *Thai J. Pharm. Sci.* **2015**, *39*, 10−20.
(34) Liu, J.; Meng, C.-g.; Yan, Y.-h.; Shan, Y.-n.; Kan, J.; Jin, C.-h. Protocatechuic acid grafted onto chitosan: Characterization and antioxidant activity. *Int. J. Biol. Macromol.* **2016**, *89*, 518−526.
(35) Lim, S.-H.; Hudson, S. M. Synthesis and antimicrobial activity of a water-soluble chitosan derivative with a fiber-reactive group. *Carbohydr. Res.* **2004**, *339*, 313−319.
(36) Zhang, H.; Li, S.; Branford White, C. J.; Ning, X.; Nie, H.; Zhu, L. Studies on electrospun nylon-6/chitosan complex nanofiber interactions. *Electrochim. Acta* **2009**, *54*, 5739−5745.
(37) Liu, J.; Wen, X.-y.; Lu, J.-f.; Kan, J.; Jin, C.-h. Free radical mediated grafting of chitosan with caffeic and ferulic acids: Structures and antioxidant activity. *Int. J. Biol. Macromol.* **2014**, *65*, 97−106.

https://doi.org/10.1021/acsapm.2c00514
ACS Appl. Polym. Mater. 2022, 4, 4961−4971

(38) Chatterjee, N. S.; Panda, S. K.; Navitha, M.; Asha, K. K.; Anandan, R.; Mathew, S. Vanillic acid and coumaric acid grafted chitosan derivatives: improved grafting ratio and potential application in functional food. J. Food Sci. Technol. 2015, 52, 7153−7162.
(39) Spizzirri, U. G.; Iemma, F.; Puoci, F.; Cirillo, G.; Curcio, M.; Parisi, O. I.; Picci, N. Synthesis of antioxidant polymers by grafting of gallic acid and catechin on gelatin. Biomacromolecules 2009, 10, 1923−1930.
(40) Fan, L.; Cao, M.; Gao, S.; Wang, T.; Wu, H.; Peng, M.; Zhou, X.; Nie, M. Preparation and characterization of sodium alginate modified with collagen peptides. Carbohydr. Polym. 2013, 93, 380−385.
(41) Yadav, S.; Ahuja, M.; Kumar, A.; Kaur, H. Gellan-thioglycolic acid conjugate: Synthesis, characterization and evaluation as mucoadhesive polymer. Carbohydr. Polym. 2014, 99, 601−607.
(42) Kanti, P.; Srigowri, K.; Madhuri, J.; Smitha, B.; Sridhar, S. Dehydration of ethanol through blend membranes of chitosan and sodium alginate by pervaporation. Sep. Purif. Technol. 2004, 40, 259−266.
(43) Lawrie, G.; Keen, I.; Drew, B.; Chandler-Temple, A.; Rintoul, L.; Fredericks, P.; Grøndahl, L. Interactions between alginate and chitosan biopolymers characterized using FTIR and XPS. Biomacromolecules 2007, 8, 2533−2541.
(44) Wang, X.; Jiang, Z.; Shi, J.; Zhang, C.; Zhang, W.; Wu, H. Dopamine-modified alginate beads reinforced by cross-linking via titanium coordination or self-polymerization and its application in enzyme immobilization. Ind. Eng. Chem. Res. 2013, 52, 14828−14836.
(45) Xie, M.; Hu, B.; Wang, Y.; Zeng, X. Grafting of gallic acid onto chitosan enhances antioxidant activities and alters rheological properties of the copolymer. J. Agric. Food Chem. 2014, 62, 9128−9136.
(46) Yu, S.; Du, J.; Zheng, Y.; Yan, L. Synthesis and characterization of carboxymethyl chitosan containing functional ultraviolet absorber substituent. J. Appl. Polym. Sci. 2007, 106, 4098−4103.
(47) Eom, T.-K.; Senevirathne, M.; Kim, S.-K. Synthesis of phenolic acid conjugated chitooligosaccharides and evaluation of their antioxidant activity. Environ. Toxicol. Pharmacol. 2012, 34, 519−527.
(48) Novoa-Carballal, R.; Riguera, R.; Fernandez-Megia, E. Disclosing an NMR-invisible fraction in chitosan and PEGylated copolymers and its role on the determination of degrees of substitution. Mol. Pharmaceutics 2013, 10, 3225−3231.
(49) Wang, J.; Liu, L. G.; Jiao, W.-Q.; Yang, H.; Liu, J.; Liu, D. Phenylboronic acid-conjugated chitosan nanoparticles for high loading and efficient delivery of curcumin. Carbohydr. Polym. 2021, 256, 117497.
(50) Belattmania, Z.; Kaidi, S.; El Atouani, S.; Katif, C.; Bentiss, F.; Jama, C.; Reani, A.; Sabour, B.; Vasconcelos, V. Isolation and FTIR-ATR and 1H NMR characterization of alginates from the main alginophyte species of the Atlantic Coast of Morocco. Molecules 2020, 25, 4335.
(51) Fertah, M.; Belfkira, A.; Dahmane, E. m.; Taourirte, M. Extraction and characterization of sodium alginate from Moroccan Laminaria digitata brown seaweed. Arabian J. Chem. 2017, 10, S3707−S3714.
(52) Golunova, A.; Velychkivska, N.; Miksŏovská, Z.; Chochola, V.; Jaroš, J.; Hampl, A.; Pop-Georgievski, O.; Proks, V. Direct and Indirect Biomimetic Peptide Modification of Alginate: Efficiency, Side Reactions, and Cell Response. Int. J. Mol. Sci. 2021, 22, 5731.
(53) Oliveira, J.; Mateus, N.; Silva, A. M.; de Freitas, V. Equilibrium forms of vitisin B pigments in an aqueous system studied by NMR and visible spectroscopy. J. Phys. Chem. B 2009, 113, 11352−11358.
(54) Cruz, L.; Petrov, V.; Teixeira, N.; Mateus, N.; Pina, F.; Freitas, V. d. Establishment of the chemical equilibria of different types of pyranoanthocyanins in aqueous solutions: evidence for the formation of aggregation in pyranomalvidin-3-O-coumaroylglucoside-(+)-catechin. J. Phys. Chem. B 2010, 114, 13232−13240.
(55) Oliveira, J.; Araujo, P.; Fernandes, A.; Brás, N. F.; Mateus, N.; Pina, F.; de Freitas, V. Influence of the structural features of amino-based pyranoanthocyanins on their acid-base equilibria in aqueous solutions. Dyes Pigm. 2017, 141, 479−486.

Recommended by ACS

Fast and Reversibly Humidity-Responsive Fluorescence Based on AIEgen Proton Transfer
Botian Li, Qiong Zhou, *et al.*
OCTOBER 18, 2022
ACS APPLIED MATERIALS & INTERFACES
READ

In Vivo Detection of Cyclic-di-AMP in *Staphylococcus aureus*
Nagaraja Mukkayyan, Som S. Chatterjee, *et al.*
AUGUST 26, 2022
ACS OMEGA
READ

β-Cyclodextrin Polymer-Based Host–Guest Interaction and Fluorescence Enhancement of Pyrene for Sensitive Isocarbophos Detection
Shanshan Gao, Chunxia Song, *et al.*
APRIL 08, 2022
ACS OMEGA
READ

Simple and Rapid Endotoxin Recognition Using a Dipicolylamine-Modified Fluorescent Probe with Picomolar-Order Sensitivity
Hiroshi Kimoto, Takashi Hayashita, *et al.*
JULY 15, 2022
ACS OMEGA
READ

Get More Suggestions >

https://doi.org/10.1021/acsapm.2c00514
ACS Appl. Polym. Mater. 2022, 4, 4961−4971

Supporting Information

Colorimetric pH-responsive Biomaterials Based on Pyranoflavylium-Biopolymer Hybrid Conjugates

Ana Sofia Pires, Vânia Gomes, Dina Neves, Nuno Mateus, Victor de Freitas, Luís Cruz*

REQUIMTE/LAQV, Department of Chemistry and Biochemistry, Faculty of Sciences, University of Porto, Rua do Campo Alegre, 687, 4169-007, Porto, Portugal.

*Corresponding author: Luís Cruz: Tel.: +351 220402558; fax: +351 220402658.

Email address: luis.cruz@fc.up.pt

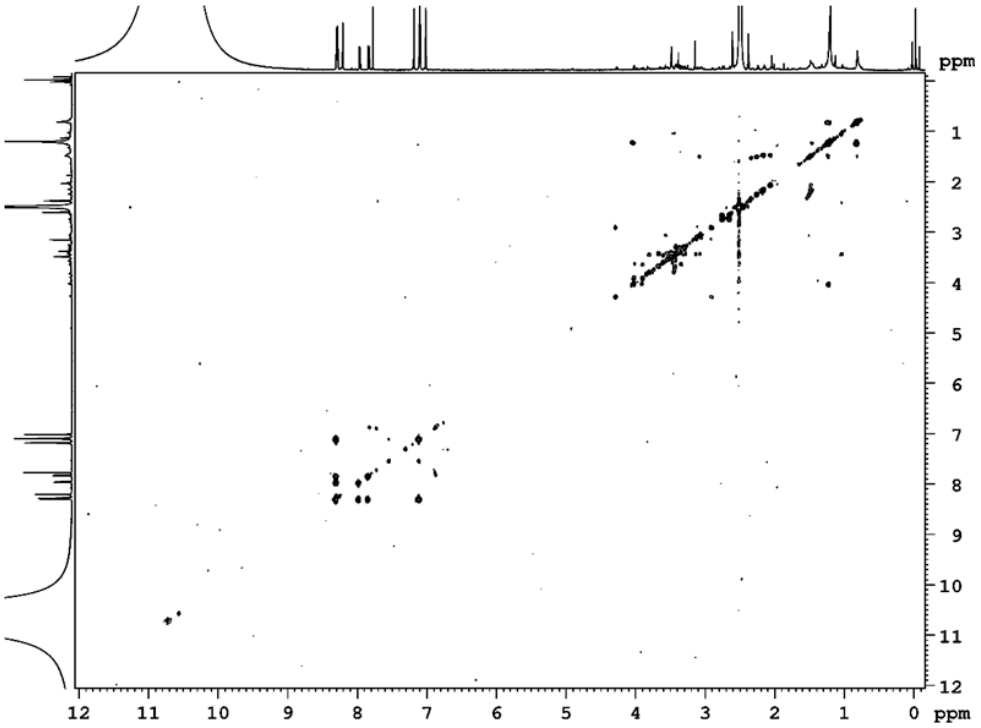


Figure S1. 1H-1H 2D COSY (600:600 MHz, DMSO-d6:TFA 9:1) spectrum of PyFlav 4.

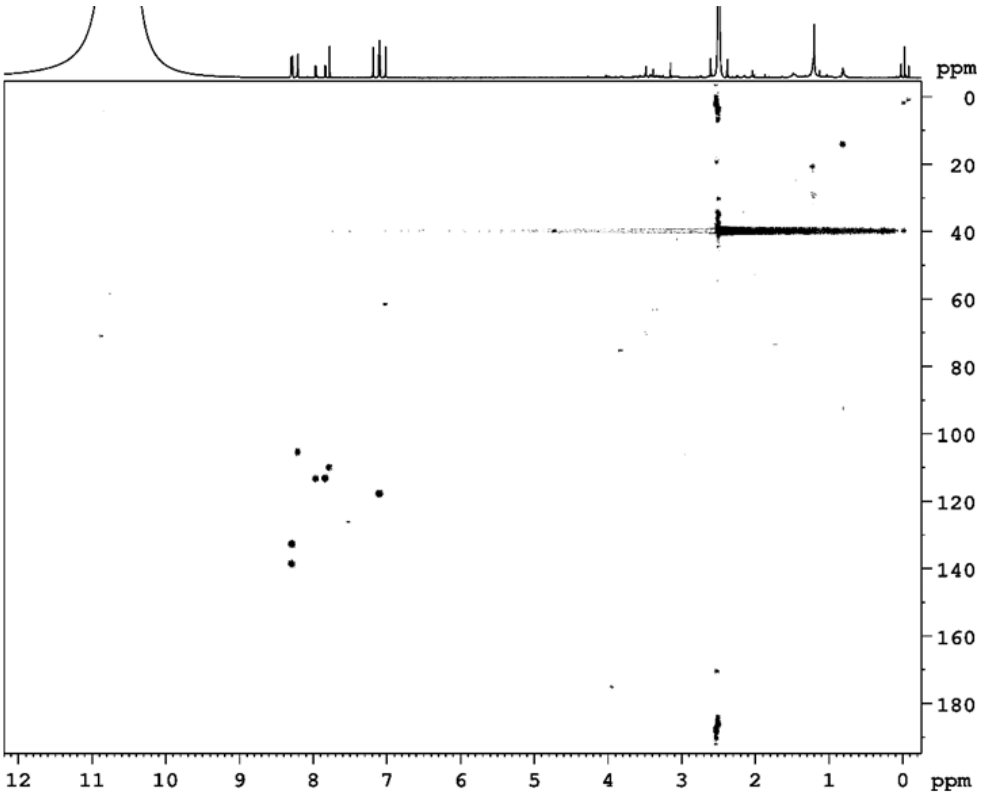


Figure S2. 1H-13C 2D HSQC (600:150 MHz, DMSO-d6:TFA 9:1) spectrum of PyFlav 4.

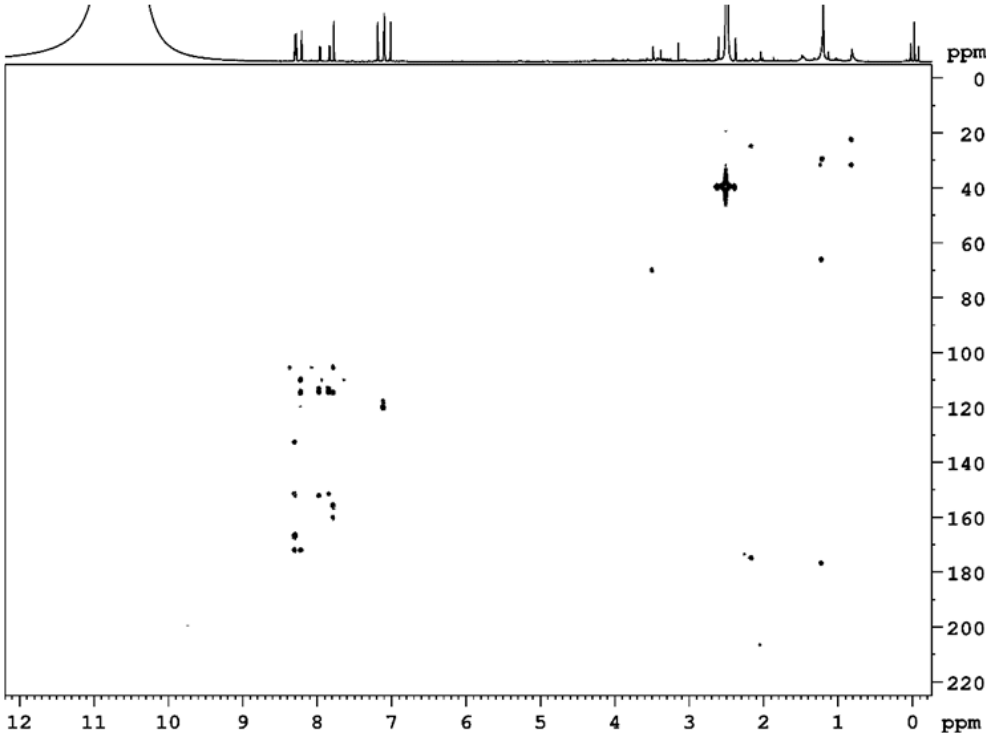


Figure S3. 1H-13C 2D HMBC (600:150 MHz, DMSO-d6:TFA 9:1) spectrum of PyFlav 4.

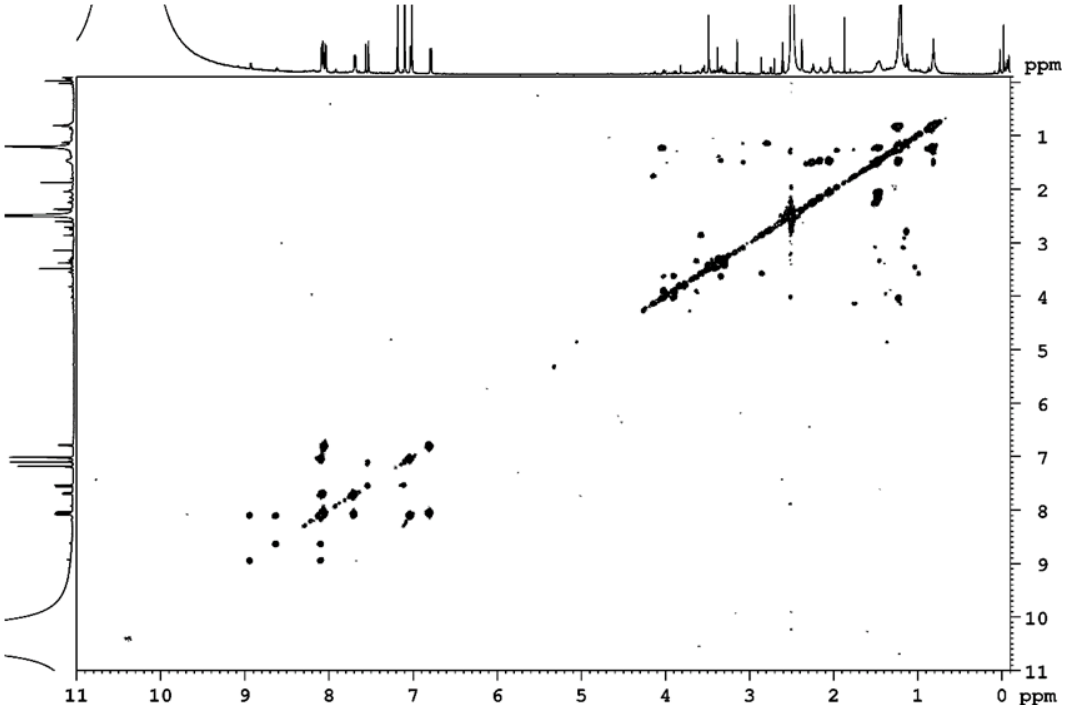


Figure S4. 1H-1H 2D COSY (600:600 MHz, DMSO-d6:TFA 9:1) spectrum of PyFlav-CHT 6.

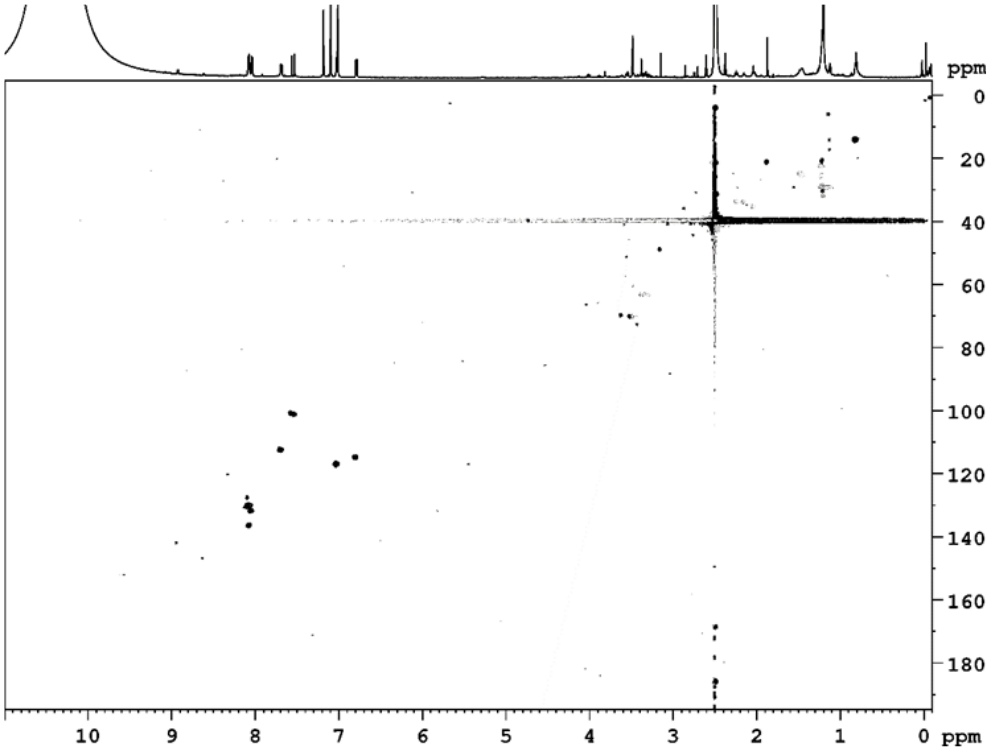


Figure S5. 1H-13C 2D HSQC (600:150 MHz, DMSO-d6:TFA 9:1) spectrum of PyFlav-CHT 6.

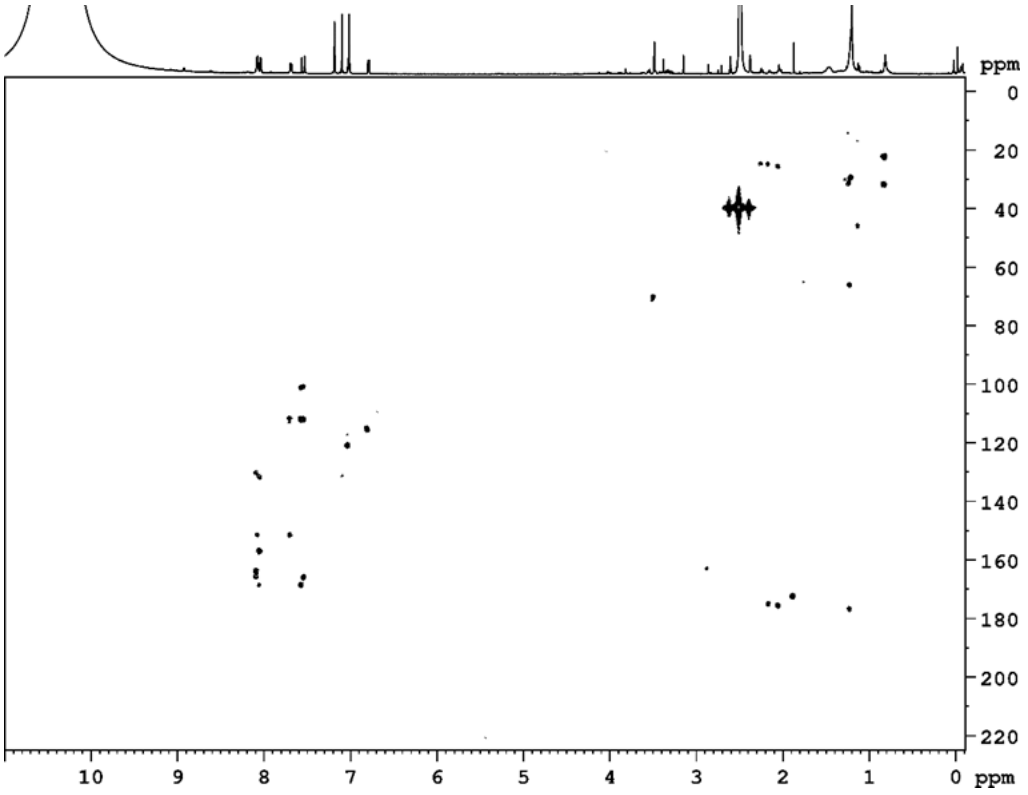


Figure S6. 1H-13C 2D HMBC (600:150 MHz, DMSO-d6:TFA 9:1) spectrum of PyFlav-CHT 6.

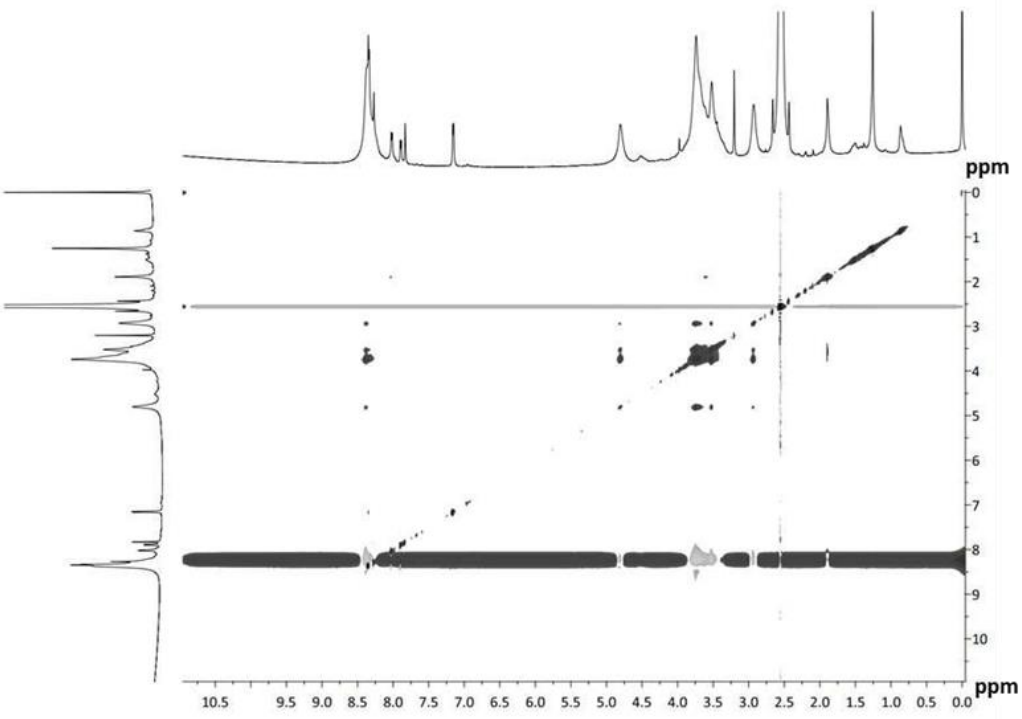


Figure S7. 1H-1H 2D NOESY (600:600 MHz, DMSO-d6:TFA 9:1) spectrum of PyFlav-CHT 6.

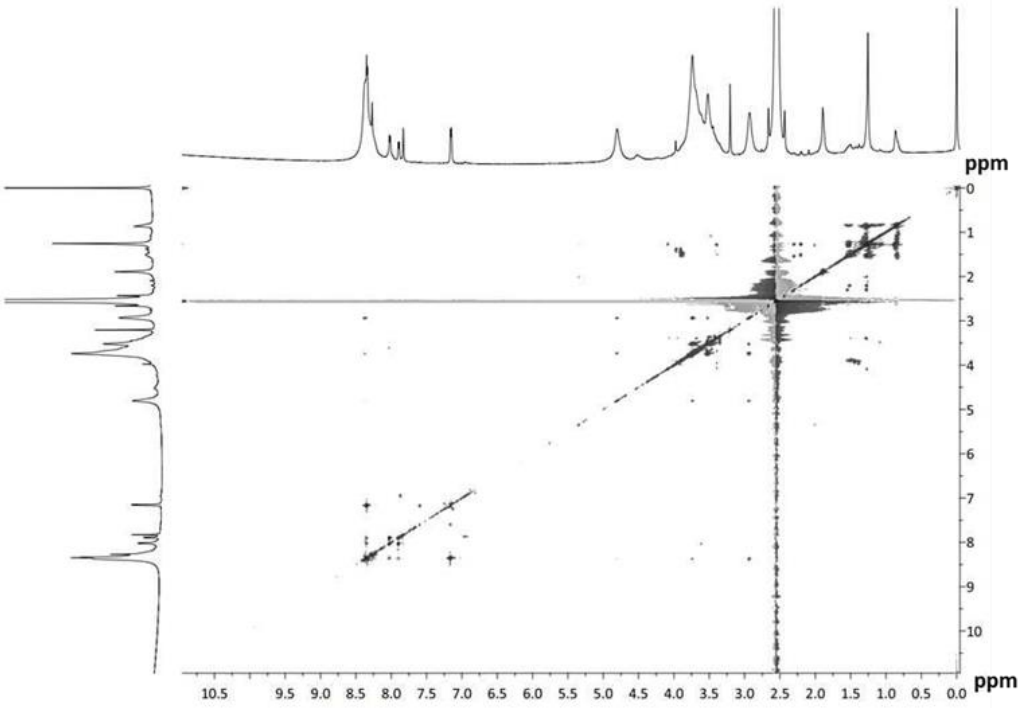


Figure S8. 1H-1H 2D TOCSY (600:600 MHz, DMSO-d6:TFA 9:1) spectrum of PyFlav-CHT 6.

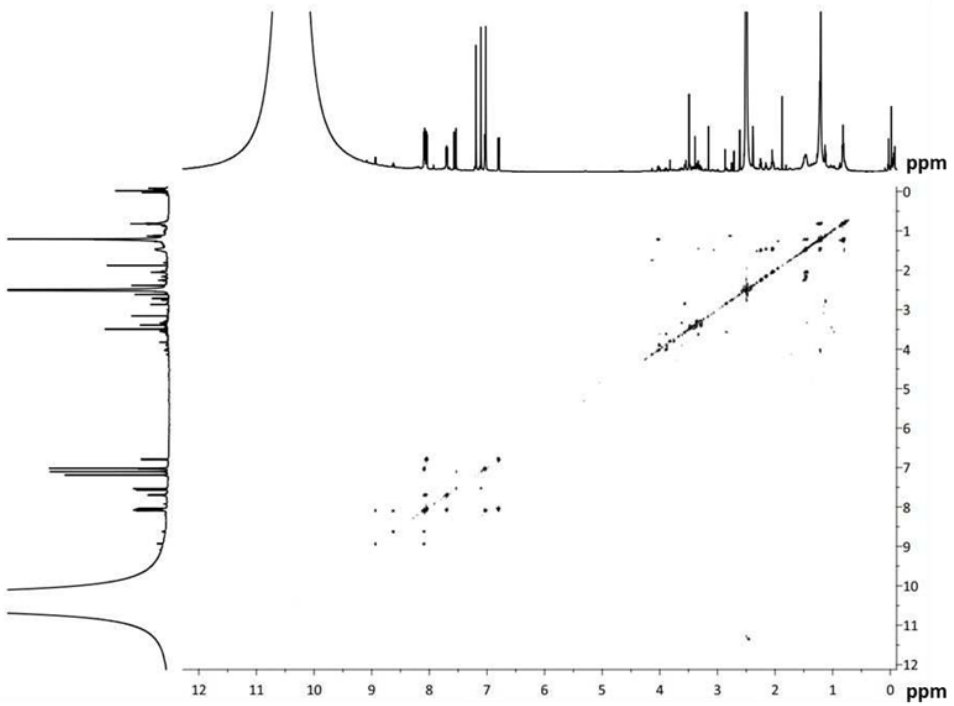


Figure S9. 1H-1H 2D COSY (600:600 MHz, DMSO-d6:TFA 9:1) spectrum of PyFlav 5.

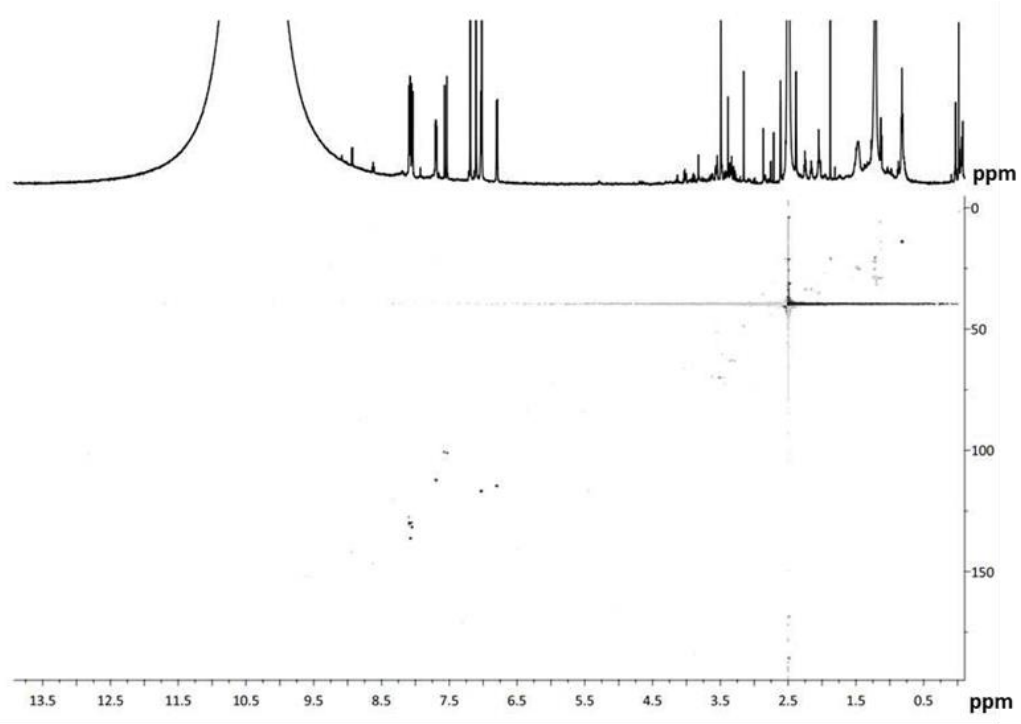


Figure S10. 1H-13C 2D HSQC (600:150 MHz, DMSO-d6:TFA 9:1) spectrum of PyFlav 5.

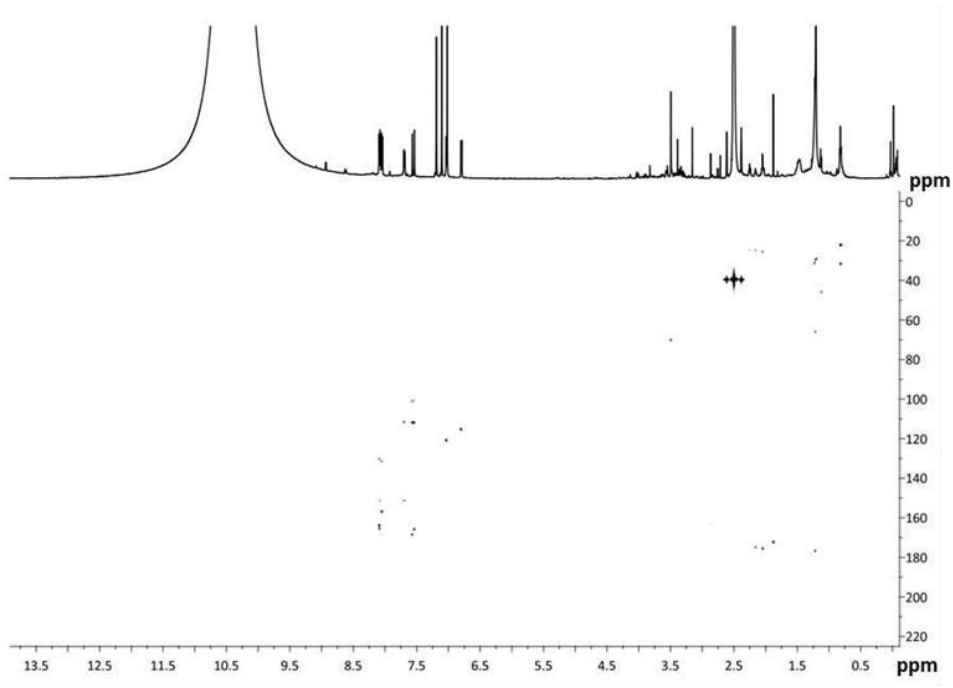


Figure S11. 1H-13C 2D HMBC (600:150 MHz, DMSO-d6:TFA 9:1) spectrum of PyFlav 5.

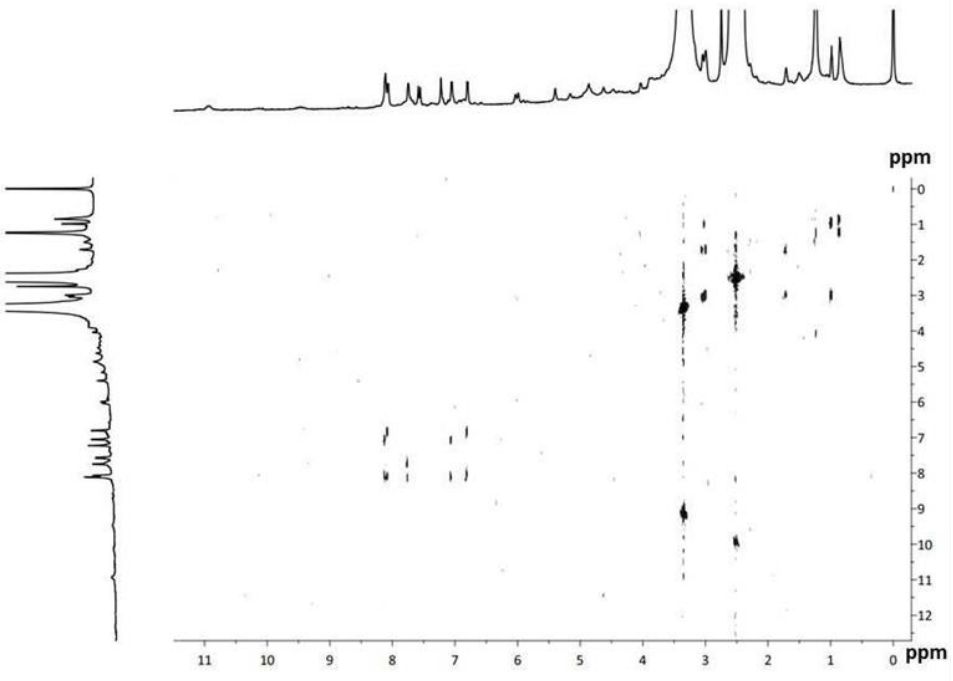


Figure S12. 1H-1H 2D COSY (600:600 MHz, DMSO-d6:NaOD 98:2 at 40 ºC) spectrum of PyFlav-ALG 7.

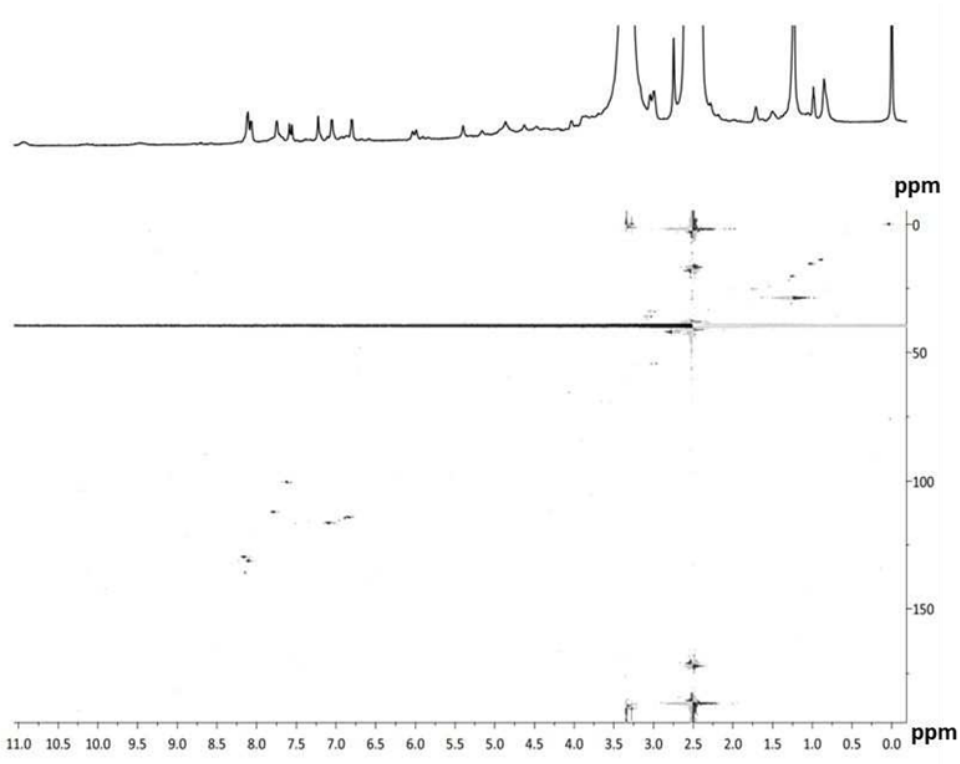


Figure S13. 1H-13C 2D HSQC (600:150 MHz, DMSO-d6:NaOD 98:2 at 40 ºC) spectrum of PyFlav-ALG 7.

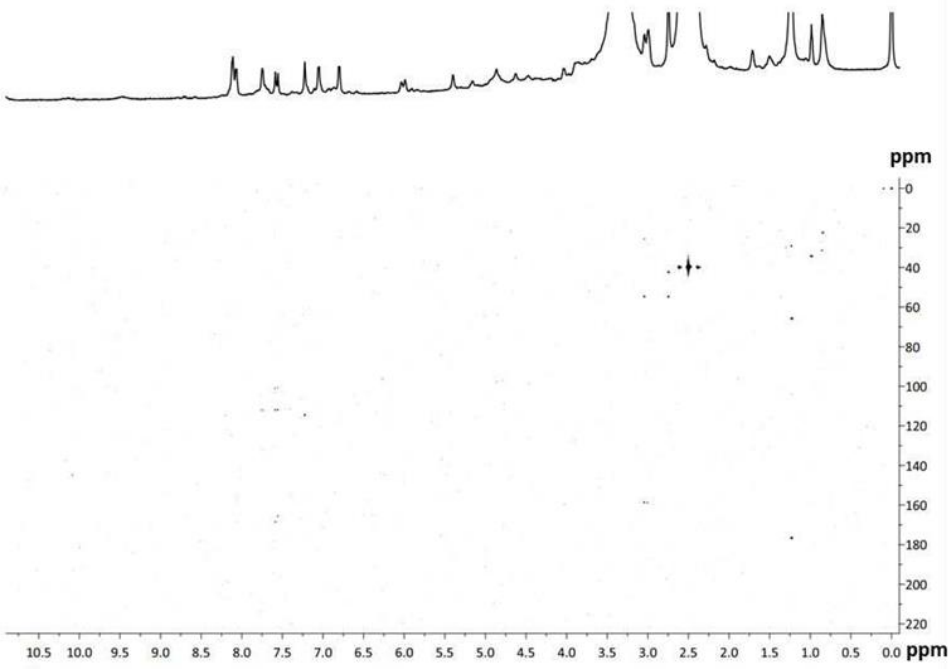


Figure S14. 1H-13C 2D HMBC (600:150 MHz, DMSO-d6:NaOD 98:2 at 40 ºC) spectrum of PyFlav-ALG 7.

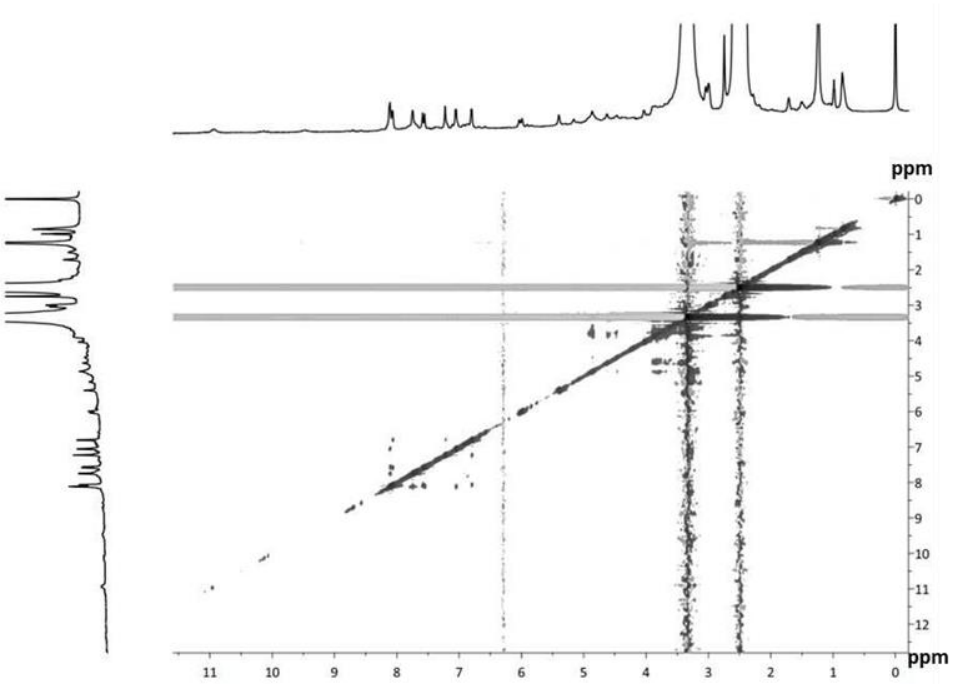


Figure S15. 1H-1H 2D NOESY (600:600 MHz, DMSO-d6:NaOD 98:2 at 40 ºC) spectrum of PyFlav-ALG 7.

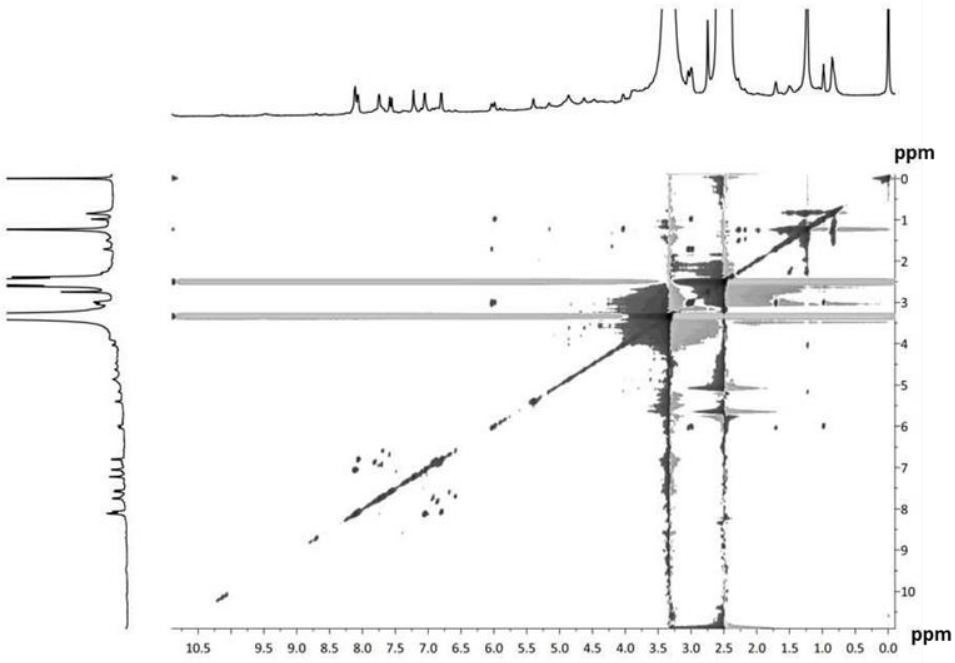


Figure S16. 1H-1H 2D TOCSY (600:600 MHz, DMSO-d6:NaOD 98:2 at 40 ºC) spectrum of PyFlav-ALG 7 .

Chapter II

Development of a pH-indicator label based on a pyranoflavylium for food packaging

Article VI

Pyranoflavylium-cellulose acetate films and the glycerol effect towards the development of pH-freshness smart label for food packaging

Vânia Gomes, Ana Sofia Pires, Nuno Mateus, Victor de Freitas, Luís Cruz*

REQUIMTE/LAQV, Departamento de Química e Bioquímica, Faculdade de Ciências, Universidade do Porto, Rua Do Campo Alegre, 687, 4169-007, Porto, Portugal

---

Gomes, V., Pires, A. P., Mateus, N., de Freitas, V, Cruz, L., Pyranoflavylium-cellulose acetate films and the glycerol effect towards the development of pH-freshness smart label for food packaging, *Food Hydrocolloids*, **2022**, 127, 10750. DOI https://doi.org/10.1016/j.foodhyd.2022.107501

Food Hydrocolloids 127 (2022) 107501

Contents lists available at ScienceDirect

Food Hydrocolloids

journal homepage: www.elsevier.com/locate/foodhyd

Pyranoflavylium-cellulose acetate films and the glycerol effect towards the development of pH-freshness smart label for food packaging

Vânia Gomes, Ana Sofia Pires, Nuno Mateus, Victor de Freitas, Luís Cruz *

REQUIMTE/LAQV, Departamento de Química e Bioquímica, Faculdade de Ciências, Universidade do Porto, Rua Do Campo Alegre, 687, 4169-007, Porto, Portugal

ARTICLE INFO

Keywords:
Pyranoflavylium salt
Dyes
pH-indicator
Water vapor permeability
Colorimetric films
Amine-rich environment
Food packaging

ABSTRACT

A bio-inspired anthocyanin-type pigment, namely a pyranoflavylium salt previously developed was incorporated into cellulose acetate-based films to build up a colorimetric pH-indicator as a smart label for monitoring food freshness. The pigment (0.1% (w/w)) was immobilized in cellulose acetate matrix in the absence and presence of different percentages of glycerol (10–40% (w/w)). The films were obtained by the casting method and characterized by the thickness, morphology and barrier properties, thermogravimetric analysis, color, among others. The chromatic responsive properties of the films were tested in solutions at different pH values (pH 4 to 8) and in the headspace of biogenic amines and ammonia-containing solutions at different concentrations. The results showed that the films without glycerol are not color-responsive to different pH values. On the other hand, the incorporation of glycerol above 20% (w/w) demonstrated effective pH responsiveness after 20 min of immersion and after exposition to an amine-rich environment. The glycerol-containing films showed relevant and remarkable color change at the pH range of food spoilage indicating a great potential for application as a food freshness indicator.

1. Introduction

Nowadays, both food safety and food waste are issues of increasing concern for society. On one hand, the World Health Organization (WHO) estimated 600 million cases of illness due to contaminated food supplies, and 420,000 people die every year as they are affected by foodborne contamination (World Health Organization, 2020). On the other hand, the Food and Agriculture Organization of the United Nations (FAO) estimated that the total food waste for the edible part is around 1.3 billion tons (FAO, 2013). Innovative food packaging systems have been extensively studied to help tackle these problems through food preservation and giving information on food quality, keeping safety the entire supply chain until the final consumer (Heising et al., 2017). Intelligent packaging is a kind of innovative packaging system concept which purpose is to monitor in real-time the condition of the packaged product (Drago et al., 2020). Behind the technologies applied in intelligent packaging, indicators are one of the most studied in research since they provide immediate visual and qualitative (or semi-quantitative) information about the packaged food through a color change (Vanderroost et al., 2014). The real-time food control in a package can be made by monitoring the different food quality indicators such as pH changes, oxygen, temperature, among others. In fact, pH changes in the food environment have been described as an effective method of identifying food spoilage (Yousefi et al., 2019). pH alterations can be affected by many microbial metabolites such as biogenic amines (Danchuk et al., 2020) and organic acids (Yousefi et al., 2019) as the main result of amino acids and glucose metabolization, leading to an increase or a decrease of pH of food samples, respectively.

Anthocyanins are natural pigments found in many fruits and vegetables that have the ability to change color depending on the pH of the environment (Cruz et al., 2022). Due to this feature, they have been widely studied as a colorimetric indicator for application in intelligent food packaging (Andretta et al., 2019; Chen et al., 2020; Liang et al., 2019; Luchese et al., 2017; Moradi et al., 2019; Shukla et al., 2016; Veiga-Santos et al., 2010; Wei et al., 2017; J. Zhang et al., 2019). Despite most published works did not refer it, these natural pigments have a complex multi-state equilibrium that leads to color fading over time (Brouillard et al., 2010; Pina, 2014; Pina et al., 2012), which could be a limitation for their application as pH-indicators. In turn, pyranoflavylium salts are anthocyanin-derived pigments that also have the ability to change color according to pH variations, but they are described as more stable than anthocyanins over time (Luís Cruz et al., 2017;

* Corresponding author.
E-mail address: luis.cruz@fc.up.pt (L. Cruz).

https://doi.org/10.1016/j.foodhyd.2022.107501
Received 3 November 2021; Received in revised form 11 January 2022; Accepted 12 January 2022
Available online 15 January 2022
0268-005X/© 2022 Elsevier Ltd. All rights reserved.

Gomes et al., 2020; Oliveira et al., 2014; Sousa et al., 2017). A specific pyranoflavylium compound (Fig. 1), developed and studied by our research group, showed promising features such as a suitable pK_a value (pK_{a1} = 6.5 ± 0.1) in the relevant food spoilage region (pH ≈ 4–8, depending on the product type) (Choi et al., 2017; Ezati & Rhim, 2020; J.; Liu et al., 2019; Pereira et al., 2015; Wei et al., 2017; X.; Zhang et al., 2014), low cytotoxicity and, also a great color variation which make it an excellent candidate to be applied as pH-indicator for food packaging (Gomes et al., 2021).

The cellulose acetate polymer was chosen as a support matrix for pigment immobilization since it is described as an essential and economical natural resource due to its biocompatibility, non-toxicity and, biodegradability, etc (Y. Liu et al., 2021). Previous studies showed that acetate cellulose films have good properties for food packaging applications (Aghaei et al., 2018; Ardila-Diaz et al., 2020; Assis et al., 2020; Freitas et al., 2020; Gemili et al., 2009; Rajeswari et al., 2020; Saha et al., 2016). Furthermore, a plasticizer was added into films formulation to improve their physical properties as well as to evaluate its effect on pH-sensing efficiency. Generally, plasticizers are low molecular weight and non-volatile compounds that are incorporated in a material to increase its flexibility, workability, or distensibility (Mekonnen et al., 2013; Vieira et al., 2011). Among the plasticizers, glycerol is one of the most studied for biodegradable polymers (Vieira et al., 2011). Although the use of glycerol as a plasticizer for cellulose acetate films is not very common, some recent works have studied its incorporation in the formulation (de Melo et al., 2018; Gonçalves et al., 2019; Moreira Gonçalves et al., 2020; Teixeira et al., 2021).

In this work, the previously developed pyranoflavylium dye was immobilized in cellulose acetate-based films and, the impact of the glycerol amount in the pH-responsive colorimetric properties of the films was studied. The aim of the best film formulation is for the development of a small label to be incorporated in food packaging for smart food packaging applications.

2. Experimental

2.1. Materials

Cellulose acetate (CA) (Mw = 30,000 g mol^{-1} and 39.8 wt % of the degree of substitution in acetyl content), sodium chloride, magnesium nitrate hexahydrate, putrescine, cadaverine, tyramine, histamine dihydrochloride, and ammonium hydroxide solution (25% (v/v)) were supplied from Sigma-Aldrich. The glycerol (Gly) was supplied from Himedia. Acetone and Methanol P.A. were purchased from Chem-Lab. Calcium chloride anhydrous granular (∼ 2–6 mm) was purchased from Supelco. Deionized water was purified with a Milli-Q water system before use. Pyranoflavylium compound (2,10-Bis-(4′,4″-hydroxyphenyl) pyranobenzopyrylium chloride – PyF) was obtained according to the procedure described elsewhere (Gomes et al., 2021).

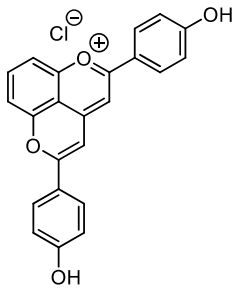


Fig. 1. Pyranoflavylium dye previously developed (Gomes et al., 2021) and used as pH-indicator in this work.

2.2. Preparation of cellulose acetate-based films

The films were obtained by the casting technique, according to the methodology described by R.Q. Assis et al.(Assis et al., 2020), with some modifications. CA 8% (w/w) was dissolved in acetone under mechanical stirring at room temperature until complete solubilization. Different percentages of Gly (0–40%) were added to CA solution. Dispersions were kept in vigorous mechanical stirring overnight. Pyranoflavylium salt solution in MeOH (1 mg/mL) was added to dispersions with final concentration 0.1% (w/w). After 1 h of homogenization, the dispersions were cast onto Petri dishes (63.6 cm^2), and solvent evaporation was carried out in an oven for 2 h at 40 °C. The concentrations of biopolymer and drying conditions were defined from preliminary tests. The obtained films were detached from the plates and conditioned in a desiccator at 20–25 °C and relative humidity (RH) of 53–54% (saturated magnesium nitrate solution) for at least 48 h until the characterization and tests.

2.3. Film characterization

2.3.1. Thickness

Film thicknesses were measured using a digital coating thickness meter (model TE 1250-0.1 F, Sauter). Measurements were taken at ten random positions for each film in five replicates, and the mean values were calculated.

2.3.2. Moisture content (MC)

Moisture content (*MC*) was defined as the amount of water taken up by the dry film until the equilibrium is established between the moisture content of the surrounding air and that of the films (Priyadarshi et al., 2018). The determination was adapted from ASTM D644-99 (ASTM, 1994). The films were cut into 1 × 1 cm square pieces and weighed (W_1), then the pieces were dried in an oven at 105 °C for 24 h. Dried films were weighted (W_2), and the moisture content was calculated using Eq. (1). The analyses were carried out for three samples of each formulation.

$$MC\ (\%) = \left(\frac{W_1 - W_2}{W_1}\right) \times 100 \quad (1)$$

2.3.3. Swelling index (SI) and water solubility (WS)

The swelling index (*SI*) of the films was defined as the water sorption capacity by the dry film after 24 h of immersion in water, while the water solubility (*WS*) was the percentage of the film material that was dissolved in water (Dick et al., 2015; Gontard et al., 2007). The dried films from the moisture content analysis with the dry weight (W_2) were immersed in 20 mL of Milli-Q water under constant agitation at 150 rpm using a mechanical shaker for 24 h at 25 °C ± 2 °C. The swollen samples were removed, and the weight was recorded as wet weight (W_3). The last weight (W_4) was obtained after re-drying the films at the same conditions of *MC* determination. *SI* and *WS* (%) were calculated according to Eqs. (2) and (3) (da Silva Filipini et al., 2020). Three replicates were carried out and averaged for each sample.

$$SI\ (\%) = \left(\frac{W_3 - W_2}{W_2}\right) \times 100 \quad (2)$$

$$WS\ (\%) = \left(\frac{W_2 - W_4}{W_2}\right) \times 100 \quad (3)$$

2.3.4. Scanning electron microscopy (SEM)

In order to evaluate the morphology of the films, SEM analyses using a High Resolution (Schottky) Environmental Scanning Electron Microscope FEI Quanta 400 FEG ESEM were performed. Samples were coated with an Au/Pd thin film, by sputtering, using the SPI Module Sputter Coater equipment. Each image contains data with the most important analysis conditions.

2.3.5. Atomic force microscopy (AFM)

In order to evaluate the topography of the film's surface, AFM analysis was performed on Veeco Multimode Nanoscope IVa in Tapping mode, using a Bruker silicon probe (model TESPA-V2, resonant frequency 320 kHz, nominal force constant 42 N/m, estimated tip radius 7 nm).

2.3.6. Thermal properties

The thermogravimetric analysis was performed on a Simultaneous Thermogravimetric Analyzer (TGA-DTA, model STA7200RV, Hitachi). Approximately 3 mg film pieces in the alumina crucible were heated from 25 to 600 °C with a heating rate of 10 °C/min, under a nitrogen atmosphere with a flow rate of 200 mL/min.

2.3.7. Water vapor permeability (WVP)

The WVP was performed according to the gravimetric method (ASTM E96-95) (ASTM, 2013) with some modifications. Anhydrous calcium chloride was used inside capsules, which were sealed with the films and packed in a desiccator containing saturated NaCl solution to promote controlled humidity (75% ± 2) and placed at room temperature (25 °C ± 2 °C). The permeability (WVP) of the films is expressed in g.h^{-1}.m^{-1}.Pa^{-1} was determined by Eqs. (4–6):

$$WVP = (WVT / \Delta p) \times X \quad (4)$$

$$WVT = (G/t)/A \quad (5)$$

$$\Delta p = S \times (R_1 - R_2) \quad (6)$$

where WVT is the water vapor transmission rate expressed in g.h^{-1}.m^{-2}; Δp is vapor pressure difference (Pa); X is the average film thickness (mm); G/t is the linear regression of the constant mass transfer region between weight gain, G (g) and time, t (s); and A is the permeation area of the sample (m^2); S is the saturation of water vapor pressure (Pa) at 25 °C; R_1 is the RH in the desiccator, R_2, the RH in the permeation cell. All measurements were performed in five replicates.

2.3.8. Color and opacity measurements

Color (CIELAB system) and opacity of the films were measured using a portable spectrophotometer (model CM-2600 d; Konica Minolta, Japan). L*, a*, and b* are the color parameters of lightness, red-green chromaticity index, and yellow-blue chromaticity index, respectively. The measurements were made by Specular Component Excluded (SCE) mode in a 3 mm illuminated sample area with a 10° angle standard observer condition, D65 illuminant condition, and white background. The opacity was measured through the surface reflectance spectra with the same conditions described above but with a white and black background. The opacity values were obtained by Spectramagic NX Colour Data Software following ISO 2471. All measurements were taken at three random positions for each film in the replicates, and the mean values were calculated.

2.4. Tests as pH-indicator

Films were cut into pieces (1 × 1 cm) and immersed in buffer solutions from pH 4 to pH 8. Solutions of pH 4 and 5 were prepared by citric acid – phosphate buffer, and solutions with pH 6 to 8 were prepared by phosphate buffer. pH measurements were made in a Radiometer Copenhagen PHM240 pH/ion meter. Films were kept submerged in the different pH solutions for 10, 20, 40, and 60 min. The color coordinates were measured before and after the immersion.

The color difference was determined over time by Eq. (7):

$$\Delta E^* = \sqrt{[(\Delta L^*)^2 + (\Delta a^*)^2 + (\Delta b^*)^2}} \quad (7)$$

where $\Delta L^* = L^* - L_0^*$; $\Delta a^* = a^* - a_0^*$; $\Delta b^* = b^* - b_0^*$; L_0^*, a_0^* and b_0^* are color values of the films before the immersion (control). The experiment was done in triplicate.

2.5. Film color response towards an amine-rich environment

Films were cut into pieces (1 × 1 cm) and placed on a floating support on the surface of a solution (30 mL) of biogenic amines (BA) or ammonium hydroxide, inside a closed flask (50 mL). BA solutions were prepared with cadaverine, putrescine, tyramine, and histamine with final concentration of 0.5, 1 and 4 g/L. The concentration of ammonium hydroxide solutions was 0.35 and 3.5 g/L (10 and 100 mM). Films were kept in a different amine-rich environment overnight at 25 °C. The color coordinates were measured before and after the experiment and the color difference was determined by Eq. (7). The experiment was done in triplicate.

2.6. Statistical analysis

A one-way ANOVA and Tukey multi comparative test were performed to detect the differences between samples with a significant level of 5% ($p < 0.05$). All statistical analyses were carried out using the software GraphPad Prism version 8.0.2.

3. Results and discussion

3.1. General appearance of the films

The films were obtained by immobilization of pyranoflavylium dye into CA matrix and combined with different percentages of Gly for further assessment of their efficiency as a pH-indicator. The casting technique was used to produce the films, and then they were removed from the casting plates. CA film prepared without Gly was brittle, rigid, and fragile, making it difficult to peel off and handle. This characteristic could be attributed to the strong inter/intramolecular hydrogen bonds of CA which provide less mobility to the macromolecular chains, resulting in brittle and rigid films (Teixeira et al., 2021). This film had to be removed carefully from the casting plate to avoid breakage, whereas the films with plasticizer were easily detached. As expected, the addition of Gly yielded more flexible and handleable films. The low molecular size of glycerol enables it to occupy the intermolecular spaces of polymer chains, reducing the intermolecular hydrogen bond strength between CA chains, hence increasing the molecular mobility (M. L. Sanyang et al., 2016). Fig. 2 shows photographs of the films under a white and black background to understand the visual aspect of the films more easily. The CA_PyF surface appeared homogeneous and slightly wavy. All of them displayed a yellow color and, CA_PyF was almost transparent, while the films with Gly showed to be opaquer, which will be discussed in more detail below. Gly led to a more heterogeneous surface, mainly in CA_PyF_Gly10 film, that exhibited the appearance of whitish spots. Films with 20% of Gly or higher showed a smoother and more homogeneous surface than the 10% Gly film. Films with 30 and 40% of Gly were slightly sticky and sticky, respectively. This property observed on these materials may mean that the plasticizer exceeded the limit of compatibility with the CA, and phase separation can occur with Gly exclusion (Vieira et al., 2011).

3.2. Thickness

The thickness measurements of the films (Table 1) revealed a significant increase ($p < 0.05$) with the plasticizer concentration up to 30% of Gly. A similar effect of Gly concentration on film thickness was reported by several authors and may be due to the role of plasticizers in disrupting and restructuring intermolecular polymer chain networks, creating more free volumes in its interstitial spaces which translate into thicker film (Mekonnen et al., 2013; Nordin et al., 2020; M. L.; Sanyang et al., 2016; Tarique et al., 2021). The increase in thickness from 30 to

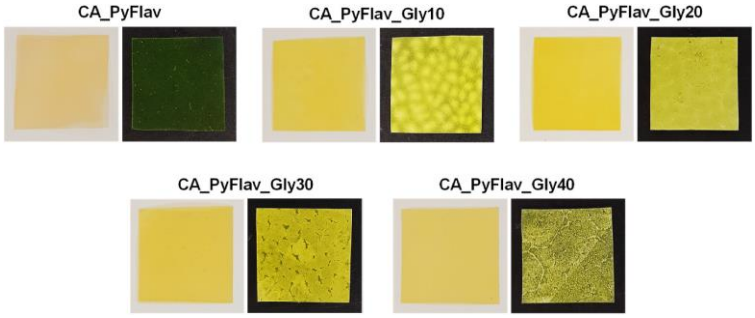


Fig. 2. Photographs of the CA films (3 × 3 cm) with PyF and different Gly percentages (0–40%) under white and black backgrounds.

Table 1
Average values of the thickness, moisture content, swelling index and, the water solubility of the CA films with PyF and different Gly percentages (0–40%).

Sample	Thickness (μm)	Moisture Content (%)	Swelling Index (%)	Water Solubility (%)
CA_PyF	60.1 ± 1.4^{a}	2.3 ± 1.1^{a}	4.9 ± 2.1^{a}	0.0 ± 0.0^{a}
CA_PyF_Gly10	65.4 ± 0.9^{b}	7.8 ± 0.3^{b}	10.7 ± 2.1^{b}	3.6 ± 1.2^{ab}
CA_PyF_Gly20	70.2 ± 1.3^{c}	15.1 ± 2.1^{c}	14.8 ± 1.5^{bc}	5.9 ± 2.1^{bc}
CA_PyF_Gly30	78.0 ± 2.3^{d}	20.9 ± 1.6^{d}	18.9 ± 2.0^{c}	7.5 ± 1.6^{bc}
CA_PyF_Gly40	81.9 ± 3.8^{d}	27.8 ± 1.3^{e}	20.3 ± 2.5^{c}	8.3 ± 1.7^{c}

40% of Gly was not significant and may be related to the limit of Gly incorporation by CA, which should reach its maximum at ≈ 30%.

3.2.1. *Moisture content (MC), swelling index (SI), and water solubility (WS)*

The film without plasticizer showed the lowest moisture content and swelling index, and no solubility in water. The moisture content increased significantly ($p < 0.05$) concomitantly with the Gly concentrations, while the swelling index and water solubility also increased although with less expression. This result is due to the high hydrophilic character of Gly, which increases the affinity of the films for the surrounding water molecules (Cerqueira et al., 2012). Moreover, the free space volumes between the polymeric chains caused by Gly addition led to an increase of water diffusion into the films and, consequently, increased the capacity to retain water within their matrix being responsible also for the superior water solubility (M. L. Sanyang et al., 2016). These properties have not been extensively studied in published works dealing with Gly plasticized CA films. However, other authors reported a similar trend for films based on another type of polymers (i.e., chia seed mucilage, semi-refined kappa-carrageenan, or arrowroot starch) plasticized with Gly (Dick et al., 2015; Farhan & Hani, 2017; Tarique et al., 2021).

3.2.2. *SEM*

The morphology of the films was analyzed by SEM on both surfaces (surface A – top of the film; and surface B – bottom of the film, in contact with the Petri dish) and in the interior by transversal fracture (Fig. 3). The film without Gly showed to be smooth and homogeneous at both interior and surfaces, as described elsewhere (Assis et al., 2020; Bruna et al., 2014). After Gly addition, pores raise at the surface as well as in the interior of the films. It was also observed differences between surface A and B, in contrast with other works that do not make any reference to it. In general, surface A of Gly-based films is characterized by a large number of pores with different sizes depending on the Gly percentage. CA_PyF_Gly10 showed the smallest pores between 0.5 and 1.5 μm. From 20% of Gly, pores had no longer a well-defined size and they seem to be more net-like. Surface B showed some irregularities, mainly for 20, 30, and 40% of Gly, but practically without pores. From the images of the cross-section, it was also possible to observe differences between both surfaces and in the interior of the films. For CA_PyF_Gly10, the interior of the film is very similar to the one of CA_PyF, only differentiated by the

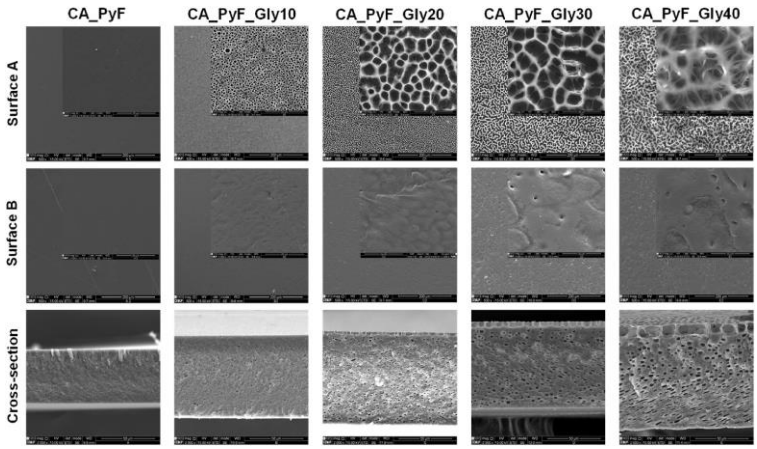


Fig. 3. SEM images of surface A and B and cross-section of the CA films with PyF and different Gly percentages (0–40%).

appearance of a small number of pores. For 20–40% Gly, the interior is characterized by a higher porosity, which could be distinguishable from the porosity of surface A. Although the number and size of the pores increase with the Gly amount, in general, they are smaller than the ones corresponding to surface A. When observed in a transversal fracture, the porosity of surface A seems to have large "caves" in comparison to the pores of the interior of the films, and surface B seems smooth. These differences are mainly related to the film production method. Surface B is the surface in contact with the Petri dish and it is shaped by this one, leading to a smoother surface. Surface A is the surface where the solvent evaporates, and the large porosity of this surface is probably a consequence of this phenomenon. Inner porosity may be more intrinsic to the material composition, namely to the dispersion of Gly into CA matrix. This porosity confirms that the presence of Gly causes internal morphological changes, yielding free volumes created as mentioned above and explaining the increased thickness, moisture content, swelling index, and water solubility. The appearance of the pores in CA-based films with specific percentages of Gly was already described (de Melo et al., 2018; Gonçalves et al., 2019; Moreira Gonçalves et al., 2020). However, the authors did not report any difference between the surfaces and also described that the films with 20% of Gly did not show porosity on the surface.

3.2.3. AFM

The AFM results of surface A (Fig. 4) corroborate the SEM behavior patterns. The topography and the roughness of ~20 nm obtained for the film without Gly reveal that the surface of the film is rather smooth and homogeneous. The topographies of the films with plasticizer have become increasingly heterogeneous and rougher when Gly concentration has increased. Similar results were reported in previous studies, suggesting that CA-based films tend to present a heterogeneous and irregular topography when additives are added to them (de Melo et al., 2018; Freitas et al., 2020). This trend was confirmed quantitatively by the mean roughness (R_a) of the films, which presented values of 47.2, 90.3, and 419 nm for Gly 10, 20, and 30%, respectively. The exception was for 40% of Gly, which decreased the roughness comparatively to the CA_PyF_Gly30. This behavior could be related to the fact of Gly had exceeded the limit of compatibility with CA. In fact, the AFM analysis of CA_PyF_Gly40 was difficult due to its sticky character.

3.2.4. Thermal properties

The thermal properties of the films were studied by thermogravimetric analysis (TGA) in the temperature range from 25 to 900 °C. The TGA curves of the films and their derivatives (DTG) are shown in Fig. 5a and b. In general, there are three main events of thermal decomposition. The first event occurred between 25 and 80 °C and it was characterized by a small weight loss related to the evaporation of the free water molecules of the films. The control film (CA_PyF) and CA_PyF_Gly10 showed residual water loss, with mass loss of 0.5 and 1%, respectively. The remaining films with Gly showed a slightly higher water loss of around 2.4–2.7%. These values follow the same trend of the moisture content results. The second event occurred in the temperature range of 85 and 254 °C and it was related to the Gly volatilization, and the evaporation of water linked by H-bonding. As expected, CA_PyF did not show this event, however, for films with Gly, it can be observed an increase of mass loss from 7.7 (CA_PyF_Gly10) to 24.4% (CA_PyF_Gly40). The third and main event occurred between 254 and 410 °C and corresponds to the thermal decomposition of the CA polymer (Assis et al., 2020), with a mass loss from 77.2 (CA_PyF) to 55.42% (CA_PyF_Gly40). In general, Gly presence showed less thermostability of the films since the thermal degradation of the films with plasticizer started at lower temperatures than the control film. The same behavior was reported in

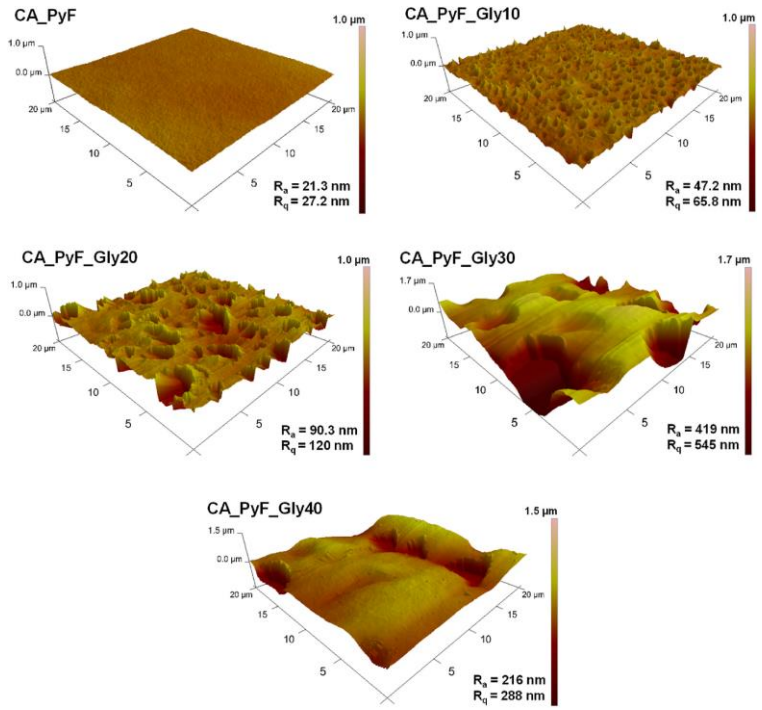


Fig. 4. AFM images of the surface of the CA films with PyF and different Gly percentages (0–40%).

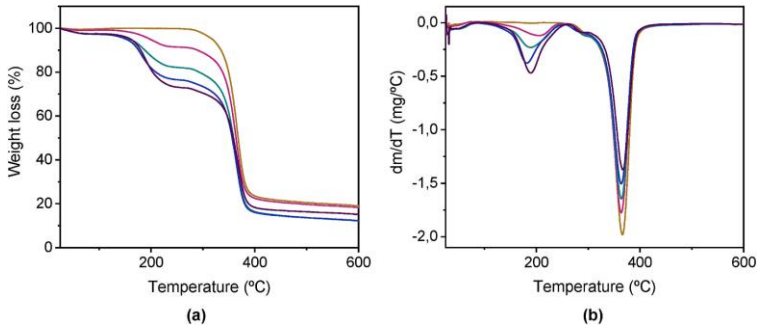


Fig. 5. Thermogravimetric (a) and derivative curves (b) of the CA films with PyF and different Gly percentages (0–40%): CA_PyF; CA_PyF_Gly10; CA_PyF_Gly20; CA_PyF_Gly30; CA_PyF_Gly40.

another work of plasticization of CA with Gly (Teixeira et al., 2021), as well as for other polymers (Muhammed L. Sanyang et al., 2015).

3.2.5. Color properties

The color properties of CA-based films were determined by color coordinates using CIELAB system (Table 2). In general, Gly produced significant changes in the color coordinates of the films. The L* and a* coordinates only were significantly affected ($p > 0.05$) by the presence of Gly, being independent of the Gly percentages ($p < 0.05$). The luminosity (L*) increased, whereas the a* decreased with the presence of Gly, leading to slightly whitish and greenish films. On the other hand, the b* coordinate had a very significant increase ($p > 0.05$) with 10% Gly, translating into an increase in the yellowish of the films, but it decreased significantly ($p > 0.05$) from 20%, where the blue content is more pronounced.

3.2.6. Water vapor permeability (WVP)

The WVP analysis of CA-based films allowed to conclude that this property significantly increased ($p < 0.05$) with Gly amounts (Table 3). This trend could also be explained by structural modifications of the polymer network caused by the hydrophilic character of the plasticizer (Farhan & Hani, 2017), namely by the appearance of pores, as it was confirmed by SEM and AFM images and discussed above. This porosity allows the water molecules to diffuse more easily and leading to a higher WVP. The WVP increase of the films with the presence of hydrophilic plasticizers such as Gly is a common phenomenon for different polymer-based films reported (Cerqueira et al., 2012; Dick et al., 2015; Farhan & Hani, 2017; Muhammed L.; Sanyang et al., 2015; Tarique et al., 2021; Teixeira et al., 2021).

3.2.7. Opacity

Through the opacity measurements (Table 3), it was possible to observe that the film without Gly was practically transparent, with ≈ 10% of opacity. The addition of 10% of Gly originated a substantial opacity enhancement from 10.3 to 30.5%. This drastic increase as well as the increase of whiteness (L*) together with the appearance of white spots (Fig. 2) in CA_PyF_Gly10 film (non-homogeneous film) is in agreement with the "blooming" or "blushing" phenomenon described by other authors (Donhowe & Fennema, 1993; Laohakunjit & Noomhorm, 2004; Saberi et al., 2017). They described that it occurs when the plasticizer concentration exceeds its compatibility in the polymer causing phase separation and physical exclusion of the plasticizer.

Table 2
Color properties of the CA films with PyF and different Gly percentages (0–40%).

Sample	L*	a*	b*
CA_PyF	85.5 ± 0.5^{a}	18.2 ± 0.6^{b}	4.0 ± 1.1^{a}
CA_PyF_Gly10	90.7 ± 0.7^{b}	9.6 ± 1.6^{a}	29.2 ± 0.7^{d}
CA_PyF_Gly20	90.1 ± 1.0^{b}	11.2 ± 1.2^{a}	29.4 ± 0.8^{d}
CA_PyF_Gly30	89.6 ± 1.0^{b}	11.4 ± 2.0^{a}	23.5 ± 1.0^{c}
CA_PyF_Gly40	90.0 ± 0.6^{b}	10.3 ± 1.0^{a}	20.1 ± 1.0^{b}

Table 3
Barrier properties, namely water vapor permeability (WVP) and opacity of the CA films with PyF and different Gly percentages (0–40%).

Sample	WVP x 10^{-10} ($g.m^{-1}.s^{-1}.Pa^{-1}$)	Opacity (%)
CA_PyF	1.42 ± 0.03^{a}	10.3 ± 0.9^{a}
CA_PyF_Gly10	1.79 ± 0.04^{b}	30.5 ± 1.0^{e}
CA_PyF_Gly20	2.24 ± 0.15^{c}	27.6 ± 1.4^{d}
CA_PyF_Gly30	2.51 ± 0.11^{d}	23.0 ± 1.6^{c}
CA_PyF_Gly40	2.70 ± 0.03^{e}	19.6 ± 1.1^{b}

Villalobos et al. (Villalobos et al., 2005) also reported that the opacity is closely related to the polymer chain rearrangement during the drying of the cast film-forming solution, which is strongly influenced by its initial nature, namely, if it is a miscible or non-miscible dispersion. In fact, Gly has low miscibility in acetone (5% (w/w)) (The Soap and Detergent Association, 1990) which might be a limitation in the blending process with CA (Quintana et al., 2013). In this work, although the Gly initial concentration in the film-forming solution was less than 5% (w/w), this concentration increases during the evaporation of acetone in the drying step. Thus, the opacity of the CA-based films with Gly could be not only related to the compatibility between the biopolymer and the plasticizer but also with the interaction of all components of the solution during the film formation. The development of the opacity in CA-Gly films was already reported elsewhere (de Melo et al., 2018; Teixeira et al., 2021), although the authors did not provide a well clear explanation.

The opacity results also showed that the opacity decreases significantly ($p > 0.05$) from 10 to 40% of Gly percentages. Moreover, in terms of visual appearance (Fig. 2), films with a percentage of Gly equal and superior to 20% were smoother and more homogeneous than the 10% Gly film, as already described above. Although this is unexpected behavior, it seems that higher concentrations of Gly led to high dispersion and spread of the plasticizer in the films, which could be also observed by SEM and AFM images. Indeed, a certain incompatibility between the components of the film during the drying stage may be responsible for the appearance of pore-like structures characteristic of films with Gly, which in turn, caused changes in the optical properties. Nevertheless, it was possible to observe by SEM and AFM images the increase in pore size with the increase of the Gly percentage, becoming a more network-like type. These larger pores can allow for more permeability to light, justifying the reduction in opacity and heterogeneity of the films.

If the films would be for application in active food packaging,

transparency is a very important property from consumers' point of view because they want to be able to see the food inside the packaging (Motelica et al., 2020). However, since the aim is the development of a smart colorimetric indicator (label or tag), the opacity can be an advantage since that transparency can lead to uncertainties in the interpretation of the color by the customer.

3.3. Tests as pH-indicator

The films were tested as pH-colorimetric indicators by doing their immersion in buffer solutions with different pH values, between 4 and 8, which is the relevant pH range for monitoring the spoilage of perishable foods. Color variations for each film were calculated by Eq. (7) after the exposure to different pH solutions over time for 1 h (Fig. 6). Almost no color variation was observed for the CA_PyF film for any pH value, while the Gly-containing films showed an increasing color variation as the solution pH increased. For those films, it was possible practically to reach a plateau of color variation after 20 min of immersion at different pH values, except for CA_PyF_Gly10, which takes longer to achieve the final color. Furthermore, CA_PyF_Gly40 showed some color fading after the maximum color variation had been achieved, mainly for higher pH values (pH 7 and 8). The presence of Gly in film formulation was essential to achieve pH sensing efficacy. In fact, in the case of the film without glycerol, the stronger inter/intramolecular hydrogen bonding of CA lead to a tight net of the polymer chains which avoids the penetration of water molecules and, consequently, the contact of H^+ and OH^- ions with the film. Since the ions cannot penetrate into the film, they also cannot interact with the dye and, thus, the dye has no fast response to the pH. The porosity and, consequently, the higher water permeability of the films with glycerol promotes the penetration of H^+ and OH^- ions, resulting in higher effectiveness and sensitivity of the indicator. In addition, the porosity also promoted by glycerol increases the superficial area of the film which increases the contact area between the dye immobilized on the film and the water molecules in the surrounding environment, rising a faster pH response. Thus, the most promising formulations to be considered for indicator development were the CA-based films containing 20 and 30% of Gly, since the 10% film presented a slower pH response. CA_PyF_Gly40 was not considered because its formulation exceeded the compatibility limit between biopolymer and plasticizer, as mentioned above, in addition to the slight loss of color demonstrated at higher pH values. Ardila-Diaz et al. (Ardila-Diaz et al., 2020) also reported that the amount of the

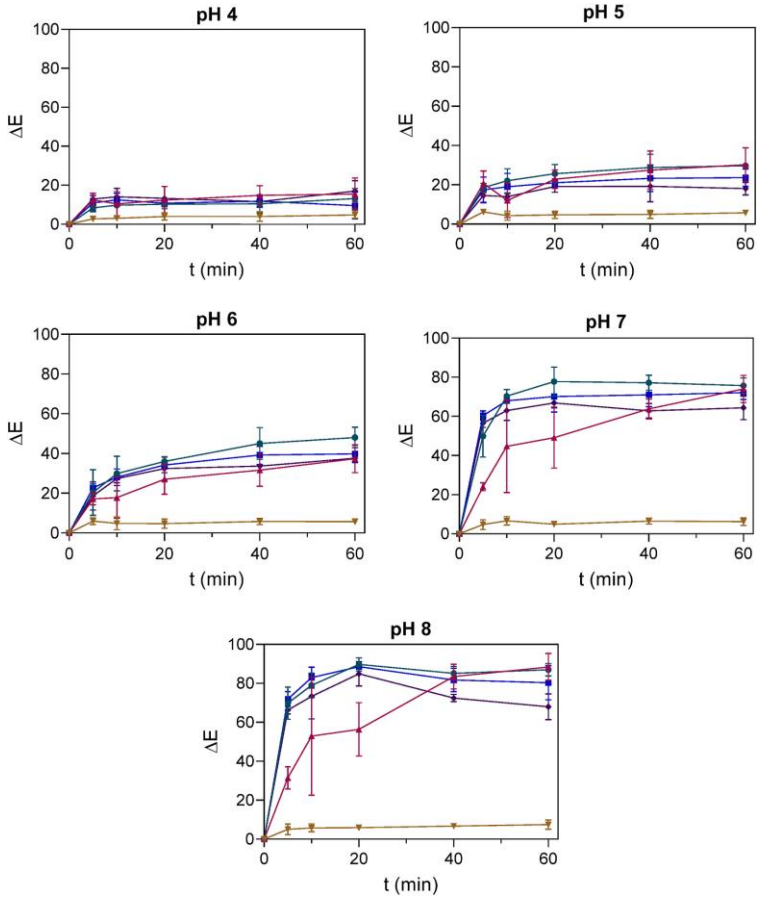


Fig. 6. Color variation calculated by Eq. (7) for each CA film with PyF and different Gly percentages (0–40%), after immersion in different buffer solutions (pH 4 to 8), over 60 min: CA_PyF; CA_PyF_Gly10; CA_PyF_Gly20; CA_PyF_Gly30; CA_PyF_Gly40. (For interpretation of the references to color in this figure legend, the reader is referred to the Web version of this article.)

plasticizer, namely triethyl citrate, is one of the important factors for the color transitioning of CA films with polydiacetylene as a colorimetric sensor substance.

The color variation between different pH buffered solutions was very noteworthy as it was possible to observe by the photographs of the films (Fig. 7A), changing gradually from yellow to purple. The most pronounced variation was observed between pH 6 and 7, with a ΔE from ≈ 37 to ≈ 75 (Fig. 7B). Generally, the spoilage pH range of perishable foods is very narrow, varying i.e. between 6.24 (fresh) and 7 (spoiled) for rainbow trout samples (Ezati et al., 2019); and from 5.82 (fresh) to 7.42 (total spoiled) for pork samples (Choi et al., 2017), etc. In contrast to most of the pH-indicators based on anthocyanin extracts, which did not have a very noticeable color change on this pH range (Jiang et al., 2020; Kang et al., 2020; Liang et al., 2019; Mohammadalinejhad et al., 2020; Moradi et al., 2019; Prietto et al., 2017), the developed pyranoflavylium-containing CA film yielded an excellent color change. Furthermore, this anthocyanin-derived pigment is more stable over time than native anthocyanins, as described elsewhere (Gomes et al., 2021), which makes this formulation a promising pH-indicator for monitoring fish and meat spoilage.

3.4. Film color response towards an amine-rich environment

Biological degradation and microbial growth are responsible for the spoilage of many perishable food products. During spoilage, various volatile basic nitrogen compounds (TVB-N – total volatile basic nitrogen), such as ammonia and BA are produced and released resulting in an increase of the pH (Ezati & Rhim, 2020). The aim of a pH-indicator label for food packaging is to give a color response to the volatile nitrogen compounds present in the headspace equilibrium of the packaging, without touching the food product. In order to evaluate the efficacy of the color response of the pH-indictor to volatile basic nitrogen compounds, CA_PyF_Gly30 film was exposed to the headspace of different solutions of BA (0.5–4 g/L) and ammonium hydroxide (0.35 and 3.5 g/L). Fig. 8a showed the experimental method and the initial color of the film before the amine solutions exposure and Fig. 8b showed the color difference (ΔE) between the initial and the final color of the films (photographs) after overnight headspace exposition.

Although the pH value at the headspace of each flask is unknown in this preliminary experiment, it was possible to observe a noticeable change of the film color with increasing concentrations of BA and ammonia-containing solutions. The pH at the headspace depends on the volatility of the amine compounds, its basicity, and its affinity to the air *versus* matrix, which in this case is water, whereas in real samples is the food product itself. Here, the color response was greater for ammonia solutions due to its higher basicity and volatility compared to BA ones. The color of pH-indicator film changed from the initial yellow to orange and pale pink in BA solutions, and to purple and finally blue in ammonia solutions. These preliminary tests proves that the colorimetric pH-indicator developed in this work is able to respond to an amine-rich environment, highlighting great evidence that it can be applied into smart food packaging.

4. Conclusions

The pyranoflavylium dye was successfully immobilized in CA-based films with different percentages of Gly (0–40% (w/w)) as a plasticizer. In general, the presence of Gly promoted a significant difference in the thickness and color, barrier, and morphological properties of the films. Gly originated the appearance of pores, which lead to an increase of the permeability of the films to water as well as the surface contact area, resulting in more efficient color-response to the pH of the environment. A great pH-responsiveness was obtained with the films enriched with 20 and 30% of Gly after 20 min of immersion. These formulations showed relevant and remarkable color change at the pH range of food spoilage, and a good response to an amine-rich environment, indicating a great potential for application as a pH freshness indicator for perishable foods.

CRediT authorship contribution statement

Vânia Gomes: Conceptualization, Methodology, Investigation, Writing - original draft. **Ana Sofia Pires:** Methodology, Investigation. **Nuno Mateus:** Writing - review & editing. **Victor Freitas:** Writing - review & editing, Project administration, Funding acquisition. **Luis Cruz:** Conceptualization, Methodology, Investigation, Writing - review & editing, Funding acquisition.

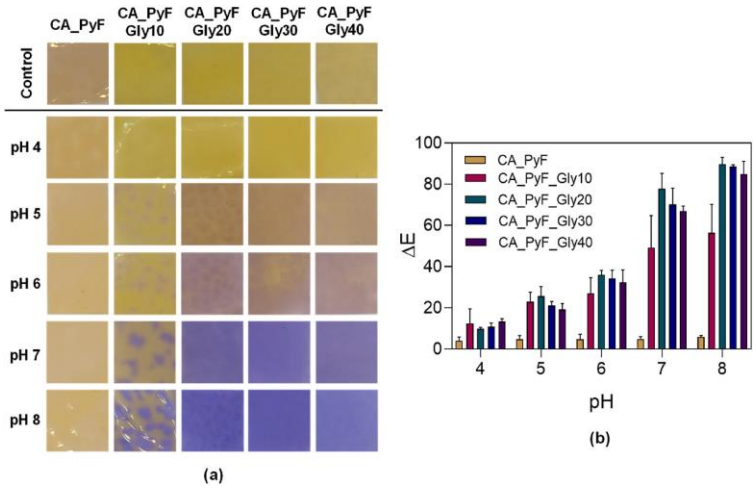


Fig. 7. Color variation of the CA films with PyF and different Gly percentages (0–40%) after 20 min of immersion in different buffer solutions (pH 4 to 8): (a) photographs and (b) calculated by Eq. (7). Controls were the films before immersion in buffer solutions. (For interpretation of the references to color in this figure legend, the reader is referred to the Web version of this article.)

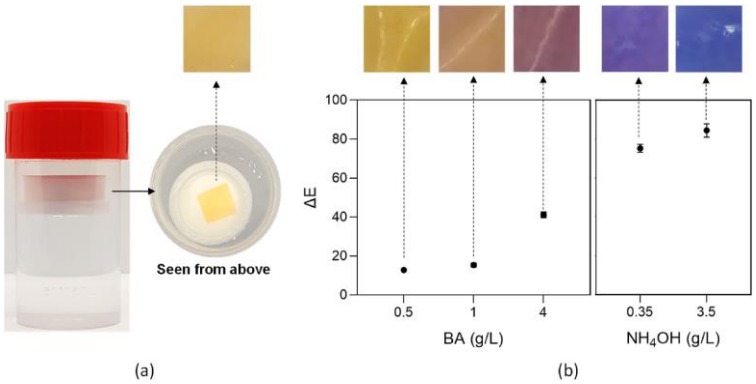


Fig. 8. (a) Experimental method and photograph of the film before the amine solutions exposure and (b) color variation calculated by Eq. (7) for CA_PyF_Gly30 film, after overnight headspace exposition to different BA (g/L) and ammonia solutions (g/L), and photographs of the final color of the films. (For interpretation of the references to color in this figure legend, the reader is referred to the Web version of this article.)

Declaration of competing interest

The authors declare that they have no known competing financial interests or personal relationships that could have appeared to influence the work reported in this paper.

Acknowledgments

The authors thank Professor Alexandra Guedes from Department of Geosciences, Environment and Spatial Plannings (Faculty of Sciences, University of Porto) for the portable spectrophotometer (model CM-2600 d; Konica Minolta, Japan) used for color and opacity analysis. This work was supported by the Associate Laboratory for Sustainable Chemistry, Clean Processes, and Technologies LAQV. The latter is financed by national funds from UIDB/50006/2020. This research is supported by AgriFood XXI I&D&I project (NORTE-01-0145-FEDER-000041) cofinanced by European Regional Development Fund (ERDF), through the NORTE 2020 (Pro-grama Operacional Regional do Norte 2014/2020). This work was also supported by the project PTDC/OCE-ETA/31250/2017 funded by FCT and FEDER. Luís Cruz acknowledges the FCT research contract (DL 57/2016/CP1334/CT0008) and Vânia Gomes acknowledges the Ph.D. grant from FCT (SFRH/BD/136556/2018).

References

Aghaei, Z., Emadzadeh, B., Ghorani, B., & Kadkhodaee, R. (2018). Cellulose acetate nanofibres containing alizarin as a halochromic sensor for the qualitative assessment of rainbow trout fish spoilage. *Food and Bioprocess Technology, 11*(5), 1087–1095. https://doi.org/10.1007/s11947-017-2046-5

Andretta, R., Luchese, C. L., Tessaro, I. C., & Spada, J. C. (2019). Development and characterization of pH-indicator films based on cassava starch and blueberry residue by thermocompression. *Food Hydrocolloids, 93*, 317–324. https://doi.org/10.1016/j.foodhyd.2019.02.019. February.

Ardila-Diaz, L. D., de Oliveira, T. V., & Soares, N. de F. F. (2020). Development and evaluation of the chromatic behavior of an intelligent packaging material based on cellulose acetate incorporated with polydiacetylene for an efficient packaging. *Biosensors, 10*(6). https://doi.org/10.3390/BIOS10060059

Assis, R. Q., Rios, P. D. A., Rios, A. de O., & Olivera, F. C. (2020). Biodegradable packaging of cellulose acetate incorporated with norbixin, lycopene or zeaxanthin. *Industrial Crops and Products, 147*, Article 112212. https://doi.org/10.1016/j.indcrop.2020.112212. February.

ASTM. (1994). Standard test methods for moisture content of paper and paperboard by oven drying. Method D644-99. *Annual Book of ASTM Standards, American Society for Testing and Materials, 99*, 1–3. Reapproved.

ASTM. (2013). *Standard test methods for water vapor transmission of materials E96/E96M*. Annual Book of ASTM Standards. https://doi.org/10.1520/E0096. *i*, 1–10.

Brouillard, R., Chassaing, S., Isorez, G., Kueny-Stotz, M., & Figueiredo, P. (2010). The visible flavonoids or anthocyanins: From research to applications. In *Recent advances in polyphenol research* (pp. 1–22). Wiley-Blackwell. https://doi.org/10.1002/9781444323375.ch1.

Bruna, J. E., Galotto, M. J., Guarda, A., & Rodríguez, F. (2014). A novel polymer based on MtCu2+/cellulose acetate with antimicrobial activity. *Carbohydrate Polymers, 102*(1), 317–323. https://doi.org/10.1016/j.carbpol.2013.11.038

Cerqueira, M. A., Souza, B. W. S., Teixeira, J. A., & Vicente, A. A. (2012). Effect of glycerol and corn oil on physicochemical properties of polysaccharide films - a comparative study. *Food Hydrocolloids, 27*(1), 175–184. https://doi.org/10.1016/j.foodhyd.2011.07.007

Chen, H. zhi, Zhang, M., Bhandari, B., & Yang, C. hui (2020). Novel pH-sensitive films containing curcumin and anthocyanins to monitor fish freshness. *Food Hydrocolloids, 100*, Article 105438. https://doi.org/10.1016/j.foodhyd.2019.105438. July 2019.

Choi, I., Lee, J. Y., Lacroix, M., & Han, J. (2017). Intelligent pH indicator film composed of agar/potato starch and anthocyanin extracts from purple sweet potato. *Food Chemistry, 218*, 122–128. https://doi.org/10.1016/j.foodchem.2016.09.050

Cruz, L., Basílio, N., Mateus, N., de Freitas, V., & Pina, F. (2022). Natural and synthetic flavylium-based dyes: The Chemistry behind the color. *Chemical Reviews, 122*(1), 1416–1481. https://doi.org/10.1021/acs.chemrev.1c00399

Cruz, L., Sousa, J. L. C., Marinho, A., Mateus, N., & de Freitas, V. (2017). Synthesis and structural characterization of novel pyranoluteolinidin dyes. *Tetrahedron Letters, 58*(2), 159–162. https://doi.org/10.1016/j.tetlet.2016.11.123

Danchuk, A. I., Komova, N. S., Mobarez, S. N., Doronin, S. Y., Burmistrova, N. A., Markin, A. V., & Duerkop, A. (2020). Optical sensors for determination of biogenic amines in food. *Analytical and Bioanalytical Chemistry, 412*(17), 4023–4036. https://doi.org/10.1007/s00216-020-02675-9

Dick, M., Costa, T. M. H., Gomaa, A., Subirade, M., Rios, A. D. O., & Flôres, S. H. (2015). Edible film production from chia seed mucilage: Effect of glycerol concentration on its physicochemical and mechanical properties. *Carbohydrate Polymers, 130*, 198–205. https://doi.org/10.1016/j.carbpol.2015.05.040

Donhowe, I. G., & Fennema, O. (1993). The effects of plasticizers on crystallinity, permeability, and mechanical properties of methylcellulose films. *Journal of Food Processing and Preservation, 17*(4), 247–257. https://doi.org/10.1111/j.1745-4549.1993.tb00729.x

Drago, E., Campardelli, R., Pettinato, M., & Perego, P. (2020). Innovations in smart packaging concepts for food: An extensive review. *Foods, 9*(11), 1628. https://doi.org/10.3390/foods9111628

Ezati, P., & Rhim, J. W. (2020). pH-responsive chitosan-based film incorporated with alizarin for intelligent packaging applications. *Food Hydrocolloids, 102*, Article 105629. https://doi.org/10.1016/j.foodhyd.2019.105629. December 2019.

Ezati, P., Tajik, H., Moradi, M., & Molaei, R. (2019). Intelligent pH-sensitive indicator based on starch-cellulose and alizarin dye to track freshness of rainbow trout fillet. *International Journal of Biological Macromolecules, 132*, 157–165. https://doi.org/10.1016/j.ijbiomac.2019.03.173

FAO. (2013). In *Food wastage footprint*. FAO. www.fao.org/publications.

Farhan, A., & Hani, N. M. (2017). Characterization of edible packaging films based on semi-refined kappa-carrageenan plasticized with glycerol and sorbitol. *Food Hydrocolloids, 64*, 48–58. https://doi.org/10.1016/j.foodhyd.2016.10.034

Freitas, P. A. V., Silva, R. R. A., de Oliveira, T. V., Soares, R. R. A., Junior, N. S., Moraes, A. R. F., Pires, A. C. dos S., & Soares, N. F. F. (2020). Development and characterization of intelligent cellulose acetate-based films using red cabbage extract for visual detection of volatile bases. *Lebensmittel-Wissenschaft & Technologie, 132*, Article 109780. https://doi.org/10.1016/j.lwt.2020.109780. June.

Gemili, S., Yemenicioğlu, A., & Altinkaya, S. A. (2009). Development of cellulose acetate based antimicrobial food packaging materials for controlled release of lysozyme. *Journal of Food Engineering, 90*(4), 453–462. https://doi.org/10.1016/j.jfoodeng.2008.07.014

Gomes, V., Guimarães, M., Gonçalves, G., De Freitas, V., & Cruz, L. (2020). Bioinspired synthesis and physical-chemical properties of a new 10-Methylpyrano-4′-

hydroxyflavylium chloride salt. *Synlett, 31*(4), 334–338. https://doi.org/10.1055/s-0039-1690744

Gomes, V., Pires, A. S., Fernandes, I., Mateus, N., de Freitas, V., & Cruz, L. (2021). Synthesis of novel pyrano-3,7-deoxyanthocyanin derivatives and study of their thermodynamic, photophysical and cytotoxicity properties. *Journal of Photochemistry and Photobiology A: Chemistry, 415*, Article 113313. https://doi.org/10.1016/j.jphotochem.2021.113313. August 2020.

Gontard, N., Duchez, C., Cuq, J.-L., & Guilbet, S. (2007). Edible composite films of wheat gluten and lipids: Water vapour permeability and other physical properties. *International Journal of Food Science and Technology, 29*(1), 39–50. https://doi.org/10.1111/j.1365-2621.1994.tb02045.x

Gonçalves, S. M., dos Santos, D. C., Motta, J. F. G., Santos, R. R. dos, Chávez, D. W. H., & Melo, N. R. de (2019). Structure and functional properties of cellulose acetate films incorporated with glycerol. *Carbohydrate Polymers, 209*, 190–197. https://doi.org/10.1016/j.carbpol.2019.01.031. January.

Heising, J. K., Claassen, G. D. H., & Dekker, M. (2017). Options for reducing food waste by quality-controlled logistics using intelligent packaging along the supply chain. *Food Additives & Contaminants Part A Chemistry, Analysis, Control, Exposure and Risk Assessment, 34*(10), 1672–1680. https://doi.org/10.1080/19440049.2017.1315776

Jiang, G., Hou, X., Zeng, X., Zhang, C., Wu, H., Shen, G., Li, S., Luo, Q., Li, M., Liu, X., Chen, A., Wang, Z., & Zhang, Z. (2020). Preparation and characterization of indicator films from carboxymethyl-cellulose/starch and purple sweet potato (Ipomoea batatas (L.) lam) anthocyanins for monitoring fish freshness. *International Journal of Biological Macromolecules, 143*, 359–372. https://doi.org/10.1016/j.ijbiomac.2019.12.024

Kang, S., Wang, H., Xia, L., Chen, M., Li, L., Cheng, J., Li, X., & Jiang, S. (2020). Colorimetric film based on polyvinyl alcohol/okra mucilage polysaccharide incorporated with rose anthocyanins for shrimp freshness monitoring. *Carbohydrate Polymers, 229*, Article 115402. https://doi.org/10.1016/j.carbpol.2019.115402. July 2019.

Laohakunjit, N., & Noomhorm, A. (2004). Effect of plasticizers on mechanical and barrier properties of rice starch film. *Starch Staerke, 56*(8), 348–356. https://doi.org/10.1002/star.200300249

Liang, T., Sun, G., Cao, L., Li, J., & Wang, L. (2019). A pH and NH3 sensing intelligent film based on Artemisia sphaerocephala Krasch. gum and red cabbage anthocyanins anchored by carboxymethyl cellulose sodium added as a host complex. *Food Hydrocolloids, 87*, 858–868. https://doi.org/10.1016/j.foodhyd.2018.08.028. July 2018.

Liu, Y., Ahmed, S., Sameen, D. E., Wang, Y., Lu, R., Dai, J., Li, S., & Qin, W. (2021). A review of cellulose and its derivatives in biopolymer-based for food packaging application. *Trends in Food Science & Technology, 112*, 532–546. https://doi.org/10.1016/j.tifs.2021.04.016. November 2020.

Liu, J., Wang, H., Guo, M., Li, L., Chen, M., Jiang, S., Li, X., & Jiang, S. (2019). Extract from Lycium ruthenicum Murr. Incorporating κ-carrageenan colorimetric film with a wide pH–sensing range for food freshness monitoring. *Food Hydrocolloids, 94*, 1–10. https://doi.org/10.1016/j.foodhyd.2019.03.008. March.

Luchese, C. L., Sperotto, N., Spada, J. C., & Tessaro, I. C. (2017). Effect of blueberry agro-industrial waste addition to corn starch-based films for the production of a pH-indicator film. *International Journal of Biological Macromolecules, 104*, 11–18. https://doi.org/10.1016/j.ijbiomac.2017.05.149

Mekonnen, T., Mussone, P., Khalil, H., & Bressler, D. (2013). Progress in bio-based plastics and plasticizing modifications. *Journal of Materials Chemistry, 1*(43), 13379–13398. https://doi.org/10.1039/c3ta12555f

de Melo, P. G., Fornazier Borges, M., Afonso Ferreira, J., Vicente Barbosa Silva, M., & Ruggiero, R. (2018). Bio-based cellulose acetate films reinforced with lignin and glycerol. *International Journal of Molecular Sciences, 19*(4), 1–13. https://doi.org/10.3390/ijms19041143

Mohammadalinejhad, S., Almasi, H., & Moradi, M. (2020). Immobilization of Echium amoenum anthocyanins into bacterial cellulose film: A novel colorimetric pH indicator for freshness/spoilage monitoring of shrimp. *Food Control, 113*, Article 107169. https://doi.org/10.1016/j.foodcont.2020.107169. January.

Moradi, M., Tajik, H., Almasi, H., Forough, M., & Ezati, P. (2019). A novel pH-sensing indicator based on bacterial cellulose nanofibers and black carrot anthocyanins for monitoring fish freshness. *Carbohydrate Polymers, 222*(June), Article 115030. https://doi.org/10.1016/j.carbpol.2019.115030

Moreira Gonçalves, S., Gomes Motta, J. F., Ribeiro-Santos, R., Hidalgo Chávez, D. W., & Ramos de Melo, N. (2020). Functional and antimicrobial properties of cellulose acetate films incorporated with sweet fennel essential oil and plasticizers. *Current Research in Food Science, 3*, 1–8. https://doi.org/10.1016/j.crfs.2020.01.001

Motelica, L., Ficai, D., Ficai, A., Oprea, O. C., & Andronescu, E. (2020). Biodegradable antimicrobial food packaging : Trends and perspectives. *Foods, 9*, 1–36. https://doi.org/10.3390/foods9101438

Nordin, N., Othman, S. H., Rashid, S. A., & Basha, R. K. (2020). Effects of glycerol and thymol on physical, mechanical, and thermal properties of corn starch films. *Food Hydrocolloids, 106*, Article 105884. https://doi.org/10.1016/j.foodhyd.2020.105884. December 2019.

Oliveira, J., Mateus, N., & Freitas, V. De (2014). Previous and recent advances in pyranoanthocyanins equilibria in aqueous solution. *Dyes and Pigments, 100*, 190–200. https://doi.org/10.1016/j.dyepig.2013.09.009

Pereira, V. A., de Arruda, I. N. Q., & Stefani, R. (2015). Active chitosan/PVA films with anthocyanins from Brassica oleraceae (Red Cabbage) as Time-Temperature Indicators for application in intelligent food packaging. *Food Hydrocolloids, 43*, 180–188. https://doi.org/10.1016/j.foodhyd.2014.05.014

Pina, F. (2014). Chemical applications of anthocyanins and related compounds. A source of bioinspiration. *Journal of Agricultural and Food Chemistry, 62*(29), 6885–6897. https://doi.org/10.1021/jf404869m

Pina, F., Melo, M. J., Laia, C.a. T., Parola, a. J., & Lima, J. C. (2012). Chemistry and applications of flavylium compounds: A handful of colours. *Chemical Society Reviews, 41*(2), 869. https://doi.org/10.1039/c1cs15126f

Prietto, L., Mirapalhete, T. C., Pinto, V. Z., Hoffmann, J. F., Vanier, N. L., Lim, L.-T., Guerra Dias, A. R., & da Rosa Zavareze, E. (2017). pH-sensitive films containing anthocyanins extracted from black bean seed coat and red cabbage. *Lebensmittel-Wissenschaft & Technologie, 80*, 492–500. https://doi.org/10.1016/j.lwt.2017.03.006

Priyadarshi, R., Sauraj, Kumar, B., & Negi, Y. S. (2018). Chitosan film incorporated with citric acid and glycerol as an active packaging material for extension of green chilli shelf life. *Carbohydrate Polymers, 195*, 329–338. https://doi.org/10.1016/j.carbpol.2018.04.089. February.

Quintana, R., Persenaire, O., Lemmouchi, Y., Sampson, J., Martin, S., Bonnaud, L., & Dubois, P. (2013). Enhancement of cellulose acetate degradation under accelerated weathering by plasticization with eco-friendly plasticizers. *Polymer Degradation and Stability, 98*(9), 1556–1562. https://doi.org/10.1016/j.polymdegradstab.2013.06.032

Rajeswari, A., Christy, E. J. S., Swathi, E., & Pius, A. (2020). Fabrication of improved cellulose acetate-based biodegradable films for food packaging applications. *Environmental Chemistry and Ecotoxicology, 2*, 107–114. https://doi.org/10.1016/j.enceco.2020.07.003

Saberi, B., Chockchaisawasdee, S., Golding, J. B., Scarlett, C. J., & Stathopoulos, C. E. (2017). Physical and mechanical properties of a new edible film made of pea starch and guar gum as affected by glycols, sugars and polyols. *International Journal of Biological Macromolecules, 104*, 345–359. https://doi.org/10.1016/j.ijbiomac.2017.06.051

Saha, N. R., Sarkar, G., Roy, I., Bhattacharyya, A., Rana, D., Dhanarajan, G., Banerjee, R., Sen, R., Mishra, R., & Chattopadhyay, D. (2016). Nanocomposite films based on cellulose acetate/polyethylene glycol/modified montmorillonite as nontoxic active packaging material. *RSC Advances, 6*(95), 92569–92578. https://doi.org/10.1039/c6ra17300d

Sanyang, M. L., Sapuan, S. M., Jawaid, M., Ishak, M. R., & Sahari, J. (2015). Effect of plasticizer type and concentration on tensile, thermal and barrier properties of biodegradable films based on sugar palm (Arenga pinnata) starch. *Polymers, 7*(6), 1106–1124. https://doi.org/10.3390/polym7061106

Sanyang, M. L., Sapuan, S. M., Jawaid, M., Ishak, M. R., & Sahari, J. (2016). Effect of plasticizer type and concentration on physical properties of biodegradable films based on sugar palm (arenga pinnata) starch for food packaging. *Journal of Food Science & Technology, 53*(1), 326–336. https://doi.org/10.1007/s13197-015-2009-7

Shukla, V., Kandeepan, G., Vishnuraj, M. R., & Soni, A. (2016). Anthocyanins based indicator sensor for intelligent packaging application. *Agricultural Research, 5*(2), 205–209. https://doi.org/10.1007/s40003-016-0211-0

da Silva Filipini, G., Romani, V. P., & Guimarães Martins, V. (2020). Biodegradable and active-intelligent films based on methylcellulose and jambolão (Syzygium cumini) skins extract for food packaging. *Food Hydrocolloids, 109*. https://doi.org/10.1016/j.foodhyd.2020.106139. June.

Sousa, J. L. C., Gomes, V., Mateus, N., Pina, F., de Freitas, V., & Cruz, L. (2017). Synthesis and equilibrium multistate of new pyrano-3-deoxyanthocyanin-type pigments in aqueous solutions. *Tetrahedron, 73*(41), 6021–6030. https://doi.org/10.1016/j.tet.2017.08.051

Tarique, J., Sapuan, S. M., & Khalina, A. (2021). Effect of glycerol plasticizer loading on the physical, mechanical, thermal, and barrier properties of arrowroot (Maranta arundinacea) starch biopolymers. *Scientific Reports, 11*(1), 1–17. https://doi.org/10.1038/s41598-021-93094-y

Teixeira, S. C., Silva, R. R. A., de Oliveira, T. V., Stringheta, P. C., Pinto, M. R. M. R., & Soares, N. de F. F. (2021). Glycerol and triethyl citrate plasticizer effects on molecular, thermal, mechanical, and barrier properties of cellulose acetate films. *Food Bioscience, 42*(June). https://doi.org/10.1016/j.fbio.2021.101202

The Soap and Detergent Association. (1990). *Glycerine : An overview*. Glycerine & Oleochemical Division.

Vanderroost, M., Ragaert, P., Devlieghere, F., & De Meulenaer, B. (2014). Intelligent food packaging: The next generation. *Trends in Food Science & Technology, 39*(1), 47–62. https://doi.org/10.1016/j.tifs.2014.06.009

Veiga-Santos, P., Ditchfield, C., & Tadini, C. C. (2010). Development and evaluation of a novel pH indicator biodegradable film based on cassava starch. *Journal of Applied Polymer Science, 120*, 1069–1079. https://doi.org/10.1002/app.33255

Vieira, M. G. A., Da Silva, M. A., Dos Santos, L. O., & Beppu, M. M. (2011). Natural-based plasticizers and biopolymer films: A review. *European Polymer Journal, 47*(3), 254–263. https://doi.org/10.1016/j.eurpolymj.2010.12.011

Villalobos, R., Chanona, J., Hernández, P., Gutiérrez, G., & Chiralt, A. (2005). Gloss and transparency of hydroxypropyl methylcellulose films containing surfactants as affected by their microstructure. *Food Hydrocolloids, 19*(1), 53–61. https://doi.org/10.1016/j.foodhyd.2004.04.014

Wei, Y. C., Cheng, C. H., Ho, Y. C., Tsai, M. L., & Mi, F. L. (2017). Active gellan gum/purple sweet potato composite films capable of monitoring pH variations. *Food Hydrocolloids, 69*, 491–502. https://doi.org/10.1016/j.foodhyd.2017.03.010

World Health Organization. (2020). *Food Safety*. https://www.who.int/news-room/fact-sheets/detail/food-safety.

Yousefi, H., Su, H. M., Imani, S. M., Alkhaldi, K., Filipe, C. D., & Didar, T. F. (2019). Intelligent food packaging: A review of smart sensing technologies for monitoring

food quality. *ACS Sensors, 4*(4), 808–821. https://doi.org/10.1021/acssensors.9b00440

Zhang, X., Lu, S., & Chen, X. (2014). A visual pH sensing film using natural dyes from Bauhinia blakeana Dunn. *Sensors and Actuators B: Chemical, 198*, 268–273. https://doi.org/10.1016/j.snb.2014.02.094

Zhang, J., Zou, X., Zhai, X., Huang, X. W., Jiang, C., & Holmes, M. (2019). Preparation of an intelligent pH film based on biodegradable polymers and roselle anthocyanins for monitoring pork freshness. *Food Chemistry, 272*, 306–312. https://doi.org/10.1016/j.foodchem.2018.08.041. August 2018.

Article VII

FoodSmarTag: An innovative dynamic labeling system based on pyranoflavylium-based colorimetric films for real-time monitoring of food freshness

Vânia Gomes[1], Roberto Bermudez[2], Jose Manuel Lorenzo[2,3], Nuno Mateus[1], Victor de Freitas[1], Luís Cruz[1]*

[1]REQUIMTE/LAQV, Departamento de Química e Bioquímica, Faculdade de Ciências, Universidade do Porto, Rua Do Campo Alegre, 687, 4169-007, Porto, Portugal

[2]Centro Tecnológico de la Carne de Galicia, Rúa Galicia Nº 4, Parque Tecnológico de Galicia, San Cibrao das Viñas, 32900 Ourense, Spain

[3]Universidade de Vigo, Área de Tecnoloxía dos Alimentos, Facultade de Ciencias, 32004 Ourense, Spain

---

Gomes, V., Bermudez, R., Lorenzo, J. M., Mateus, N., de Freitas, V, Cruz, L., FoodSmarTag: An innovative dynamic labeling system based on pyranoflavylium-based colorimetric films for real-time control of food freshness. *In preparation.*

FoodSmarTag: An innovative dynamic labeling system based on pyranoflavylium-based colorimetric films for real-time monitoring of food freshness

Vânia Gomes[1], Roberto Bermudez[2], Nuno Mateus[1], Jose Manuel Lorenzo[2,3], Victor de Freitas[1], Luís Cruz[1]*

[1]REQUIMTE/LAQV, Departamento de Química e Bioquímica, Faculdade de Ciências, Universidade do Porto, Rua Do Campo Alegre, 687, 4169-007, Porto, Portugal
[2]Centro Tecnológico de la Carne de Galicia, Rúa Galicia Nº 4, Parque Tecnológico de Galicia, San Cibrao das Viñas, 32900 Ourense, Spain
[3]Universidade de Vigo, Área de Tecnoloxía dos Alimentos, Facultade de Ciencias, 32004 Ourense, Spain

*Corresponding author: Luís Cruz: Tel.: +351 220402558; fax: +351 220402658.

Email address: luis.cruz@fc.up.pt

ABSTRACT

A colorimetric pyranoflavylium-based pH-indicator with an improved formulation was obtained and studied as an intelligent label for food freshness monitoring. Pyranoflavylium pigment at 0.2% (w/w) and glycerol at 30% (w/w) were immobilized in a cellulose acetate matrix, and a thin film was obtained by the solvent casting method. The pH-responsive properties of the film were evaluated in solutions at different pH values (pH 4 to 8) and compared with a previous formulation. Film photostability and pigment migration over time were assessed. The label's performance was evaluated using real samples (fish and meat) at controlled conditions (4 ± 1 ºC and modified atmosphere packaging). The results showed that increased pigment concentration visually favored its colorimetric efficacy. Regarding pigment migration and photostability, the label showed to be suitable for application in fresh meat and fish packaging. The best performance was observed for the freshness monitoring of fish samples. The indicator demonstrated high efficacy in detecting spoilage of Atlantic horse mackerel (*Trachurus trachurus*). After 5 days of storage, freshness parameters exceeded the limit defined by EU regulations, indicating that the fish was unfit for consumption. Simultaneously, the yellow label started to turn purple, effectively indicating the beginning of the spoilage process.

Keywords: Pyranoflavylium dye; pH-indicator; colorimetric films; food packaging; fish and meat spoilage

1. Introduction

The challenges of modern society are driving innovation in the field of food packaging at an ever-increasing rate. "Food safety" and "food waste" are issues on the agenda, and the development of innovative food packaging can be part of the solution. Although its use is often controversial due to the excessive use of plastic-based materials, the truth is that packaging has played a crucial role in maintaining the quality and safety of foods during their storage, transportation, and sale. For this reason, there has been an increased interest in designing and producing more sustainable packaging materials using polymers derived from biodegradable sources. Moreover, food packaging systems able to extend the quality/shelf life of food – active packaging – and/or to provide information on food quality or freshness – intelligent packaging – have also been a focus of research.

The European Union defines intelligent packaging materials as "materials and articles that monitor the condition of packaged food or the environment surrounding the food" [1]. Its principal purpose is to detect and provide real-time food quality information, ensuring the food safety entire supply chain until the final consumer [2]. In addition, intelligent packaging can play an essential role in reducing food waste by replacing static "best before" or "use by" dates with the "dynamic shelf-life" concept, even among products of the same lot [3].

The real-time food control in a package can be made by monitoring different quality parameters, such as pH, oxygen, temperature, or specific compounds. In fact, pH change in the food environment has been described as an effective method of identifying food spoilage, especially in perishable food products, such as animal-origin products [4]. pH alterations can be affected by many microbial metabolites, such as biogenic amines [5] and organic acids [4], resulting from amino acids and glucose metabolization, leading to an increase or a decrease in the pH of food samples, respectively.

Behind the technologies applied in intelligent packaging, colorimetric pH indicators are the most studied in research since they provide immediate visual and qualitative (or semi-quantitative) information about the packaged food through a color change [6]. In the last decade, colorimetric indicators have been studied based on natural pH-sensitive dyes, such as anthocyanins, curcumin, alizarin, and betalains. Natural dyes are chosen instead of synthetic ones due to their lower toxicity, environmental impact, and high availability [3,7,8]. Among these pigments, anthocyanins are the most widely studied [9–13] due to their notable color change from red to blue with pH increases. However, natural pigments are often not stable outside their native habitat, and color fading may

occur quickly owing to environmental factors (e.g., light, temperature, etc.), limiting their use as colorimetric pH indicators [8]. Even though most published works did not refer to it, anthocyanins are an example since they have a complex multistate equilibrium that leads to color fading over time [14–17]. On the other hand, synthetic dyes are generally described as potentially hazardous for food applications due to their toxic, carcinogenic, and mutagenic characteristics. Nevertheless, synthetic pigments are not necessarily unsafe; e.g., when designed based on natural pigments with improved or simplified properties, they may be the answer to the instability problems of natural pigments.

Synthetic pigments inspired by anthocyanins, namely pyranoflavylium salts, have been recently developed, being also able to change color in response to pH variations; however, they are more stable over time than anthocyanins [18–21]. In previous work, a pyranoflavylium-based pigment designed with specific features, such as a suitable color variation and low cytotoxicity [22], was immobilized in cellulose acetate and glycerol as a plasticizer, giving rise to a colorimetric pH-indicator film [23]. The film exhibited a remarkable color variation in buffer solutions within the pH range relevant for food spoilage (from pH 4 to 8). In addition, according to preliminary results obtained in the headspace of biogenic amine solutions, colorimetric films showed a promising ability to detect the real-time freshness state of perishable food products such as meat and fish samples. In this work, an improved formulation of the pH-indicator previously developed work was deeply tested, focusing on its application which included pigment migration assays according to European regulation and photostability studies over time. Furthermore, the label's performance was evaluated using real samples and conditions, including modified atmosphere packaging (MAP).

2. Experimental

2.1. Materials

Cellulose acetate (CA) (Mw = 30,000 g·mol^{-1} and 39.8% (wt) of the degree of substitution in acetyl content), magnesium nitrate hexahydrate, were supplied from Sigma-Aldrich. The glycerol (Gly) was supplied from Himedia. Acetone and methanol were purchased from Chem-Lab. Deionized water was purified with a Milli-Q water system-Pyranoflavylium compound (2,10-Bis-(4′,4″-hydroxyphenyl)pyranobenzopyrylium chloride – PyF) was obtained according to the procedure described elsewhere [22].

2.2. Preparation of cellulose acetate-based films

Films were obtained by the casting technique, according to the methodology described by Assis *et al.*[24], with some modifications. CA 8% (w/w) was dissolved in acetone under mechanical stirring at room temperature until complete solubilization. Gly 30% (w/w) was added to the CA solution, and the dispersion was kept in vigorous mechanical stirring overnight. Pyranoflavylium salt solution in MeOH (1 mg/mL) was added to dispersion with a final concentration of 0.2% (w/w). After 1 h of homogenization, the dispersion was cast onto a Petri dish (63.6 cm^2), and solvent evaporation was carried out in an oven for 2 h at 40 ºC. The obtained films were detached from the plates and conditioned in a desiccator at 20 – 25 ºC and relative humidity (RH) of 53 – 54% (saturated magnesium nitrate solution) for at least 48 h until to be tested.

2.3. Color measurements

Color (CIELAB system) was measured using a portable spectrophotometer (model CM-2600d; Konica Minolta, Japan). L*, a*, b*, C*, and h are the color parameters of lightness, red-green chromaticity index, yellow-blue chromaticity index, total chromaticity, and hue, respectively. The measurements were made by Specular Component Excluded (SCE) mode in a 3 mm illuminated sample area with a 10° angle standard observer condition, D65 illuminant condition, and white background. All measurements were taken at three random positions for each film in the replicates, and the mean values were calculated. All photographs were taken with a smartphone (model A53, Samsung).

2.4. Tests as pH-indicator in pH buffer solutions

Films were cut into pieces (1 cm^2) and immersed in buffer solutions from pH 4 to pH 8. Buffer solutions of pH 4 and 5 were prepared by citric acid – phosphate buffer, and solutions with pH 6 to 8 were prepared by phosphate buffer. pH measurements were made in a Radiometer Copenhagen PHM240 pH/ion meter. The films were kept submerged in the different pH solutions for 60 minutes, and the color coordinates were measured before and after the immersion.

The color difference was determined over time by Eq. (1):

$$\Delta E^* = \sqrt{[(\Delta L^*)^2 + (\Delta a^*)^2 + (\Delta b^*)^2} \quad (1)$$

where $\Delta L^* = L^* - L_0^*$; $\Delta a^* = a^* - a_0^*$; $\Delta b^* = b^* - b_0^*$; L_0^*, a_0^* and b_0^* are color values of the films before the immersion (control). The experiment was done in triplicate.

2.5. Pigment migration analysis

The migration of pigment from the label was performed following the method described by Cerqueira *et al.* [25] with slight modifications and based on Commission Regulation (EU) No 10/2011 on plastic materials and articles intended to come into contact with food [26]. EtOH 10% (v/v) and EtOH 50% (v/v) solutions were used as food simulants A and D1, respectively. Migration tests in food simulant A were also made with different pH values, substituting water for the buffer solutions pH 4 – 8 (described in the 2.4. section). The film samples (4 cm^2) were weighted and immersed into 5 mL of simulant solutions at 25°C under moderate stirring (150 rpm). A sample of the simulant solution sample was taken at predetermined time intervals (1, 4, 8, 12, 24, 48, 72, 96, 120, and 144 hours), and the absorption spectra were recorded from 250 to 850 nm using a UV–vis spectrophotometer (Genesys 10S, Thermo Scientific). Of note, the samples were immediately returned to keep the total volume of the original solution constant (vestigial sample losses were neglected). The amount of pigment in simulant solutions was determined based on regression equations established for each experimental condition (50%EtOH: $y = 26.13x - 0.0063$, 10%EtOH: $y = 15.78x + 0.0038$, 10%EtOH pH 4: $y = 10.65x - 0.0034$, 10%EtOH pH 5: $y = 14.67x + 0.0004$, 10%EtOH pH 6: $y = 8.17x + 0.0046$, 10%EtOH pH 7: $y = 8.45x + 0.0038$, 10%EtOH pH 8: $y = 9.83x + 0.0064$) and the accumulative release percentage was calculated as follows:

$$Migration\ (\%) = \frac{M_t}{M_0} \times 100 \quad (2)$$

where M_t (mg) is the amount of pigment released from the label to food simulant at time t, and M_0 (mg) is the total amount of pigment incorporated in the label.

The amount of pigment migrated was also presented in mg of pigment per 1 dm^2 of the film's superficial area (mg/dm^2). The experiment was done in triplicate.

2.6. Color photostability of indicator

The color stability of the film indicator was evaluated in the presence (LIGHT) or absence (DARK) of light as a function of time. Samples (1 cm^2) were stored in two different chambers at 21 ± 2 ºC and RH of 55 ± 3%. Both chambers were protected from extern light with a box in each one. While one of the chambers was kept without light (DARK), another chamber was exposed to a constant light (LED, power 6 W), with 20 cm from the samples (LIGHT). The color coordinates were measured every three days for 30 days. Then, color variation (ΔE) was calculated according to Equation (1).

2.7. Application of indicator on real samples

In order to test the performance of the label in monitoring spoilage of perishable food products, experiments with real samples were carried out. First, a screening with different types of food products was made to evaluate the label's response to the pH changes over the deterioration stages of each one. Fresh samples of fish (Atlantic horse mackerel and Gilt-head bream) and meat (chicken breast and pork loin) were used and purchased from a local market. Then, a complete analysis of degradation parameters, such as the total volatile basic nitrogen (TVB-N) content, microbiology, and lipidic oxidation, was made for Atlantic horse mackerel (*Trachurus trachurus*). The packaging was produced in the pilot plant of the Meat Technology Center of Galicia (San Cibrao das Viñas, Ourense, Spain). Fish samples were packed whole without any prior handling. The labels were placed inside the package in cup-type support to protect them from possible contact with fluids released by the samples.

The samples and labels were packaged using a packaging machine (Caveco, model V900, Milano, Italy) with a modified atmosphere similar to the retail conditions. The atmosphere used for the fish and chicken samples was 30% CO_2 and 70% N_2 (PRAXAIR, Madrid, Spain), while for the pork samples, it was 20% O_2 and 80% N_2 (PRAXAIR, Madrid, Spain). The packaged samples were stored at 4 ± 1 °C (simulating retail conditions at supermarkets in a refrigeration chamber) for 8 and 15 days, respectively. The chamber was illuminated by a standard supermarket fluorescent lamp. For each day of analyses, packages were opened, and the color of the labels was quickly measured to avoid any color change due to their contact with the atmosphere outside the package. The ΔE values of the indicator were calculated according to Eq. 1. Then, the samples were ground in a food processor for further analysis. When the microbiological study was performed, samples for this analysis were first taken. In the case of fish samples, only muscles were ground and analyzed without the skin and bones. For the first experiment, three samples of each fish type and five of each meat type were used, which were carried out without replicates (screening). For the second experiment, thirty-five samples of Atlantic horse mackerel were used, with five replicates for each analysis day (days 0, 1, 4, 5, 6, 7, and 8). In this experiment, pH and TVB-N were analyzed on all days, while the microbiological profile and lipid oxidation were only studied at the experiment's beginning, middle, and end (days 0, 4, and 7).

2.7.1. pH measurement

For the pH measurement, 5 g of the ground sample was vigorously homogenized in 45 mL of distilled water, and pH values of dispersions were measured by a digital pH meter (Hanna HI, Woonsocket, EEUU).

2.7.2. Total volatile basic nitrogen (TVB-N) content

Total volatile basic nitrogen (TVB-N) content was assessed according to the Commission Regulation (EC) No 2074/2005 [27]. A 10 g sample of muscle was homogenized with 90 mL of perchloric acid, and the resulting suspension was centrifuged at 10,000g for 10 min using an Allegra X-22 centrifuge (Beckman Coulter, California, EEUU). 50 mL of the supernatant was analyzed for the nitrogen content following the Kjeldahl method using a Vapodest 50S analyzer (Gerhardt, Königswinter, Germany). The TVB-N values were expressed as mg N/100 g of sample.

2.7.3. Microbiological analysis

The microbiology quality of the samples was evaluated by the counts of aerobic mesophilic microorganisms (TVC). 10 g of fish samples were aseptically weighed and homogenized with 90 mL of 0.1% sterile peptone water (Merck, Darmstadt, Germany) in a masticator blender (IUL Instruments, Barcelona, Spain) for 2 min at room temperature. Serial decimal dilutions were prepared for each sample in 0.1% peptone solutions.

The TVC was carried out using the TEMPO® system (Biomérieux S.A., Madrid, Spain) based on the most probable number (MPN) technology. The TEMPO® system comprises two ergonomic stations, a preparation station for filling disposable cards (each card contains 16 x 3 tubes) with culture medium inoculated with the samples, and a reading station. The cards were read after the pre-established incubation time of 24 hours at 30 °C. TVC was calculated and expressed as log CFU/g of the fish sample.

2.7.4. Lipidic oxidation

Lipid oxidation was evaluated through the thiobarbituric acid reactive substances (TBARS) index according to the method proposed by Vyncke (1975). 2 g of the ground sample was homogenized with 10 mL of TCA 5% with Ultraturrax (IKA/T25) over 2 minutes in an ice bath. Samples were centrifuged at 3500 rpm for 10 min using an Allegra X-22 centrifuge (Beckman Coulter, California, EEUU). The supernatant was gravity filtered in an ice bath. In a test tube, 5 ml of sample and 5 ml of 0.2 M TBA were mixed and the mixture was incubated in a hot water bath at 97°C for 40 minutes. After that, the

tubes were cooled in a cold-water bath for 15 minutes. Finally, the absorption spectra were recorded at 532 nm using a UV–vis spectrophotometer (Agilent / 8453). TBARS values were calculated from a standard curve of malonaldehyde (MDA) with 1,1,3,3-tetraethoxypropane (TEP) and expressed as mg MDA/kg sample.

2.8. Statistical analysis

A one-way ANOVA and Tukey multi-comparative test were performed to detect the differences between samples with a significant level of 5% ($p < 0.05$). All statistical analyses were carried out using the software GraphPad Prism version 8.0.2.

3. Results and discussions

3.1. Color variation

Color quality is an essential feature of a colorimetric pH-indicator label. When food freshness is assessed, indicators with faded or less intense colors might raise some questions. Furthermore, color variations on the label should be visually more noticeable with stronger colors. The pyranoflavylium-based pH-indicator film developed in our previous work demonstrated an interesting color variation within the pH range of food spoilage [23]. However, herein we have decided to study its color improvement by increasing the pigment concentration in the formulation. The new film formulation included 0.2% (w/w) pigment, and the color was compared to the formulation from the previous study (0.1% (w/w)). The comparison was made before and after the immersion in buffer solutions (pH 4 – 8). Figure 1 shows photographs of films with 0.1% (w/w) and 0.2% (P0.2%) (w/w) of pigment before and after 60 minutes immersed in buffer solutions (pH 4 to 8). The three tristimulus components of color, namely the lightness (L*), chromaticity (C*), and hue (h), were used to compare both formulations (Figure 2). Moreover, each film formulation's color variation (ΔE) after immersion in the buffer solutions was compared (Figure 2).

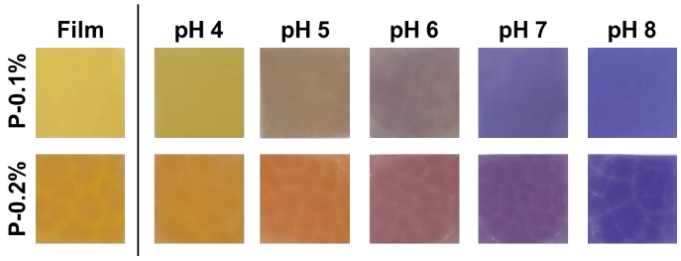


Figure 1. Photographs of films (1 cm^2) with 0.1% (m/m) (**P-0.1%**) and 0.2% (w/w) (**P-0.2%**) of pigment before and after 60 minutes immersed in buffer solutions (pH 4 to 8)

By analyzing Figure 1, the colors from P0.2% films are more intense than P0.1% films, and this observation can be quantitatively correlated with the luminosity (Figure 2A). In both cases, the luminosity decreases from high values (100) to neutral values (50). However, P0.2% films always had significantly lower values, translating into less clear and less faded colors than P0.1% films. In addition, the chromaticity of P0.2% films was higher than P0.1%, except for pH 5 and 6 (Figure 2B). Although the hues of P0.1% and P0.2% films were significantly different for all conditions except for pH 8, they were very similar. Color changes in the correspondent film before the immersion were not significantly different between P0.1% and P0.2% films. Although the color variation was statistically equal, the highest color intensity of P0.2% films makes its color variation more distinguishable. In both films, the color variation occurs between a hue from quadrant I (0º to 90º) to quadrant IV (270º to 359º) along the b* axis, from yellow (+b) to blue (-b). Overall, increasing the pigment film concentration improved its efficacy as an intelligent label by increasing the intensity of the colors in all pH studies and color coordinates evaluated.

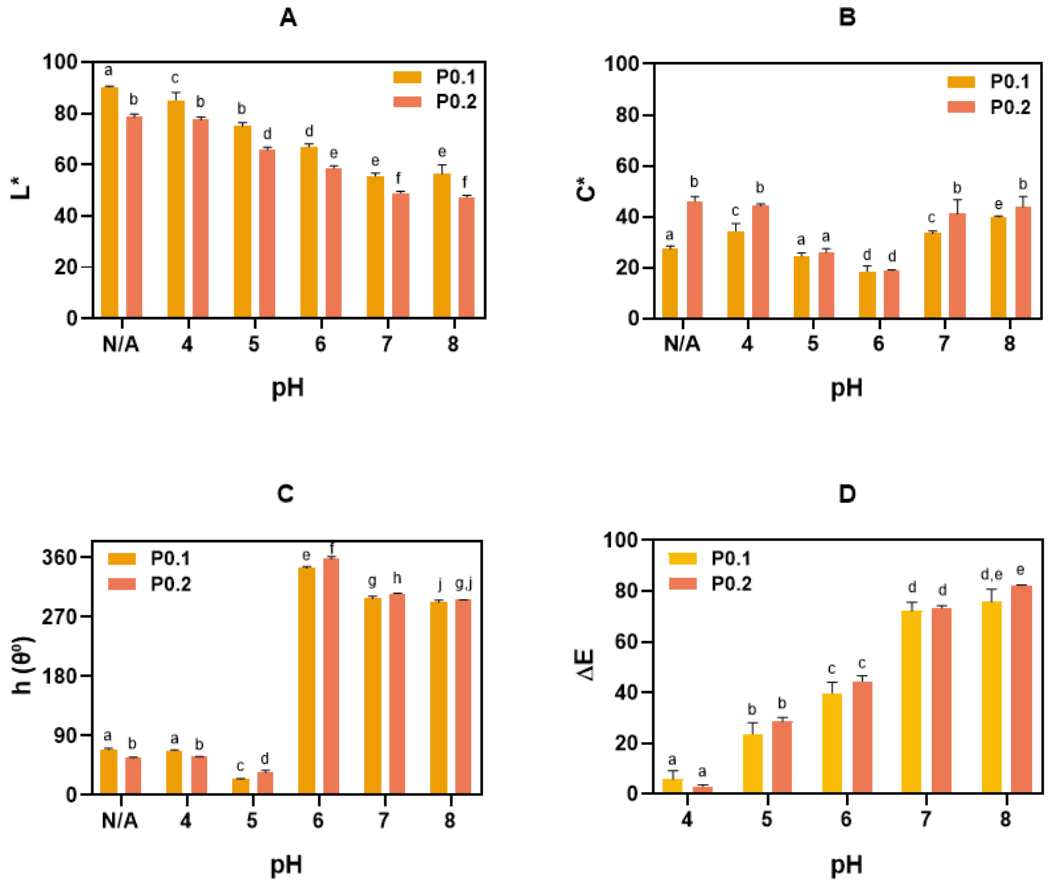


Figure 2. The three tristimulus components of color: **(A)** lightness (L*), **(B)** chromaticity (C*), and

(C) hue (h)[1]; and **(D)** the color variation (ΔE) before (N/A) and after immersion in the buffer solutions (pH 4 to 8) of formulations 0.1% (w/w) (**P0.1**) and 0.2% (w/w) (**P0.2**) of pigment. Significantly differences are represented by different letters. Comparisons were made between all columns. The same letter means no significant differences between the columns (a-j $p < 0.05$).

3.2. Pigment migration analysis

Although the principle of the label is not to be in contact with the food product, this could happen since it will be fixed inside the packaging. The components released from packaging material to food can compromise food safety. For this reason, regulatory authorities, such as the European Union (EU) Commission, set limits on the migration of the constituents of plastic materials and articles intended to come into contact with foodstuffs [26]. In addition, since all substances have an associated cytotoxicity, even the natural ones, it is essential that the amount released be far below its cytotoxicity. Furthermore, depending on the amount of pigment released, the label might lose effectiveness.

Migration largely depends on the affinity between the material components and the type (polarity) of the food matrix. The pigment migration study was conducted with food simulants A (EtOH 10%, v/v) and D1 (EtOH 50%, v/v) of EU No 10/2011. Simulant A was used for foods with a hydrophilic character, which can extract hydrophilic substances, such as fresh fish and meat. Food simulant D1 was used for foods made from oil-in-water emulsions, such as milk and some dairy products. In addition, simulant A solution at different pH values was also assayed, replacing the water with buffer solutions from pH 4 to 8. The pigment migration throughout the food deterioration period considering solutions at different pH values is important since the color displayed results from the presence of different dye chemical species, which may have different affinities for the food matrix, which must be considered.

The results of pigment release are presented in two different ways: 1) the percentage of pigment release from the label (4 cm^2) over time (Figure 3); 2) the total pigment release amount per area of the film (mg/dm^2) (Table 1).

Regarding releasing kinetics, they were practically similar for all solutions tested, reaching a *plateau* after 48 h (Figure 3).

[1] Hue values are given by their angle position in relation to the central axis of the theoretical three-dimensional sphere of color (0 – 359°). For the statistical analysis of these values, specifically, the statistical analysis of data that transverse the IV and I quadrants, the I quadrant values must be compensated (hue + 360°) for its analysis to be viable [44]. This compensation was done for the hue values for the films of pH 6.

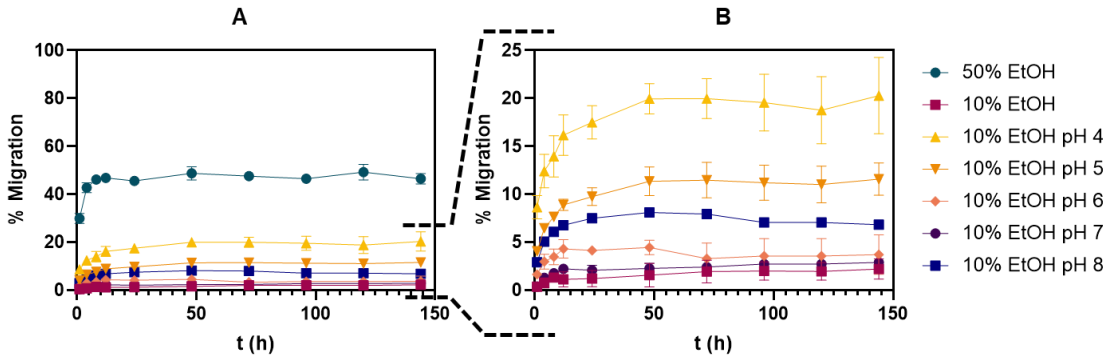


Figure 3. A) Migration percentages of pigment from the label (4 cm^2) over time in different conditions; B) Re-size graphic of migration percentages of pigment.

The highest pigment released from the label was observed for the food simulant D1, with a total of 45%, corresponding to 0.55 ± 0.02 mg/dm^2. The regulation set the migration limit to 10 mg of substances per 1 dm^2 of the surface area of material in contact with food. Since the label will be fixed inside the packaging, both sides were considered for the total contact area. Although the amount of pigment released for the D1 food simulant was much lower than the defined limit, this migration led to a substantial decrease in the effectiveness of the label. Thus, the developed label is not indicated to be used in oil-in-water emulsion-type foods.

On the other hand, the migration results in simulant A were quite promising. Pigment migration in solution without pH control and for the solutions at pH 6 and 7 did not exceed 5%. Higher percentages of migration were obtained for the pH 4 simulant solution, with 20%, followed by the solutions at pH 5 and 8, with 12 and 7%, respectively. These results demonstrated that the predominant species at neutral pH, the non-ionic quinoidal base, had less affinity for this type of simulant. On the other hand, the predominant species at a more acidic pH, the flavylium cation (highest hydrophilic character), is the one that demonstrated the highest affinity for the simulant. In this way, the label developed proves to be suitable for application in packages of fresh products of animal origin (*e.g.,* meat and fish) since 1) the amount of pigment that migrates in the real pH conditions of these foods (pH between 5.5 and 7.5) is low and does not affect the efficacy of the label; 2) the amount of pigment that migrates per dm^2 of material is residual compared to the defined limit value (Table 1).

Table 1. Total amount of pigment migrated from the label to different food simulant conditions during the assay period (144 hours).

Simulant	Migration (mg/dm^2)
50% EtOH	0.55 ± 0.02
10% EtOH	0.02 ± 0.01
10% EtOH pH 4	0.19 ± 0.02
10% EtOH pH 5	0.092 ± 0.002
10% EtOH pH 6	0.03 ± 0.01
10% EtOH pH 7	0.021 ± 0.002
10% EtOH pH 8	0.070 ± 0.002

3.3. Photostability of the pH-indicator film

A colorimetric pH-indicator must have an excellent color variation that follows the pH variation in its entire range or a specific range for a given application. However, this color must be stable to other stimuli, such as light and temperature, since these other variations may compromise its efficiency. The dye's planar structure and physicochemical properties are the main factors for this stability; however, the structural features of the polymer matrix can also affect it [28]. The photostability of the indicator was studied in the dark and with incident light at the same temperature (20 ± 2 ºC) and relative humidity (53 ± 2%). Figure 4 shows the color variation (∆E), lightning (L*), and chromaticity (C*) over 30 days. The color of the films that were not exposed to light remained practically the same over 30 days. In contrast, the films exposed to light suffered a slight variation (∆E ≈ 10), being very similar in the first 12 days. However, from the 12th day onwards, the variation was significantly more pronounced (Figure 4a), mainly due to an increase in luminosity and a slight decrease of chromaticity (a* and b* coordinates) (data not shown), leading to a loss of the film color. These results indicated that the label must be stored in the dark before its use. Furthermore, it is possible considering the stability over 12 days, which is usually the spoilage time for perishable foods, such as fish and meat fresh products.

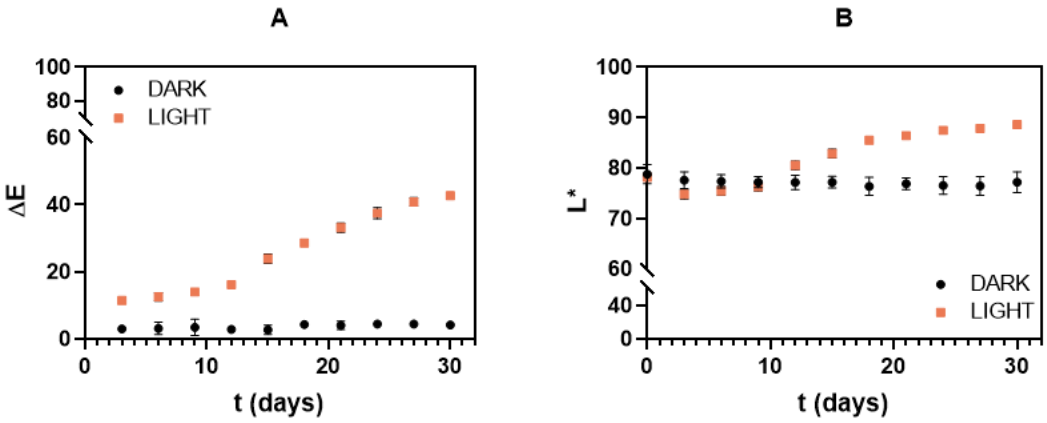


Figure 4. (A) Color variation (ΔE) and **(B)** luminosity (L*) of labels in the dark and with incident light over 30 days. DARK means that films were protected from light while LIGHT means that films were submitted to incident light.

3.4. Application of the pH-indicator films on real samples

3.4.1. Screening with different food products

A preliminary test was conducted with two different fish and meat samples to assess the film indicator performance regarding the color change in real packaged samples. A sample of oily fish (Atlantic horse mackerel) and white fish (Gilt-head bream) were used in the case of fish. Chicken breast and pork loin were used as meat samples. Samples were packaged in modified atmosphere packaging (MAP), a technique used to protect food products from the air and, consequently, to increase their shelf-life. Different MAPs can be used depending on product type. Fish and chicken samples were packaged in N_2 70% + CO_2 30%, a MAP used in fish and white meat products. The pork sample was packaged in O_2 80% + CO_2 20%, a MAP used in red meat products to keep their red coloration [29]. Since the shelf-life of fresh fish samples is shorter than meat, different study times were established for different types of samples (8 days for fish and 15 days for meat samples). The color variation and its correlation with the pH of each sample per day were evaluated (Figure 5).

In general, a very notable correlation was observed between the food pH and label color changes during the storage of all samples. However, the best color variations were observed for fish samples. The highest ΔE value observed was obtained for the oily fish sample (ΔE = 50.7), which had an increase of 0.80 in pH, the highest pH variation. Also, this sample showed higher pH values, starting with 6.45 on day 0 and reaching 7.21 after 8 days.

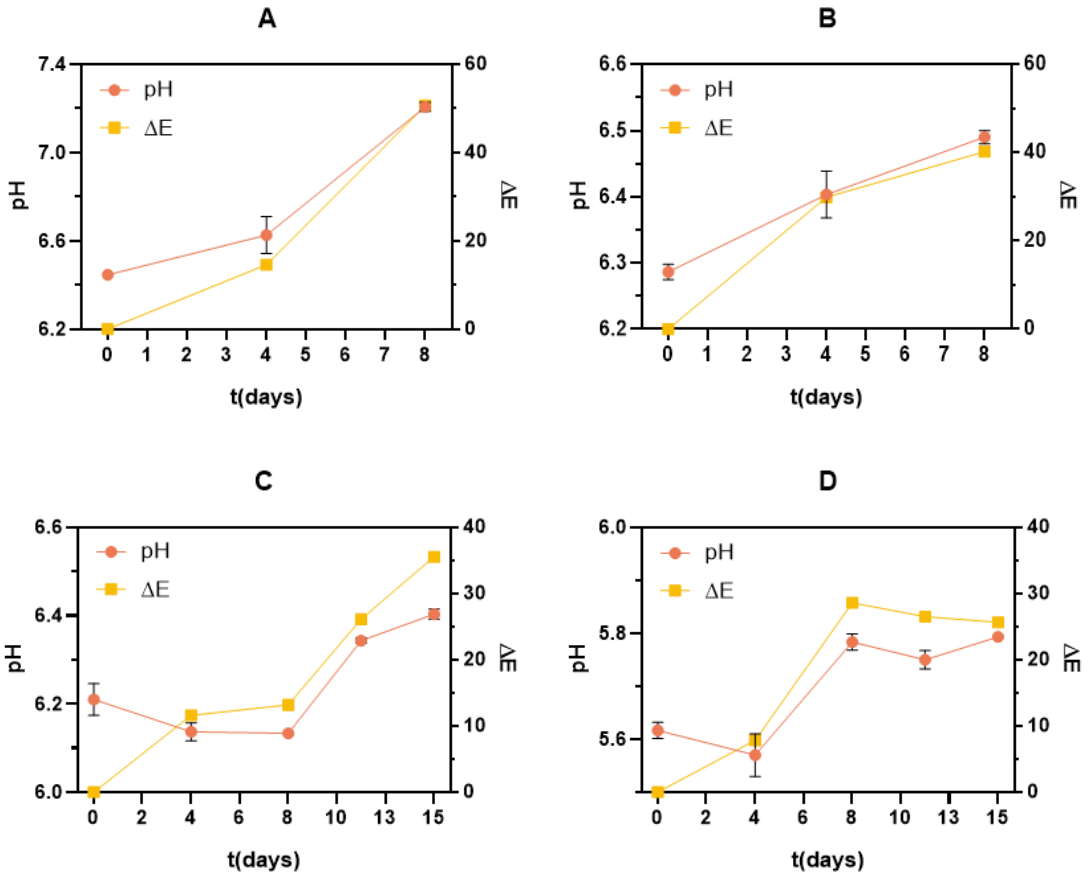


Figure 5. pH variation of (A) Atlantic horse mackerel, (B) Gilt-head bream, (C) Chicken, and (D) pork samples of and the corresponding color variation of the label over storage time at 4 ± 1 ºC.

The label in whitefish packages exhibited a maximum ΔE of 40.2 for a pH variation of 0.2, with a pH of 6.29 and 6.49 before and after 8 days of packaging. Both meat samples showed a similar pH variation during the spoilage period evaluated (15 days), with a slight pH decrease in the first four days and then a pH variation of 0.19 and 0.17 for chicken and pork, respectively. The decrease in pH in the first days owes to the anaerobic glycolysis (first step of spoilage), which produces acid compounds, and, consequently, the decrease of the pH of meat. This behavior also happens in fish products but occurs quicker than in meat, making its detection more difficult [29].

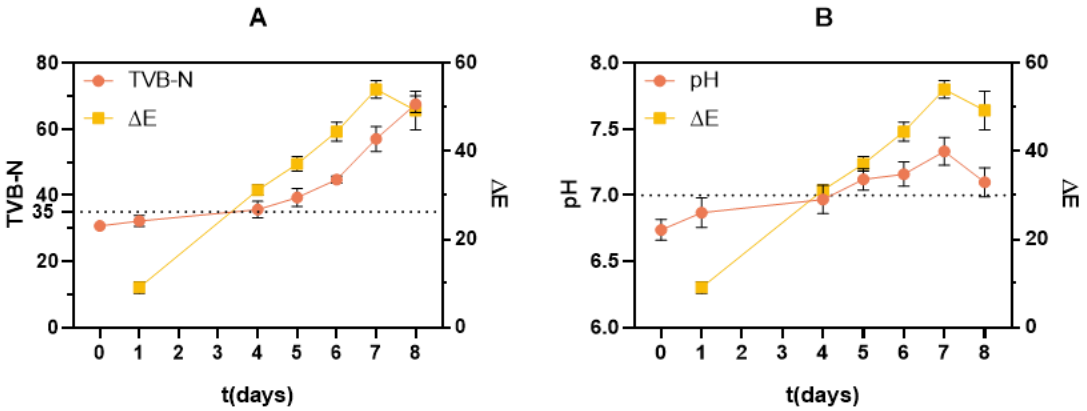
The label of the chicken packaging had an ΔE of 35.6 after 15 days. The lowest value was obtained for the pork packaging, with an ΔE of 28.6 after 15 days. Although the pH variation of whitefish and meat samples were similar, the color variation of the labels differed. The main difference was the pH range within which the variation occurred. While the chicken pH changed between 6.21 and 6.40, slightly below that obtained for the whitefish sample, the pork sample had a pH variation in the lower range of 5.62 and 5.79.

Although this represents a preliminary study, without replies to confirm the data, it was possible to conclude that the efficacy of the label depends on two factors: pH variation during the spoilage process and the occurring pH range. The best label responses were seen in the pH ranges above 6, which matches the pK_a values of the pigment used. The pK_{a1} of the pyranoflavylium pigment is 6.5 [22], and the pH variations around this value will conduct more noticeable color changes. Since fish samples usually have higher pH values as well as high pH variations during the spoilage process, the label developed seems to be more suitable for monitoring the freshness of fish samples.

3.4.2. Case study with Atlantic horse mackerel (Trachurus trachurus)

The Atlantic horse mackerel sample was used to validate the effectiveness of the label in monitoring the freshness. Also, the label was tested to detect spoilage, namely when the product becomes unsafe for human consumption. The Atlantic horse mackerel is a species of pelagic fish, which is a valuable food source due to its high nutritive value and essential nutrients such as long-chain omega-3 fatty acids, fat-soluble vitamins, and easily digestible proteins [30]. However, pelagic fish is also characterized by its highly perishable nature [30], which makes monitoring its freshness advantageous for guaranteeing consumption safety.

In this study, a more in-depth examination of the freshness state over time was conducted by increasing the number of data points and by measuring additional parameters, namely the total volatile basic-nitrogen (TVB-N) content, the microbiological profile, and the degree of lipid oxidation (Figure 6).



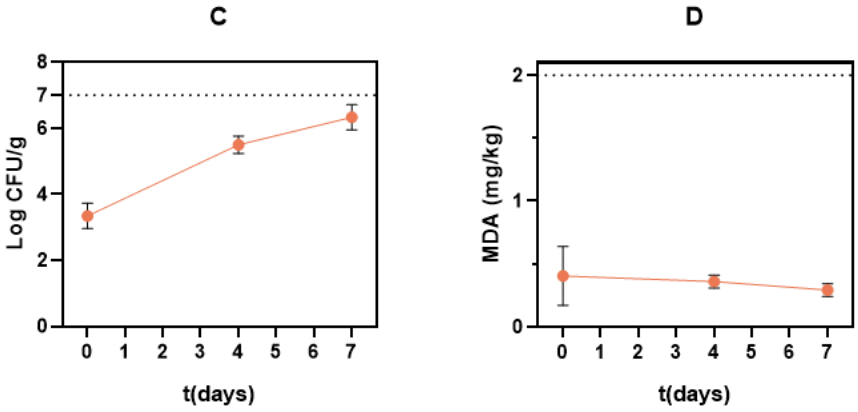


Figure 6. TVB-N content (A) and pH (B) and correspondent DE, and TVC (C) and TBARS index (D) evolution over time for Atlantic horse mackerel sample.

The TVB-N content is one of the parameters most used to evaluate fish freshness [31]. This parameter measures the total volatile nitrogen from organic amines (i.e., ammonia, triethylamine, and biogenic amines) generated by the decomposition of proteins and other nitrogen (N)-containing molecules as a consequence of enzymatic autolysis and microbiological spoiling mechanisms [32]. On the other hand, the total viable bacteria count (TVC) was used to evaluate the microbiological profile of the samples since it is one of the most powerful degrading agents, which has a close relation with the formation of biogenic amines [31].

Fish, especially oily fish, are rich in lipids, such as fatty acids, that are highly prone to oxidation, causing changes in fish quality attributes. The lipidic oxidation was evaluated by the determination of the thiobarbituric acid reactive substances (TBARS) index that quantifies malondialdehyde (MDA) in samples, which is a major compound from the secondary oxidation of lipids [33,34]. The TVC and TBARS index were studied only at the beginning, middle, and final of the experiment (days 0, 4, and 7), giving general information about their evolution over time.

The initial freshness level of the samples was evaluated by the values obtained for each parameter on day 0. The TVB-N value (30.7 ± 0.6 mg of N/100 g) indicated that the freshness level of the fish was lower than expected. Super fresh fish samples usually have TVB-N values between 0 to 20 mg N/100 g, but they depend on several factors, such as the type of fish, the time of transport since they are caught until the analysis and the temperature in the transport. In the specific case of Atlantic horse mackerel specie (*Trachurus trachurus*), TVB-N content of 15.3 mg of N/100 g [34], 18.64 ± 8.32 mg of N/100 g [35] and 25.48 ± 0.79 mg of N/100 g [36] have been reported. These values are also high for fresh fish, especially the last one described. The authors of the work that

reported an initial value of 25.48 ± 0.79 mg of N/100 g refer that the fish samples were delivered to the laboratory within 48 h of harvesting [36], which could reduce the freshness of the sample. The time elapsed after catching and the temperature history of fish are considered to be the key determining factors for the quality of a fish product [37]. In these samples, the high initial value of TVB-N may also be due to the time elapsed between the capture of the fish and the analysis, as well as to the transport and storage conditions, which are unknown. However, despite being high, this value is below the limit value of 35 mg of N/100 g defined by the EU regulations [27] and in other works reported in the literature for the same species [34,36]. The initial pH of 6.7 ± 0.1 was also slightly higher than values found in the literature (pH 6.2–6.5) for the same species [35,36,38], as well as the value obtained in the first screening experiment (pH of 6.45 ± 0.01). This discrepancy in initial pH is most likely to be attributed to the different levels of the freshness of the samples on day 0 of analysis. Despite the relatively high TVB-N and pH values for fresh fish, the total mesophilic aerobic bacterial count was low (3.5 ± 0.3 log $CFUg^{-1}$) and below the lowest values reported for the same species in the literature [35,38]. Since most organic amines are the product of microbial activity, high pH and TVB-N levels are usually connected with their high activity. In these samples, pH and TVB-N values may be due to the autolytic process by endogenous enzymes (first phase of fish spoiled), or the activity of other types of microorganisms not included in the mesophilic aerobic bacterial count [29]. Furthermore, the characteristic off-odors of a spoiled fish were not detected on day 0 by sensorial perception. Considering that the acceptability limit for TBARS is around 2 mg MDA/kg muscle, the initial value of 0.4 mg/kg of samples suggests low lipid oxidation and is in agreement with the literature [34]. The evolution of the freshness of Atlantic horse mackerel samples packaged in MAP (70% N_2 and 30% CO_2) was monitored over 8 days through TVB-N content and pH values (Figure 6) and correlated with the color variation (ΔE) of the label. Analyzing the evolution of freshness may be divided into two distinct phases. In the first phase, the evolution of the pH and TVB-N was slow, with an increase of around 0.2 and 5 mg N/100 g, respectively, over the first 4 days. The second phase was characterized by a more pronounced progression of the pH and TVB-N, with a pH rise of 0.36 over 3 days (from 4^{th} to 7^{th} day) and a TVB-N content increase of 31.91 mg N/100 g over 4 days (from 4^{th} to 8^{th} day). The decline in pH on the 8^{th} day may be related to advanced decomposition processes. In opposition to pH and TVB-N, the TVC had a higher increase from day 0 until the 4^{th} day (5.5 ± 0.3 log $CFUg^{-1}$) of storage and packaging and a less pronounced increase between the 4^{th} and 7^{th} day (6.3 ± 0.4 log $CFUg^{-1}$). The fish degradation begins *post-mortem*, initiating the autolysis process by anaerobic glycolysis, followed by

proteolysis induced by endogenous enzymes. The degradation of protein and nonproteic nitrogen (NPN) molecules produces short-chain peptides, amino acids, and nitrogen compounds, which consist of an ideal substrate for microorganisms [29]. The autolytic phenomenon predominates in some fish species, especially at low temperatures (close to 0 ºC) [36]. The elevated TVB-N and pH levels observed on day 0 of the experiment may have been induced by the possible storage of fish samples on ice for a few days before their acquisition and analysis. After packaging, their slow increase may be due to MAP since it is able to slow down the spoiling, raising the product shelf-life, as reported elsewhere [39]. However, a significant increase in bacterial growth was observed, namely, the TVC values from day 0 until day 4. This increase may result from several factors, such as the increase in the temperature of the storage. Temperature plays an essential role in microbial growth. Initially, fish samples were stored at approx. 0 °C in ice (in the supermarket), and then samples packaged were stored at 4 ± 1 °C in the refrigeration chamber. In addition, TVB-N results showed that the muscles of these samples are rich in nitrogen, an ideal substrate for microbial growth. Moreover, handling the sample during the preparation and packaging may lead to contamination of the samples, increasing further bacterial growth. The bacterial growth caused a more accentuated increase in the production of organic amines and, consequently, the TVB-N and pH values from the 4th day. Therefore, most of the organic amines responsible for off-odors in the fish, such as biogenic amines, are produced by bacterial activity, which explains some off-odors detected on the 5th day by the sensory perception. Despite being blue fish rich in fatty acids, lipid oxidation remained low during the experiment. This behavior was most likely due to the type of modified atmosphere in which it was packaged. The use of an atmosphere composed only of 70% N_2 and 30% CO_2, and without O_2, prevents the oxidation of fatty acids in the fish.

The TVB-N limit value defined by the EU regulations [27] is achieved on day 4th of storage (35.7 ± 2.2 mg N/100 g). In terms of pH, the limit value considered for acceptable quality fish is pH 7 [34], which was also reached on the 4th day of storage (pH of 6.97). According to Comi [29], the limit of the total bacterial count can generally be between 10^6 and 10^7 CFU/g. Thus, all parameters indicated the 4th day as the last day on which these Atlantic horse mackerel samples may be safely consumed. In addition, the sensory perception was consistent with the results since some off-odors began to be detected from the 5th day. Although modified atmosphere packaging increases the food shelf-life, the quality and freshness of the product at the time of packaging are crucial. Studies demonstrated that the shelf-life of fish samples could be extended up to 12 days in the same MAP [33].

However, in this case, the fish lasted only 5 days packed, suggesting one more time that its freshness on the day of packaging (day 0 of analysis) was below expected.
By evaluating the performance of the indicator label, a very interesting color change from yellow to purple was observed (Figure 7).

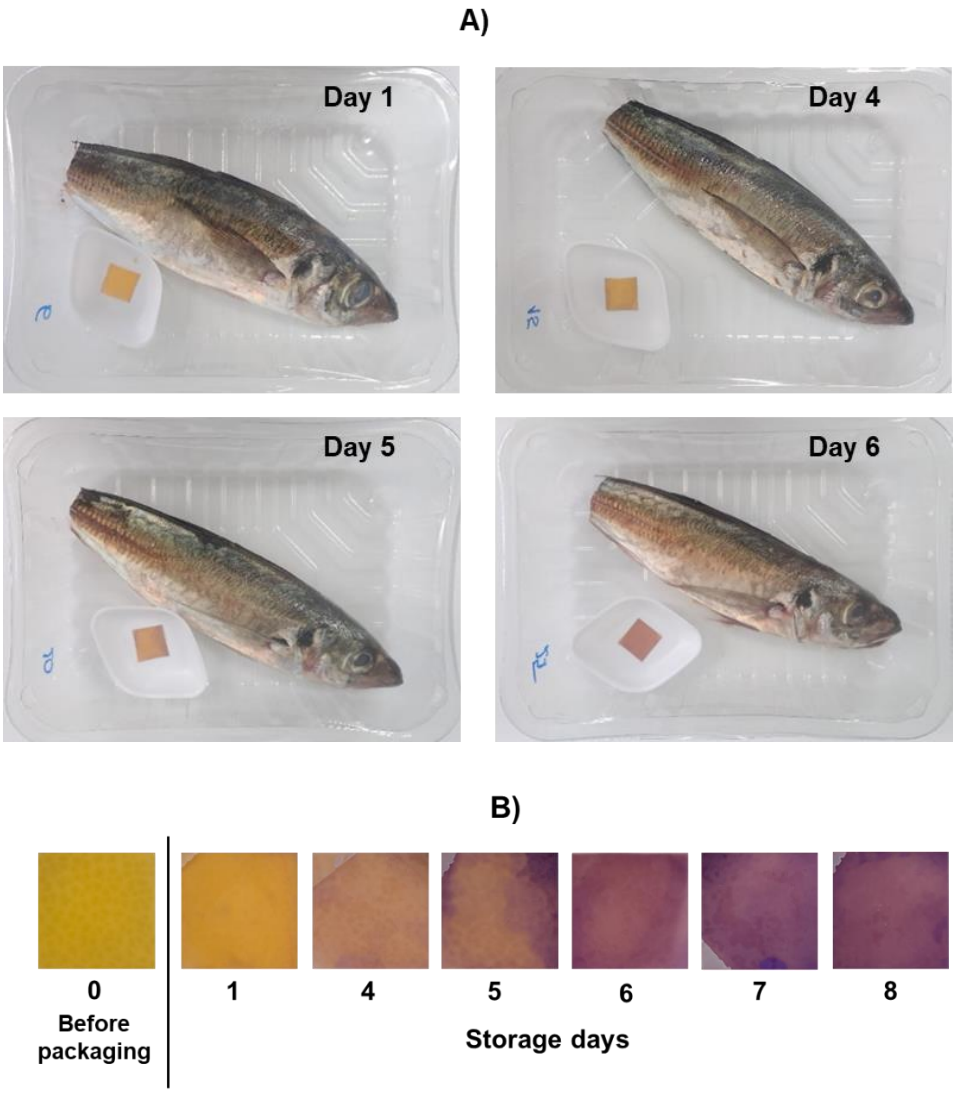


Figure 7. A) Photographs of packages on days 1, 4, 5, and 6, and B) photographs of the label before packaging and after different days of packaging storage.

The color variation of the label followed the evolution of the TVB-N and, particularly, the pH, since all values increased until the 7th day, where pH and ΔE registered a slight decrease on the 8th day, contrary to the TVB-N value. In quantitative terms, a ΔE of 9.0 ± 1.2 was detected on the 1st day as a consequence of certain variations in freshness as well as the color variation associated with the adaptation of the label to the conditions within the packaging (relative humidity, pH, etc.). The maximum ΔE value of 54.0 ± 1.7

was recorded after 7 days of storage, indicating that fish samples were completely spoiled. The ΔE value corresponds to the 5th day, in which the samples were considered as "spoiled" according to the established limits, which was 37.1 ± 1.4. Compared to the ΔE of day 4, the last day of freshness for consumption, the color variation was not quantitatively superior as expected, rising by just 6 units of ΔE.

In qualitative terms and visual aspects, however, labels of the 4th and 5th days are very distinguishable, as shown in Figure 7. The label of the 5th day is characterized by the appearance of a purple hue in certain regions, resulting in a non-homogeneous color that may not be accurately represented by ΔE values. Thus, the yellow color means that the product is "fresh", pale yellow denotes the "last day for consumption", and the purple color, in part or its whole, indicates that the product is "spoiled".

Compared to previous pH-indicators developed in the literature and tested to monitor the freshness of fish samples, this label is simpler, easier to read, and more efficient. Conversely, some of the produced indicators did not visually show a pronounced color change [40–42] or have multiple color changes [43], which might result in confusion and inaccurate readings by the consumer at the evaluation moment.

Therefore, and in opposition to most of the works published, the experimental conditions with real samples were practically the same as the real ones, mainly the packaging (size, MAP, sample/package ratio) and storage conditions (temperature and light). In fact, to our knowledge, this is the first work that tests the label's performance in a MAP. These conditions enhance the accuracy of the obtained results.

4. Conclusions

The new film formulation showed an improvement of color intensity in entire pH variations, which constitutes an advantage for a colorimetric label to indicate food freshness. Although the migration amount for all simulant conditions tested was considerably lower than the defined limit, the label is only suitable for foods with a hydrophilic character, such as fresh meat and fish products. In the case of lipophilic foods, the migration amount may substantially decrease the label effectiveness. Regarding photostability, the color of the label was kept valid and functional over 12 days with incident light, suitable for packaging perishable foods.

Through the preliminary tests in real samples, it was possible to observe a good correlation between the food pH and label color changes during the storage of all

samples. However, the best performance was observed for the freshness monitoring of fish samples since they had higher pH values as well as high pH variations during the spoilage process. In the test of freshness monitoring of fish Atlantic horse mackerel, the label exhibited an excellent correlation with pH and TVB-N during the spoilage. Following the limit values for pH, TVB-N, and TVC for fish products reported in the literature, the indicator demonstrated high efficacy in detecting spoilage of Atlantic horse mackerel.

CRediT authorship contribution statement

Vânia Gomes: Conceptualization, Methodology, Investigation, Writing - original draft.
Roberto Bermúdez: Methodology, Investigation, Writing - review & editing.
Nuno Mateus: Writing - review & editing.
Alexandra Guedes: Writing - review & editing.
Jose Manuel Lorenzo: Writing - review & editing.
Victor Freitas: Writing - review & editing, Project administration, Funding acquisition.
Luis Cruz: Conceptualization, Methodology, Investigation, Writing - review & editing, Funding acquisition.

Declaration of competing interest

The authors declare that they have no known competing financial interests or personal relationships that could have appeared to influence the work reported in this paper.

Acknowledgments

This work was supported by the Associate Laboratory for Sustainable Chemistry, Clean Processes, and Technologies LAQV. The latter is financed by national funds from UIDB/50006/2020. This research is supported by the AgriFood XXI I&D&I project (NORTE-01-0145-FEDER-000041), co-financed by European Regional Development Fund (ERDF), through the NORTE 2020 (Pro-grama Operacional Regional do Norte 2014/2020). This work was also supported by the project PTDC/OCE-ETA/31250/2017, funded by FCT and FEDER. Luís Cruz acknowledges the FCT research contract (DL 57/2016/CP1334/CT0008), and Vânia Gomes acknowledges the Ph.D. grant from FCT (SFRH/BD/136556/2018).

References

[1] European Commision. Commission Regulation (EC) No. 450/2009 of on active and intelligent materials and articles intended to come into contact with food. Off J Eur Union 2009:3–11.

[2] Heising JK, Claassen GDH, Dekker M. Options for reducing food waste by quality-controlled logistics using intelligent packaging along the supply chain. Food Addit Contam - Part A Chem Anal Control Expo Risk Assess 2017;34:1672–80. https://doi.org/10.1080/19440049.2017.1315776.

[3] Priyadarshi R, Ezati P, Rhim J-W. Recent Advances in Intelligent Food Packaging Applications Using Natural Food Colorants. ACS Food Sci Technol 2021;1:124–38. https://doi.org/10.1021/acsfoodscitech.0c00039.

[4] Yousefi H, Su HM, Imani SM, Alkhaldi K, Filipe CD, Didar TF. Intelligent Food Packaging: A Review of Smart Sensing Technologies for Monitoring Food Quality. ACS Sensors 2019;4:808–21. https://doi.org/10.1021/acssensors.9b00440.

[5] Danchuk AI, Komova NS, Mobarez SN, Doronin SY, Burmistrova NA, Markin A V., et al. Optical sensors for determination of biogenic amines in food. Anal Bioanal Chem 2020;412:4023–36. https://doi.org/10.1007/s00216-020-02675-9.

[6] Vanderroost M, Ragaert P, Devlieghere F, De Meulenaer B. Intelligent food packaging: The next generation. Trends Food Sci Technol 2014;39:47–62. https://doi.org/10.1016/j.tifs.2014.06.009.

[7] Alizadeh-Sani M, Mohammadian E, Rhim JW, Jafari SM. pH-sensitive (halochromic) smart packaging films based on natural food colorants for the monitoring of food quality and safety. Trends Food Sci Technol 2020;105:93–144. https://doi.org/10.1016/j.tifs.2020.08.014.

[8] Zheng L, Liu L, Yu J, Shao P. Novel trends and applications of natural pH-responsive indicator film in food packaging for improved quality monitoring. Food Control 2021;134:108769. https://doi.org/10.1016/j.foodcont.2021.108769.

[9] Oliveira Filho JG de, Braga ARC, Oliveira BR de, Gomes FP, Moreira VL, Pereira VAC, et al. The potential of anthocyanins in smart, active, and bioactive eco-friendly polymer-based films: A review. Food Res Int 2021;142:110202. https://doi.org/10.1016/j.foodres.2021.110202.

[10] Ghareaghajlou N, Hallaj-Nezhadi S, Ghasempour Z. Red cabbage anthocyanins: Stability, extraction, biological activities and applications in food systems. Food Chem 2021;365:130482. https://doi.org/10.1016/j.foodchem.2021.130482.

[11] Becerril R, Nerín C, Silva F. Bring some colour to your package: Freshness indicators based on anthocyanin extracts. Trends Food Sci Technol 2021;111:495–505. https://doi.org/10.1016/j.tifs.2021.02.042.

[12] Roy S, Rhim JW. Anthocyanin food colorant and its application in pH-responsive color change indicator films. Crit Rev Food Sci Nutr 2021;61:2297–325. https://doi.org/10.1080/10408398.2020.1776211.

[13] Neves D, Andrade PB, Videira RA, de Freitas V, Cruz L. Berry anthocyanin-based films in smart food packaging: A mini-review. Food Hydrocoll 2022;133:107885. https://doi.org/10.1016/j.foodhyd.2022.107885.

[14] Pina F, Melo MJ, Laia C a. T, Parola a. J, Lima JC. Chemistry and applications of flavylium compounds: a handful of colours. Chem Soc Rev 2012;41:869. https://doi.org/10.1039/c1cs15126f.

[15] Pina F. Chemical applications of anthocyanins and related compounds. A source of bioinspiration. J Agric Food Chem 2014;62:6885–97. https://doi.org/10.1021/jf404869m.

[16] Brouillard R, Chassaing S, Isorez G, Kueny-Stotz M, Figueiredo P. The Visible Flavonoids or Anthocyanins: From Research to Applications. Recent Adv. Polyphen. Res., Oxford, UK: Wiley-Blackwell; 2010, p. 1–22. https://doi.org/10.1002/9781444323375.ch1.

[17] Cruz L, Basílio N, Mateus N, de Freitas V, Pina F. Natural and Synthetic Flavylium-Based Dyes: The Chemistry Behind the Color. Chem Rev 2022;122:1416–81. https://doi.org/10.1021/acs.chemrev.1c00399.

[18] Oliveira J, Mateus N, De Freitas V. Previous and recent advances in pyranoanthocyanins equilibria in aqueous solution. Dye Pigment 2014;100:190–200. https://doi.org/10.1016/j.dyepig.2013.09.009.

[19] Cruz L, Sousa JLC, Marinho A, Mateus N, de Freitas V. Synthesis and structural characterization of novel pyranoluteolinidin dyes. Tetrahedron Lett 2017;58:159–62. https://doi.org/10.1016/j.tetlet.2016.11.123.

[20] Sousa JLC, Gomes V, Mateus N, Pina F, de Freitas V, Cruz L. Synthesis and equilibrium multistate of new pyrano-3-deoxyanthocyanin-type pigments in aqueous solutions. Tetrahedron 2017;73:6021–30. https://doi.org/10.1016/j.tet.2017.08.051.

[21] Gomes V, Guimarães M, Gonçalves G, De Freitas V, Cruz L. Bioinspired Synthesis and Physical-Chemical Properties of a New 10-Methylpyrano-4′-hydroxyflavylium Chloride Salt. Synlett 2020;31:334–8. https://doi.org/10.1055/s-0039-1690744.

[22] Gomes V, Pires AS, Fernandes I, Mateus N, de Freitas V, Cruz L. Synthesis of novel pyrano-3,7-deoxyanthocyanin derivatives and study of their thermodynamic, photophysical and cytotoxicity properties. J Photochem Photobiol A Chem 2021;415:113313. https://doi.org/10.1016/j.jphotochem.2021.113313.

[23] Gomes V, Pires AS, Mateus N, de Freitas V, Cruz L. Pyranoflavylium-cellulose acetate films and the glycerol effect towards the development of pH-freshness smart label for food packaging. Food Hydrocoll 2022;127. https://doi.org/10.1016/j.foodhyd.2022.107501.

[24] Assis RQ, Rios PDA, Rios A de O, Olivera FC. Biodegradable packaging of cellulose acetate incorporated with norbixin, lycopene or zeaxanthin. Ind Crops Prod 2020;147:112212. https://doi.org/10.1016/j.indcrop.2020.112212.

[25] Cerqueira MA, Fabra MJ, Castro-Mayorga JL, Bourbon AI, Pastrana LM, Vicente AA, et al. Use of Electrospinning to Develop Antimicrobial Biodegradable Multilayer Systems: Encapsulation of Cinnamaldehyde and Their Physicochemical Characterization. Food Bioprocess Technol 2016;9:1874–84. https://doi.org/10.1007/s11947-016-1772-4.

[26] European Union. Commission Regulation (EU) No 10/2011 of 14 January 2011. 2011. https://doi.org/10.3000/17252555.L_2011.012.eng.

[27] EC. Determination of the concentration of TVB-N in fish and fishery products. Commission Regulation, Chapter III. (EC) No 2074/2005. Off J Eur Union 2005:L338/37-39.

[28] Moazami Goodarzi M, Moradi M, Tajik H, Forough M, Ezati P, Kuswandi B. Development of an easy-to-use colorimetric pH label with starch and carrot anthocyanins for milk shelf life assessment. Int J Biol Macromol 2020;153:240–7.

https://doi.org/10.1016/j.ijbiomac.2020.03.014.

[29] Comi G. Spoilage of Meat and Fish. Elsevier Ltd; 2017. https://doi.org/10.1016/B978-0-08-100502-6.00011-X.

[30] Rustad T. The utilisation of pelagic fish: Challenges and possibilities. Open Access Gov 2018. https://www.openaccessgovernment.org/pelagic-fish-deparment-of-biotechnology-food-science/55576/ (accessed December 28, 2022).

[31] Prabhakar PK, Vatsa S, Srivastav PP, Pathak SS. A comprehensive review on freshness of fish and assessment: Analytical methods and recent innovations. Food Res Int 2020;133:109157. https://doi.org/10.1016/j.foodres.2020.109157.

[32] Bekhit AEDA, Holman BWB, Giteru SG, Hopkins DL. Total volatile basic nitrogen (TVB-N) and its role in meat spoilage: A review. Trends Food Sci Technol 2021;109:280–302. https://doi.org/10.1016/j.tifs.2021.01.006.

[33] Bouletis AD, Arvanitoyannis IS, Hadjichristodoulou C. Application of modified atmosphere packaging on aquacultured fish and fish products: A review. Crit Rev Food Sci Nutr 2017;57:2263–85. https://doi.org/10.1080/10408398.2013.862202.

[34] Zarandona I, López-Caballero ME, Montero MP, Guerrero P, de la Caba K, Gómez-Guillén MC. Horse mackerel (Trachurus trachurus) fillets biopreservation by using gallic acid and chitosan coatings. Food Control 2021;120. https://doi.org/10.1016/j.foodcont.2020.107511.

[35] Mol S, Cosansu S, Ucok Alakavuk D, Ozturan S. Survival of Salmonella Enteritidis during salting and drying of horse mackerel (Trachurus trachurus) fillets. Int J Food Microbiol 2010;139:36–40. https://doi.org/10.1016/j.ijfoodmicro.2010.01.046.

[36] Alfaro B, Hernández I, Baliño-Zuazo L, Barranco A. Quality changes of Atlantic horse mackerel fillets (Trachurus trachurus) packed in a modified atmosphere at different storage temperatures. J Sci Food Agric 2013;93:2179–87. https://doi.org/10.1002/jsfa.6025.

[37] Tzikas Z, Ambrosiadis I, Soultos N, Georgakis S. Quality assessment of Mediterranean horse mackerel (Trachurus mediterraneus) and blue jack mackerel (Trachurus picturatus) during storage in ice. Food Control 2007;18:1172–9. https://doi.org/10.1016/j.foodcont.2006.07.014.

[38] Rodríguez Ó, Losada V, Aubourg SP, Barros-Velázquez J. Sensory, microbial and chemical effects of a slurry ice system on horse mackerel (Trachurus trachurus). J Sci Food Agric 2005;85:235–42. https://doi.org/10.1002/jsfa.1960.

[39] Babic Milijasevic J, Milijasevic M, Djordjevic V. Modified atmosphere packaging of fish – an impact on shelf life. IOP Conf. Ser. Earth Environ. Sci., vol. 333, 2019, p. 012028. https://doi.org/10.1088/1755-1315/333/1/012028.

[40] Ezati P, Rhim JW. pH-responsive chitosan-based film incorporated with alizarin for intelligent packaging applications. Food Hydrocoll 2020;102:105629. https://doi.org/10.1016/j.foodhyd.2019.105629.

[41] Sani MA, Tavassoli M, Hamishehkar H, McClements DJ. Carbohydrate-based films containing pH-sensitive red barberry anthocyanins: Application as biodegradable smart food packaging materials. Carbohydr Polym 2021;255:117488. https://doi.org/10.1016/j.carbpol.2020.117488.

[42] Li Y, Wu K, Wang B, Li X. Colorimetric indicator based on purple tomato anthocyanins and chitosan for application in intelligent packaging. Int J Biol Macromol 2021;174:370–6. https://doi.org/10.1016/j.ijbiomac.2021.01.182.

[43] Amaregouda Y, Kamanna K, Gasti T. Fabrication of intelligent/active films based on chitosan/polyvinyl alcohol matrices containing Jacaranda cuspidifolia anthocyanin for real-time monitoring of fish freshness. Int J Biol Macromol 2022;218:799–815. https://doi.org/10.1016/j.ijbiomac.2022.07.174.

[44] Mclellan MR, Lind LR, Kime RW. Hue angle determinations and statistical analysis for multiquadrant hunter L,a,b data. J Food Qual 1995;18:235–40. https://doi.org/10.1111/j.1745-4557.1995.tb00377.x.

General Discussion and Final Remarks

The present work focused on developing a colorimetric smart label for food freshness monitoring of perishable muscle-based products. The aim of the work was generically divided into two parts: 1) the development of a suitable a pH-responsive pigment based on pyranoflavylium salts, and 2) building cellulose acetate-based materials (thin-films) containing the pH-sensitive pigment.

Different pigments were synthesized and structurally characterized in the first part of the work, and their chromatic properties toward pH variation were studied. Figure 1. shows all pigments developed in this work.

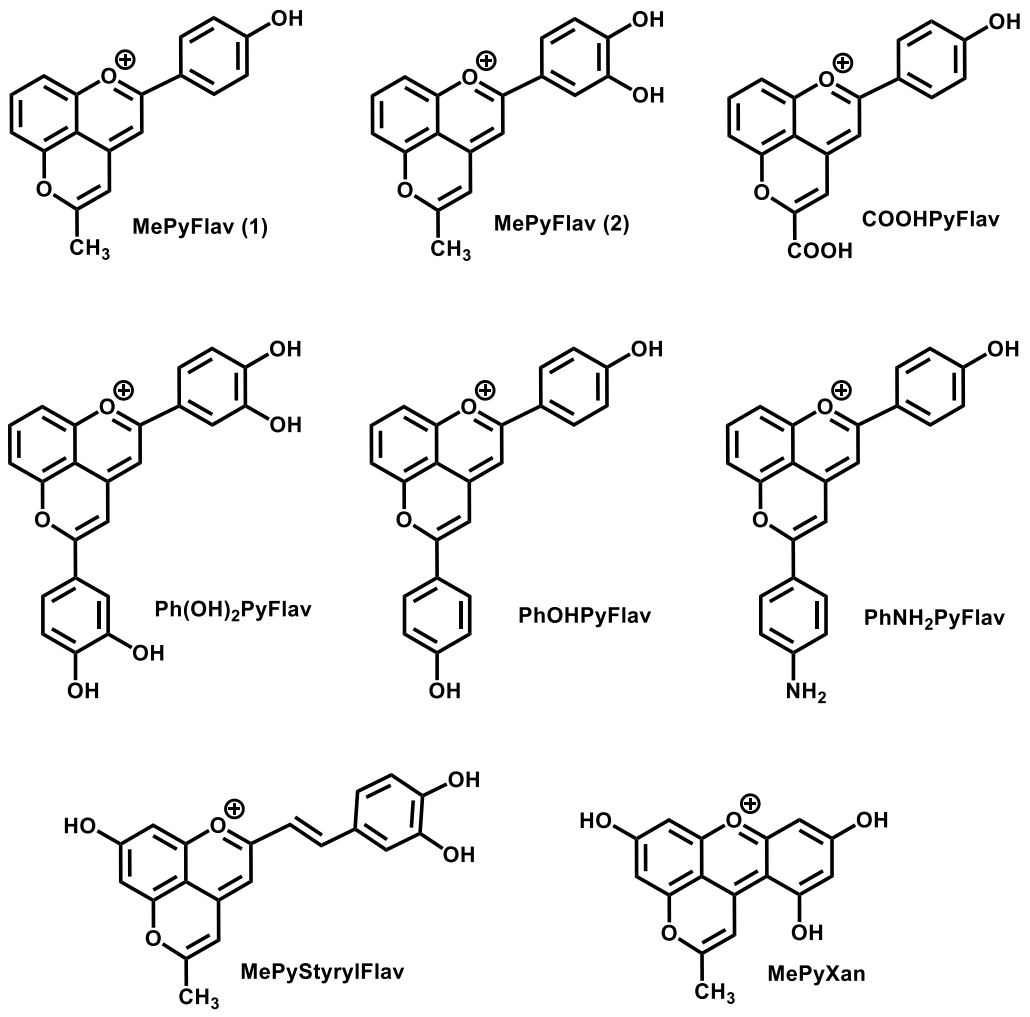


Figure 1. Structure of pyranoflavylium dyes synthesized in the present work.

The chemical equilibria of the dyes were studied in aqueous/ethanol solution (EtOH 25% (v/v)) by spectrophotometric titrations, and equilibria constants (pK_a) were determined (Table 1).

Table 1. pK_a values from hydroxylic deprotonations of pyranoflavylium and related compounds obtained by UV−Vis Spectroscopy in a H_2O/EtOH 75:25 (v/v) solution.

		pK_{a1}(OH)	pK_{a2}(OH)	pK_{a3}(OH)
MePyStyrylFlav		5.1 ± 0.1	7.3 ± 0.2	11.3 ± 0.1
Micellar system	**SDS**	6.8 ± 0.2	9.5 ± 0.2	-
	TRITON X-100	5.1 ± 0.1	9.7 ± 0.1	-
	CTAB	4.5 ± 0.1	6.9 ± 0.1	9.2 ± 0.1
MePyXan		4.80 ± 0.03	6.51 ± 0.05	8.64 ± 0.01
MePyFlav (1)		6.8 ± 0.1	10.8 ± 0.1	-
MePyFlav (2)		5.80 ± 0.02	8.7 ± 0.1	-
Ph(OH)$_2$PyFlav		5.5 ± 0.1	9.77 ± 0.02	-
PhOHPyFlav		6.5 ± 0.1	8.9 ± 0.1	-
COOHPyFlav*		6.22 ± 0.01	-	-
COOHPyFlav_CH		6.43 ± 0.04	-	-
PhNH$_2$PyFlav*		7.2 ± 0.1	-	-
PhNH$_2$PyFlav_ALG		7.17 ± 0.02	-	-

*The pigments COOHPyFlav and PhNH2PyFlav presented a lower pK_a value corresponding to the deprotonation of carboxylic acid and ammonia cation groups, respectively.

Since the relevant pH range in the spoilage process of fresh animal products is between pH 5.5 and 7, one of the aims of this work was the rational design of new pyranoflavylium pigments in order to their pK_a values (at least one) could match that range. Regarding the existing pyranoflavylium salts at the time of this work, the pK_a values described in the literature are between 3.6 and 5.4 which is due to the first deprotonation occurring at the C7-hydroxyl group[1].

The pK_a of the first studied pigment (MePyStyrylFlav) was lower than pretended; however, its modulation in SDS micellar system yielded good color tuning. Nevertheless, the development of pigments lacking a hydroxyl group at position 7 allowed, in general, to push the pK_a values toward the desired range. In addition to possessing the requisite pK_a value, the symmetric PhOHPyFlav demonstrated a remarkable color change from yellow to purple without a decrease in color intensity over the pH range, making it the most suitable dye, and exhibited the lowest cytotoxicity as well. The pigments COOHPyFlav and PhNH$_2$PyFlav were essentially designed to be covalently linked to chitosan (CHT) and alginate (ALG) biopolymers, respectively, via amide-type bonding

[1] L. Cruz, N. Basílio, N. Mateus, V. de Freitas, and F. Pina, “Natural and Synthetic Flavylium-Based Dyes: The Chemistry Behind the Color,” *Chem. Rev.*, vol. 122, no. 1, pp. 1416–1481, Jan. 2022, doi: 10.1021/acs.chemrev.1c00399.

using EDC/NHS coupling chemistry. Although the remainder of the work was not completed during this project, the purpose of these conjugates is to build multilayered films by electrostatic interactions between oppositely charged polyelectrolytes through Layer-by-Layer assembly technology. Particularly, the COOHPyFlav_CHT conjugate showed a suitable pK_a to be applied in food freshness monitoring.

The study of pigment MePyXan arose from the fact that it is a by-product formed in large quantities from the reaction from Article I. In the acidic aldol condensation between 2,4,6-trihydroxybenzaldehyde and the acetophenone, the by-product xanthylium results from the condensation between two aldehyde molecules. Since it is a secondary product formed in large quantities, this pigment was used to synthesize a new pyranic compound and study its potential. Despite not having demonstrated chromatic variation (yellow color in the entire pH range), it had interesting fluorescence properties. The "*off-on-off*" fluorescence behavior and the pK_a values within the neutral pH region make this pigment a promising candidate as a pH-responsive fluorescent probe for several applications in the biomedical field.

In the work's second part, the PhOHPyFlav pigment was immobilized by physical entrapment in a polymeric matrix. After some preliminary tests (data not shown) with different biopolymers, cellulose acetate was the polymer chosen due to showed more water resistance. Unlike the other biopolymers tested, the cellulose acetate films remained strong when immersed in water. Since the first formulation with pigment and cellulose acetate did not change de color in the pH buffer solution (pH 4 - 8), the addition of a plasticizer, namely, glycerol was tested. The effect of adding glycerol was crucial to the performance of the smart label because of two reasons. Firstly, glycerol provided the appearance of pores in films, which led to an ideal water vapor permeability of the films as well as the surface contact area, resulting in a more efficient color response to the environmental pH. Secondly, the glycerol content also promoted an increase in opacity, leading to a more distinguishable color. After testing different concentrations of glycerol, films with 30% showed the best performance in solutions with different pH values. In addition, films with 0.2% (w/w) of pigment showed greater color intensity in entire pH variations than films with 0.1% (w/w). These films exhibited a relevant and remarkable color change at the pH range of food spoilage, such as observed for the pigment in the solution. However, the best performance in real samples was observed for the freshness monitoring of fish since they had higher pH values as well as high pH variations during the spoilage process. In the test of freshness monitoring of fish Atlantic horse mackerel, the label color variation (ΔE) showed a directly proportional correlation with pH 7 and

TVB-N during the spoilage process. Following the limit values for pH, TVB-N, and TVC for fish products reported in the literature, the indicator demonstrated high efficacy in detecting spoilage of Atlantic horse mackerel. The color of the label changed from yellow ($\Delta E = 9.05 \pm 1.4$) to purple ($\Delta E = 37.1 \pm 1.4$) when the freshness parameters exceeded the limit defined by EU regulations on day 5 (TVB = 39.4 ± 2.7 and pH = 7.1 ± 0.1), indicating that the fish was unfit for consumption. In terms of photostability, the label kept its color for over 15 days by exposition to light. However, it would also be relevant to study its photostability at different pH values, with higher relative humidities and lower temperatures, since these are more realistic conditions.

In conclusion, in this work, it was possible to successfully obtain a pH indicator label to monitor the freshness of packaged fish products. Contrary to most of the works found in the literature, the development of this indicator was based on knowledge regarding the physical-chemical properties (pK_a values) of compounds, which are designed for the purpose. Future work would be important to consolidate these results by increasing the reproducibility, testing more Atlantic horse mackerel samples, and testing with other species. In the case of meat samples, it could be interesting to develop indicator films containing structurally different pigments with lower pK_a values such as the case of MePyFlav (2). It would also be interesting to develop the films with the COOHPyFlav_CHT conjugate by layer-by-layer methodology, as originally planned.